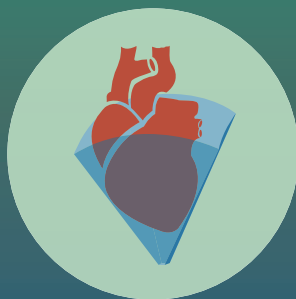# SIMULTANEOUS MULTIPLANE
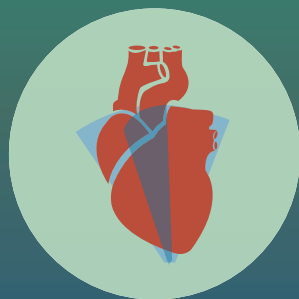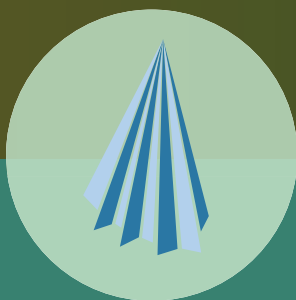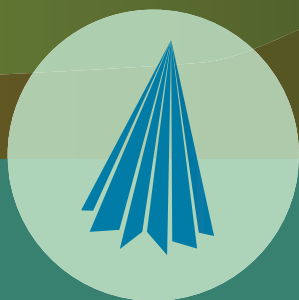# 2D-ECHOCARDIOGRAPHY

Jackie McGhie

Simultaneous Multiplane 2D-Echocardiography

Jackie McGhie

Simultaneous Multiplane 2D-Echocardiography

Simultaneous Multiplane 2D-Echocardiografie

Proefschrift

ter verkrijging van de graad van doctor aan de
Erasmus Universiteit Rotterdam
op gezag van de
rector magnificus

Prof.dr. H.A.P. Pols

en volgens besluit van het College voor Promoties.
De openbare verdediging zal plaatsvinden op
dinsdag 27 juni 2017 om 15.30

door

Jacqueline Susan McGhie
geboren te Edinburgh, Scotland, UK

Erasmus University Rotterdam

To all those who I have met
and those I still have to meet
during my walk of life

CONTENTS

PART I

Simultaneous multiplane
2D-echocardiography

CHAPTER 1

General introduction and
outline of the thesis

GENERAL INTRODUCTION

Since the future is based on the past, this chapter will provide a brief history of echocardiography and the knowledge gained that has led to transthoracic simultaneous multiplane 2D-echocardiography.

The Evolution of Echocardiography

The evolution of echocardiography has been dramatic and it is still ongoing. The ultrasound instruments of today are derived from sound and ranging navigation (sonar) instruments. The existence of ultrasound was recognised by L. Spallanzani (1729–1799); he demonstrated that bats, although blind, could navigate using echo-reflections of inaudible sound. In 1917, during World War I, the idea was born to use the piezo-electric quartz crystal, discovered in 1880 by Jacques and Piere Curier, not only as a transmitter but also as a receiver. In 1941, K.T. Dussik, an Austrian neurologist, demonstrated for the first time the use of ultrasound for medical practise. He aimed to outline the ventricles of the brain using echo transmission, a principle similar to X-ray.[1] The first use of echocardiography, as we know it today, is to the credit of Edler and Hertz[3], (Figure 1).

In the 1950s, doctors were searching for a technique that could measure the expansion of the left atrium (LA) wall to exclude patients with significant mitral regurgitation from closed mitral valve surgery. The first A-mode display of the heart was visualized. They noted high-speed movement of what they thought to be reflections coming from the LA

Figure 1 Helmut Hertz (left) and Inger Edler (right) standing with the first echocardiograph. From E. Braunwald with permission.[2]

wall; however, the echoes displayed were actually from the anterior mitral valve leaflet. Hertz realized the importance of recording these echoes. This could be realized by moving the B-mode display over the oscilloscope screen for immediate visualization or by moving a recording surface past the B-mode display for documentation, the time-motion mode, or M-mode (Figure 2A, 2B). **Thus the field of echocardiography was born.** During the 1960s, the Americans, after working a few years with M-mode echocardiography, were convinced that there were many potential applications for this diagnostic technique. It was Harvey Feigenbaum who realized that with its popularity, the demand on a physician's time for performing the examination would be high. He felt that a productive, dedicated, non-physician could perform the examination, if the acquiring of images could be standardized leaving the final interpretation to the physician. This idea was successful and a new breed of specialist was created, "the cardiac sonographer".[5]
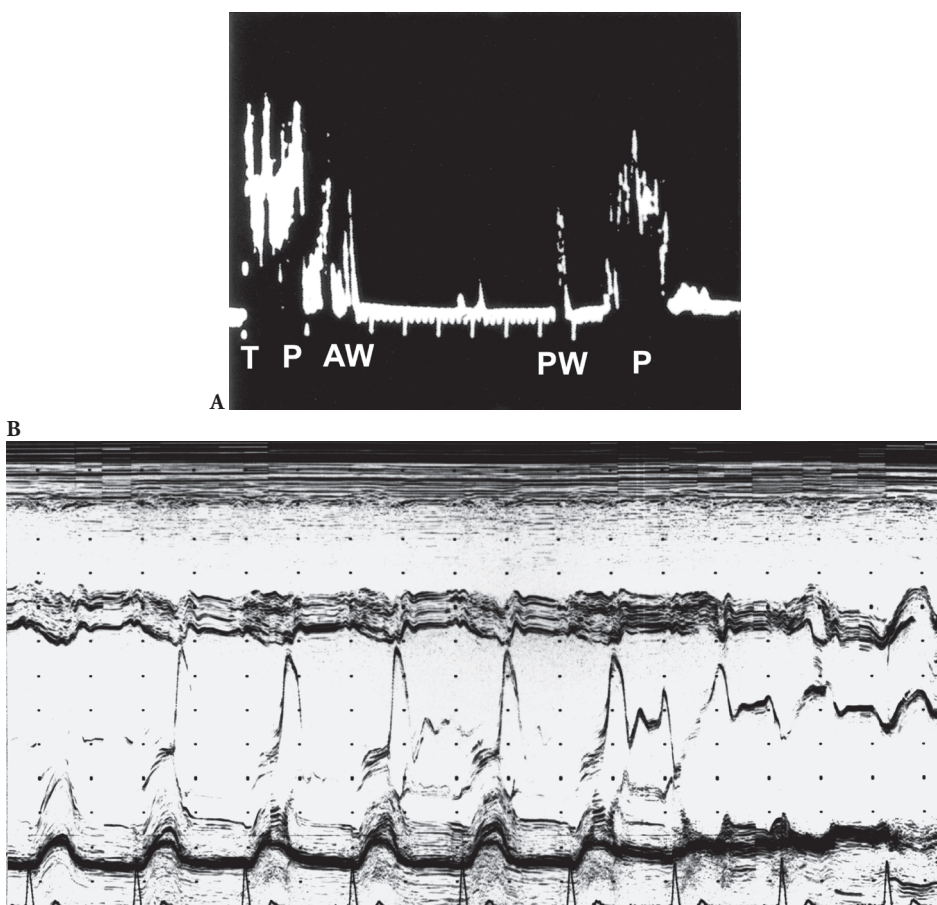

Figure 2 A. A-mode recording. (T = transducer signal; P = pericardium; AW = anterior wall, PW = posterior wall). From H.Feigenbaum with permission.[4] **B.** Time motion or M-mode echo.

There have been many important developments in the field of cardiac ultrasound, too numerous to mention them all. In the 1960s, great progress was made in developing two-dimensional (2D) echocardiography (2DE). In the late sixties and early seventies, contrast echocardiography came on the scene; the technique was extremely helpful in identifying and delineating the various cardiac structures and intra-cardiac shunts.[6–8] Further advances in this technique did result in the use of contrast for myocardial perfusion studies.[9] The oscillation of the contrast bubbles caused by the ultrasound waves inspired the development of harmonic imaging; the main imaging setting of all echo-machines today. In 1971, at the Thoraxcenter, Erasmus University Medical Center, Rotterdam, Professor Bom and colleagues developed the linear array transducer demonstrating the potential of real-time 2DE imaging.[10] It was Professor Jos Roelandt, considered to be one of the godfathers of clinical echocardiography who ensured that the potential of these technical developments fully investigated in the clinical setting.[11] In 1974, the first mechanical 2DE sector scanner was launched [12], followed later that year by the first phased-array 2DE scanner, this technology still has a very prominent place in cardiac imaging today. [13] Further development and miniaturization has led to pocket size echo-machines available to every doctor; in reality a modern stethoscope.[14] In 1982 transoesophageal echocardiography (TEE), which allows a view of the heart less compromised by artefacts due to the lung and ribcage, entered the clinical setting, first with a mono-and biplane probe followed in 1985 by a multiplane probe.[15]

Alongside the development of echocardiography, the Doppler technique was also evolving. A major step forward for clinical acceptance was the duplex scanner.[16,17] In 1982, the revolutionary colour Doppler flow imaging system showing a non-invasive 'angiogram' of normal and abnormal blood flow entered the market scene.[18] Further development in Doppler technology resulted in tissue Doppler imaging for the quantification of myocardial function. Flawed by its angle dependencies, progress in development continued, leading to speckle tracking echocardiography. This technique, that is relatively angle-independently, quantifies myocardial wall motion, not only in a longitudinal direction but also radial and circumferential directions.[19,20]

Clinical Impact of Echocardiography

We now have a patient friendly diagnostic console, which is versatile, low cost and available at bedside, providing integrated structural, functional and haemodynamic data of the heart. 2D imaging is the core of every echocardiographic examination along with M-mode, pulsed-wave, continuous-wave and colour Doppler flow imaging. There are three essential ingredients for an optimal diagnostic echocardiogram: the machine, the machine operator and the echogenicity of the patient. The second making the technique operator dependent and the third frustrating the sonographer.

Once the images have been acquired, other drawbacks of the 2DE technique have to be taken into consideration. First, the quantification of the left ventricular and atrial volume; these are calculated using either the ellipsoid (linear) method or the modified bi-plane Simpsons method of disks.[21] Measurements are performed on two assumed orthogonal

planes: apical 4 and 2-chamber view. Errors can occur in both of these methods either from the geometric assumption or from acquiring foreshortened apical views.[21–23] Second, cardiac anatomy, sometimes so complex that conceptualization of the true anatomy viewed from several 2D cut-planes can be very difficult. There is no way of knowing and controlling if everybody is visualizing the same conceptualized image.[24]

The pioneers of echocardiography realized this and published their first manuscript on three-dimensional (3D) echocardiography (3DE) in 1974.[25] In the early 1990s the first real-time 3D matrix phased array transducer containing 512 elements came onto the market with a frame-rate high enough to depict cardiac motion.[26] Since then numerous studies have been performed and articles published worldwide showing the benefits of this technique. The European Association of Echocardiography/American Society of Echocardiography now recommends 3DE for volume quantification.[27] However, "all that glitters is not gold" and in the real world, the cardiac sonographer is faced with several problems produced by this new technology: an intensive learning curve, a bulky transducer with a too large footprint, poor 2DE image quality compared to the dedicated 2D transducer and a number of 3DE-datasets had to be acquired to answer the clinical question. The analysis, often tedious, has to be performed off-line and quantification software was predominantly manual, all of which hampered the introduction of 3DE into routine practice. With significant technological developments in both digital techniques and miniaturization Philips recently introduced a new generation 2DE/3DE matrix transducer containing more than 3,000 elements with operating frequencies from 2–4MHz (Figure 3), size and
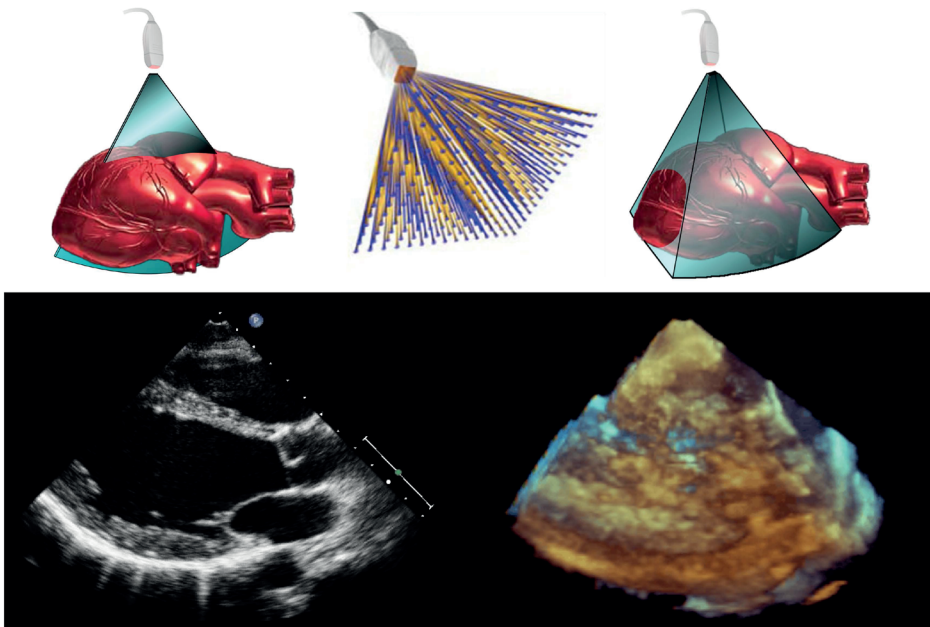
Figure 3 The matrix-array transducer: 2D to 3D echocardiography. (Left 2D B-mode, center matrix-array transducer, right 3D echocardiography)

image quality being very similar to that of the dedicated 2D transducer. Pulsed-wave, continuous-wave and colour Doppler were also incorporated which resulted in an "all-in-one" transducer.

Even with the marked improvement in 3DE image quality, the 2DE image quality taken from a 3D dataset remains inferior, especially with a less than optimal acoustic window. With the increase in obese patients, this has become a daily problem resulting in a substantial group of patients who will not benefit from the advantages of 3DE. The learning curve still remains and it is difficult to implement in a high productivity
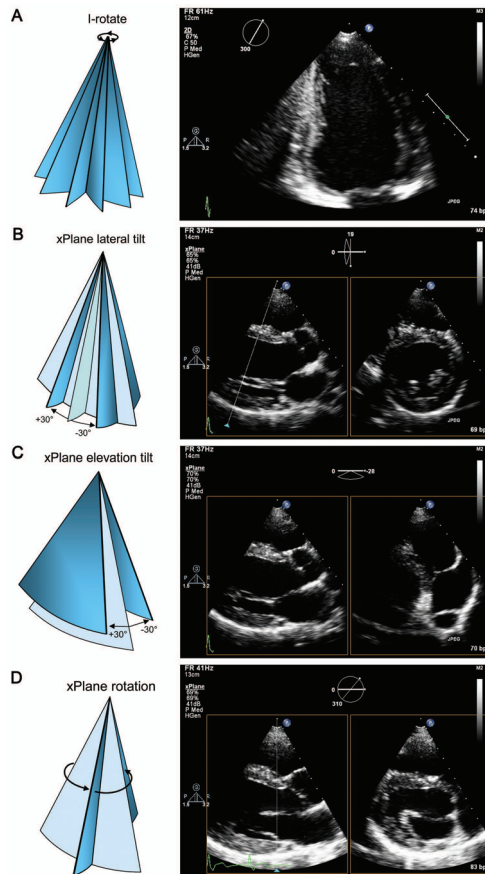
Figure 4 Simultaneous multiplane imaging modes.
A. I-Rotate: a 2-chamber view is obtained by rotation of 60° (to 300°) from a standard 4-chamber view (defined as 0° or 360°). The degree of rotation is displayed in the upper left-hand corner of the screen.
B. xPlane with lateral tilt: from a standard parasternal long-axis view (primary image or reference plane) an orthogonal short-axis view at the chordal–papillary muscle level can be obtained by a lateral tilt of +10°.
C. xPlane with elevation tilt: from the same view a right ventricular inflow view can be obtained by an elevation tilt of -28°.
D. xPlane with rotation: from the same view an unorthodox short-axis view of the mitral valve by a rotation of +50°.

outpatient environment. However, with this marked increase in the 2DE image quality of this second generation matrix transducer, a new echocardiographic imaging modality has become available; "simultaneous multiplane 2D-echocardiography imaging" (SMPI). This new modality permits the use of a full electronic rotation of 360° of the 2D image (iRotate) and a simultaneously adjustable biplane 2D image from the same heartbeat (xPlane) (Figure 4). SMPI has the potential to reduce the scanning time, increase 2DE standardisation and bridge the gap from 2D to 3D thinking, accelerating the 3DE learning curve and securing its place in routine cardiac imaging.

AIMS AND OUTLINE OF THIS THESIS

In 2011, this new generation transthoracic 2DE/3DE matrix transducer became available in our center and the studies featured in this thesis were initiated. The aim of this thesis is to investigate the potential contributions of this new imaging modality to cardiovascular imaging and patient care. The thesis is divided into three parts.

Part I: Simultaneous multiplane 2D-echocardiography
In addition to a general introduction (**Chapter 1**), the 2DE imaging modes from this new matrix transducer technology and how they can be utilized on day-to-day bases in the echo laboratory are described (**Chapter 2**).

Part II: Simultaneous multiplane 2D-echocardiography in congenital and valvular heart disease
The atrial septal secundum defect (ASD) is one of the most common lesions in adult congenital heart disease. Transcatheter closure of an ASD has gradually become the treatment of choice. However, the size of the defect and length of rims is important for the choice of closure and in the adult patient transesophageal echocardiography (TEE) is considered the pre-interventional imaging method of choice. We assessed the value of SMPI in measurement of ASD size and rim length (**Chapter 3**). The site and extent of prolapse of the mitral valve (MV) is essential in defining the suitability for MV repair. We assessed the value of 2D, 2D xPlane imaging and 3D echocardiography for the definition and the extent of MV prolapse in patients that underwent MV surgery (**Chapter 4**). Paravalular aortic regurgitation following trans-catheter aortic valve implantation (TAVI) is a common finding, particularly in the older generation of prosthesis (**Chapter 5**). Short-axis imaging suffers from intrinsic acoustic shadowing of the prosthesis and calcification, making recording of paravalular leakage difficult. We assessed the value of SMPI in estimating the circumferential extent of paravalular leakage from a standard apical view. With the experience gained from transcatheter pulmonary and aortic valve replacement there is a need to extend catheter interventions to the tricuspid valve (TV). This so called forgotten valve has shown renewed interest, but relevant information in current literature is scarce. In **Chapter 6**, a book section, we describe, in depth, all the different transthoracic

echocardiographic modalities that can be applied for a comprehensive evaluation of the tricuspid valve. A detailed morphologic assessment of the TV leaflets and its annulus, functional information and grading of the severity of the tricuspid regurgitation will be of paramount importance for a successful intervention.3D echocardiography (3DE) has come a long way and experts in this field found that the time was ripe for an expert consensus document providing a review of the optimal applications of 3D echocardiography and its short-comings in congenital heart (**Chapter 7**).

Part III: Simultaneous multiplane 2D-echocardiography imaging and ventricular function

Quantification of cardiac chambers and function is the cornerstone of cardiac imaging.[28] Increasing published data suggest that speckle tracking echocardiography (STE) can detect ventricular dysfunction in a pre-clinical phase.[19] However, interpretation of data depends on robust normal limits that define "normalcy" and information on normal range STE-derived measures for the left ventricle (LV) and right ventricle (RV) is limited.[29–32] We initiated an echocardiographic study with 155 healthy individuals, the Navigator study, to obtain normal values of all echocardiographic parameters for the Dutch population. LV images were recorded from the apical window with conventional or iRotate 2DE. Longitudinal strain values using speckle-tracking echocardiography were established and associations with anthropometrics identified (**Chapter 8**). Before initiating the Navigator study we formed the concept of using iRotate mode to evaluate the entire RV from a fixed transducer position, as was already done for the LV. First we had to establish, like the LV, unique anatomic landmarks that could be used as reference points to accurately depict the entire RV from the apical window. In a population of normal healthy adult subjects and in a small cohort of patients with abnormally loaded RVs the feasibility of iRotate mode to evaluate the entire RV was evaluated (**Chapter 9**). The feasibility of the technique described in chapter 9 was promising. Normal values of the different RV parameters were established and associations with anthropometrics identified. In addition, we studied the potential use of this multi-view iRotate model in a small group of patients with abnormally loaded RVs (**Chapter 10**). Finally (**Chapter 11)** we discuss our findings and the place of Simultaneous multiplane imaging in daily cardiac imaging. With continuous innovations in ultrasound technology we reflect on the pressure placed on the day-to-day running of the department of echocardiography and the importance of a good working relationship between clinicians and engineers to achieve these goals.

By reading this thesis, we hope that the reader will appreciate the unique features of this SMPI technique and its additional value in cardiovascular imaging.

REFERENCES

1. Dussik KT. Über die Moglichkeit Hochfrequente Mechanische Schwingungen als Diagnostisches Hilfsmitel zu Verwerten. *ZNeurol* 1941;174:153.

2. Braunwald E. The Simon Dack lecture. Cardiology: the past, the present, and the future. *J Am Coll Cardiol* 2003;42:2031-2041.

3. Edler I, Hertz CH. The use of ultrasonic reflectoscope for the continuous recording of the movements of heart walls. 1954. *Kurgl Fysiogr Salad i Lund Forhandl* 1954;24:5.

4. Feigenbaum H. The first long-lasting use of echocardiography: a result of a false advertisement. *JACC Cardiovasc Imaging* 2008;1:522-524.

5. Feigenbaum H. Evolution of echocardiography. *Circulation* 1996;93:1321-1327.

6. Feigenbaum H, Stone JM, Lee DA, Nasser WK, Chang S. Identification of ultrasound echoes from the left ventricle by use of intracardiac injections of indocyanine green. *Circulation* 1970;41:615-621.

7. Gramiak R, Shah PM. Echocardiography of the aortic root. *Invest Radiol* 1968;3:356-366.

8. Seward JB, Tajik AJ, Spangler JG, Ritter DG. Echocardiographic contrast studies: initial experience. *Mayo Clin Proc* 1975;50:163-192.

9. Feinstein SB, Cheirif J, Ten Cate FJ, Silverman PR, Heidenreich PA, Dick C, Desir RM, Armstrong WF, Quinones MA, Shah PM. Safety and efficacy of a new transpulmonary ultrasound contrast agent: initial multicenter clinical results. *J Am Coll Cardiol* 1990;16:316-324.

10. Bom N, Lancee CT, Honkoop J, Hugenholtz PG. Ultrasonic viewer for cross-sectional analyses of moving cardiac structures. *Biomed Eng* 1971;6:500-503, 505.

11. Kamp O. History of echocardiography in the Netherlands: 30 years of education and clinical applications. *Neth Heart J* 2008;16:16-20.

12. Griffith JM, Henry WL. A sector scanner for real time two-dimensional echocardiography. *Circulation* 1974;49:1147-1152.

13. Thurstone F.L. vROT. A new ultrasound imaging technique employing two dimensional electronic beam steering. In: Green PS, ed. Acoustic Holographyy. New York Plenum press, 1974:149-159.

14. Vourvouri EC, Poldermans D, De Sutter J, Sozzi FB, Izzo P, Roelandt JR. Experience with an ultrasound stethoscope. *J Am Soc Echocardiogr* 2002;15:80-85.

15. Souquet J, Hanrath P, Zitelli L, Kremer P, Langenstein BA, Schluter M. Transesophageal phased array for imaging the heart. *IEEE Trans Biomed Eng* 1982;29:707-712.

16. Barber FE, Baker DW, Nation AW, Strandness DE, Jr., Reid JM. Ultrasonic duplex echo-Doppler scanner. *IEEE Trans Biomed Eng* 1974;21:109-113.

17. D.W. B. Pulsed ultrasonic Doppler blood flow sensing. *IEEE Trans Sonics Ultrason* 1970;17:170-185.

18. Kasai C, Namekawa K, Koyano A, al. E. Real-time two-dimensional blood flow imaging using autocorrection technique. *IEEE Trans Sonics Ultrason* 1985;32:460-463.

19. Mondillo S, Galderisi M, Mele D, Cameli M, Lomoriello VS, Zaca V, Ballo P, D'Andrea A, Muraru D, Losi M, Agricola E, D'Errico A, Buralli S, Sciomer S, Nistri S, Badano L, Echocardiography Study Group Of The Italian Society Of C. Speckle-tracking echocardiography: a new technique for assessing myocardial function. *J Ultrasound Med* 2011;30:71-83.

20. Valsangiacomo Buechel ER, Mertens LL. Imaging the right heart: the use of integrated multimodality imaging. *Eur Heart J* 2012;33:949-960.

21. Lang RM, Badano LP, Mor-Avi V, Afilalo J, Armstrong A, Ernande L, Flachskampf FA, Foster E, Goldstein SA, Kuznetsova T, Lancellotti P, Muraru D, Picard MH, Rietzschel ER, Rudski L, Spencer KT, Tsang W, Voigt JU. Recommendations for cardiac chamber quantification by echocardiography in adults: an update from the American Society of Echocardiography and the European Association of Cardiovascular Imaging. *J Am Soc Echocardiogr* 2015;28:1-39 e14.

22. Khankirawatana B, Khankirawatana S, Porter T. How should left atrial size be reported? Comparative assessment with use of multiple echocardiographic methods. *Am Heart J* 2004;147:369-374.

23. Moller JE, Hillis GS, Oh JK, Seward JB, Reeder GS, Wright RS, Park SW, Bailey KR, Pellikka PA. Left atrial volume: a powerful predictor of survival after acute myocardial infarction. *Circulation* 2003;107:2207-2212.

24. Kasliwal RR, Chouhan NS, Sinha A, Gupta P, Tandon S, Trehan N. Real-time three-dimensional transthoracic echocardiography. *Indian Heart J* 2005;57:128-137.

25. Dekker DL, Piziali RL, Dong E, Jr. A system for ultrasonically imaging the human heart in three dimensions. *Comput Biomed Res* 1974;7:544-553.

26. von Ramm OT, Smith SW. Real time volumetric ultrasound imaging system. *J Digit Imaging* 1990;3:261-266.

27. Lang RM, Badano LP, Tsang W, Adams DH, Agricola E, Buck T, Faletra FF, Franke A, Hung J, de Isla LP, Kamp O, Kasprzak JD, Lancellotti P, Marwick TH, McCulloch ML, Monaghan MJ, Nihoyannopoulos P, Pandian NG, Pellikka PA, Pepi M, Roberson DA, Shernan SK, Shirali GS, Sugeng L, Ten Cate FJ, Vannan MA, Zamorano JL, Zoghbi WA, American Society of E, European Association of E. EAE/ASE recommendations for image acquisition and display using three-dimensional echocardiography. *J Am Soc Echocardiogr* 2012;25:3-46.

28. Lang RM, Badano LP, Mor-Avi V, Afilalo J, Armstrong A, Ernande L, Flachskampf FA, Foster E, Goldstein SA, Kuznetsova T, Lancellotti P, Muraru D, Picard MH, Rietzschel ER, Rudski L, Spencer KT, Tsang W, Voigt JU. Recommendations for cardiac chamber quantification by echocardiography in adults: an update from the American Society of Echocardiography and the European Association of Cardiovascular Imaging. *Eur Heart J Cardiovasc Imaging* 2015;16:233-270.

29. Fine NM, Chen L, Bastiansen PM, Frantz RP, Pellikka PA, Oh JK, Kane GC. Reference Values for Right Ventricular Strain in Patients without Cardiopulmonary Disease: A Prospective Evaluation and Meta-Analysis. *Echocardiography* 2015;32:787-796.

30. Sachdev A, Villarraga HR, Frantz RP, McGoon MD, Hsiao JF, Maalouf JF, Ammash NM, McCully RB, Miller FA, Pellikka PA, Oh JK, Kane GC. Right ventricular strain for prediction of survival in patients with pulmonary arterial hypertension. *Chest* 2011;139:1299-1309.

31. Yang H, Marwick TH, Fukuda N, Oe H, Saito M, Thomas JD, Negishi K. Improvement in Strain Concordance between Two Major Vendors after the Strain Standardization Initiative. *J Am Soc Echocardiogr* 2015;28:642-648 e647.

32. Yingchoncharoen T, Agarwal S, Popovic ZB, Marwick TH. Normal ranges of left ventricular strain: a meta-analysis. *J Am Soc Echocardiogr* 2013;26:185-191.

CHAPTER 2

Contributions of simultaneous multiplane echocardiographic imaging in daily clinical practice

Jackie S. McGhie
Wim B. Vletter
Lotte E. de Groot - de Laat
Ben Ren
René Frowijn
Annemien E. van den Bosch
Osama I.I. Soliman
Marcel L. Geleijnse

INTRODUCTION

Two-dimensional (2D) transthoracic echocardiography is one of the most frequently used techniques for diagnosis, management and follow-up of patients with any suspected or known cardiovascular disease. It is based on multiple single cardiac planes taken from standard positions on the chest wall. With the development of the matrix transducer, three-dimensional echocardiography (3D) can now be performed in the routine lab reducing the number of cross-sections needed for the information required.[1] However, there are several challenges for the use of 3D echocardiography in daily clinical practice. First, there is the need for a separate 3D transducer, which has a lower temporal resolution compared to the standard 2D transducer.[1,2] Second, the acquisition time of 3D images is time-consuming and most often requires offline analysis. Third, 3D echocardiography is a relatively new technique, which requires extra training and it has a learning curve.

Recently, a new generation 2D/3D matrix transducer has become available, overcoming some of these drawbacks and even introducing a new image modality called "Simultaneous Multiplane Imaging" (SMPI). This new modality permits the use of a full electronic rotation of 360° of the 2D image (iRotate) and a simultaneously adjustable biplane 2D image (xPlane). In this article we will discuss the potential contributions of SMPI in daily clinical practice.

The Biplane –Triplane Era before SMPI

Bi-plane and triplane echocardiography has been available since 1988. However, literature data are currently scarce suggesting that the potential of this technique was not fully appreciated and/or the technology has not been sufficient.

In 1988, Omoto et al.[3] reported their clinical experience with a self-developed biplane transesophageal echocardiographic transducer. In 2003, transthoracic biplane echocardiography was introduced by Sugeng et al.[4] In their initial study the focus was on the value of simultaneous display of two imaging planes during stress echocardiography from the same heartbeat rather than an entire 3D volume.[2,5,6] They suggested that although image quality is maintained, examination time would be reduced. Later, Wang et al. reported the potential for this technique as a single beat assessment of LV function in patients with atrial fibrillation.[7,8] In 2005, Sengupta et al. revealed the biplane potential as a goal-orientated (limited) echocardiogram to cut down time in a high volume echocardiography laboratory, although they recognized that improvements in technology and transducer size were necessary.[9] Meanwhile some vendors developed matrix transducers that could acquire simultaneously the three standard apical views during one single heartbeat (triplane echocardiography) providing a potentially even more effective tool to estimate LV function accurately in routine clinical practice.[10]

Up until now an additional matrix transducer, on top of the conventional 2D transducer, was necessary to apply biplane and/or triplane scanning. Because of the lower frequency, larger footprint and inability to perform a pulsed-wave or continuous-wave Doppler study, the use in daily routine was limited. SMPI is based on a relatively new

matrix transducer, which has 2D and 3D capabilities. It has the potential to overcome those limitations of bi- and tri-plane imaging.

The SMPI Ultrasound System

Simultaneous Multiplane Imaging is performed using the iE33 ultrasound system (Philips Medical systems, Best, The Netherlands) equipped with an X5–1 transthoracic (TTE) or X7–2t transesophageal (TEE) matrix transducer. These transducers are composed of 3040 (TTE) and 2500 (TEE) elements, respectively, with a 1–5MHz and 2–7MHz frequency range, respectively.

SMPI Imaging Modes

The primary image (reference plane) is defined by the transducer position, chosen by the operator and optimized in the same manner as for a conventional 2D image. From this primary image, a secondary image can be visualized by applying one of the four SMPI modes. The four SMPI modes are iRotate, xPlane with lateral tilt, xPlane with elevation tilt and xPlane with iRotate. The spatial relation of the secondary image plane can be modified in three directions: rotation around a central longitudinal axis, elevation tilt and lateral tilt (Figure 1).

iRotate

In the primary image a full electronic rotation of 360° (adjustable by 5° steps) during TTE (Figure 1A) and 180° (adjustable by 1° steps) during TEE can be performed. In contradiction to the below-described xPlane modes the frame rate in the iRotate mode will not be compromised because only the secondary image is displayed.

xPlane with Lateral Tilt

From a primary image an orthogonal view can be acquired through the midline and displayed as a secondary image. From the midline, additional secondary images can be visualized by a lateral tilt of up to maximal +30° to -30°. As in all xPlane modes, the frame rate will be half of the original image (Figure 1B).

xPlane with Elevation Tilt

From a primary image, additional secondary images can be visualized by an elevation tilt of up to maximal +30° to -30° (Figure 1C).

xPlane with iRotate

This mode combines the xPlane and iRotate mode. From a primary image a secondary image can be visualized by applying the xPlane mode, subsequently this secondary image can be adjusted by rotation around the central longitudinal axis in the primary image (Figure 1D).
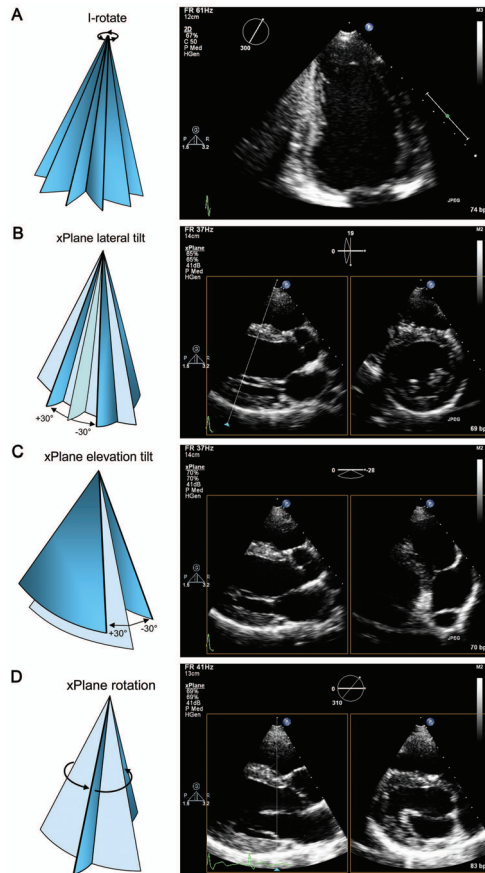
Figure 1 Simultaneous multiplane imaging mode. **A.** iRotate: a two-chamber view is obtained by rotation of 60° (to 300°) from a standard four-chamber view (defined as 0° or 360°). The degree of rotation is displayed in the upper left- hand corner of the screen. **B.** xPlane with lateral tilt: from a standard parasternal long-axis view (primary image or reference plane) an orthogonal short-axis view at the chordal–papillary muscle level can be obtained by a lateral tilt of +10°. **C.** xPlane with elevation tilt: from the same view a right ventricular inflow view can be obtained by an elevation tilt of -28°. **D.** xPlane with rotation: from the same view an unorthodox short-axis view of the mitral valve by a rotation of +50°.

UNIQUE APPLICATIONS OF SMPI

iRotate

Stress echocardiography

During stress echocardiography, the iRotate mode makes it possible to obtain standard apical two- and three-chamber views from a standard non-foreshortened four-chamber view without changing the transducer position. The number of degrees corresponding to the two- and three-chamber views, obtained at baseline, can be used as a default setting

during the rest of the study (Figure 2). It may even be better to analyze the LV not according to these arbitrary cross-sections (that are present at different degrees in different patients) but to standard cross section at three 60° intervals or even smaller intervals. If such a mode is set up as the default setting, the variability of the standard imaging planes throughout stress may be reduced and as a result LV segments may be better compared during stress with less false positive or negative test results.[2,11–13]
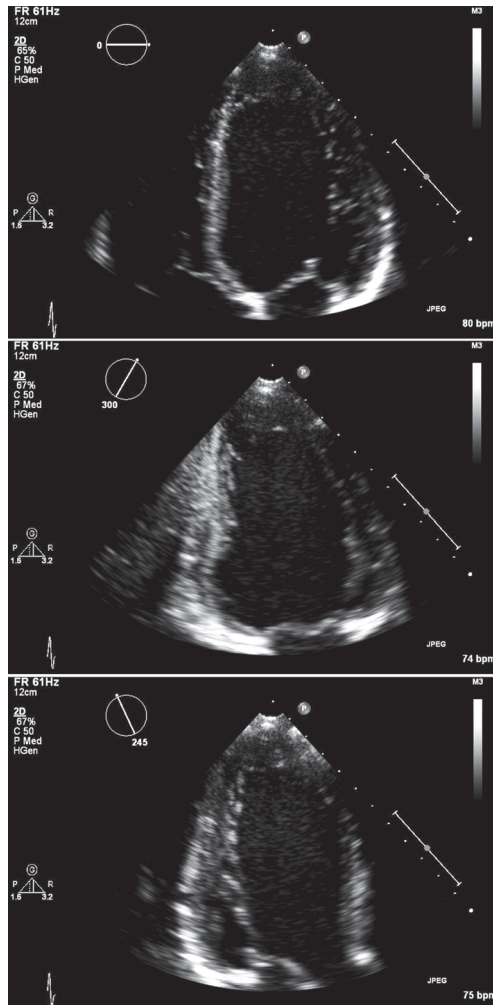
Figure 2 iRotate mode. iRotate: from a standard nonforeshortened four-chamber view (primary image or reference plane, top) reproducible two-chamber (middle) and three-chamber (bottom) views can be obtained at different stress levels.

Mitral regurgitation severity

Mitral regurgitation is not always present or maximally visualized in the standard 2D cross-sections as it will depend on mechanism and jet morphology. The iRotate applied with the transducer in the apical position will give a comprehensive evaluation of the mitral regurgitant jet. In Figure 3, it can be seen that the origin of the regurgitation jet (and thus the most representative vena contracta and proximal isovelocity surface area) is seen in non-conventional image planes between 320° and 340°.
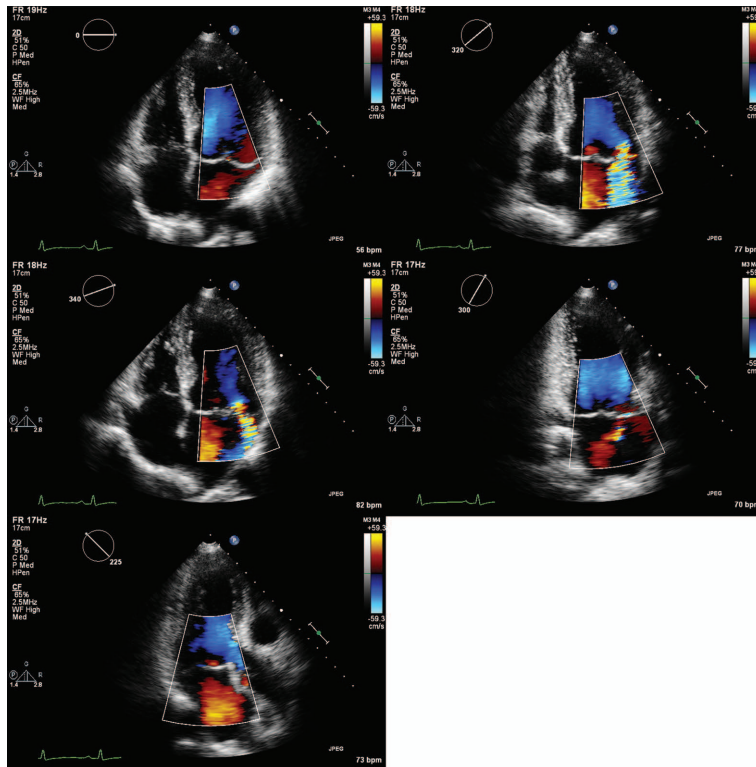
Figure 3 Mitral regurgitation. iRotate: the maximal vena contracta and proximal isovelocity surface area of mitral regurgitation can be easily seen in non-standard 2D cross-sections at 320° and 340° as opposed to the standard cross-sections at 0° (apical four chambers), 300° (apical two chambers), and 225° (apical three chambers).

xPlane with Lateral Tilt

Left ventricular outflow tract

Measurement of the left ventricular outflow tract (LVOT) area is crucial in estimation of LV stroke volume, mitral regurgitation severity, and aortic valve area[14]. Unfortunately, in routine 2D TTE, important geometric errors can be made in calculating the cross-sectional area of the LVOT. The measurements are monoplane and the LVOT is assumed to have a circular geometry, whereas in reality, the LVOT is a (dynamic) oval structure

with a major and minor axis. In fact, by the recommended measurement of the LVOT dimension in the parasternal long-axis view the true LVOT area is underestimated by > 20% because this dimension corresponds to the minor axis of the oval LVOT.[14,15] By use of the SMPI xPlane with lateral tilt mode, a cross-sectional image from the LVOT can be acquired from the parasternal long-axis view showing the major and minor axes, the perimeter and area of the LVOT (Figure 4).
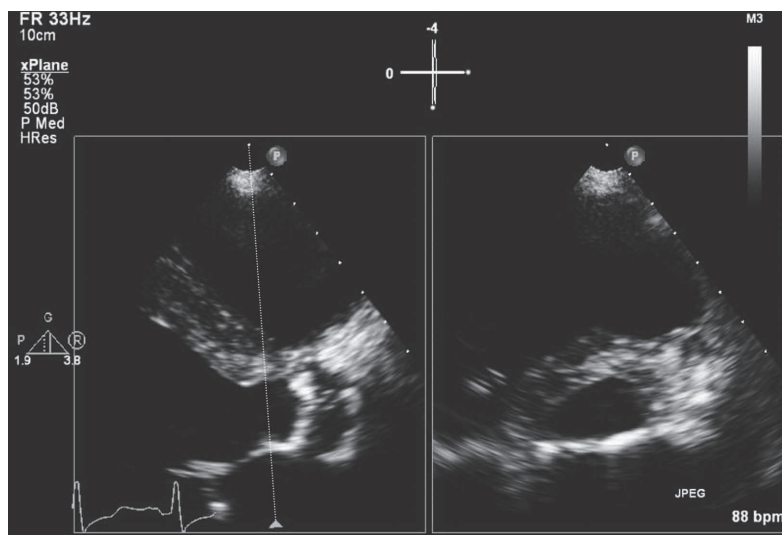
Figure 4 Left ventricular outflow tract. xPlane with lateral tilt of -4°: the reference line transects the left ventricular out-flow tract allowing major and minor-axis, perimeter, and area measurements in the secondary image.

Mitral and tricuspid annulus

The mitral annulus (MA) is a vital component of the mitral valve apparatus and dilatation of the MA is one of the main mechanisms of mitral regurgitation.[16] However, like the LVOT the MA is not circular in shape but rather oval or D-shaped and different cross-sections result in different dimensions.[17] An xPlane from a correctly orientated apical 2-chamber view in which the mitral valve scallops P3, A2, P1 and both papillary muscle are intersected symmetrically will allow a measurement of the major (primary image) and minor (secondary image) axis diameters of the mitral valve annulus (Figure 5). In most patients, an xPlane image at mitral annulus level, from a parasternal long-axis window will reveal an orthogonal short-axis view on the secondary image. Therefore, the major and minor axes, the perimeter and the mitral annular area could be measured. However, these measurements will be limited to some extent because of the saddle-shaped MA. Likewise, in normal and dilated right ventricles, an xPlane from a parasternal short-axis view will allow a measurement of two axes diameters of the tricuspid valve annulus, although due to the complex non-planar morphology of the tricuspid annulus these measurements may be limited (Figure 6A). Also, from the right ventricle inflow view with xPlane all three leaflets from the tricuspid valve leaflets can be imaged (Figure 6B).[18]
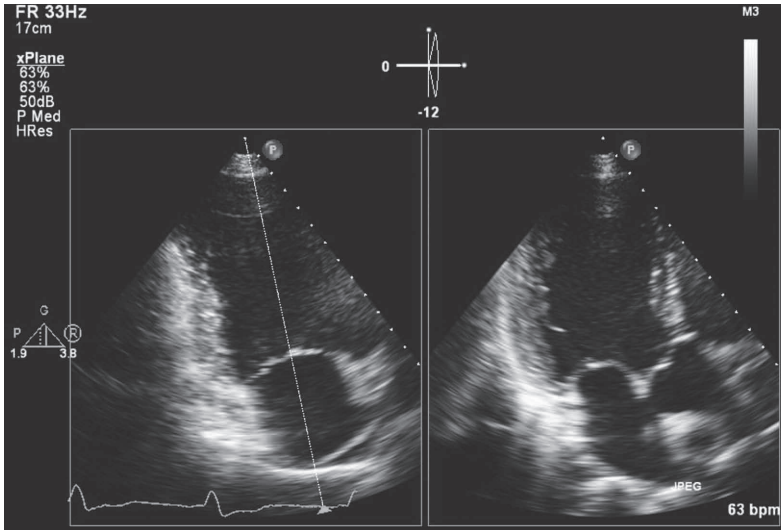
Figure 5 Mitral valve annulus. xPlane with lateral tilt of -12°: the reference line transects the mitral valve annulus in a bi-commissural view allowing measurements of the major and minor axis diameters in end-diastole.
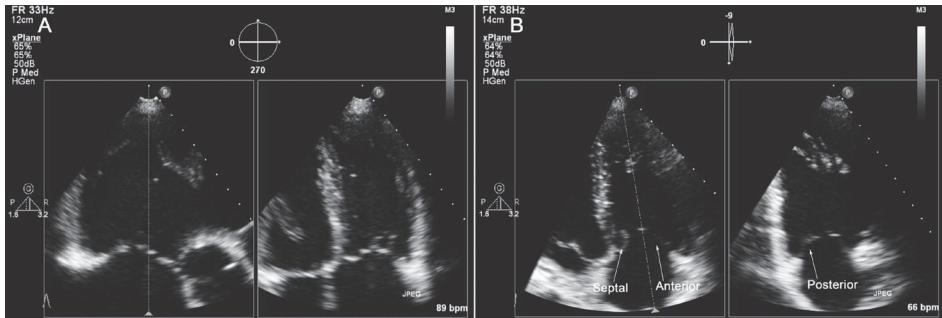
Figure 6 Tricuspid valve annulus. **A.** The reference line, in this dilated right ventricle, transects the tricuspid valve annulus in a short-axis view allowing measurements of two axes diameters in end-diastole. **B.** xPlane with lateral tilt of -9°. The reference line, in this dilated right ventricle, transects the tricuspid anterior leaflet in a foreshortened four-chamber view allowing visualization of all three tricuspid leaflets (the arrows).

Aortic and mitral stenosis

Direct measurement of aortic and mitral valve area on short-axis 2D images is possible in patients with excellent transthoracic image quality. However, planimetry of the valve area should always be interpreted with caution due to the complex 3D anatomy of the orifice and the image plane may not be aligned with the narrowest point at the leaflet tips. In particular in the "domelike" opening of the mitral valve and the bicuspid aortic valve, with sometimes an eccentric closure line, this is an important source of error in estimation of stenosis severity. By use of the xPlane mode with lateral tilt, a cross-sectional image from

the valve at the correct valvular level may be acquired guided by the parasternal long-axis view.[19]

Left ventricular and left atrial volumes and ejection fraction

Two-dimensional echocardiography has, apart from image quality issues, limited value in the calculation of LV volumes and ejection fraction. This is because LV images (in particular the two-chamber view) are often foreshortened, the four-chamber and two-chamber views are not perpendicular to each other [20] and the geometrical assumptions applied in the Bi-plane Simpson calculation.[1,21–23]

   With the use of the xPlane two true perpendicular image planes can be acquired. Provided that the primary image (four-chamber view) shows the true long axis of the LV the same will apply to the secondary image. The two planes are now acquired from the same heart beat, an advantage in particular in patients with atrial fibrillation. Such an analysis based on biplane or triplane imaging may be a simple and reasonable alternative to the 3D echocardiographic technique[1,7,8,21–23]. Likewise, SMPI may also be a simple and reasonable alternative to the 3D echocardiographic technique to analyze LA volumes (Figure 7).[24] With iRotate it is also possible to analyze the LV and LA volumes; this will result in a much higher (primary image) frame rates but it should be noted that now non-identical beats will be analyzed.
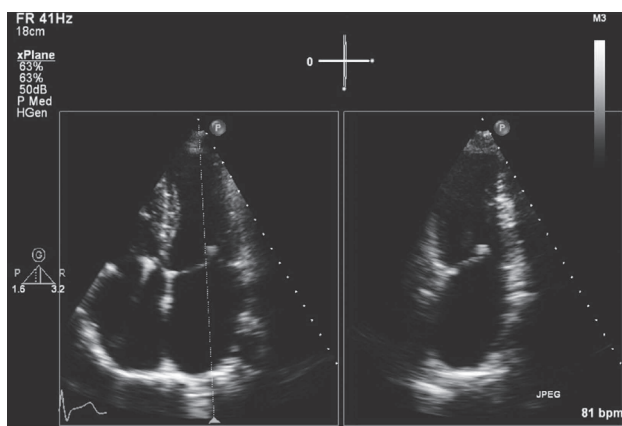
Figure 7 Left atrium. From a four-chamber view showing a nonforeshortened left atrium a true perpendicular image can be obtained with xPlane, allowing correct volume measurements.

Mitral valve prolapse

The correct identification of the etiology and underlying lesions that result in mitral valve dysfunction is important for management decisions. In Europe, degenerative mitral valve disease is the most common etiology.[25] In such patients, a precise morphologic assessment is necessary to predict the likelihood of successful reconstructive valve surgery. Although in most patients the localization of the pathology (assessment of the involved mitral leaflet segments) can be identified with standard 2D echocardiography, this requires extensive

expertise.[26] As seen in Figure 8, with SMPI segmental analysis of the scallops involved in mitral valve prolapse may become easier with a lateral sweep across the mitral valve co-optation line seen in the parasternal short-axis view.
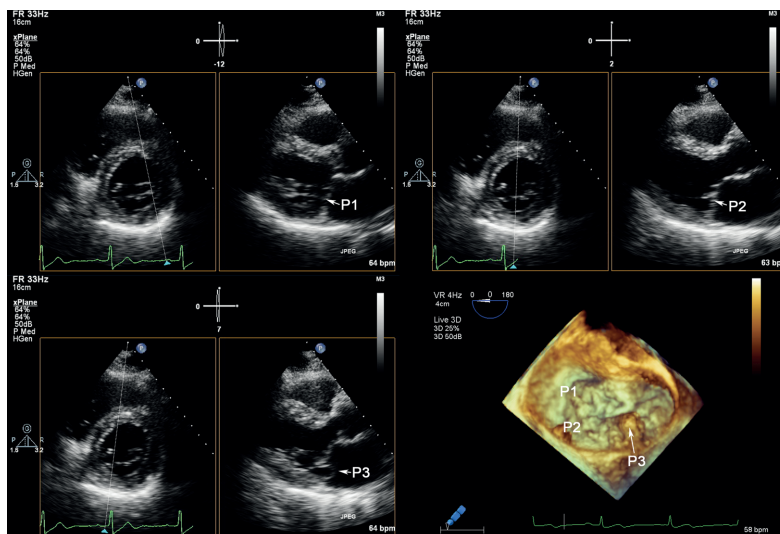
Figure 8 Mitral valve morphology. Segmental analysis of the mitral valve scallops (the arrows) with xPlane imaging with lateral tilt, a P3 prolapse (the arrow) as seen in the xPlane and 3D image.

xPlane with Elevation Tilt

The xPlane with elevation mode is probably the least useful mode in SMPI. One application is to visualize the right ventricular inflow (Figure 1C) and outflow view from the parasternal long-axis view. This mode is probably most useful in pediatric echocardiography where numerous sweeps are part of the routine examination, for example a sweep from posterior to anterior from the apical 4-chamber (the coronary sinus) to the apical 5-chamber view (aortic valve).

iRotate and xPlane with Lateral Tilt

Transesophageal echocardiography SMPI, available earlier than TTE SMPI, is gradually being accepted as part of the standard TEE examination in daily clinical practice and during interventions and surgery. The iRotate images acquired during TEE are identical to the images acquired with a traditional TEE transducer only the steering mechanism is electronic and not mechanical. xPlane lateral and elevation tilt work the same way as for TTE.

Left atrial appendage

The left atrial appendage (LAA) may harbor thrombi that may cause a transient ischemic attack or cerebral vascular accident. TEE is the standard procedure to exclude LAA thrombi. Unfortunately it may sometimes be difficult to differentiate thrombi from

pectinate muscles. A sweep across the LAA in xPlane mode may more easily differentiate an organized thrombus from these small pectinate muscles (Figure 9).[27]
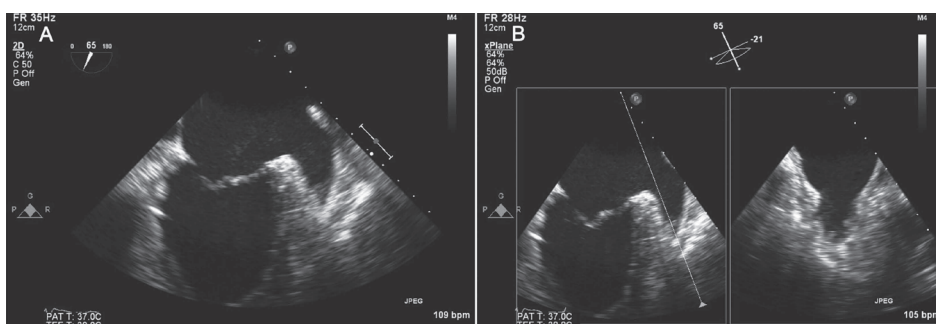
Figure 9 Left atrial appendage thrombus. **A.** iRotate of 65° during transesophageal echocardiography showing a suspected thrombus in the left atrial appendage. **B.** xPlane with lateral tilt of -21° showing in the secondary image clear pectinate muscles rather than organized thrombus.

MitraClip mitral valve repair

During the percutaneous MitraClip procedure for treatment of mitral regurgitation, the middle portions of the anterior and posterior mitral valve leaflets are approximated by stitching them together.[28] This procedure critically depends on echocardiographic imaging. A mid-esophageal aortic valve short-axis view at approximately 30° in combination with an xPlane image showing the bicaval view may guide correct trans-septal puncture. Positioning of the delivery catheter toward the mitral valve regurgitant jet and grasping of the leaflets from their underside may be facilitated by use of an inter-commissural view in combination with an xPlane image showing a long-axis view. The use of lateral and elevation tilt easily allows continuous monitoring of the clip in the primary image and thus the exact position of the clip during deployment in the two orthogonal planes (Figure 10).
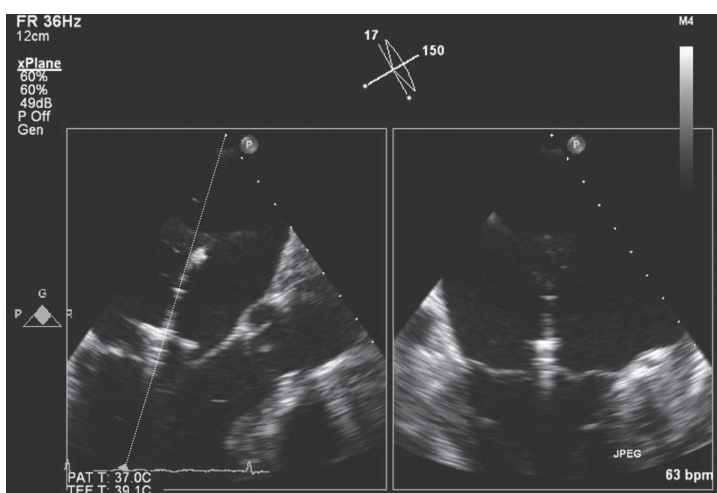
Figure 10 MitraClip monitoring. iRotate of 150° with lateral tilt of 17° during transesophageal echocardiography allowing continuous monitoring of the positioning and deployment of the mitral clip.

Patent foramen ovale

A patent foramen ovale (PFO) has been associated with many diseases.[29] Detection of a PFO requires a structured protocol to detect the passage of contrast bubbles through the PFO from the right to left atrium. Typically, contrast images are made from at least two views (aortic short-axis and bicaval views) at rest, coughing and a Valsalva maneuver. By use of iRotate (to select the primary image) combined with xPlane mode during contrast injection the total number of needed contrast injections (and thus time) will be reduced by 50% (Figure 11).
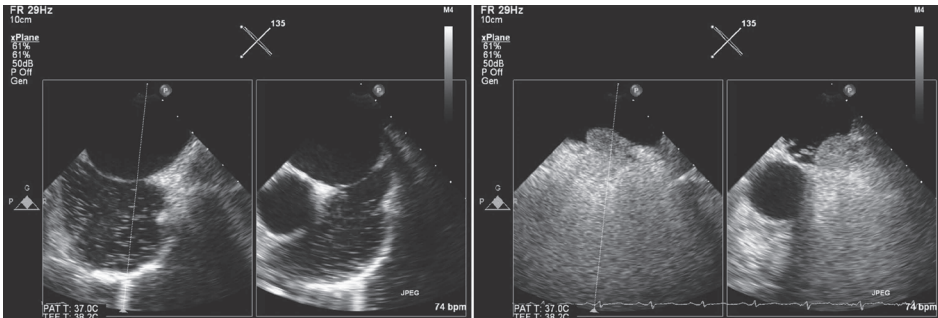
Figure 11 Contrast echocardiography. iRotate of 135° during transesophageal echocardiography allowing with xPlane simultaneous visualization of contrast passage through the foramen ovale in the bicaval 135° view (negative for right to left shunt) and the short-axis 45° view (positive for right to left shunt).

Atrial septal defect

The size of the atrial septal defect and surrounding rims are crucial determinants in the selection of percutaneous or surgical closure. Defects larger than 30mm or defects that have a supporting rim of tissue around the defect of less than 5mm are not suited for percutaneous closure.[30,31] Also, it is well known that, in particular, in non-circular defects the maximal diameter may be underestimated with monoplane 2D-echocardiography. With SMPI, even in TTE an infinite number of cutting planes and true orthogonal planes can be visualized giving complete visualization of the defect and its surrounding rims (Figure 12).[30]

Limitations

When studying the LV or LA in the iRotate (high frame rate, non-identical beats) or xPlane biplane mode (lower frame rate, identical beats) the primary image should not be fore-shortened to ensure proper views. In patients with asymmetric wall motion, 3D echocardiography will remain the imaging modality of choice.[1,21–23]

The spatial resolution remains somewhat inferior to the stand alone 2D transducer and in addition the frame rate (temporal resolution) drops by half when entering the xPlane mode. This latter can be problematic for colour Doppler flow imaging that already suffers from lower frame rates in the standard (primary) 2D images. The drop in temporal resolution can be brought to a minimum by ensuring that the smallest sector able to encompass the cardiac structure of interest is used.
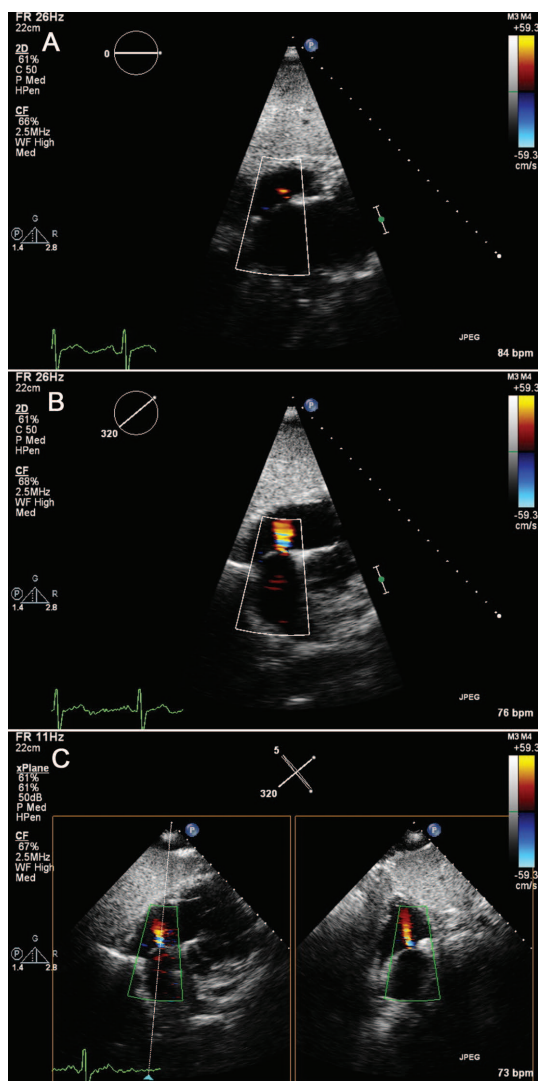
Figure 12 Atrial septal defect. **A.** subcostal four-chamber view with colour Doppler suggestive of a small atrial septal defect at 0°. **B**. iRotate at 320° reveals the exact origin of the defect. **C:** xPlane with a lateral tilt of 5° showing the long and short-axis views of the atrial septal defect.

Although this X5–1 transducer is equipped with spectral Doppler in the standard and iRotate setting this is not available in xPlane mode.

Also, the motion of the heart throughout the cardiac cycle may result in a reference line not transecting the region of interest at any time point in the heart cycle. For example, the longitudinal motion of the mitral annulus[32] will limit the study of the dynamic changes of the mitral annulus in the xPlane mode with lateral tilt.

CONCLUSIONS

The SMPI modality allows full electronic rotation of 360° of the 2D image (iRotate) and a simultaneously adjustable biplane 2D image (xPlane) from the same heart beat. This quick, simple to use, and easy to understand echo modality may save on scanning time in a high-volume echocardiography laboratory and will provide unique 2D information on cardiac function and morphology. Also, SMPI may ultimately bridge the gap between 2D and 3D thinking, making the integration of 3D echocardiography onto the work floor easier.

REFERENCES

1. Soliman OI, Geleijnse ML, Theuns DA, van Dalen BM, Vletter WB, Jordaens LJ, Metawei AK, Al-Amin AM, ten Cate FJ. Usefulness of left ventricular systolic dyssynchrony by real-time three-dimensional echocardiography to predict long-term response to cardiac resynchronization therapy. *Am J Cardiol* 2009;103:1586-1591.
2. Nemes A, Geleijnse ML, Krenning BJ, Soliman OI, Anwar AM, Vletter WB, Ten Cate FJ. Usefulness of ultrasound contrast agent to improve image quality during real-time three-dimensional stress echocardiography. *Am J Cardiol* 2007;99:275-278.
3. Omoto R, Kyo S, Matsumura M, Adachi H, Maruyama M, Matsunaka T. New direction of biplane transesophageal echocardiography with special emphasis on real-time biplane imaging and matrix phased-array biplane transducer. *Echocardiography* 1990;7:691-698.
4. Sugeng L, Kirkpatrick J, Lang RM, Bednarz JE, Decara JM, Lammertin G, Spencer KT. Biplane stress echocardiography using a prototype matrix-array transducer. *J Am Soc Echocardiogr* 2003;16:937-941.
5. Nemes A, Geleijnse ML, van Geuns RJ, Soliman OI, Vletter WB, Krenning BJ, Ten Cate FJ. Dobutamine stress MRI versus threedimensional contrast echocardiography: It's all Black and White. *Neth Heart J* 2008;16:217-218.
6. Nemes A, Leung KY, van Burken G, van Stralen M, Bosch JG, Soliman OI, Krenning BJ, Vletter WB, ten Cate FJ, Geleijnse ML. Side-by-side viewing of anatomically aligned left ventricular segments in three-dimensional stress echocardiography. *Echocardiography* 2009;26:189-195.
7. Wang CL, Lin KH, Luqman N, Chu PH, Hsu LA, Kuo CT. Simultaneous biplane single-beat assessment of left ventricular systolic function in patients with atrial fibrillation. *Am J Cardiol* 2004;94:942-944.
8. Wang CL, Ho WJ, Luqman N, Hsu LA, Kuo CT. Biplane assessment of left ventricular function during atrial fibrillation at beats with equal subsequent cycles. *Int J Cardiol* 2006;113:54-60.
9. Sengupta PP, Chandrasekaran K, Prince DJ, Dyke RA, Khandheria BK. Role of biplane echocardiography in a large-volume clinical practice: revamping strategies for echocardiography in a limited time. *J Am Soc Echocardiogr* 2005;18:757-760.
10. Nucifora G, Badano LP, Dall'Armellina E, Gianfagna P, Allocca G, Fioretti PM. Fast data acquisition and analysis with real time triplane echocardiography for the assessment of left ventricular size and function: a validation study. *Echocardiography* 2009;26:66-75.
11. Geleijnse ML, Fioretti PM, Roelandt JR. Methodology, feasibility, safety and diagnostic accuracy of dobutamine stress echocardiography. *J Am Coll Cardiol* 1997;30:595-606.

12.   Krenning BJ, Nemes A, Soliman OI, Vletter WB, Voormolen MM, Bosch JG, Ten Cate FJ, Roelandt JR, Geleijnse ML. Contrast-enhanced three-dimensional dobutamine stress echocardiography: between Scylla and Charybdis? *Eur J Echocardiogr* 2008;9:757-760.

13.   Amzulescu MS, Slavich M, Florian A, Goetschalckx K, Voigt JU. Does two-dimensional image reconstruction from three-dimensional full volume echocardiography improve the assessment of left ventricular morphology and function? *Echocardiography* 2013;30:55-63.

14.   Ren B, de Groot-de Laat LE, McGhie J, Vletter WB, Ten Cate FJ, Geleijnse ML. Geometric errors of the pulsed-wave Doppler flow method in quantifying degenerative mitral valve regurgitation: a three-dimensional echocardiography study. *J Am Soc Echocardiogr* 2013;26:261-269.

15.   Silva CD, Pedro F, Deister L, Sahlen A, Manouras A, Shahgaldi K. Two-dimensional color Doppler echocardiography for left ventricular stroke volume assessment: a comparison study with three-dimensional echocardiography. *Echocardiography* 2012;29:766-772.

16.   Carpentier A. Cardiac valve surgery--the "French correction". *J Thorac Cardiovasc Surg* 1983;86:323-337.

17.   Anwar AM, Soliman OI, ten Cate FJ, Nemes A, McGhie JS, Krenning BJ, van Geuns RJ, Galema TW, Geleijnse ML. True mitral annulus diameter is underestimated by two-dimensional echocardiography as evidenced by real-time three-dimensional echocardiography and magnetic resonance imaging. *Int J Cardiovasc Imaging* 2007;23:541-547.

18.   Anwar AM, Geleijnse ML, Soliman OI, McGhie JS, Frowijn R, Nemes A, van den Bosch AE, Galema TW, Ten Cate FJ. Assessment of normal tricuspid valve anatomy in adults by real-time three-dimensional echocardiography. *Int J Cardiovasc Imaging* 2007;23:717-724.

19.   Sebag IA, Morgan JG, Handschumacher MD, Marshall JE, Nesta F, Hung J, Picard MH, Levine RA. Usefulness of three-dimensionally guided assessment of mitral stenosis using matrix-array ultrasound. *Am J Cardiol* 2005;96:1151-1156.

20.   Nosir YF, Vletter WB, Boersma E, Frowijn R, Ten Cate FJ, Fioretti PM, Roelandt JR. The apical long-axis rather than the two-chamber view should be used in combination with the four-chamber view for accurate assessment of left ventricular volumes and function. *Eur Heart J* 1997;18:1175-1185.

21.   Soliman OI, Kirschbaum SW, van Dalen BM, van der Zwaan HB, Mahdavian Delavary B, Vletter WB, van Geuns RJ, Ten Cate FJ, Geleijnse ML. Accuracy and reproducibility of quantitation of left ventricular function by real-time three-dimensional echocardiography versus cardiac magnetic resonance. *Am J Cardiol* 2008;102:778-783.

22.   Soliman OI, Krenning BJ, Geleijnse ML, Nemes A, Bosch JG, van Geuns RJ, Kirschbaum SW, Anwar AM, Galema TW, Vletter WB, ten Cate FJ. Quantification of left ventricular volumes and function in patients with cardiomyopathies by real-time three-dimensional echocardiography: a head-to-head comparison between two different semiautomated endocardial border detection algorithms. *J Am Soc Echocardiogr* 2007;20:1042-1049.

23.   Soliman OI, Krenning BJ, Geleijnse ML, Nemes A, van Geuns RJ, Baks T, Anwar AM, Galema TW, Vletter WB, ten Cate FJ. A comparison between QLAB and TomTec full volume reconstruction for real time three-dimensional echocardiographic quantification of left ventricular volumes. *Echocardiography* 2007;24:967-974.

24.   Anwar AM, Soliman OI, Geleijnse ML, Nemes A, Vletter WB, ten Cate FJ. Assessment of left atrial volume and function by real-time three-dimensional echocardiography. *Int J Cardiol* 2008;123:155-161.

25.   Iung B, Baron G, Butchart EG, Delahaye F, Gohlke-Barwolf C, Levang OW, Tornos P, Vanoverschelde JL, Vermeer F, Boersma E, Ravaud P, Vahanian A. A prospective survey of patients with valvular heart disease in Europe: The Euro Heart Survey on Valvular Heart Disease. *Eur Heart J* 2003;24:1231-1243.

26.   Monin JL, Dehant P, Roiron C, Monchi M, Tabet JY, Clerc P, Fernandez G, Houel R, Garot J, Chauvel C, Gueret P. Functional assessment of mitral regurgitation by transthoracic echocardiography using standardized imaging planes diagnostic accuracy and outcome implications. *J Am Coll Cardiol* 2005;46:302-309.

27.   Shah SJ, Bardo DM, Sugeng L, Weinert L, Lodato JA, Knight BP, Lopez JJ, Lang RM. Real-time three-dimensional transesophageal echocardiography of the left atrial appendage: initial experience in the clinical setting. *J Am Soc Echocardiogr* 2008;21:1362-1368.

28.   Cavalcante JL, Rodriguez LL, Kapadia S, Tuzcu EM, Stewart WJ. Role of echocardiography in percutaneous mitral valve interventions. *JACC Cardiovasc Imaging* 2012;5:733-746.

29.   Soliman OI, Geleijnse ML, Meijboom FJ, Nemes A, Kamp O, Nihoyannopoulos P, Masani N, Feinstein SB, Ten Cate FJ. The use of contrast echocardiography for the detection of cardiac shunts. *Eur J Echocardiogr* 2007;8:S2-12.

30.   Baker GH, Shirali G, Ringewald JM, Hsia TY, Bandisode V. Usefulness of live three-dimensional transesophageal echocardiography in a congenital heart disease center. *Am J Cardiol* 2009;103:1025-1028.

31.   Prokselj K, Kozelj M, Zadnik V, Podnar T. Echocardiographic characteristics of secundum-type atrial septal defects in adult patients: implications for percutaneous closure using Amplatzer septal occluders. *J Am Soc Echocardiogr* 2004;17:1167-1172.

32.   van Dalen BM, Bosch JG, Kauer F, Soliman OI, Vletter WB, ten Cate FJ, Geleijnse ML. Assessment of mitral annular velocities by speckle tracking echocardiography versus tissue Doppler imaging: validation, feasibility, and reproducibility. *J Am Soc Echocardiogr* 2009;22:1302-1308.

PART II

Simultaneous multiplane
2D-echocardiography in congenital and
valvular heart disease

CHAPTER 3

Characterization of atrial septal defect by simultaneous multiplane two-dimensional echocardiography

Jackie S. McGhie
Annemien E. van den Bosch
Meindina G. Haarman
Ben Ren
Jolien W. Roos-Hesselink
Maarten Witsenburg
Marcel L. Geleijnse

ABSTRACT

Aims

The aim of this study was to assess the value of two-dimensional (2D) transthoracic simultaneous multiplane imaging (SMPI) in the evaluation of suitability for percutaneous ASD closure compared to the golden standard 2D transesophageal echocardiography (TEE).

Methods and results

Twenty-nine patients with an ASD underwent both SMPI and TEE. Ten patients (34%) were male (age 41 ± 18 years, range 20–74). SMPI assessment of ASD size and rims included xPlane and iRotate modes. Rims were defined as suitable for ASD percutaneous closure using a cut-off value of 5mm. There were no significant differences between SMPI in xPlane mode and TEE regarding the sizes of the anterior-posterior dimension (13.7 ± 4.5 mm vs. 14.5 vs. ± 5.2 mm) and superior-inferior dimension (13.5 ± 3.9 mm vs. 14.1 vs. ± 5.0 mm, respectively). Agreement for the aortic, atrioventricular, inferior, right upper pulmonary vein and superior rims was 100%, 100%, 100%, 96% and 96%, respectively.

Conclusion

The SMPI technique can reliably assess the dimensions and rim size of a secundum ASD for pre-interventional selection when compared with TEE and has thus the potential to replace TEE.

INTRODUCTION

The atrial septal secundum defect (ASD) is one of the most common lesions in adult congenital heart disease. In the past decade, transcatheter closure of an ASD has gradually become the treatment of choice, rather than surgery. [1,2] However, not all ASDs are anatomically suitable for a transcatheter approach, as the ASD size should be limited and sufficient rims of inter-atrial septal tissue between the defect and adjacent structures are required to position the ASD device. Standard two-dimensional (2D) transthoracic echocardiography (TTE) is limited in the assessment of these rims, due to the fixed number of set cut planes and the difficulty entailed in acquiring some of them. Due to these limitations, transesophageal echocardiography (TEE) is considered the pre-interventional imaging method of choice. [3,4] Nevertheless TEE is a semi-invasive method and is not without procedural risk and it has the short comings of an observational blind area. [5–7]

With the introduction of 2D transthoracic Simultaneous Multiplane Imaging (SMPI) a new image modality has become available. [8] Alongside the standard 2D images taken from the standard transducer positions, images can now also be acquired using the xPlane (bi-plane) and iRotate (any-plane) modes, providing true orthogonal planes that can be acquired in lateral and elevation directions, and an infinite number of 2D cutting planes. The current study sought to assess the value of SMPI in measurement of ASD size and its rims.

METHODS

Study population

Between March 2011 and June 2013, 39 consecutive adult patients with an ASD were referred to our centre for evaluation of an ASD and suitability for treatment by either a transcatheter device or surgical closure. There was an indication for ASD closure when there was right heart dilatation reflecting the significant volume overload of the right ventricle. A defect diameter of > 30mm and total or partial deficiency of rims (< 5mm) were an indication for surgical closure. [1] The institutional review board approved the study and informed consent was obtained from all patients.

Transthoracic 2D SMPI echocardiography

A comprehensive 2D echocardiogram with SMPI was performed using an iE33 ultrasound system (Philips Medical Systems, Best, the Netherlands) equipped with an X5–1 matrix transthoracic probe composed of 3040 elements, with a 1–5MHz extended operating frequency range. For the evaluation of the ASD and its surrounding rims, standard views were examined including the xPlane mode in all patients and since November 2011 also including the iRotate mode in the most recent 23 patients. In the xPlane mode, an orthogonal view can be acquired through the midline of a primary image and displayed as a secondary image. From the midline, additional secondary images can be visualized

by a lateral tilt of up to maximal +30° to -30°. In the xPlane mode, the frame rate will be half of the frame rate of the original image. In the iRotate mode a full electronic rotation of 360° (adjustable by 5° steps) can be performed in the primary image. In contradiction to the xPlane modes the frame rate in the iRotate mode will not be compromised because only the secondary image is displayed. [8]

Measurement of the ASD dimensions

ASD dimensions were acquired by SMPI with the standard subcostal four-chamber (4CH) view as the primary image and making a lateral xPlane sweep through the inter-atrial septum to identify the secondary image with the largest ASD diameter. The end-systolic maximal diameters of the ASD were measured, with the help of colour flow mapping. [3,9–11]

The atrioventricular (AV: inferior / anterior rim between the ASD and the AV valve) and right upper pulmonary vein (RUPV: posterior rim between the ASD and the right pulmonary veins) rims were assessed from the standard subcostal 4CH view. The inferior (IVC: inferior/posterior rim between the ASD and IVC) and superior (SVC: superior/ posterior rim between ASD and the SVC) caval vein rims were assessed using xPlane SMPI from the above-described standard subcostal 4CH view (Figure 1). [1] In four patients with a poor subcostal window the right parasternal (RPS) view and its xPlane view were used to assess the AV, RUPV, IVC and SVC rims. [12,13] The aortic rim (superior/anterior rim between the ASD and aortic valve) was assessed from the standard parasternal short-axis
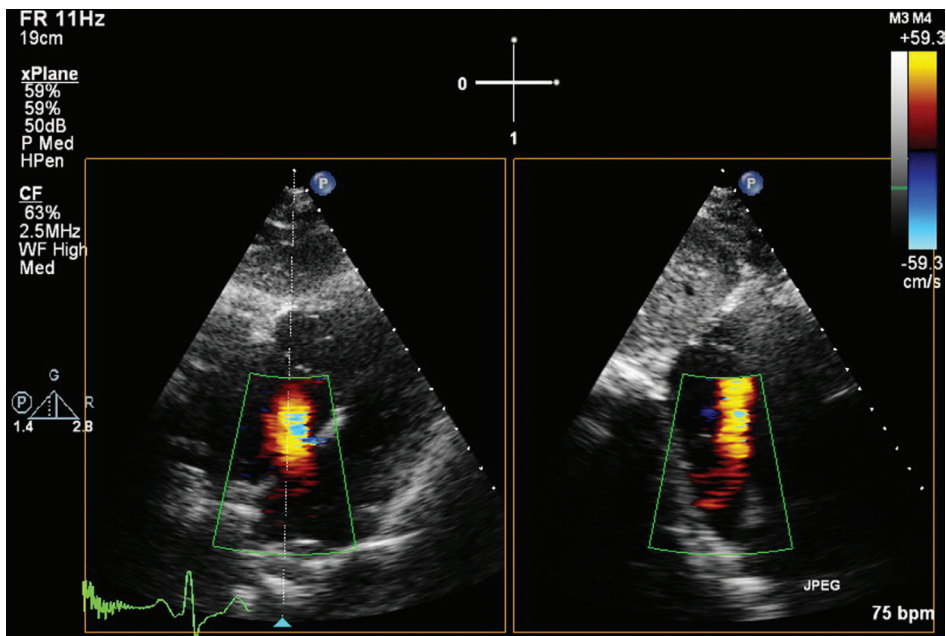
Figure 1 Assessment of the major and minor ASD diameters and main rims: the standard subcostal 4CH view (left) and its xPlane image (right) providing the superior-inferior ASD dimension and IVC and SVC rims.

(SAX) view at the level of the aortic valve view and in the most recent 23 patients also with iRotate SMPI from a standard subcostal 4CH (or RPS) view.

For all rims, the maximal rim size was measured and the measures were subsequently divided using a cut-off value of 5mm because a rim length < 5mm is considered unsuitable for positioning a closure device. [2,4,12]

Two-dimensional transesophageal echocardiography

A 2D TEE examination was performed using an iE33 ultrasound system (Philips Medical Systems, Best, the Netherlands) equipped with a X7–2t matrix transducer composed of 2500 elements, with a 2–7MHz extended operating frequency range. The inter-atrial septum (IAS) was evaluated from the standard transverse (4CH) view, the longitudinal view at the level of the caval veins, and the transverse view at the level of the aorta. [1] The end-systolic maximal diameters of the ASD were measured in the 4CH view and the bi-caval view with help of colour flow mapping.

Contrast fluoroscopy

In the patients who underwent transcatheter closure, a sizing balloon was filled with diluted contrast until the appearance of a waist and disappearance of left-to-right shunt. Once this occurred, a cine-image was performed and the size of the waist was measured using the markers positioned in the balloon for calibration.

STATISTICAL ANALYSIS

Continuous variables are presented as mean ± standard deviation. The paired sample *t*-test was done because all variables were normally distributed. For comparison of normally distributed continuous variables between two groups Student's *t*-test was used. Inter-observer variability was tested by analysing the anterior-posterior and the superior-inferior ASD dimensions and the rim cut-off values (binary) by two blinded observers (J.McG, A.v.d.B). The results were analysed by the relative difference (expressed as the absolute difference divided by mean) and Bland–Altman method, in which biases and 95% limits of agreement were calculated. All statistical analyses were performed using SPSS version 20.0 (SPSS, Inc., Chicago, IL, USA). A *P*-value of < 0.05 was considered significant.

RESULTS

Of the 39 patients referred for ASD closure, 7 had no indication for ASD closure as there was no right heart volume overload present and 3 had an indication for surgical closure because of a defect diameter of > 30mm and total or partial deficiency of rims (< 5mm) on the basis of 2D TTE. The remaining 29 patients had evidence of substantial right heart volume overload at 2D TTE (and thus an indication for intervention), and therefore

underwent not only a 2D SMPI study but also a TEE study. These 29 patients formed the final study population. Ten patients (34%) were male, and the mean (± SD) age of the patients was 41 ± 18 years (range 20–74). Sixteen patients were suitable for percutaneous closure, 12 for surgical closure, and 1 no indication for closure.

Diameters of ASD

In the 16 patients who finally underwent percutaneous closure of the ASD, the SMPI dimensions of the ASD could be compared to the dimensions measured with 2D TEE, balloon sizing and device size. As seen in Table 1, there were no significant differences between SMPI in xPlane mode and 2D-TEE regarding the sizes of the anterior-posterior dimension (13.7 ± 4.5 mm vs. 14.5. ± 5.2 mm) and superior-inferior dimension (13.5 ± 3.9 mm vs. 14.1. ± 5.0 mm). The mean echocardiographic SMPI (13.6 ± 4.2 mm) and TEE dimensions (14.3 ± 5.1mm) were smaller than the balloon sizing diameter (16.7 ± 5.8 mm, both $P < 0.05$) and the actual device size (18.2 ± 6.0 mm, both $P < 0.05$).

Table 1 Atrial septal defect dimensions according to echocardiography and sizing balloon (n = 16).

Dimension	SMPI	TEE	Sizing balloon	Device size
Anterior-posterior (mm)	13.7 ± 4.5	14.5 ± 5.2	---	---
Superior-inferior (mm)	13.5 ± 3.9	14.1 ± 5.0	---	---
Mean (mm)	13.6 ± 4.2[*]	14.3 ± 5.1[*]	16.7 ± 5.8	18.2 ± 6.0

* P < 0.05 compared to sizing balloon and device size

Visualization of ASD rims

As seen in Table 2, in the transthoracic subcostal 4CH view (or RPS view in the four patients with poor subcostal window) and TEE transverse 4CH view, the AV rim could be visualized in all patients. In the 29 patients, SMPI and TEE for assessment of the AV rim size (using the clinically relevant cut-off value of 5mm) had a 100% agreement. With TEE, the RUPV could not be visualized in one patient; with SMPI, the RUPV was visualized in all patients. The IVC rim could be visualized in all patients with SMPI, but not in two patients with TEE. The SVC rim could not be visualized in one patient with SMPI and in two patients with TEE.

In the 23 patients with all imaging techniques (2D, iRotate SMPI and TEE) used for assessment of the aortic rim, rim visualization was 100% for both the standard parasternal SAX view, iRotate SMPI from the subcostal 4CH view (or RPS view in four patients), and TEE. The agreement with TEE was 100% for SMPI and 79% for the 2D TTE parasternal SAX view. In the other four patients, rim size was underestimated by the transthoracic SAX analysis when compared to TEE: 4 vs. 8 mm, 3 vs. 7 mm, and 4 vs. 6 mm and from the RPS view 4 vs. 14 mm for TEE.

Table 2 Atrial septal defect rim size when compared with TEE (n = 29).

Rim of atrial septal defect	2D / SMPI technique	TEE Visualization (%)	SMPI Visualization (%)	Concordance[$] TEE – SMPI (%)
AV	Standard 4CH subcostal view[a]	100	100	100
RUPV	Standard 4CH subcostal view[a]	97	100	96
Inferior caval vein	Biplane SMPI subcostal SAX view[a]	93	100	100
Superior caval vein	Biplane SMPI subcostal SAX view[a]	93	97	96
Aortic	Standard parasternal SAX view	100	100	79
	iRotate SMPI subcostal view	100	100	100

[$]Based on patients with visible rims both in TEE and SMPI.
[a]In four patients the RPS view was used because of a poor quality subcostal window.

Agreement on suitability for percutaneous closure between SMPI and TEE

In 26 patients, all rims could be completely assessed with both SMPI and TEE. According to SMPI, 20 of these patients were considered suitable for implantation of a percutaneous device and in all 20 patients this was confirmed by TEE (positive predictive value 100%). In six patients one or more rims were too small according to SMPI, in five patients this was confirmed by TEE (negative predictive value 83%).

Inter-observer agreement for SMPI measurements

The inter-observer 95% limits of agreement for the anterior-posterior dimension of ASD was -3.4 to 3.6 mm, with a bias of 0.1 mm, and a relative inter-observer variability of 10% ± SD (Figure 2). The inter-observer 95% limits of agreement for the superior-inferior
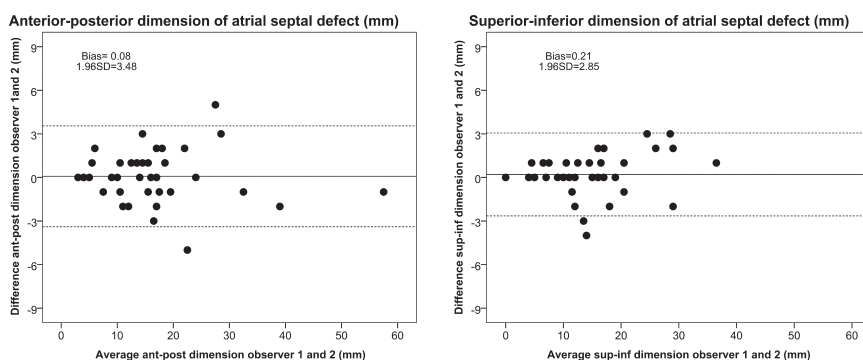
Figure 2 Results of Bland-Altman analyses from the anterior-posterior dimension (left) and the superior-inferior dimension for 39 patients (right). Ant-post, anterior-posterior, sup-in, superior-inferior.

dimension of ASD were -2.7 to 3.1 mm, with a bias of 0.2 mm, and a relative inter-observer variability of 7% ± SD. The inter-observer agreement, using the cut-off value of 5mm, was for all rims 100%.

DISCUSSION

Patient selection for percutaneous closure of an ASD relies on two essential criteria: maximal ASD diameter and tissue rim length. A defect diameter of > 30mm and total or partial deficiency of rims (< 5mm) exclude patients from referral to percutaneous ASD closure. [1,14] The main finding of this study was that the SMPI technique could reliably assess the dimensions and rim size of a secundum ASD for pre-interventional selection as compared to 2D TEE.

ASD diameter

As an ASD may be oval or slit like in shape, it is important that both the major and minor axis of the defect are visualized. Through a thorough 2D TTE multi-view examination of the inter-atrial septum from the subcostal 4CH view, an experienced sonographer may record sufficient data to decide whether a patient is suitable for percutaneous ASD closure. [10,15] However, one is never completely sure whether the true orthogonal plane of the defect has been crossed and the maximum superior-inferior diameter measured. For the less experienced sonographer, it is technically demanding to image the subcostal SAX (lateral) view for the superior-inferior diameter. Incorrect measurements may easily be made, and defects that are not within the oval fossa and not seen in the standard subcostal 4CH view could be missed. TEE is superior to TTE in evaluating an ASD not only because of its superior image quality, but also because of its multiplane character. Once the largest diameter has been visualized in the transverse (4CH) view, a true orthogonal plane can be acquired with a simple 90º rotation. The same results may now be achieved with transthoracic SMPI. Once the largest diameter of the ASD has been identified from the standard subcostal 4CH view, the true orthogonal plane of the defect can be acquired in xPlane mode and the superior-inferior diameter measured in the same heartbeat as the anterior-posterior diameter. As shown in this study, no significant differences in the two diameters were seen between SMPI and TEE. As well known, the anterior-posterior and superior-inferior dimensions measured with SMPI in xPlane mode and TEE were both significantly smaller compared to balloon sizing (a stretch diameter) and the actual device size.[14,16]

An additional benefit of SMPI over standard TTE is that the diagnoses of an ASD becomes less operator dependant. Also a controlled sweep across the inter-atrial septum, with xPlane mode, from the standard 4CH subcostal view allows defects outside the oval fossa (which are often missed) to be detected more easily (Figure 3).
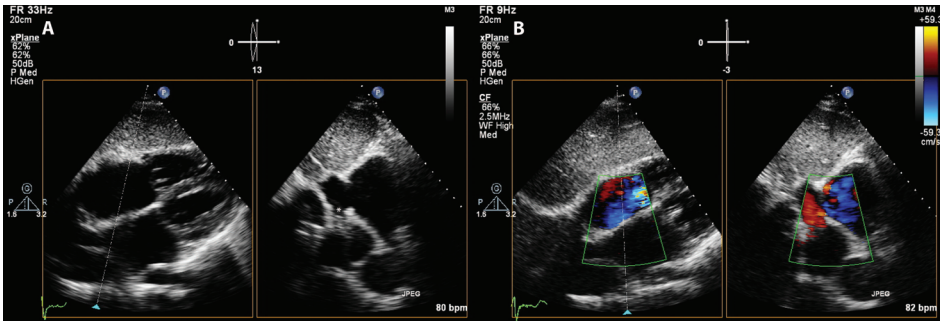
Figure 3 Grey scale standard subcostal 4CH view illustrating an intact atrial septum (*A*, left) and the secondary image with xPlane lateral tilt + 13° (**A**, right) illustrating the ASD (asterisk) with an absent inferior rim. Colour flow mapping illustrating (**B**, left) intact septum and (B, right) the ASD.

ASD rims

To ensure stability of the closure device and to avoid encroachment on surrounding structures, an adequate rim size of septal tissue (> 5mm) around the defect is of vital importance. [1,17] Apart from one SVC rim, all rims could be assessed with SMPI. The AV rim was evaluated from the standard subcostal 4CH view (or in a few patients with a poor subcostal window from the RPS view); in full concordance with TEE. The RUPV rim was also evaluated from the standard subcostal 4CH view. Only one RUPV rim showed a discrepancy in cut-off measurement between SMPI and TEE (3mm at SMPI versus 6mm at TEE). Underestimation of this rim, which appeared thin and floppy at TEE, may have been caused by reduced transthoracic image quality. The SVC and IVC rims were measured from an xPlane image taken from the standard subcostal 4CH view. The IVC rim could be visualized in all patients with SMPI, in full concordance with TEE. The SVC rim that was scored absent was most likely due to it being in alignment with the ultrasound beam and its position in the far-field in combination with reduced transthoracic image quality (the RUPV rim was also underestimated in this patient). In the patient in whom the SVC rim could not be visualised, this was also true for the TEE so maybe this was due to the rotation of the heart itself rather than the technique.

Assessment from the standard parasternal SAX of the aortic rim is known for its inaccurate measurement, as was shown in six patients in our study. As seen in Figure 4A, misinterpretation of the IAS as being intact and signal dropout due to the inability to evaluate the aortic rim perpendicularly will result in inadequate assessment. [16,18,19] iRotate from the subcostal 4CH and RPS view resulted in a more perpendicular visualization of this rim and perfect correlation with TEE. With the ASD centred on the midline of the sector, a complete 360º rotation around the defect can be performed and the full extent of the rims evaluated (Figure 4B)
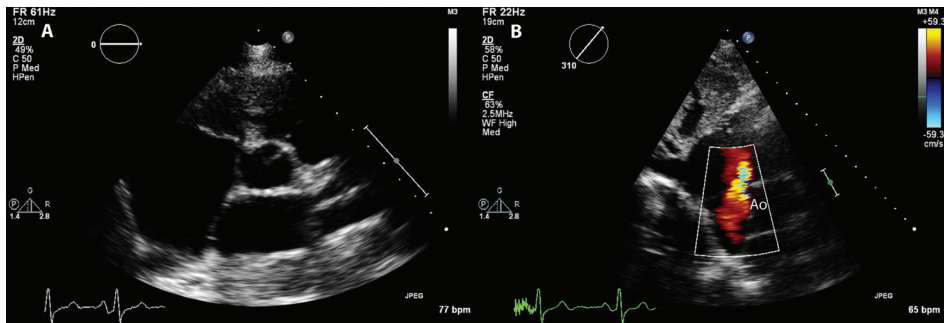
Figure 4 Standard parasternal SAX view at the aortic valve level: showing the misinterpreted intact aortic rim (left) whereas with a 310° rotation the true absent aortic rim can be appreciated (right).

Clinical Implications

Our results show that with an optimal quality SMPI echo, the diagnostic (especially in patients with defects outside the oval fossa) and pre-interventional TEE could be avoided. In children where a pre-interventional TEE is not routinely performed, SMPI would give more detailed information. In addition, it has been reported in studies that catheter closure of central ASD's can be successfully monitored by standard 2D TTE and fluoroscopic guidance. [6,7,15,20] Because multiple cross-sectional views are needed throughout the procedure, SMPI can reduce the number of transducer positions and provides bi-plane (xPlane) imaging, the benefit of which has already been described with TEE, while monitoring the positioning of the device. [21] iRotate may also accurately check if all aspects of the closure device are well seated and no residual shunts are present before the final deployment of the device. As TTE monitoring is a very economical (compared with the use of intra-cardiac echocardiography) and patient friendly (compared with intra-interventional TEE monitoring necessitating general anaesthesia) imaging technique, more centres may be tempted to use it given the additional value of SMPI, especially in patients who have a good acoustic window.

Limitations

We did not compare 2D-SMPI measurements to 3D TTE echo. Despite the valuable 'enface views', this technique is not without limitations. Difficulties in image acquisition, loss of image resolution, and ASD size being dependent on 3D gain settings may result in inaccurate measurements. [3,22,23]

The spatial resolution of the X5–1 matrix transthoracic probe remains somewhat inferior to the stand-alone 2D transducer and in addition the frame rate (temporal resolution) drops by half when entering the xPlane mode. This latter can be problematic for colour Doppler flow imaging that already suffers from lower frame rates in the standard (primary) 2D images. The drop in temporal resolution can be brought to a minimum by ensuring that the smallest sector able to encompass the cardiac structure of interest is used. Also this can be overcome with iRotate mode if the ASD can be positioned in the centre of the sector as frame rate in this mode is not compromised at all.

Two-dimensional TEE is considered the gold standard. However, in one patient the RUPV rim could not be visualised due to a very large ASD and the position of the RUPV in the corner of the sector. Also, in two patients the IVC and SVC rims were not visualized on TEE. Both TEE studies suffered from reduced image quality, and it is known that due to the extreme proximity of the VCI rim to the transducer it can be difficult to visualize. [24]

Finally, the motion of the heart throughout the cardiac cycle may result in the reference line not transecting the ASD at any time point in the heart cycle.

CONCLUSION

The SMPI technique, which allows a full electronic rotation of 360° of the ASD and displays the true orthogonal plane of the defect in xPlane mode, can reliably assess the dimensions and rim size of a secundum ASD for pre-interventional selection when compared with 2D TEE. If the SMPI study is of optimal quality, it has the potential to replace the TEE for ASD evaluation and guidance of device placement.

REFERENCES

1. Podnar T, Martanovic P, Gavora P, Masura J. Morphological variations of secundum-type atrial septal defects: feasibility for percutaneous closure using Amplatzer septal occluders. *Catheter Cardiovasc Interv* 2001;53:386-391.
2. Roberson DA, Cui W, Patel D, Tsang W, Sugeng L, Weinert L, Bharati S, Lang RM. Three-dimensional transesophageal echocardiography of atrial septal defect: a qualitative and quantitative anatomic study. *J Am Soc Echocardiogr* 2011;24:600-610.
3. Chau AK, Leung MP, Yung T, Chan K, Cheung Y, Chiu S. Surgical validation and implications for transcatheter closure of quantitative echocardiographic evaluation of atrial septal defect. *Am J Cardiol* 2000;85:1124-1130.
4. Prokselj K, Kozelj M, Zadnik V, Podnar T. Echocardiographic characteristics of secundum-type atrial septal defects in adult patients: implications for percutaneous closure using Amplatzer septal occluders. *J Am Soc Echocardiogr* 2004;17:1167-1172.
5. Erdem A, Saritas T, Zeybek C, Yucel IK, Erol N, Demir H, Odemis E, Yalcin Y, Celebi A. Transthoracic echocardiographic guidance during transcatheter closure of atrial septal defects in children and adults. *Int J Cardiovasc Imaging* 2013;29:53-61.
6. Li GS, Kong GM, Ji QS, Li JF, Chen YG, You BA, Zhang Y. Reliability of transthoracic echocardiography in estimating the size of Amplatzer septal occluder and guiding percutaneous closure of atrial septal defects. *Chin Med J (Engl)* 2008;121:973-976.
7. Li GS, Li HD, Yang J, Zhang WQ, Hou ZS, Li QC, Zhang Y. Feasibility and safety of transthoracic echocardiography-guided transcatheter closure of atrial septal defects with deficient superior-anterior rims. *PLoS One* 2012;7:e51117.
8. McGhie JS, Vletter WB, de Groot-de Laat LE, Ren B, Frowijn R, van den Bosch AE, Soliman OI, Geleijnse ML. Contributions of Simultaneous Multiplane Echocardiographic Imaging in Daily Clinical Practice. *Echocardiography* 2013.

9.   Huang X, Shen J, Huang Y, Zheng Z, Fei H, Hou Y, Xu Y, Huang T, Huang W, Zhang C. En face view of atrial septal defect by two-dimensional transthoracic echocardiography: comparison to real-time three-dimensional transesophageal echocardiography. *J Am Soc Echocardiogr* 2010;23:714-721.

10.   Mehta RH, Helmcke F, Nanda NC, Pinheiro L, Samdarshi TE, Shah VK. Uses and limitations of transthoracic echocardiography in the assessment of atrial septal defect in the adult. *Am J Cardiol* 1991;67:288-294.

11.   Sahin M, Ozkutlu S, Yildirim I, Karagoz T, Celiker A. Transcatheter closure of atrial septal defects with transthoracic echocardiography. *Cardiol Young* 2011;21:204-208.

12.   Luckie M, Buckley H, Khattar R. Echocardiographic detection of atrial septal defects: the forgotten view. *Echocardiography* 2010;27:97-99.

13.   Watanabe N, Taniguchi M, Akagi T, Tanabe Y, Toh N, Kusano K, Ito H, Koide N, Sano S. Usefulness of the right parasternal approach to evaluate the morphology of atrial septal defect for transcatheter closure using two-dimensional and three-dimensional transthoracic echocardiography. *J Am Soc Echocardiogr* 2012;25:376-382.

14.   El-Said HG, Bezold LI, Grifka RG, Pignatelli RH, McMahon CJ, Schutte DA, Smith EO, Mullins CE. Sizing of atrial septal defects to predict successful closure with transcatheter cardioSEAL device. *Tex Heart Inst J* 2001;28:177-182.

15.   Li GS, Kong GM, Wang YL, Jin YP, Ji QS, Li JF, You BA, Zhang Y. Safety and efficacy of transcatheter closure of atrial septal defects guided by transthoracic echocardiography: a prospective study from two Chinese Medical Centers. *Ultrasound Med Biol* 2009;35:58-64.

16.   Mesihovic-Dinarevic S, Begic Z, Halimic M, Kadic A, Gojak R. The reliability of transthoracic and transesophageal echocardiography in predicting the size of atrial septal defect. *Acta Med Acad* 2012;41:145-153.

17.   Graham R, Gelman J. Echocardiographic aspects of percutaneous atrial septal defect closure in adults. *Heart Lung Circ* 2001;10:75-78.

18.   McMahon CJ, Feltes TF, Fraley JK, Bricker JT, Grifka RG, Tortoriello TA, Blake R, Bezold LI. Natural history of growth of secundum atrial septal defects and implications for transcatheter closure. *Heart* 2002;87:256-259.

19.   Mehmood F, Vengala S, Nanda NC, Dod HS, Sinha A, Miller AP, Khanna D, Misra VK, Lloyd SG, Upendram S, Bodiwala K, McMahon WS, Kasliwal RR, Chouhan N, Govinder M, Pacifico AD, Kirklin JK, McGiffin DC. Usefulness of live three-dimensional transthoracic echocardiography in the character-ization of atrial septal defects in adults. *Echocardiography* 2004;21:707-713.

20.   Kardon RE, Sokoloski MC, Levi DS, Perry JS, 2nd, Schneider DJ, Allada V, Moore JW. Transthoracic echocardiographic guidance of transcatheter atrial septal defect closure. *Am J Cardiol* 2004;94:256-260.

21.   Yared K, Baggish AL, Solis J, Durst R, Passeri JJ, Palacios IF, Picard MH. Echocardiographic assessment of percutaneous patent foramen ovale and atrial septal defect closure complications. *Circ Cardiovasc Imaging* 2009;2:141-149.

22.   Faletra FF, Nucifora G, Ho SY. Imaging the atrial septum using real-time three-dimensional trans-esophageal echocardiography: technical tips, normal anatomy, and its role in transseptal puncture. *J Am Soc Echocardiogr* 2011;24:593-599.

23.   van den Bosch AE, Ten Harkel DJ, McGhie JS, Roos-Hesselink JW, Simoons ML, Bogers AJ, Meijboom FJ. Characterization of atrial septal defect assessed by real-time 3-dimensional echocardiography. *J Am Soc Echocardiogr* 2006;19:815-821.

24.   Remadevi KS, Francis E, Kumar RK. Catheter closure of atrial septal defects with deficient inferior vena cava rim under transesophageal echo guidance. *Catheter Cardiovasc Interv* 2009;73:90-96.

CHAPTER 4

Transthoracic two-dimensional xPlane and three-dimensional echocardiographic analysis of the site of mitral valve prolapse

Jackie S. McGhie
Lotte de Groot- de Laat
Ben Ren
Wim Vletter
René Frowijn
Frans Oei
Marcel L. Geleijnse

ABSTRACT

Purpose
This study sought to assess the value of two-dimensional (2D) transthoracic echocardiography (TTE), 2D xPlane imaging and three- dimensional (3D) TTE for the definition of the site and the extent of mitral valve (MV) prolapse.

Method and Results
Fifty patients underwent transthoracic 2D, 2D xPlane and 3D echocardiography. With 2D xPlane a segmental analysis of the MV was performed, by making a lateral sweep across the MV coaptation line as seen in the parasternal short-axis view.

Inter-observer agreement for specific scallop prolapse was for 2D xPlane excellent (97%, kappa = 0.94) and for 3D TTE moderate (85%, kappa = 0.67). The respective sensitivities of standard 2D TTE, 2D xPlane, and 3D TTE for the identification of the precise posterior scallop prolapse were for P1 92, 85, and 92%, for P2 96, 96, and 82%, and for P3 86, 81, and 71%. In total, 5 (8%) prolapsing MV scallops were missed by 2D TTE, 7 (12%) by 2D xPlane, and 12 (20%) by 3D TTE. The sensitivity of 3D TTE was significantly lower than standard 2D imaging (80% versus 93%, P < 0.05). The extent of P2 prolapse was under or overestimated in 5 patients with 2D xPlane and in 9 patients with 3D TTE.

Conclusion
2D xPlane imaging is an accurate, easy to use (compared to 3D TTE) and easy to interpret (compared to 2D and 3D TTE) imaging modality to study the site and the extent of MV prolapse.

INTRODUCTION

Mitral valve (MV) prolapse (MVP) is one of the most common valvular abnormalities in industrialized countries.[1] The site and extent of the prolapse is essential in defining the suitability for MV repair.[2] Many physicians are of the opinion that two-dimensional (2D) transthoracic echocardiography (TTE) is not reliable enough to provide the surgeon with the essential pre-operative information and consider transesophageal echocardiography (TEE) obligatory. However, it should be recognized that newer technology (beam formers and harmonic imaging) has improved TTE quality and TEE is a semi-invasive imaging technique not totally without procedural risk.[3–5] More recently, three-dimensional (3D) TTE has been developed; a technique that is thought to be able to define more precisely the site and extent of the prolapse in a non-invasive manner.[6,7] However, 3D imaging requires expertise and suffers from limited temporal and spatial resolution.[8] With the 3D matrix transducer, it is also possible to identify the prolapse site and the extent from multiple 2D xPlane views taken from a standard parasternal short axis view of the MV by simultaneous multiplane imaging (SMPI).[9,10] This technique requires less expertise and the spatial resolution is only minimally reduced compared to 3D imaging. Therefore, this study sought to assess the value of 2D TTE, 2D xPlane imaging and 3D TTE for the definition of the site and the extent of MV prolapse in patients that underwent MV surgery.

METHODS

Study population

Between May 2012 and August 2013, 57 consecutive patients with MVP were referred to our center for surgical MV repair because of isolated severe mitral regurgitation (MR). The institutional review board approved the study and informed consent was obtained from all patients.

Prior to surgery a transthoracic 2D, 2D xPlane and 3D echocardiogram in harmonic imaging was performed using an iE33 ultrasound system (Philips Medical Systems, Best, The Netherlands) equipped with an X5–1 matrix probe composed of 3040 elements, with a 1–5MHz extended operating frequency range, with the patient in the left lateral decubitus position.

2D echocardiography

As recommended, four standard 2D imaging planes were used: the parasternal long-axis and short-axis views and the apical four- and two-chamber views.[5]

2D xPlane mode

A segmental analysis of the MV was performed with SMPI in xPlane mode, by making a lateral sweep across the MV coaptation line as seen in the parasternal short-axis view (Figure 1). In the xPlane mode an orthogonal view can be acquired through the midline of
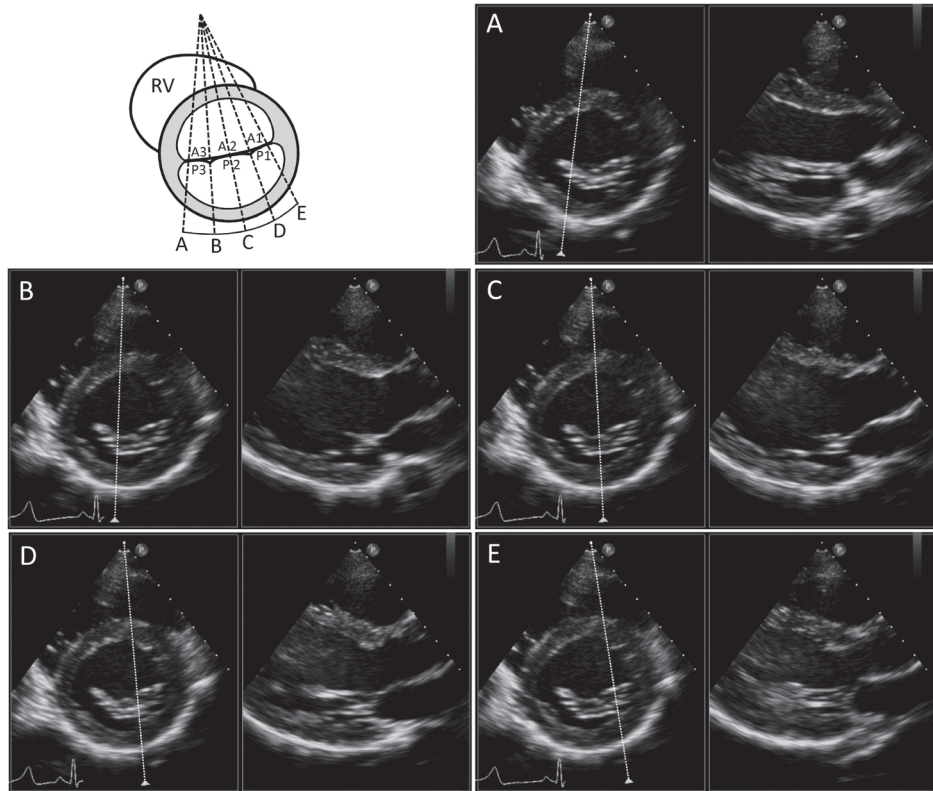
Figure 1 Segmental sweep analysis of the mitral valve scallops with 2D xPlane imaging with lateral tilt. **A - E** correspond to the *P3,P2* medial, *P2* central, *P2* lateral and *P1* scallops

a primary image and displayed as a secondary image. From the midline, additional secondary images can be obtained by a lateral tilt of up to a maximum of +30º to -30º allowing precise visualization of the prolapsing scallop in the secondary image which will resemble a parasternal long axis view. A clear example of a P1, P2 and P3 prolapsing scallop is seen in Figure 2. The smallest sector able to encompass the mitral valve should be used because in the xPlane mode frame rate will be half of the frame rate of the original image.[10] Mean xPlane frame rate was 37 ± 6 frames per second.

3D echocardiography

In patients in sinus rhythm a full-volume data set from four to six R-wave gated sub-volumes during a single end-expiratory breath-hold was acquired and in patients with atrial fibrillation a live 3D data set was acquired to avoid the concerns about stitching artefacts. All full-volume and live 3D data sets were taken from a parasternal or an apical window.[11,12] The 3D data set was manipulated, off-line, using QLAB version 9 (Philips Medical Systems, Best, The Netherlands) to show an 'en-face' or 'surgical' view of the MV as seen from the left atrium. The mean 3D volume rate was 36 ± 16 volumes per second.
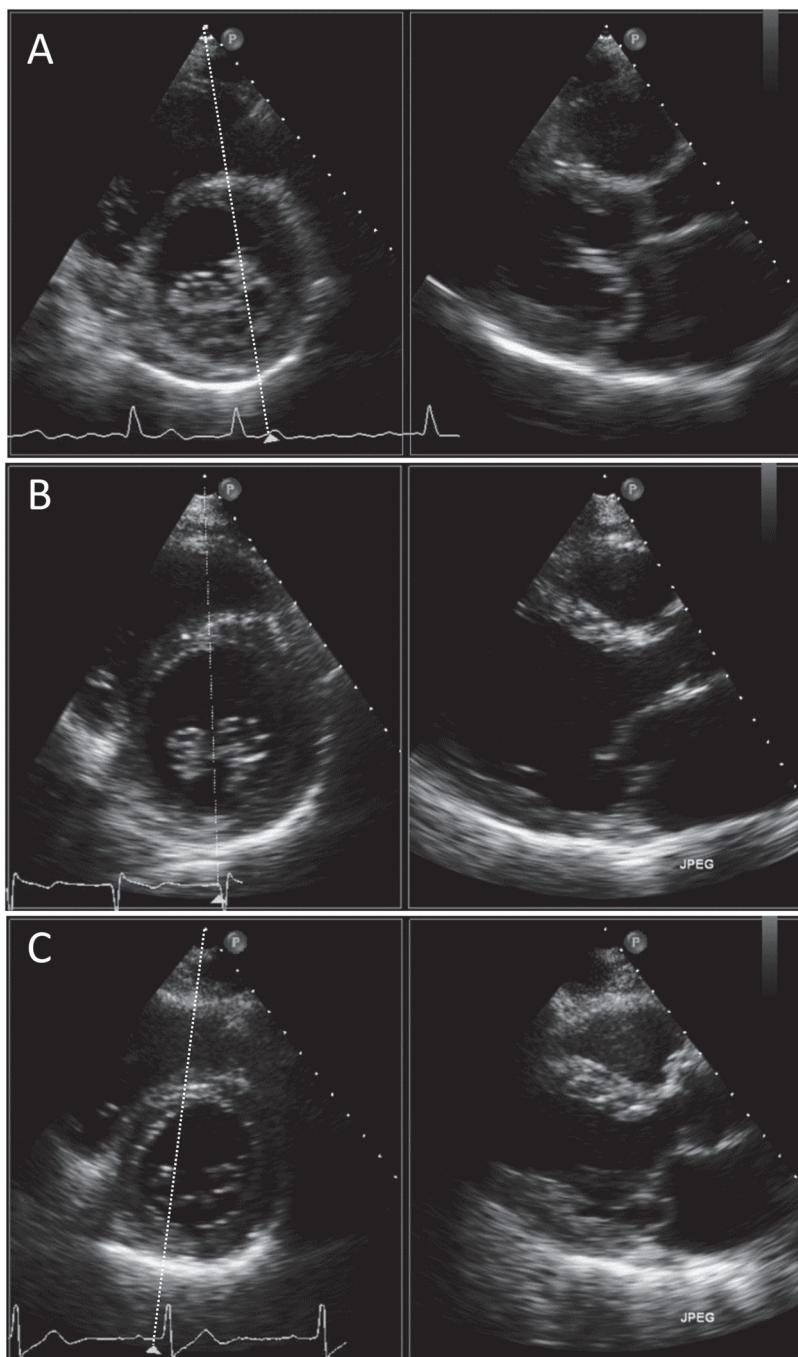
Figure 2 Segmental analysis of the mitral valve scallops with 2D xPlane imaging with lateral tilt.
a P1 prolapse **b** P2 prolapse **c** P3 prolapse

Scoring protocol

A senior cardiologist with extensive experience in 2D and 3D echocardiography and MV disease analyzed all echocardiographic data sets blinded to other patient information with at least 10 days between each specific analysis in a random order. MV prolapse and segmental visualization of the affected scallop was classified according to the Carpentier nomenclature.[13] The extent of P2 prolapse was only assessed with 2D xPlane and 3D echocardiography since standard 2D echocardiography is not capable of doing so. The surgical findings served as the gold standard. However, in 6 cases the surgeon only described a P2 prolapse without a clear description on the specific extent of the prolapse. In these 6 cases, intra-operative 3D transesophageal data were used as supplementary gold standard data to describe the extent of the P2 prolapse.

The sensitivity of scoring a P1, P2 or P3 prolapse was calculated as the positive findings of the different modalities divided by the positive surgical findings. The specificity was calculated as the negative findings of the different modalities divided by the negative surgical findings.

The identification of the extent of the P2 prolapse examined with 2D xPlane and 3D TTE was split up into five categories and compared with the surgical finding. The five categories are; Barlow disease (including P1 and P3 prolapse), broad P2 (central, including the centro-medial and centro-lateral edges of the P2 scallop but without P1 or P3 prolapse), small P2 (only central prolapse without incorporation of the centro-medial and centro-lateral edges), asymmetric P2 (central and only one edge) and edge P2 (one centro-medial or centro-lateral part only).

Statistical analysis

Prolapse site sensitivity and specificity were calculated according to standard formulas.

The degree of inter-observer agreement between the two blinded observers (MLG and JSMcG) for specific scallop prolapse using 2D xPlane and 3D echocardiography was assessed by calculating the Kappa coefficient (a value > 0.80 indicating excellent agreement).

RESULTS

Of the 57 patients referred for surgical repair, 7 patients (12%) were excluded because a 3D TTE was not possible due to inadequate 2D image quality. In the remaining 50 patients mean age was 61 ± 16 years and 33 (66%) were men. Forty (80%) patients were in sinus rhythm and 10 (20%) in atrial fibrillation. Eleven patients (22%) had Barlow's disease involving both the anterior and posterior mitral valve leaflet. In 24 patients (48%) the prolapse was confined to one or more posterior mitral valve scallops (P1 in 1, P2 in 13, P2+P3 in 2, P3 in 8 patients). In the remaining 15 patients (30%) no prolapse was seen and MR was due to mitral annular dilatation with or without retraction in 10 patients (20%), endocarditis in 3 patients (6%), and rheumatic disease in 2 patients (4%).

Anterior mitral valve scallop

In 16 patients, a prolapsing anterior MV leaflet was seen. In the eleven patients with Barlow disease all prolapsing anterior MV leaflets were recognized with all techniques, apart from one patient in which 3D echocardiography missed the prolapse. In the 5 remaining patients the prolapse was confined to the A2 part in one patient, the A2-A3 part in one patient and the A3 part in three patients. Standard 2D analysis detected anterior MV leaflet prolapse in all patients although distinction between the specific scallops was problematic. 2D xPlane identified the specific prolapse part in all patients where as 3D echocardiography missed the prolapse in two patients with A3 prolapse.

Localization of posterior mitral valve scallop

As seen in Figure 3a, the respective sensitivities of 2D TTE, 2D xPlane, and 3D TTE for the identification of the precise posterior scallop prolapse were for P1 92, 85, and 92%, for P2 96, 96, and 82%, and for P3 86, 81, 71%. In total, 5 (8%) prolapsing MV scallops were missed by 2D TTE, 7 (12%) by 2D xPlane, and 12 (20%) by 3D TTE. The sensitivity of 3D TTE was significantly lower than standard 2D imaging (80% vs. 93%, $P < 0.05$). As seen in Figure 3b, the respective specificities of 2D TTE, 2D xPlane, and 3D TTE for the identification of the precise posterior scallop prolapse were for P1 100, 97, and 97%, for P2 100, 91, and 91%, and for P3 100, 97, and 97%.
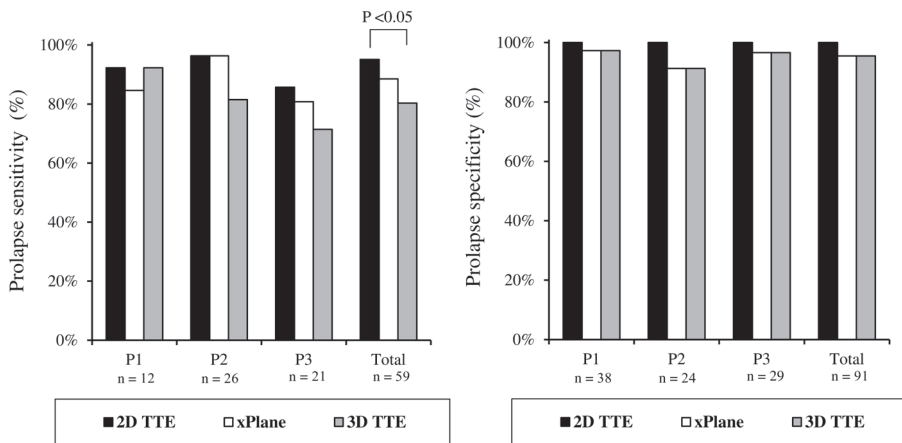
Figure 3 Sensitivity (**left**) and specificity (**right**) for the identification of posterior mitral valve scallop prolapse by the different echo techniques

Identification of the extent of the P2 prolapse

The results of 2D xPlane and 3D TTE for accurately diagnosing the extent of the P2 prolapse are shown in Table 1. All 11 patients with a Barlow MV (that is involvement of the complete anterior and posterior MV leaflet) were correctly diagnosed by both modalities. Seven patients had a broad P2 prolapse. With 2D xPlane 4 were identified correctly and in 3 patients, a prolapsing P2 was seen, but the extent of prolapse was to

some extent underestimated (one edge was missed). Whereas with 3D TTE, one was missed completely and 3 were underestimated (in two patient's one edge was missed and in one patient only a prolapsing edge was identified). Five patients had a small central P2 prolapse, 2D xPlane identified three correctly, overestimated one (that is one edge was also scored as prolapsing) and missed one. 3D TTE identified two correctly and missed three. In the three patients with asymmetric P2 prolapse (center and one edge), all three were correctly diagnosed with 2D xPlane, but two were underestimated (only a prolapsing edge was identified in one patient and only a prolapsing central part in one other patient) with 3D TTE. One patient had a P2 one edge only prolapse that was diagnosed correctly with 2D xPlane and missed by 3D TTE. So, in total 4 and 9 scallop parts were missed or underestimated with 2D xPlane and 3D, respectively.

Table 1 Identification of the extent of P2 prolapse with transthoracic xPlane and 3D echocardiography.

Surgical findings	Barlow		Broad P2 (central + 2 edges)		Small P2 (central)		Asymmetric P2 (central + 1 edge)		Edge P2 (1 edge only)	
Echo findings	N = 11		N = 7		N = 5		N = 3		N = 1	
	xPlane	3D	xPlane	3D	xPlane	3D	xPlane	3D	xPlane	3D
Broad	11	11	4	3	0	0	0	0	0	0
Small	0	0	0	0	3	2	0	1	0	0
Asymmetric	0	0	3	2	1	0	3	1	0	0
Edge only	0	0	0	1	0	0	0	1	1	0
Negative (missed)	0	0	0	1	1	3	0	0	0	1

Colour legend: □ = correct, ▪ = overestimation, ▪ = underestimation, ▪ = missed.

Inter-observer agreement

Seven additional 3D TTE were excluded because the second observer determined the 3D quality too poor to reliably assess the site of MV prolapse. Inter-observer agreement for specific scallop prolapse is shown in Figure 4. For 2D xPlane the agreement was excellent (97%, kappa = 0.94). For 3D TTE the agreement was moderate (85%, kappa = 0.67)

	P1		P2		P3		Total	
	+	-	+	-	+	-	+	-
2D xPlane +	11	0	25	0	15	0	51	0
2D xPlane -	1	31	1	17	2	26	4	74
	Agreement 98% Kappa 0.94		Agreement 98% Kappa 0.95		Agreement 95% Kappa 0.90		Agreement 97% Kappa 0.94	
3D +	9	1	19	4	9	4	37	9
3D -	3	30	3	17	5	25	11	72
	Agreement 91% Kappa 0.76		Agreement 84% Kappa 0.67		Agreement 79% Kappa 0.51		Agreement 85% Kappa 0.67	

Figure 4 Interobserver variability in assessment of posterior mitral valve scallop prolapse by 2D xPlane and 3D echocardiography

DISCUSSION

In this study we sought to assess the relative value of transthoracic standard 2D imaging, 2D xPlane imaging, and 3D imaging for the definition of the site and extent of MV prolapse. The main results of the study are (1) transthoracic 2D imaging has excellent diagnostic value in detection of the prolapsing MV scallop, (2) 2D xPlane and 3D imaging do not improve detection of the prolapsing MV scallop, (3) the extent and asymmetry of P2 prolapse can, however, only be assessed by xPlane and 3D imaging, and (4) 2D xPlane imaging may be superior to en-face 3D imaging in this latter aspect because it is (a) easier to implement as it is a 2D technique, (b) has a better interobserver agreement, and (c) misses less prolapsing MV scallop parts because of less artifacts (dropouts and side-lobe artifacts) and better spatial resolution.

The definition of the site and extent of MV prolapse plays a crucial role not only in surgical referral but also for the operative plan since different pathology require different levels of surgical expertise based on the complexity of lesions seen with echocardiography.[14,15] Some authors have reported poor sensitivities of 2D TTE for the identification of prolapse,[16] and in particular of the not centrally-located P1 and P3 scallops.[4,17,18] Minardi et al. reported sensitivities of 64, 99 and 50% for respectively P1, P2, and P3 scallop prolapse (although they claimed overall sensitivity was excellent since the middle scallop P2 "represents almost the totality of prolapses"). Also, Beraud et al. reported a correct description in only 22% in patients with a prolapse other than isolated P2 prolapse. Pepi et al. reported a sensitivity of 40% for the antero-lateral commissure and 54% for the postero-medial commissure.

In contrast, Monin et al. reported sensitivities of 95% and 93% for respectively the central P2 prolapse and the not centrally-located P1 and P3 scallops based on a similar 2D analysis. Our results of sensitivities of 92, 96, and 86% for respectively P1, P2, and P3 prolapse are in line with these results of Monin et al. Of note, like in our study the echo studies were performed by dedicated "senior" sonographers and analyzed by a cardiologist with extensive experience in MV assessment. As a result of the excellent transthoracic 2D diagnostic results 2D xPlane and 3D imaging was not able to add diagnostic value. On the contrary, 2D xPlane imaging and in particular 3D imaging resulted in more false negative results.

In the literature there is some controversy over the accuracy of 3D TTE for the evaluation of the site and extent of the MV prolapse. All investigators stated that 3D TTE is a feasible technique in the majority of patients. This was confirmed in our study as in only 7 patients (12%) the 3D images were deemed not possible because of image quality by the sonographer and in another 7 patients the 3D image quality was found to be inadequate for analysis by one of the two observers. Several investigators stated that the accuracy of 3D TTE for the identification of scallop prolapse is high[7,17–20] and may even be superior to 2D TTE [17–19] or even 2D TEE. [7] Although Gutiérrez-Chico already noted imperfect results for the not centrally-located (lateral and medial) scallops, [20] Zekry et al. pointed out clearly the difficulty in using 3D TTE to localize mitral valve segmental

disease especially for the not centrally-located scallops: sensitivities were 7, 93, and 29% for respectively P1, P2, and P3 scallop prolapse [21]. In our 3D study the sensitivity for the detection of P3 prolapse was also somewhat lower. Of note, Agricola et al. and Beraud et al. used a combination of en-face "surgical" views and 3 to 5 reconstructed longitudinal views ("representing the A1-P1, A2-P2, A3-P3 scallops and the two commissures") and it was claimed to be, in particular, helpful in patients with commissural prolapse, although results were still sub-optimal.

The identification of 3D volume-rendered images may be difficult even for the experienced observer since a prolapsing scallop should be identified as a convexity or bulge, and often as a bright area when compared with the rest of the mitral valve. Despite exclusion of patients with poor echocardiographic images, the current spatial and temporal resolution of 3D transthoracic transducers in our opinion still limits the interpretation of images. This was evidenced not only by the 12 missed prolapsing scallops (compared to 5 and 7 with respectively 2D TTE and 2D xPlane), but also by the underestimation of P2 scallop extent by 3D.

2D xPlane imaging

With the introduction of 2D xPlane imaging it is possible to identify not only a prolapsing MV leaflet but also to assess, like 3D imaging, in a systematic manner the extent of MV prolapse. It is important to realize that the xPlane technique in fact mimics the 3D multiplane reconstruction with as opposite to 3D imaging only a minimal impact on spatial resolution compared to standard 2D imaging with a 2D transducer. Compared to the surgical findings 2D xPlane was a sensitive technique (overall 2D xPlane sensitivity 88vs 80% for 3D) to identify MV prolapse and the inter-observer agreement for identification of the prolapsing MV scallop was excellent. Also, the sensitivity of 2D xPlane imaging for the identification of MV prolapse was not lower than standard 2D imaging, whereas 3D TTE was significantly lower compared to standard 2D imaging. In addition, good results were seen in the identification of the extent of P2 prolapse.

Any sonographer will be able to perform an accurate, rapid, online segmental analysis of the entire coaptation line of the MV with xPlane imaging. Virtually the images do not suffer from a loss in spatial resolution and rhythm irregularities will not affect the data. Although in the present study the identification of MV prolapse presence was not superior to standard 2D imaging it should be realized that the 2D images were interpreted by a senior cardiologist highly experienced in MV evaluation

Clinical implications

Although not discussed in this article, 2D and 3D TEE imaging are excellent imaging tools to describe the MV geometry and mechanism of regurgitation and to guide the surgical approach. However, TEE is a semi-invasive imaging technique not totally without procedural risk. [3,22] Because 2D xPlane is an easy, accurate and noninvasive imaging modality we suggest standard 2D supplemented with 2D xPlane to be used in the outpatient clinic for optimal assessment of MV geometry and mechanism of regurgitation. Only in the few patients in whom doubt persists (in particular the involvement of the para-commissural

scallops) 2D and/or 3D TEE imaging should be performed in the outpatient's clinic. Finally, pre-operative TEE in the operating room (the ideal circumstance for studying the geometry and mechanism of the MV) may further refine the diagnosis and guide the surgical approach.

Limitations

The spatial resolution of the X5–1 matrix transthoracic probe remains somewhat inferior to the stand-alone 2D transducer and in addition the frame rate (temporal resolution) drops by half when entering the xPlane mode. This drop in temporal resolution however, does not seem very important in the assessment of the site and extent of MV prolapse and can be brought to a minimum by ensuring that the smallest sector able to encompass the MV is used.

Care must be taken with the interpretation of the extent of prolapse from the standard parasternal short axis view analysis since the motion of the heart throughout the cardiac cycle may result in the reference line not transecting the same region of interest at any time point in the heart cycle.

The echo studies were performed by dedicated "senior" sonographers and analyzed by a cardiologist with extensive experience in MV assessment. Therefore, our results may not be generalized to less experienced centers. In addition, TEE imaging was not considered in the design of the study because the aim of the study was to assess the relative value of transthoracic standard 2D imaging, transthoracic 2D xPlane imaging, and transthoracic 3D imaging for the definition of the site and extent of MV prolapse defined by the surgical standard.

Finally, the anatomical findings at surgery served as the gold standard. It should be recognized that surgeons assess an immobile valve in a flaccid heart whereas echocardiography assesses a dynamic valve. Unfortunately, there is no practical alternative to this approach.

CONCLUSION

2D xPlane imaging is an accurate, easy to use (compared to 3D TTE) and easy to interpret (compared to 2D and 3D TTE) imaging modality to study the site and the extent of MV prolapse.

REFERENCES

1. Iung B, Baron G, Butchart EG, Delahaye F, Gohlke-Barwolf C, Levang OW, Tornos P, Vanoverschelde JL, Vermeer F, Boersma E, Ravaud P, Vahanian A. A prospective survey of patients with valvular heart disease in Europe: The Euro Heart Survey on Valvular Heart Disease. *Eur Heart J* 2003;24:1231-1243.
2. Maffessanti F, Mirea O, Tamborini G, Pepi M. Three-dimensional echocardiography of the mitral valve: lessons learned. *Curr Cardiol Rep* 2013;15:377.
3. Daniel WG, Erbel R, Kasper W, Visser CA, Engberding R, Sutherland GR, Grube E, Hanrath P, Maisch B, Dennig K, et al. Safety of transesophageal echocardiography. A multicenter survey of 10,419 examinations. *Circulation* 1991;83:817-821.

4.   Minardi G, Pino PG, Manzara CC, Pulignano G, Stefanini GG, Viceconte GN, Leonetti S, Madeo A, Gaudio C, Musumeci F. Preoperative scallop-by-scallop assessment of mitral prolapse using 2D-transthoracic echocardiography. *Cardiovasc Ultrasound* 2010;8:1.

5.   Monin JL, Dehant P, Roiron C, Monchi M, Tabet JY, Clerc P, Fernandez G, Houel R, Garot J, Chauvel C, Gueret P. Functional assessment of mitral regurgitation by transthoracic echocardiography using standardized imaging planes diagnostic accuracy and outcome implications. *J Am Coll Cardiol* 2005;46:302-309.

6.   Sharma R, Mann J, Drummond L, Livesey SA, Simpson IA. The evaluation of real-time 3-dimensional transthoracic echocardiography for the preoperative functional assessment of patients with mitral valve prolapse: a comparison with 2-dimensional transesophageal echocardiography. *J Am Soc Echocardiogr* 2007;20:934-940.

7.   Tamborini G, Muratori M, Maltagliati A, Galli CA, Naliato M, Zanobini M, Alamanni F, Salvi L, Sisillo E, Fiorentini C, Pepi M. Pre-operative transthoracic real-time three-dimensional echocardiography in patients undergoing mitral valve repair: accuracy in cases with simple vs. complex prolapse lesions. *Eur J Echocardiogr* 2010;11:778-785.

8.   Nemes A, Geleijnse ML, Krenning BJ, Soliman OI, Anwar AM, Vletter WB, Ten Cate FJ. Usefulness of ultrasound contrast agent to improve image quality during real-time three-dimensional stress echocardiography. *Am J Cardiol* 2007;99:275-278.

9.   McGhie JS, van den Bosch AE, Haarman MG, Ren B, Roos-Hesselink JW, Witsenburg M, Geleijnse ML. Characterization of atrial septal defect by simultaneous multiplane two-dimensional echocardiography. *Eur Heart J Cardiovasc Imaging* 2014;15:1145-1151.

10. McGhie JS, Vletter WB, de Groot-de Laat LE, Ren B, Frowijn R, van den Bosch AE, Soliman OI, Geleijnse ML. Contributions of simultaneous multiplane echocardiographic imaging in daily clinical practice. *Echocardiography* 2014;31:245-254.

11. Lancellotti P, Tribouilloy C, Hagendorff A, Popescu BA, Edvardsen T, Pierard LA, Badano L, Zamorano JL, Scientific Document Committee of the European Association of Cardiovascular I. Recommendations for the echocardiographic assessment of native valvular regurgitation: an executive summary from the European Association of Cardiovascular Imaging. *Eur Heart J Cardiovasc Imaging* 2013;14:611-644.

12. Sugeng L, Coon P, Weinert L, Jolly N, Lammertin G, Bednarz JE, Thiele K, Lang RM. Use of real-time 3-dimensional transthoracic echocardiography in the evaluation of mitral valve disease. *J Am Soc Echocardiogr* 2006;19:413-421.

13. Carpentier AF, Lessana A, Relland JY, Belli E, Mihaileanu S, Berrebi AJ, Palsky E, Loulmet DF. The "physio-ring": an advanced concept in mitral valve annuloplasty. *Ann Thorac Surg* 1995;60:1177-1185; discussion 1185-1176.

14. Adams DH, Anyanwu AC. Seeking a higher standard for degenerative mitral valve repair: begin with etiology. *J Thorac Cardiovasc Surg* 2008;136:551-556.

15. Adams DH, Anyanwu AC. The cardiologist's role in increasing the rate of mitral valve repair in degenerative disease. *Curr Opin Cardiol* 2008;23:105-110.

16. Ghosh N, Al-Shehri H, Chan K, Mesana T, Chan V, Chen L, Yam Y, Chow BJ. Characterization of mitral valve prolapse with cardiac computed tomography: comparison to echocardiographic and intraoperative findings. *Int J Cardiovasc Imaging* 2012;28:855-863.

17. Beraud AS, Schnittger I, Miller DC, Liang DH. Multiplanar reconstruction of three-dimensional transthoracic echocardiography improves the presurgical assessment of mitral prolapse. *J Am Soc Echocardiogr* 2009;22:907-913.

18. Pepi M, Tamborini G, Maltagliati A, Galli CA, Sisillo E, Salvi L, Naliato M, Porqueddu M, Parolari A, Zanobini M, Alamanni F. Head-to-head comparison of two- and three-dimensional transthoracic

and transesophageal echocardiography in the localization of mitral valve prolapse. *J Am Coll Cardiol* 2006;48:2524-2530.

19. Agricola E, Oppizzi M, Pisani M, Maisano F, Margonato A. Accuracy of real-time 3D echocardiography in the evaluation of functional anatomy of mitral regurgitation. *Int J Cardiol* 2008;127:342-349.

20. Gutierrez-Chico JL, Zamorano Gomez JL, Rodrigo-Lopez JL, Mataix L, Perez de Isla L, Almeria-Valera C, Aubele A, Macaya-Miguel C. Accuracy of real-time 3-dimensional echocardiography in the assessment of mitral prolapse. Is transesophageal echocardiography still mandatory? *Am Heart J* 2008;155:694-698.

21. Ben Zekry S, Nagueh SF, Little SH, Quinones MA, McCulloch ML, Karanbir S, Herrera EL, Lawrie GM, Zoghbi WA. Comparative accuracy of two- and three-dimensional transthoracic and transesophageal echocardiography in identifying mitral valve pathology in patients undergoing mitral valve repair: initial observations. *J Am Soc Echocardiogr* 2011;24:1079-1085.

22. El-Chami MF, Martin RP, Lerakis S. Esophageal dissection complicating transesophageal echocardiogram--the lesson to be learned: do not force the issue. *J Am Soc Echocardiogr* 2006;19:579 e575-577.

CHAPTER 5

A new method to measure circumferential extent of paravalvular leakage after transcatheter aortic valve implantation: iRotate Echocardiography

Luigi F.M. Di Martino
Jackie S. McGhie
Ernest Spitzer
Ben Ren
Osama I.I. Soliman
Nicolas M. Van Mieghem
Peter P.T. de Jaegere
Marcel L. Geleijnse

ABSTRACT

Introduction

Parasternal short-axis (SAX) assessment of circumferential extent of paravalvular leakage (PVL) in patients who had undergone transcatheter aortic valve implantation (TAVI) potentially underestimates PVL. iRotate echocardiography from an apical recording may be a new method to assess the circumferential extent of PVL.

Methods

The study included 41 consecutive outpatient patients (21 men, mean age 80±10 years) who had undergone TAVI with the CoreValve System©. All patients underwent assessment of PVL circumferential extent by SAX analysis and iRotate echocardiography. From the standard 5-chamber view the probe was held in the same position and images were recorded at 15 degrees intervals to cover the whole circumference of the TAVI prosthesis.

Results

iRotate echocardiography was feasible in all patients and induced no loss in spatial or temporal resolution so image quality. Circumferential extent correlated well with SAX (r = 0.84, p < 0.001) although a bias of 6.0% (limits of agreement: ±19.7%) with a significant larger circumferential extent with iRotate (13.7% ± 17.0% vs. 7.7% ± 10.1%, p < 0.001) was observed. Individual case analyses revealed, apart from suspected underestimation due to acoustic shadowing, impaired SAX quality and jets separated by echo-dense areas as causes for PVL underestimation by SAX analysis and non-central alignment in the stent by iRotate echocardiography as a possible cause for (relative) overestimation by iRotate echocardiography.

Conclusions

iRotate echocardiography from an apical view is a feasible method to study the circumferential extent of PVL after TAVI. Future studies should provide more insight whether iRotate overestimates or SAX analysis underestimates circumferential extent of PVL.

INTRODUCTION

Paravalvular leakage (PVL) is an important issue in transcatheter aortic valve implantation (TAVI) because of its impact on mortality.[1,2] Ideally, the circumferential extent of PVL serves as measure of severity. Unfortunately, the colour Doppler analysis of the parasternal short-axis (SAX) TAVI view suffers from important limitations that may result in PVL severity underestimation because of impaired echocardiographic window quality and interaction of calcium, crushed native material or the stent prosthesis with the echo beam.[3,4] Colour Doppler imaging from an apical window does not suffer from this limiting interaction but the routinely used 3-chamber and 5-chamber apical views reflect only a very small proportion of the TAVI prosthesis circumference.

Newly developed iRotate echo transducers may allow a full electronic rotation of 360° (adjustable by 5° steps) around the TAVI prosthesis with excellent spatial and temporal resolution.[5–8] Similarly as studying the PVL extent of a mitral prosthesis with transoesophageal echocardiography it may now be possible to study the circumferential PVL extent of a TAVI prosthesis by use of iRotate colour Doppler from one standard transthoracic apical view. Importantly, by this imaging PVL method interference by calcium, crushed native material or the stent prosthesis is avoided. The aim of this paper is to propose this novel approach to assess the extent of PVL in patients who had undergone TAVI because of severe aortic stenosis.

METHODS

Patients

After exclusion of one patient with poor parasternal and apical window quality, forty-one consecutive patients (21 men, mean age 80 ± 10 years) were included in the study. All patients had undergone TAVI with the CoreValve Revalving System© and were evaluated by transthoracic echocardiography by one single highly experienced sonographer at 6 (n = 11), 12 (n = 17), 24 (n = 10) and 36 (n = 3) months after TAVI, respectively.

Standard echocardiographic evaluation

Standard transthoracic echocardiographic evaluation was performed using an iE33 ultrasound system (Philips Medical System, Best, the Netherlands) equipped with an X5–1 three-dimensional transducer. The circumferential extent of PVL was determined in the SAX view according to the standard method.[4,9] Stent shape eccentricity at the inflow part of the CoreValve prosthesis was defined as described before.[10]

iRotate echocardiographic evaluation

The ultrasound beam was aligned to the stent longitudinal axis in a standard apical long-axis 5-chamber view. Care was taken to image the stent in its maximal diameter (central axis) to avoid foreshortened views. With the probe held still in the same position, the

iRotate feature was applied to obtain color Doppler images from the entire TAVI prosthesis circumference. Images were stored every 15° until 180°, identifying the presence of PVL at both of the visible tips of the stent as seen in Figure 1. Thus, in total 14 images - including 28 stent sites - covering the whole 360° circumference of the TAVI stent were acquired (note the first and last image are mirror images and were only once considered). An image was considered "positive" for PVL at that site as a regurgitant aortic jet was clearly visible and in direct connection with the stent prosthesis. A color signal not directly connected to the TAVI prosthesis was considered as spreading of adjacent jets, and thus not scored. By counting the positive sites and multiplying for 15 degrees, derived the total circumferential extent of PVL. This iRotate circumferential extent was than compared with the circumferential extent assessed in the standard SAX view. By this method patients were classified (according to the average score of the two observers) as, 1) no PVL (note for this category no discrepancies were found between the two observers, 2) less PVL by iRotate, or 3) more PVL by iRotate. For individual analysis the last group was divided into patients with < 10%, between 10–20%, and > 20% larger circumferential extent by iRotate echocardiography.
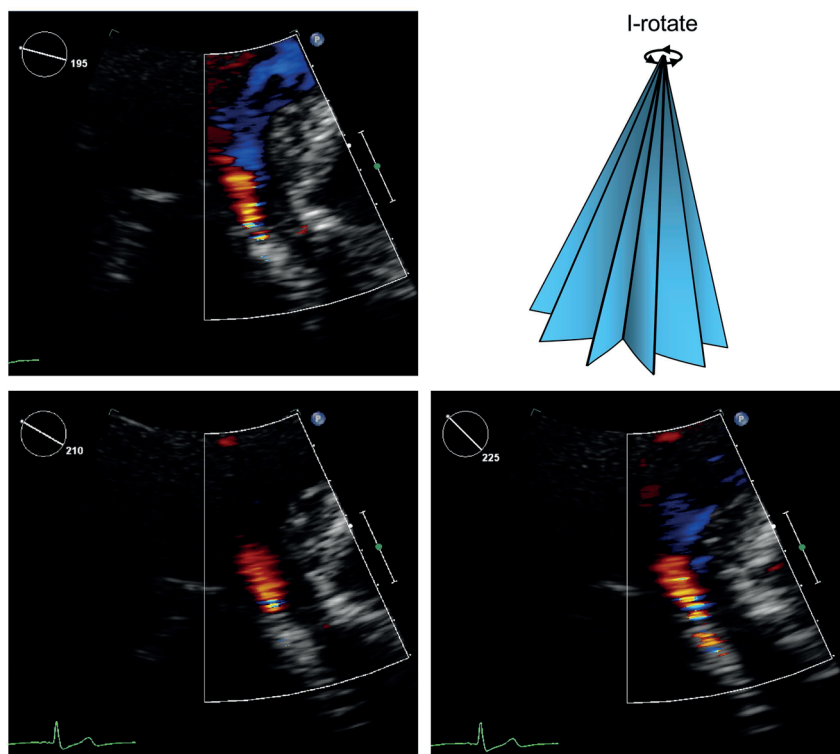
Figure 1 iRotate echocardiography from an apical window of PVL .Colour Doppler images are acquired at 15 degrees intervals covering the whole circumference of the TAVI prosthesis (in the Figure only 3 from the total number of 14 acquired images are displayed).

Inter-observer and test-retest variability

All 41 cases were analyzed independently by two observers for the assessment of inter-observer variability of SAX and iRotate circumferential extents. Test-retest analysis of iRotate was done in 10 patients studied at least 1 month apart but showing identical SAX circumferential extent of PVL by one observer.

Statistical analysis

Continuous variables were compared using the Student's t test, and the association between them was tested using Pearson's correlation and Bland-Altman analyses. A comparisons between populations was done according to the two-tailed Z-test. Test-retest and inter-observer variability were expressed as coefficient of variation (CV) calculated as the standard deviation of the inter-observer difference divided by the population mean; and, as the intra-class correlation coefficient with absolute agreement for single measures. Statistical analysis was performed with SPSS 23.0 (IBM, Armonk, NY, USA). All probability values were two-tailed, and a value of $P < 0.05$ was considered significant.

RESULTS

Feasibility of iRotate imaging

In the 41 included patients iRotate was analyzable in all. Because iRotate induces no loss in spatial or temporal resolution image quality was similar as standard apical 5-chamber quality and frame rate was 19 ± 2 frames per second.

Inter-observer and test-retest reproducibility

Reproducibility results are depicted in Table 1. Inter-observer variability was numerically lower for the iRotate-derived circumferential extent than for the SAX-derived (coefficient of variation 20% vs. 28%), while intra-class correlation coefficient was ≥ 0.95 for both. Test-retest reproducibility for iRotate-derived circumferential extent yielded a coefficient of variation of 17% and an intra-class correlation coefficient of 0.97.

Table 1 Inter-observer and test-retest reproducibility

n	Parameter	CV (%)	ICC
42	SAX CE inter-observer	28	0.95
42	iRotate CE inter-observer	20	0.97
10	iRotate CE test-retest	17	0.97

n = number of subjects; CV = coefficient of variation; ICC = intra-class correlation coefficient; SAX = short-axis; CE = circumferential extent.

Comparison of apical iRotate and parasternal SAX circumferential extent

Overall, iRotate circumferential extent was highly correlated with SAX circumferential extent (r = 0.84, *p* < 0.001). A bias of 6.0% (limits of agreement: ± 19.7%) with a significant

larger circumferential extent with iRotate (13.7% ± 17.0% vs. 7.7% ± 10.1%, p < 0.001) was observed. In 15 (37%) patients both the SAX and iRotate circumferential extent were 0% (no PVL present). When only patients with PVL were included in the analysis a larger difference was observed (20.8% ± 17.0% vs. 11.7% ± 10.4%, p < 0.001; r = 0.77, p < 0.001), with a mean bias of 9.2% ± 22.0%. More PVL with iRotate was seen in 10 (25%), 5 (12%), and 7 (17%) patients for the groups with < 10%, between 10–20% and > 30% difference, respectively. Mean differences in these groups between iRotate and SAX circumferential extent were 2% ± 2%, 15% ± 2%, and 27% ± 41%, respectively. Less PVL with iRotate was only seen in 4 (10%) patients (3% ± 1%).

Individual case analysis with large discrepant results (> 20%)

To identify specific causes of discrepancies we looked in detail to all 7 patients with large (> 20%) discrepancies in circumferential extent between the SAX and iRotate method.

False-negative SAX imaging

In 1 case with abnormal iRotate imaging at 6-months the SAX image was clearly false-negative (also at earlier and later dates). In addition to a recorded SAX level probably not distal enough from the stent reduced parasternal image quality may have contributed to this finding. Although a large difference was found in circumferential extent between the two techniques the overall impression with iRotate was that PVL was only mild because jets were minimal.

Multiple PVL localizations in connection with iRotate imaging

In 2 patients multiple PVL localizations were seen. With iRotate echo these spots seemed to be connected as one continuous jet (Figure 2).
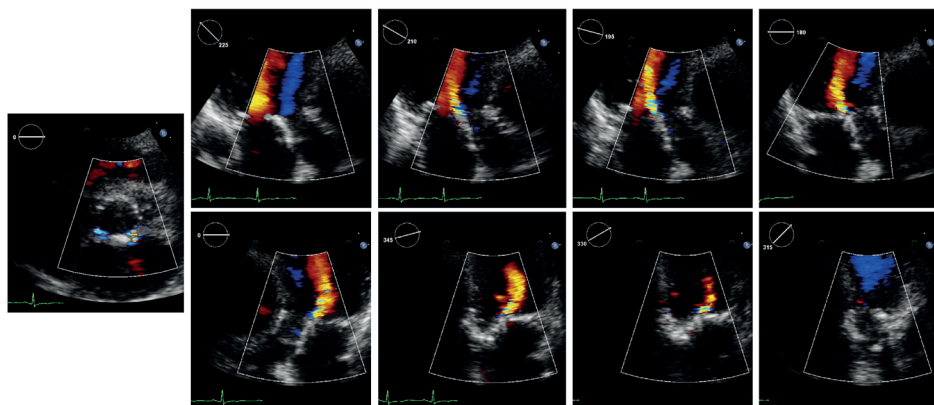
Figure 2 A patient with two small jets at SAX, separated by an echo-dense area whereas iRotate shows only one continuous broader jet

Other reasons

In the 4 remaining patients it was noted that they all had abnormally shaped stent frames (3 had a W-shape, 1 a R-shape, Figure 3) compared to 15 of the other 37 patients (100% vs. 39%, P < 0.05). In two patients with more extensive abnormalities at iRotate echocardiography it was suspected that rotation did not occur around the central axis of the stent (Figure 4).
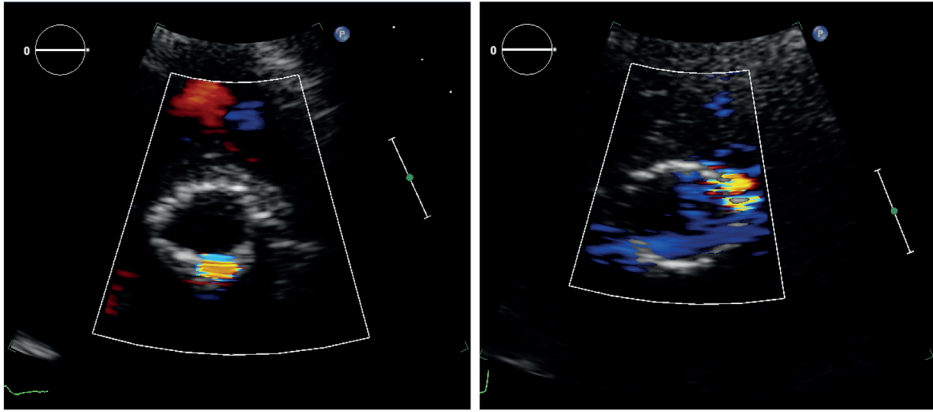
Figure 3 Examples of abnormal stent shapes in 2 patients with discrepancies between the SAX and iRotate circumferential extent of PVL.
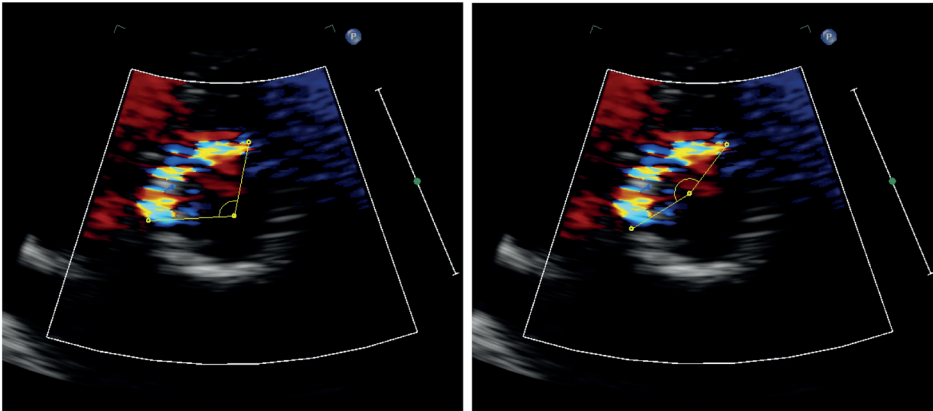
Figure 4 Potential overestimation of PVL with iRotate echocardiography. Correct imaging around the central axis gives a PVL circumferential extent of 105° (left) versus 160° with incorrect imaging (right).

DISCUSSION

The main findings of this study are 1) iRotate echocardiography is a feasible method to study the circumferential extent of PVL after TAVI from an apical view, and 2) although well correlated to the parasternal SAX analysis, circumferential extent of PVL was higher in a substantial number of patients.

The final estimation of PVL severity in TAVI patients should always integrate all available echocardiographic data.[4] The parasternal SAX circumferential extent of PVL is an essential part of the echocardiographic data.[9,11] Unfortunately, while giving an immediate result, this view may suffer from serious limitations linked to the ultrasound scan plane, inadequate parasternal window quality, eccentric jets and masking of PVL jets due to acoustic shadowing by the stent or the crushed native aortic annular material.[3] The latter is in particular important in the CoreValve prosthesis because compared to other TAVI stent designs it is supra-annular positioned and thus more susceptible for interference of crushed native material with imaging of PVL jets distal to the new leaflet plane. The standard apical 3-chamber and 5-chamber views do not suffer from these problems, but include only a very limited part of the TAVI prosthesis circumference. Three-dimensional echocardiographic visualization of PVL may seem a promising technique but suffers from reduced spatial resolution and extremely low color Doppler volume rates.[12]

The iRotate echocardiographic technique has recently been successfully used in multiple clinical settings.[5–8] In the present study it is shown that the whole TAVI prosthesis circumference can be reconstructed without a loss in spatial and temporal resolution compared to normal 2D scanning with a X5–1 transducer. When 15° intervals are used 13 images should be acquired rather than the 2 standard (3-chamber and 5-chamber) views. Other intervals such as 5°, 10° or 30° may also be chosen but the used interval is in our opinion a good balance between not missing jets and time-consumption of acquisition and analysis. Of note, as the standard apical views, iRotate echocardiography does not suffer from problems of acoustic shadowing. Identical or quite similar results between SAX analysis and iRotate were seen in 29 patients (71%). iRotate echocardiography showed significantly more circumferential extent of PVL in 12 patients (29%). The main issue not answered by this study is obviously whether iRotate overestimates or SAX analysis underestimates circumferential extent of PVL. In general several arguments can be given to support the hypothesis that parasternal SAX underestimates PVL severity. It has been shown that echocardiography (in contrast to angiography) does not correlate well with magnetic resonance in the assessment of PVL.[13] Echocardiographic analysis from a parasternal (long-axis) window underestimated regurgitation with approximately 25% of patients having a false negative study and 25% having a positive but underestimated study. In an echocardiographic study by our group also 14% of SAX images were false negative.[3] Also, in studies in which post-implantation angiographic and transthoracic parasternal echocardiographic data were compared the number of patients without PVL was clearly (up to three times) lower for echocardiography.[14] Apart from reduced parasternal window quality as seen in one patient with discrepant results seen in our series it is well known that increased gain settings and echogenic spots have destructive effects on color Doppler.[3] Interestingly, in

2 patients in our series two separately localizations of PVL seemed on iRotate analysis one continuous PVL jet. Finally, it remains intriguing that mild aortic regurgitation was linked to mortality in studies such as the PARTNER trial. It is well understood why severe PVL is related to mortality,[1,2] but the mechanism that underlies the association between less than severe PVL and mortality is still not well understood. Normally, patients with native aortic regurgitation can withstand the volume overload relatively well with an excess of mortality only seen in severe, symptomatic patients, as reflected in the surgical guidelines.[15] The relationship between PVL in TAVI patients and mortality is sometimes explained by the sudden change from a pressure overload to a volume overload regime in a stiff left ventricle.[16,17] However, it should be recognized that many patients have already aortic regurgitation before TAVI. One possible other explanation could be the underestimation of PVL regurgitation by the current method of analysis. Conversely, also arguments can be given that iRotate echocardiography overestimates PVL. Because the TAVI prosthesis is in motion in diastole in both the longitudinal direction and the elevation plane regurgitant jets in one part of the circumference may become visible in more than one iRotate image. Also, the resolution in the elevation plane is worst (about 3.0 mm). An important reason in a few patients for (relative) overestimation of PVL may be the non-central position of the echo beam in the TAVI stent, in particular in patients with abnormally shaped stent frames. From Figure 4 it can be appreciated that imaging not along the central axis of the stent prosthesis can easily lead to overestimation of the circumferential extent of PVL.

Limitations of the study

As mentioned in the previous section this study does not provide an answer whether iRotate overestimates or SAX analysis underestimates circumferential extent of PVL. This issue should be explored in future studies. Ideally, the circumferential extent of PVL should be correlated with regurgitant volumes. Unfortunately, calculation of regurgitant volumes in TAVI patients by the echo Doppler method seems not reliable.[18] A study incorporating PVL volume assessment by magnetic resonance imaging seems therefore necessary.[13,14]

The role of iRotate echocardiography in the specific interpretation of severity of eccentric PVL jets frequently seen in the CoreValve prosthesis should also be further explored.[3]

The exact orientation of the iRotate images with respect to the SAX can be extremely troublesome because the angle from which the 5-chamber view is recorded is not a fixed constant.

CONCLUSIONS

iRotate echocardiography from an apical view is a feasible method to study the circumferential extent of PVL after TAVI. It correlates well to the SAX analysis but in a substantial number of patients circumferential extent of PVL is higher. Future studies should provide more insight whether iRotate overestimates or SAX analysis underestimates circumferential extent of PVL.

REFERENCES

1. Kodali SK, Williams MR, Smith CR, Svensson LG, Webb JG, Makkar RR, Fontana GP, Dewey TM, Thourani VH, Pichard AD, Fischbein M, Szeto WY, Lim S, Greason KL, Teirstein PS, Malaisrie SC, Douglas PS, Hahn RT, Whisenant B, Zajarias A, Wang D, Akin JJ, Anderson WN, Leon MB, Investigators PT. Two-year outcomes after transcatheter or surgical aortic-valve replacement. *N Engl J Med* 2012;366:1686-1695.

2. Lefevre T, Kappetein AP, Wolner E, Nataf P, Thomas M, Schachinger V, De Bruyne B, Eltchaninoff H, Thielmann M, Himbert D, Romano M, Serruys P, Wimmer-Greinecker G, Group PEI. One year follow-up of the multi-centre European PARTNER transcatheter heart valve study. *Eur Heart J* 2011;32:148-157.

3. Geleijnse ML, Di Martino LF, Vletter WB, Ren B, Galema TW, Van Mieghem NM, de Jaegere PP, Soliman OI. Limitations and difficulties of echocardiographic short-axis assessment of paravalvular leakage after corevalve transcatheter aortic valve implantation. *Cardiovasc Ultrasound* 2016;14:37.

4. Pibarot P, Hahn RT, Weissman NJ, Monaghan MJ. Assessment of paravalvular regurgitation following TAVR: a proposal of unifying grading scheme. *JACC Cardiovasc Imaging* 2015;8:340-360.

5. McGhie JS, Menting ME, Vletter WB, Frowijn R, Roos-Hesselink JW, Soliman OI, van der Zwaan HB, Geleijnse ML, van den Bosch AE. A Novel 13-Segment Standardized Model for Assessment of Right Ventricular Function Using Two-Dimensional iRotate Echocardiography. *Echocardiography* 2016;33:353-361.

6. McGhie JS, Menting ME, Vletter WB, Frowijn R, Roos-Hesselink JW, van der Zwaan HB, Soliman OI, Geleijnse ML, van den Bosch AE. Quantitative assessment of the entire right ventricle from one acoustic window: an attractive approach. *Eur Heart J Cardiovasc Imaging* 2016.

7. McGhie JS, van den Bosch AE, Haarman MG, Ren B, Roos-Hesselink JW, Witsenburg M, Geleijnse ML. Characterization of atrial septal defect by simultaneous multiplane two-dimensional echocardiography. *Eur Heart J Cardiovasc Imaging* 2014;15:1145-1151.

8. McGhie JS, Vletter WB, de Groot-de Laat LE, Ren B, Frowijn R, van den Bosch AE, Soliman OI, Geleijnse ML. Contributions of simultaneous multiplane echocardiographic imaging in daily clinical practice. *Echocardiography* 2014;31:245-254.

9. Kappetein AP, Head SJ, Genereux P, Piazza N, van Mieghem NM, Blackstone EH, Brott TG, Cohen DJ, Cutlip DE, van Es GA, Hahn RT, Kirtane AJ, Krucoff MW, Kodali S, Mack MJ, Mehran R, Rodes-Cabau J, Vranckx P, Webb JG, Windecker S, Serruys PW, Leon MB, Valve Academic Research C. Updated standardized endpoint definitions for transcatheter aortic valve implantation: the Valve Academic Research Consortium-2 consensus document. *J Thorac Cardiovasc Surg* 2013;145:6-23.

10. Di Martino LF, Soliman OI, Vletter WB, Mieghem NM, Ren B, Galema TW, Schultz C, de Jaegere PP, Di Biase M, Geleijnse ML. Relation Between Calcium Burden, Echocardiographic Stent Frame Eccentricity and Paravalvular Leakage After CoreValve Transcatheter Aortic Valve Implantation. *EurJCI 2017 in press* 2017.

11. Leon MB, Piazza N, Nikolsky E, Blackstone EH, Cutlip DE, Kappetein AP, Krucoff MW, Mack M, Mehran R, Miller C, Morel MA, Petersen J, Popma JJ, Takkenberg JJ, Vahanian A, van Es GA, Vranckx P, Webb JG, Windecker S, Serruys PW. Standardized endpoint definitions for transcatheter aortic valve implantation clinical trials: a consensus report from the Valve Academic Research Consortium. *Eur Heart J* 2011;32:205-217.

12. Goncalves A, Almeria C, Marcos-Alberca P, Feltes G, Hernandez-Antolin R, Rodriguez E, Cardoso JC, Macaya C, Zamorano JL. Three-dimensional echocardiography in paravalvular aortic regurgitation assessment after transcatheter aortic valve implantation. *J Am Soc Echocardiogr* 2012;25:47-55.

13. Sherif MA, Abdel-Wahab M, Beurich HW, Stocker B, Zachow D, Geist V, Tolg R, Richardt G. Haemodynamic evaluation of aortic regurgitation after transcatheter aortic valve implantation using cardiovascular magnetic resonance. *EuroIntervention* 2011;7:57-63.

14. Sherif MA, Abdel-Wahab M, Stocker B, Geist V, Richardt D, Tolg R, Richardt G. Anatomic and procedural predictors of paravalvular aortic regurgitation after implantation of the Medtronic CoreValve bioprosthesis. *J Am Coll Cardiol* 2010;56:1623-1629.

15. Vahanian A, Alfieri O, Andreotti F, Antunes MJ, Baron-Esquivias G, Baumgartner H, Borger MA, Carrel TP, De Bonis M, Evangelista A, Falk V, Lung B, Lancellotti P, Pierard L, Price S, Schafers HJ, Schuler G, Stepinska J, Swedberg K, Takkenberg J, Von Oppell UO, Windecker S, Zamorano JL, Zembala M, Guidelines ESCCfP, Joint Task Force on the Management of Valvular Heart Disease of the European Society of C, European Association for Cardio-Thoracic S. Guidelines on the management of valvular heart disease (version 2012): the Joint Task Force on the Management of Valvular Heart Disease of the European Society of Cardiology (ESC) and the European Association for Cardio-Thoracic Surgery (EACTS). *Eur J Cardiothorac Surg* 2012;42:S1-44.

16. Azadani AN, Jaussaud N, Matthews PB, Ge L, Guy TS, Chuter TA, Tseng EE. Energy loss due to paravalvular leak with transcatheter aortic valve implantation. *Ann Thorac Surg* 2009;88:1857-1863.

17. Gotzmann M, Lindstaedt M, Mugge A. From pressure overload to volume overload: aortic regurgitation after transcatheter aortic valve implantation. *Am Heart J* 2012;163:903-911.

18. Di Martino LFM, Soliman OII, Vletter WB, Ren B, de Vries T, Galema TW, Van Mieghem NM, de Jaegere PP, Geleijnse ML. Quantitative Doppler for Estimation of Paravalvular Leakage after Transcatheter Aortic Valve Implantation. *J Heart Valve Dis* 2016;25:289-295.

CHAPTER 6

Tricuspid valve disease: imaging using transthoracic echocardiography

Osama Ibrahim Soliman
Jackie S. McGhie
Ashraf M. Anwar
Mihai Strachinaru
Mohammad Abdelghani
Marcel L. Geleijnse
Folkert J. ten Cate

CHAPTER 7

Three-dimensional echocardiography in congenital heart disease: an expert consensus document from the European Association of Cardiovascular Imaging and the American Society of Echocardiography

John Simpson
Leo Lopez
Philippe Acar
Mark Friedberg
Nee Khoo
Helen Ko
Jan Marek
Gerald Marx
Jackie McGhie
Folkert Meijboom
David Roberson
Annemien Van den Bosch
Owen Miller
Girish Shirali

INTRODUCTION

Three-dimensional echocardiography (3DE) has become important in the management of patients with congenital heart disease (CHD), particularly with pre-surgical planning, guidance of catheter intervention and functional assessment of the heart. 3DE is increasingly used in children because of good acoustic windows and the non-invasive nature of the technique. The aim of this paper is to provide a review of the optimal application of 3DE in CHD including technical considerations, image orientation, application to different lesions, procedural guidance and functional assessment.

THREE-DIMENSIONAL ECHOCARDIOGRAPHIC IMAGING TECHNIQUES

Transducers

The evolution of 3DE techniques and transducer technology has been well described.[1–3] The development of the matrix array probe with parallel processing has made real-time 3DE possible since the 1990s.[4,5] Later generations of transducers have become smaller with footprints similar to two-dimensional echocardiography (2DE) transducers. The development of a small high frequency paediatric 3DE transducer (2–7MHz) has enhanced spatial and temporal resolution; especially pertinent for small children with high heart rates.[6,7] Similarly, miniaturisation has enabled the development of adult-size 3D transoesophageal echocardiography (TOE) probes.[8]

Workflow

Ideally, 3DE transducers should be capable of producing 2D images which are at least equivalent to 2DE transducers. Some 3D transoesophageal transducers achieve this, but transthoracic 3DE probes still do not generally match the image quality of a dedicated 2D transducer. The difference remains most marked for high frequency paediatric 3DE probes compared to the 2DE equivalent transducer. Consequently, the use of the combined 2DE-3DE transducer is not routine in smaller patients. Manufacturer recommendations suggest current 3D TOE probes are used for patients > 30kg. Some paediatric cardiologists will extend use of such probes to smaller patients. Those undertaking such procedures should be aware of the specific manufacturer recommendation for the transducer. In any patient, the risk of complications such as damage to the oropharynx and oesophagus caused by an oversized probe needs to be balanced against the additional value of 3DE. For patients who are currently too small to accommodate 3D TOE transducers, epicardial 3D imaging with a transthoracic 3DE transducer is a feasible alternative technique during surgery.[9]

Data Acquisition modes

Good spatial and temporal resolution in 3DE is a priority for imaging of CHD, particularly valve pathology and complex lesions. The matrix transducer has different modalities

of data acquisition whose use is dictated by the clinical question. For example, in the assessment of double outlet RV, incorporation of the AV valves, ventricular septum and great arteries is necessary for decision-making, whereas measuring the size of an isolated VSD does not require such an extended field of view. The exact configuration and nomenclature of different modes is vendor specific but with features in common.

2D Simultaneous multiplane mode

Current matrix probes allow 360° electronic rotation of the imaging plane as well as simultaneous display of more than one 2D imaging plane that can be electronically steered in the elevation or lateral plane. The crop plane is marked on the projection but with the drawback that temporal resolution is reduced.[10] Applications include assessment of atrial septal defect (ASD) size and rim length,[11] size and shape of VSDs, AV valve morphology and regurgitation (Figure 1A and B), outflow tracts and arterial valves.
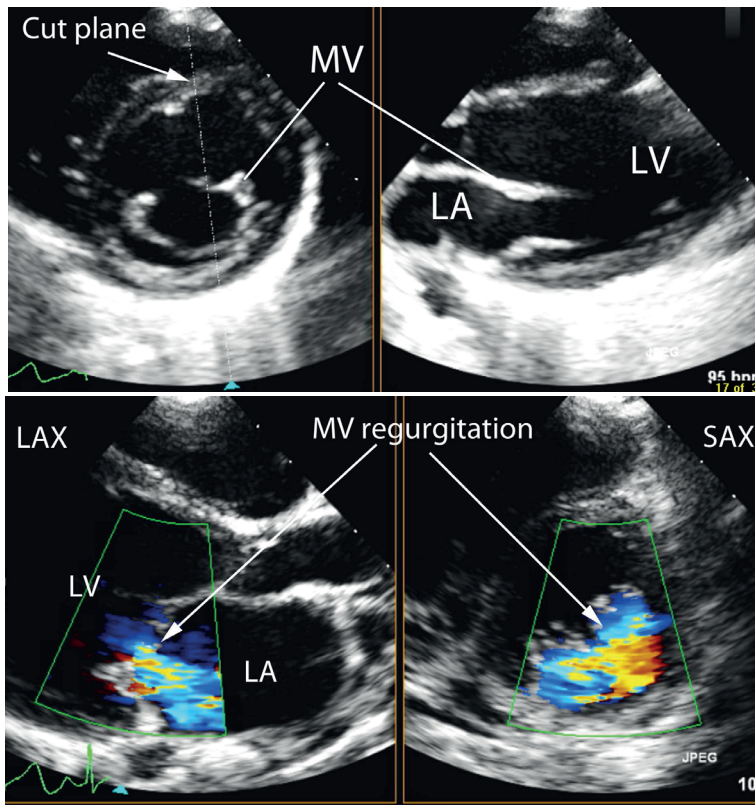
Figure 1 Cross-plane imaging. (**A**) Cross-plane imaging of the mitral valve by transthoracic echocardiography showing the user defined cut plane (dotted line and triangle) to show a short-axis view of the mitral valve (left panel) and the corresponding long-axis view (right panel). (**B**) Cross-plane imaging of mitral valve regurgitation which permits precise localisation of regurgitant jets in the long-axis (left panel) and short-axis views (right panel). The cut plane is indicated by the triangle. LAX, long axis; SAX, short axis; LV, left ventricle; LA, left atrium; MV, mitral valve.

Real-time 3DE mode

Real-time 3DE permits a display of an adjustable pyramidal volume, minimising the issue with poor co-operation in children because there is no potential for "stitch" artefacts between adjacent subvolumes. Increasing the region of interest decreases frame rate, and the limited field of view is a disadvantage for complex CHD where the relationship of different structures to each other is crucial for decision-making. Some manufacturers have a further 3D mode which permits the operator to select an area of interest but with relatively low frame rates particularly if colour flow Doppler is added. This mode is mainly used during catheter intervention, particularly ASDs, VSDs and the AV valves. Depending on the system, vendor settings may be adjusted to allow the operator to prioritise volume rate at the expense of line density, thus achieving a higher temporal but lower spatial resolution.

ECG gated multi-beat acquisition

With current imaging technology, ECG-gated multi-beat image acquisition is frequently used for paediatric 3DE because it acquires a large field of view with sufficient temporal resolution. However, the electronic "stitching" of narrow volumes of data over 2–6 heartbeats may produce artefacts related to patient breathing or movement, particularly in young children. This is not an issue in ventilated children under general anaesthesia, because ventilation can be suspended briefly, and is less of a problem during sleep or with sedation. Although "single beat" volume acquisition has been introduced, the limited temporal resolution is insufficient for high heart rates of infants and children unless the region of interest is small thereby permitting narrowing of the imaging sector, or if the region of interest is relatively static.

3DE colour flow Doppler

3DE colour flow Doppler can be added to any of the above modalities. In common with 2DE, the addition of colour flow Doppler reduces temporal resolution. Depending on the size of the region of interest, the achievable frame rate may be too low for fast moving structures such as AV valves. Some manufacturers may permit the user to prioritise temporal resolution over spatial resolution to maintain an acceptable frame rate. The alternative is to use an ECG gated multi-beat acquisition to maintain an acceptable frame rate.

Principles of 3DE acquisition

3DE for CHD utilises the same transducers and ultrasound systems as adults with the addition of high frequency probes suitable for imaging babies and children. General points are summarised below with emphasis on points relevant to the child or adult with CHD. In all patients, meticulous attention to 2D image quality is necessary to optimise the quality of the 3DE dataset. A high-frequency 3DE transducer should be used where possible, especially in small children where ultrasound penetration is not an issue, and the sector width narrowed to include only the regions of interest. Axial resolution is higher than either lateral or elevational planes which impacts on the optimal transducer position for the lesion being evaluated. For example, the mitral valve may be interrogated either from apical or paraster-

nal view to delineate both leaflets and the subvalvar apparatus.[12] Review of the multiplanar images is particularly important prior to display of rendered images to avoid diagnostic error. Comprehensive reviews of 3DE artefacts have been published for reference.[13]

Imaging of relatively static cardiac structures, such as ASDs and VSDs, may be achieved using live 3DE or 3DE 'zoom' modes because temporal resolution is sufficient. Gain settings during acquisition and post-processing are particularly important in smaller patients with thin valves to reduce 'noise' that may impede visualisation (Figure 2A and B) while avoiding "holes" or other artefacts from inadequate gain. The normal gain setting for a 3DE acquisition is slightly higher than conventional 2DE as gain can be reduced during post-processing to optimise the image whereas if too little gain is used during acquisition, increasing gain during post-processing does not restore parts of the image which have not been adequately visualised during the acquisition. This affects thin structures such as valve leaflets in particular.
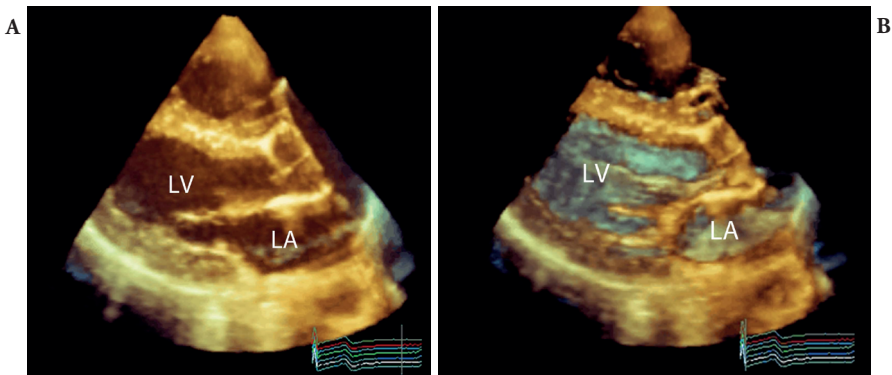
Figure 2 Effect of gain setting on 3D images. (**A**) Transthoracic PSLAX view of the LV with inappropriately high gain settings. The cavity of the LA and LV is opaque and consequently there is no perception of depth in the image. (**B**) With appropriate reduction of gain, intracavity noise has been removed and far-field structures can be visualised. In this example, far-field structures are colour coded blue grey and near field brighter and yellow-brown. LV, left ventricle; LA, left atrium

Presentation of 3DE images of CHD merits particular consideration, especially for valves, and individualised tilt or rotation to display the region of interest can help (Figure 3A and B). The 3D display modes for CHD are analogous to those used for adults and include (i) volume rendering, (ii) surface rendering and (iii) multi-planar reformatted (MPR) image display.[14,15] Volume rendered datasets can be electronically segmented, allowing the operator to 'crop' the heart in multiple sections to expose the cardiac structure of interest from any desired angle. This is especially useful for CHD prior to surgery or intervention. Surface rendering presents the surfaces of structures or organs with a solid appearance and is mainly used to visualise size, shape and function of cardiac structures.[16] Analysis software for this mode includes semi and fully automated endocardial border detection for quantification of left ventricular (LV) and RV function[17,18] as well as semi-automated mitral leaflet motion detection for quantification of valve function, both of which may be limited by the abnormal ventricular shape or valve morphology found in CHD.
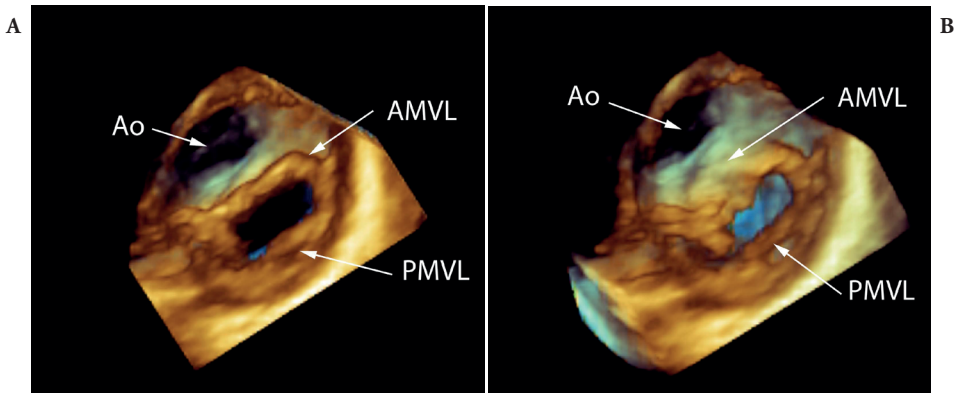
Figure 3 Rendered views of the mitral valve by transthoracic 3DE. (**A**) This is a projection of a normal mitral valve viewed from the ventricular aspect. The mitral valve is viewed directly en face so that the leading edge of the anterior and posterior leaflets can be visualised along with the aorta in the far-field. (**B**) This is a similar projection of the mitral valve to that shown in (**A**). However, the rendered image has been angulated slightly so that the depth of the anterior leaflet of the mitral valve can be visualised. This assists in imaging of abnormalities in this region such as true clefts of the mitral valve or the bridging leaflets in atrioventricular septal defects. Ao, aorta; AMVL, anterior mitral valve leaflet; PMVL, posterior mitral valve leaflet.

MPR allows the 3DE dataset to be viewed on a quad screen with the 3D dataset cut into three planes (sagittal, coronal, transverse), which are configurable, by the user. Adjustment of the MPR planes is illustrated in see Supplementary data online, *Powerpoint 1*. This display of planes not available by 2DE can aid with understanding complex anatomies and facilitate measurement of many CHDs such as ASD and VSD size. Valve areas, effective orifice areas and *vena contracta* areas of regurgitant jets can all be measured by manipulating cutting planes to avoid foreshortening or oblique measurements.[19–21]

Future Directions

Improved temporal resolution of single-beat acquisitions or post-processing software to deal with stitch artefacts would enhance 3DE in younger patients. Software packages that can accommodate analysis of valves and chambers of abnormal morphology would also benefit the patient with CHD.

Recommendations

The 3DE approach should be tailored according to the patient. Small footprint and high frequency 3DE transducers should be used in infants and young children and for epicardial 3DE.

3D TOE should be considered when patient size permits if 3D TTE provides insufficient imaging to plan therapy.

IMAGE DISPLAY AND ORIENTATION

Published standards have been produced for the echocardiographic assessment of patients with paediatric and CHD, including TTE,[22] TOE,[23] and quantification.[24] Recent published work has defined standards for adult practice using 3DE,[14] but the latter specifically excluded CHD. In the patient with CHD, cardiac position, situs, connections and alignments may be abnormal which presents a major challenge compared to acquired heart disease. 3DE facilitates *en face* projections of cardiac septums and AV valves,[25] which can be rotated in the z-plane to any desired orientation. If the analogy of a clock face is used, use of z-plane rotation turns the image in a clockwise or counter clockwise direction to achieve an anatomically correct orientation (see Supplementary data online, *Presentation 1*). The retention of adjacent anatomic landmarks is desirable, where possible, to assist orientation. Echocardiographic evaluation of the patient with CHD is often complemented by other imaging modalities including magnetic resonance imaging (MRI), computed tomography (CT) and angiography. To gain maximum value, the orientation of 3DE images should be both consistent and intuitive, as exemplified by the 'anatomic' approach to image display,[26] projecting the heart in the same orientation as a person standing in an upright position. With this approach, superiorly positioned structures will be displayed uppermost on the image. This anatomically correct approach is consistent with the projection of MRI and CT images.[26,27] The application of an anatomic orientation can be illustrated with specific examples.

The atrial septum

The atrial septum can be visualised from the right or left atrial aspect. A projection from the right atrium permits visualisation of important landmarks such as the superior vena cava, inferior vena cava, ascending aorta, tricuspid valve, oval fossa and os of the coronary
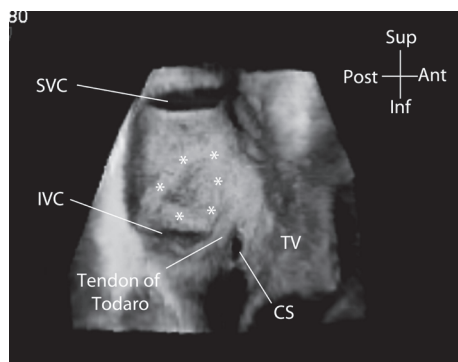
Figure 4 Normal atrial septum. Transoesophageal 3DE view of the normal atrial septum viewed from the right atrial aspect. The orientation of the image is anatomic so the superior vena cava and inferior vena cava are shown uppermost and lowermost on the image respectively. This image was acquired by 3D TOE using a full-volume acquisition over 4 cardiac cycles. The asterisk marks the margins of the oval fossa.
SVC, superior vena cava; IVC, inferior vena cava; TV, tricuspid valve; CS, coronary sinus.

sinus. The preferred anatomic image orientation has the superior vena cava uppermost and tricuspid valve seen to the right of the atrial septum (Figure 4).

The ventricular septum

The ventricular septum can be visualised from either the RV or LV aspect. By convention, the components of the ventricular septum are named as if the septum is viewed from the RV side with the free wall of the RV removed. With the anatomic approach, the diaphragmatic border of the heart is lowermost, the RV apex is seen to the right and the RV outflow tract viewed uppermost on the projected image so that landmarks such as the tricuspid valve,
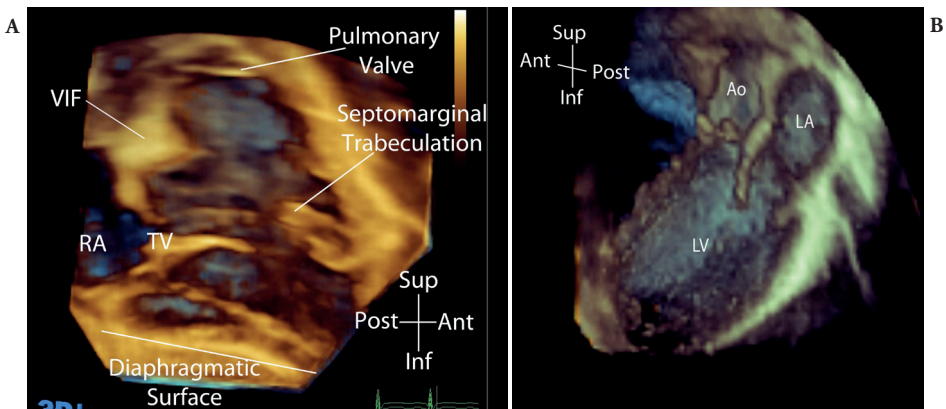
Figure 5 (**A**) Transthoracic rendered 3DE image of the right ventricular side of the normal ventricular septum. The free wall of the right ventricle has been cropped away in post-processing. The important landmarks can be readily identified including the tricuspid valve (TV), ventriculo-infundibular fold (IVF) and septomarginal trabeculation (septal band). This type of view can be used to project all types of ventricular septal defects. (**B**) Left side of the normal ventricular septum. A full-volume 3DE dataset was obtained by transthoracic 3DE in a parasternal long-axis view. The free wall of the left ventricle has been cropped away so that the ventricular septum can be directly visualised from the LV cavity. The smooth wall of the left ventricle can be appreciated.

VIF, ventriculo-infundibular fold; RA, right atrium; TV, tricuspid valve; Ao, aorta; LA, left atrium; LV, left ventricle.

moderator band and septomarginal trabeculation are seen in anatomically appropriate position (Figure 5A). Similarly, the LV aspect of the ventricular septum can be viewed in an anatomic projection (Figure 5B), to include both the septum and LV outflow tract.

AV valves

In CHD, the left-sided AV valve may not be a bileaflet valve of 'mitral' type and the right-sided AV valve may not be the tricuspid valve. Regardless of the morphology of the valve, or whether an *en face* view is projected from the ventricular or atrial aspect, the 3D rendered image is rotated so that the diaphragmatic surface of the heart is shown lowermost (Figure 6A and B). This means, for example, that the superior bridging leaflet
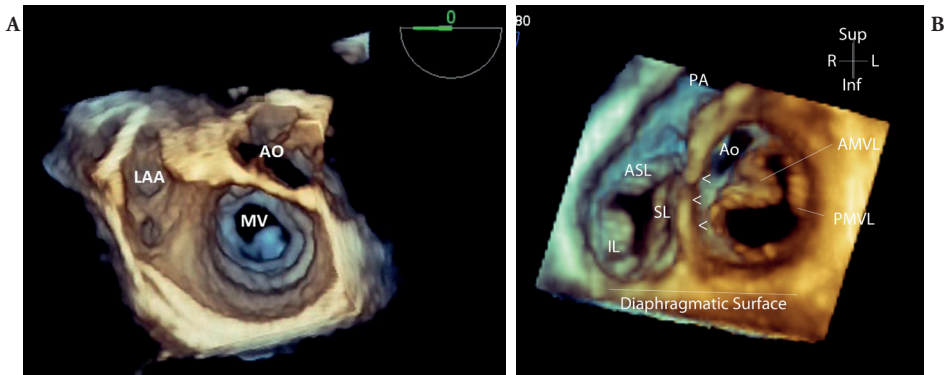
Figure 6 (**A**) Transoesophageal 3DE view of the mitral valve from the atrial side. The mitral valve, aortic valve and left atrial appendage are visualised from the atrial aspect in an anatomic orientation. If the annulus of the mitral valve is viewed as a clock-face, the aortic valve is at two o'clock with reference to the mitral valve. (**B**) Transososphageal 3DE view of the mitral and tricuspid valves from the ventricular side. The mitral and tricuspid valves are viewed from the ventricular aspect in an anatomic orientation. The aorta is at a 10 o'clock position with reference to the mitral valve. The inferior, septal and anterosuperior leaflets of the tricuspid valve are seen in anatomic orientation as well as the curved shape of the ventricular septum.

LAA, left atrial appendage; MV, mitral valve; ASL, anterosuperior leaflet of the tricuspid valve; IL, inferior leaflet of the tricuspid valve; SL, septal leaflet of the tricuspid valve; PA, pulmonary artery; Ao, aorta; AMVL, anterior mitral valve leaflet; PMVL, posterior mitral valve leaflet.
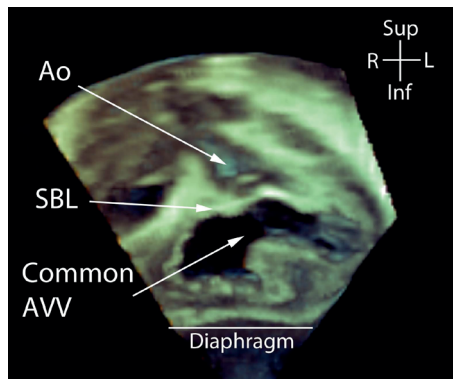
Figure 7 Transthoracic 3DE en face view of atrioventricular septal defect.En face view of a complete atrioventricular septal defect from the ventricular aspect, obtained using a subcostal view. The depth of field means that the superior bridging leaflet and the common atrioventricular valve are seen as well as the aorta in the far field.

Ao, aorta; SBL, superior bridging leaflet; AVV, Atrioventricular valve.

in an AV septal defect will be shown uppermost on the image and the inferior bridging leaflet lowermost (Figure 7).

Aortic and pulmonary valves

The morphology, position and patency of the aortic and pulmonary valves cannot be assumed in CHD. These valves are therefore projected in an anatomic format using the standard conventions for nomenclature of the valve leaflets. For example, the aortic valve may be projected as if seen from the ascending aorta or from the LV outflow tract. The conventional nomenclature of left, right and non-coronary leaflets and sinuses is used in exactly the same fashion as in 2DE. An example of the preferred orientation of the aortic valve is shown (Figure 8) and a similar approach is used for the pulmonary valve.
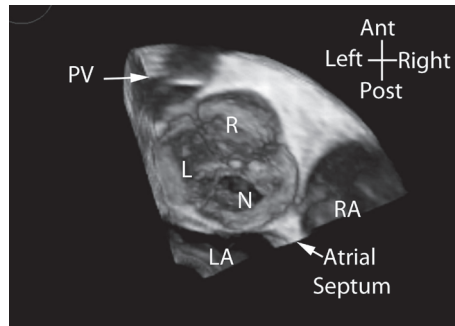
Figure 8 En face view of the normal aortic valve. Transoesophageal 3DE view of a normal aortic valve viewed from the aortic side of the valve.
R, right coronary leaflet; L, left coronary leaflet; N, noncoronary leaflet; LA, left atrium; RA, right atrium; PV, pulmonary valve.

Complex abnormalities of cardiac connections

When the main cardiac connections are abnormal, an anatomic presentation of images is particularly important so that the abnormal anatomy is displayed in a manner as close as possible to the actual spatial locations. An accurate understanding of the relationship of intracardiac structures has a direct impact on the surgical approach.

'Surgical' views of the heart

The term "surgical" view has been used to describe 3D projections that are most akin to the surgeon's view during an operation. There are specific considerations for this term, particularly in contrast to the 'anatomic' view. The anatomic view is projected as if the person is standing upright, whereas a surgical view is projected as if the patient is lying supine with the lead surgeon operating from the right side of the patient. The effect of this is that an anatomic *en face* view of the right side of the atrial or ventricular septum would be rotated counter clockwise 90 degrees when projecting a 'surgical' view (Figure 9). Views of the atrial aspect of the AV valves are often referred to as "surgical" even though the surgeon may take a different access route to repair the valve in question. For example, the truly surgical view of the mitral valve would be presented with the patient supine with the left atrium accessed through the atrial septum. This contrasts with the usual projected 3DE view obtained by cropping away the posterior aspect of the atriums and rotating the

AV valves *en face* with rotation of the whole dataset into an anatomic position. In practice, our preference is an anatomic orientation, which maintains consistency with projections of MRI and CT scans, knowing that 'surgical' visualisation of the structures may be different. A visual demonstration of the common manipulations of 3D datasets accompanies this document (see Supplementary data online, *Presentation 1*).
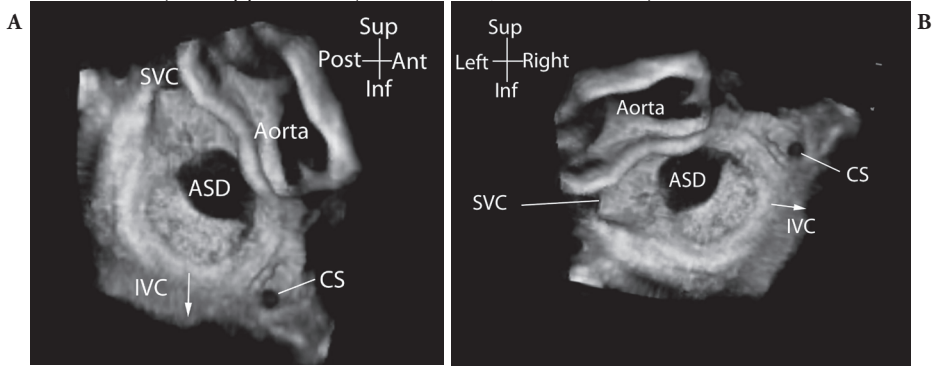
Figure 9 3D TOE views of 'Surgical' versus anatomic views of an atrial septal defect. (**A**) Atrial septal defect viewed from the right atrial aspect in an anatomic orientation with the superior vena cava uppermost and inferior vena cava lowermost on the image. (**B**) Atrial septal defect viewed from the right atrial aspect in a 'surgical' orientation where the defect is viewed from the right side in an analogous fashion to the patient in a supine position. This amounts to a 90° anticlockwise rotation of the anatomic projection.
SVC, superior vena cava; IVC, inferior vena cava; CS, coronary sinus.

Future Directions

The availability of orientation markers, already available for CT angiography and MRI, is needed for 3DE to mark, for example, the true left/right or superior/inferior orientation of an image. This should be coupled with the ability to 'landmark' important anatomical structures to enhance display of complex CHD as the data is manipulated. Fusion imaging, where 3DE datasets can be co-registered with datasets from other modalities (fluoroscopy, CT angiography, and MRI), will allow for both automated anatomic orientation of 3DE images and visualisation of regions which may be sonographically inaccessible. Widespread implementation would require co-registration across vendors, modalities, and platforms.

Recommendations

An 'anatomic' approach to image display is recommended as it reflects the real position of structures in space and is consistent with other modalities such as MRI and CT.

En face views of septums and AV valves should retain important landmarks and be rotated into a correct anatomic orientation.

The term "surgical" view should be used only for projections that show anatomy as the surgeon would visualise the region of interest.

OPTIMAL SONOGRAPHIC PROJECTIONS FOR DIFFERENT CONGENITAL HEART LESIONS

Standard imaging planes in 2DE have been developed from a combination of anatomical constraints and accessible sonographic windows, forming the basis for published standards.[22] 3DE is less constrained since post-processing will allow interrogation of structures contained within the acquired volume. A corollary is that a structure of interest can be displayed similarly after post-processing despite being acquired from a range of different echocardiographic windows. However, the principles of imaging physics apply as much to 3DE as they do to 2DE. For this reason, there are optimal approaches for data acquisition that should allow for optimal demonstration of the structure of interest. General recommendations can be made about the optimal acoustic windows to show different regions of interest. These include the following:

Table 1 Suggested transthoracic acoustic windows and utility of 3DE for CHD

	Subcostal	Apical	PLAX	PSAX	3D-TOE
ATRIAL SEPTUM					
ASD	+++	+ (modified)	+ (modified)	+ (modified)	+++
SV ASD	+++	-			+++
AV JUNCTION					
AVSD	+++	+++	++ (LAVV)	+ (LAVV)	+++
Ebstein's/TV dysplasia	+++	++ (Anterior angulation)	+	++	+
MV chordal structure	-	+ (smaller patients)	+++	++	**+++**
Double orifice MV	++	++	+	++	**++**
MVP	-	++	+++	++	**+++**
Parachute MV	++	++	++	++	**++**
Supra mitral membrane	-	++	+++	+	**+++**
VENTRICULAR SEPTUM					
mVSD (except anterior defects)	+++	++	+	+	**++**
Membranous VSD	+++	+	+	+	++
Doubly committed subarterial VSD	++	-	++ (Angled to PA)	+	++
OUTLETS					
Aortic valve	-	+	++	++	+++
Pulmonary valve	-	+	-	+	++
Double outlet right ventricle	+++	+	-	+	+

PLAX – parasternal long axis, PSAX – parasternal short axis, ASD – atrial septal defect, SV – sinus venosus, AVSD – atrioventricular septal defect, LAVV – left atrioventricular valve, TV – tricuspid valve, MV – mitral valve, MVP – mitral valve prolapse, VSD – ventricular septal defect, PA – pulmonary artery.

i.   Clear visualisation of the region of interest on 2DE
ii. Insonation orthogonal to the plane of the structure of interest where possible
iii. Inclusion of clinically relevant adjacent structures
iv. Optimisation of volume width and depth

For example, acquiring a 3D dataset to display an ASD is best achieved in a subcostal window because insonation from this view is orthogonal to the plane of the atrial septum. With TOE there is less flexibility to adjust the sonographic window; however, this is off-set by higher image quality than TTE.[28]

Although image quality is central to interrogation of regions of interest and good 3D reconstruction, there are important differences from 2DE. For example, parasternal long axis (PLAX) and parasternal short axis (PSAX) views are used in 2DE to evaluate a peri-membranous VSD (pmVSD) because the defect is in the near field, and good alignment to Doppler jets can be achieved. However, 3DE is especially useful for its ability to display VSDs *en face* and to delineate adjacent structures. PLAX and PSAX views are limited because of the small size of the ultrasound sector in the near field. Thus, subcostal and modified apical views may better define adjacent structures because the VSD is in the centre of the imaging field with a wider sector. This tailored approach is also employed for more complex lesions such as double outlet RV where AV valves, ventricular septum and outlets all have to be incorporated into the 3DE volume.[29] Table 1 summarises optimal TTE sonographic views and usefulness of 3D TOE for common forms of CHD.

Technical limitations may, however, persist irrespective of the imaging plane. Both the aortic and pulmonary valves are thin, rapidly moving structures. These are often imaged by 3D TTE using a PLAX or PSAX view where the plane of insonation does not lend itself to good quality rendering of the entirety of individual valve leaflets, particularly the body of the leaflet. This issue can be overcome by TOE in patients large enough to accommodate the 3D TOE probe.

Recommendations

Optimal sonographic projections for different congenital heart lesions
The angle of insonation should be tailored to the region of interest and ideally should be orthogonal to the relevant structure.

The size of 3DE region of interest should be adjusted to optimise temporal and spatial resolution.

Added value of 3DE for different congenital heart lesions
The literature on application of 3DE to CHD covers a wide variety of lesions including the AV valves, atrial septum, ventricular septum, as well as the outflow tracts. The use of 3DE techniques has increased as technology has improved, but there is wide institutional variability in the adoption of the technique. A central point in this regard is the evidence of additional diagnostic information compared to either 2DE or other imaging modalities. There have been no randomised trials relating to procedural success, morbidity or

Table 2 Use of 3DE in congenital lesions with normal cardiac connections

Region of interest	3D Modalities	Information acquired (I) Comment (C)	Strength of recommendation
Atrial septum	GS / CFM TTE/TOE	I: Size / number / shape /location of defects C: High value for multiple defects, multiple device deployment, residual leaks, spiral defects	HIGH for complex or residual defects MODERATE for single central defects LOW for PFO [11,28,30–33]
Tricuspid valve abnormality	GS / CFM TTE/TOE	I: Leaflet morphology Chordal support Delineation of regurgitant jets C: Mechanism/severity of regurgitation refined	HIGH [34–39]
Mitral valve	GS / CFM TTE/TOE	I: Leaflet morphology Chordal support Delineation of regurgitant jets C: Mechanism/severity of regurgitation refined	HIGH [9,12,40–42]
Ventricular septum	GS / CFM TTE/TOE	I: Size / number / shape /location of defects C: High value for multiple defects, unusually located defects or consideration of interventional closure	HIGH for more complex defects LOW for other defects [43–48]
Left ventricular outflow tract	GS / CFM TTE/TOE	I: Morphology of subaortic obstruction and aortic valve C: Clarify mechanism of obstruction and/or regurgitation	HIGH [19,49,50]
Aortic valve	GS / CFM TTE/TOE	I: Measurement of aortic valve Morphology of aortic valve leaflets Mechanism of aortic regurgitation C: Imaging of aortic valve leaflets more difficult by 3D TTE, 3D TOE preferred	HIGH Especially by TOE [21,51,52]
Aortic arch	GS / CFM TTE	I: Morphology and sizing of aortic arch C: Imaging may be difficult due to probe size, acoustic access	LOW / MOD [53]
Right Ventricular Outflow tract	GS / CFM TTE/TOE	I: RVOT morphology Visualisation of site of RVOT obstruction C: Questionable benefit over 2DE	LOW /MODERATE [54,55]
Pulmonary valve	-	I: PV morphology and function C: May be able to visualise PV morphology better than 2DE	Low [54,55]
Branch pulmonary arteries	-	Not routinely used	None

GS – greyscale, CFM – colour flow mapping, TTE – transthoracic echocardiography, TOE – transoesophageal echocardiography.

mortality related to the application of 3DE. Rather, 3DE has been adopted into practice on the basis of a clinical need to provide additional diagnostic information. Tables 2 and 3 present our consensus view of the added value of 3DE to assess some major groups of lesions. A selection of the key references relating to each of the different lesions is

Table 3 Use of 3D echo for the heart with abnormal cardiac connections

Abnormal cardiac connection	3D modalities	Information acquired (I) Comment (C)	Strength of recommendation
Systemic venous abnormalities	-	Not routinely used	No recommendation
Abnormal pulmonary venous drainage	-	Not routinely used	No recommendation
Atrioventricular septal defect	GS / CFM TTE/TOE	I: Size of atrial and ventricular components of the defect Leaflet morphology and chordal support Delineation of regurgitant jets Valvar and ventricular size in unbalanced defects C: Enhances measurement of valve size, chordal support and relative size of AV valves and ventricles	HIGH 9,40,41,56–59
Discordant atrioventricular connections	GS / CFM TTE/TOE	I: TV and MV morphology and function Location and size of associated VSDs Right and left ventricular outflow tract C: Improves assessment of feasibility of Senning / Rastelli approach. Improves localisation of VSDs	HIGH 60,61
Simple transposition of the great arteries	-	Not routinely used	No recommendation
Complex transposition of the great arteries	GS / CFM TTE/TOE	I: MV and TV morphology and size. Size, location of associated VSDs Anatomy of left or RV outflow tract obstruction C: Suitability for procedures such as Rastelli, Nikaidoh and arterial switch operations	HIGH 62,63
Tetralogy of Fallot	GS / CFM TTE	I: VSD size / location and RVOT anatomy C: Indicated where specific concerns e.g. VSD position or RVOT anatomy More extensive use for RV volume estimation postoperatively	LOW
Common arterial trunk	GS / CFM TTE / TOE	I: Truncal valve morphology / regurgitation C: Not routinely indicated in infancy May assist delineation of truncal valve morphology / regurgitation in older patients by TEE	HIGH for truncal valve in older patients LOW in infancy
Double outlet RV	GS / CFM TTE	I: Relationship of AV valves VSD size and location Relative position of great arteries C: High value for guiding appropriate type of repair	HIGH 29,63

GS – greyscale, CFM – colour flow mapping, TTE – transthoracic echocardiography, TOE – transoesophageal echocardiography.

also included within the tables as well as a summary of the additional information provided. The type of lesions for which 3DE has a major role is heavily weighted towards valvar lesions and defects in both the atrial and ventricular septum (see Supplementary
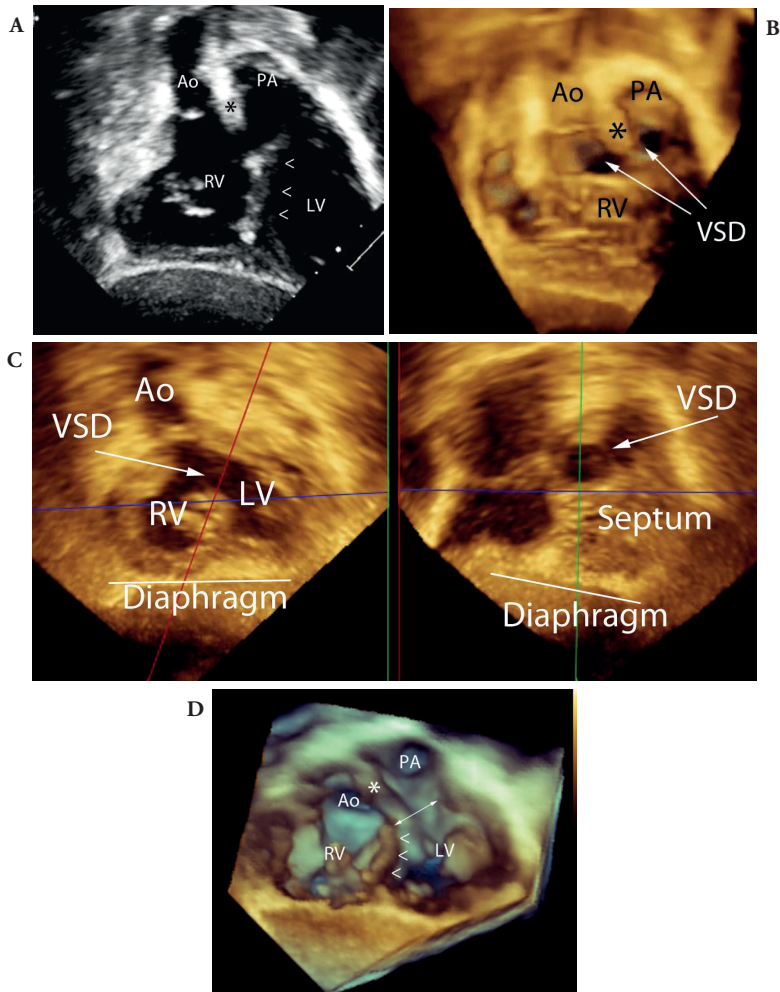
Figure 10 Transthoracic 3DE of double outlet right ventricle from a subcostal projection using a multi-beat acquisition. (**A**) Subcostal 2D echocardiographic view of double outlet right ventricle. The plane if the ventricular septum is shown by the arrows (<) and the outlet septum between the aorta and the pulmonary artery is shown by the asterisk. Note that the ventricular septal defect is not visualised as the outlet septum is entirely within the right ventricle and the plane of the ventricular septum would be posterior to the plane used in this image. (**B**) Subcostal 3D echocardiographic image of the same patient. The aorta (Ao) and the pulmonary artery (PA) are separated by the outlet septum (*). Due to the depth of field provided by the 3D image, the margins of the ventricular septal defect are clearly visualised. This is clinically important because the size and position of the ventricular septal defect may determine whether the left ventricle may be baffled to the aorta as part of the surgical repair. (**C**) MPR images showing the relationship of the ventricular septal defect to the aorta. The red plane is en face to the ventricular septal defect which is profiled in the right pane. This permits accurate measurement of the size of the ventricular septal. (**D**) 3D rendered image from the ventricular apex. The left ventricle and right ventricle are shown in short axis. The ventricular septum is shown by the arrowhead (<) and the ventricular septal defect is shown by the double-headed arrow. The depth of field of this projection shows the location of the ventricular septal defect, the outlet septum (*), and the relative position of the great arteries.

Ao, aorta; PA, Pulmonary artery; RV, right ventricle; LV, left ventricle; RV, right ventricle.

online *Appendix 1*, *Presentation*1). A good example of the application of 3DE to more complex CHD is decision-making in patients with double outlet RV where particular considerations include the size and location of the VSD, and the relative position of the great arteries (Figure 10A-D, Supplementary data online, Video *1A-D*). The depth of field enhances visualisation of the position and size of the VSD relative to the great arteries, and projections are achieved from the RV aspect and apex which cannot be achieved by 2DE.

Recommendations

Added value of 3DE for different congenital heart lesions
3DE is recommended for the assessment of valvar lesions, septal defects and complex abnormalities of the cardiac connections.

3DE should be regarded as a technique that complements rather than replaces 2DE for assessment of CHD

USE OF 3DE TO GUIDE CATHETER INTERVENTION

3D TOE is a rapid and useful imaging technique for the assessment of CHD during catheter-based interventions, including device closure of ASDs,[11,28,30–33,64–68] and VSDs.[43–45,68–70] 3D TOE complements rather than replaces 2D TOE, and both modalities are used to assess defects and adjacent margins, rims and structures. 3DE is particularly helpful for irregularly or asymmetrically shaped defects where 2D assessment of size by rotation of the TOE probe is insufficient. *En face* views of defects permit more precise appreciation of adjacent structures than 2D TOE alone, particularly for more complex lesions. 3D TOE of younger patients is typically done under general anaesthesia and is only feasible in patients large enough to accommodate the 3D TOE probe. Current manufacturers' recommendations propose a minimum patient weight of 30kg. Time is limited during the procedure; therefore rapid, simple, minimal post-processing real-time 3D acquisition modes are often most effective. A 3D full volume acquisition is favoured at some centres to produce a high-resolution view of the entire region of interest at the start of the procedure, followed by more focused imaging using live techniques. Lesion-specific targeted views have to be obtained, as discussed in subsequent sections. *En face* views are consistently used to demonstrate the relevant anatomy and interventional hardware. In addition to rendered 3D views, MPR imaging is useful for quantitation and image display during interventions[19] (Figure 10).

ASD device closure
Transcatheter device closure of a secundum ASD has become the preferred method of treatment when the anatomy is favourable.[71,72] Accurate assessment of ASD type, size, position, number of orifices, shape, and rim sizes (Figure 11) is essential for correct patient selection, device selection and deployment. Detailed analysis of device position, configu-
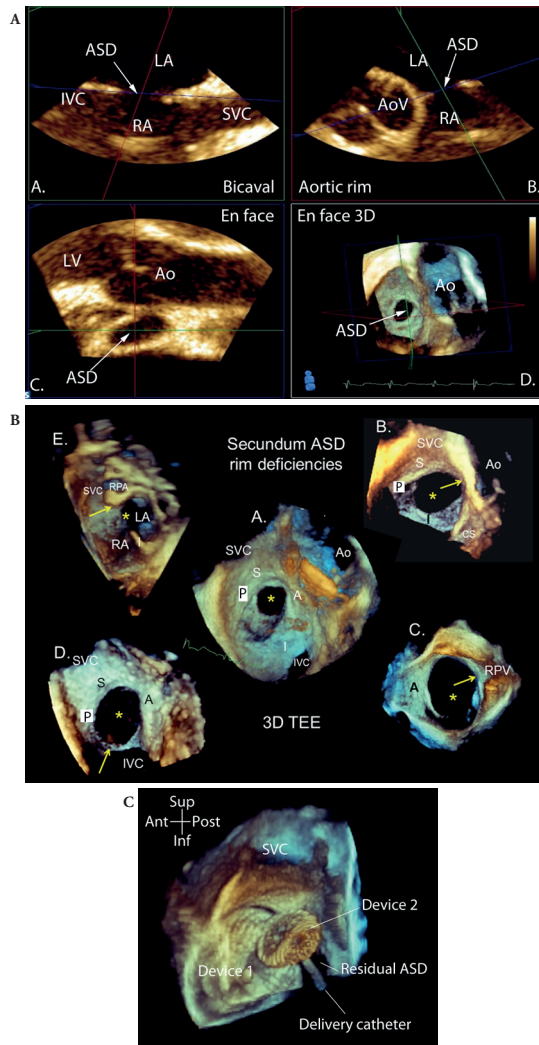
Figure 11 (**A**) 3D transoesophageal projection of MPR images of a secundum atrial septal defect. The blue plane is orientated to include the margins of the defect (*A* and *B*) which defines the en face projection shown in cross-section in (C) and rendered view in (D). The rims of the defect can be measured either on the MPR images or rendered image. (**B**). Transoesophageal 3DE rendered images of the morphology, size and rims of the atrial septal defect (*) of atrial septal defects with deficient rims in different regions. The zones where there is a deficient rim are marked with an arrow. The rims appear adequate throughout (*A*), deficient aortic rim (*B*), deficient right pulmonary vein rim (*C*), deficient inferior vena caval rim (*D*) and superior vena caval rim (*E*). Images (*A*), (*B*), and (*D*) are viewed from the right atrial side and Image (*C*) from the left atrial side. Image (*E*) cuts through the atrial septum so that the crest of the septum and the superior position of the defect can be visualised. (**C**). Transoesophageal real-time 3DE image of deployment of a second septal occluder to close a residual atrial septal defect. This 3D rendered projection from the left atrial aspect shows the relative position of the two septal occluders, the residual defect and the delivery catheter.

SVC, superior vena cava; IVC, inferior vena cava; LA, left atrium; RA, right atrium; Ao, aorta; RPV, right upper pulmonary vein; S, superior; P, posterior; A, anterior; I, inferior; LV, left ventricle; ASD, atrial septal defect; AoV, aortic valve; MPR, multiplanar reformatted.

ration, anchorage, residual shunt as well as the relationship of the device to the aorta, mitral valve, tricuspid valve, superior and inferior vena cava, and the pulmonary veins is necessary (Figure 11). Demonstration of these features is usually enhanced and at times only possible with 3DE.[30,31,64–67,73]

The 3D TOE right atrial *en face* views from the mid-oesophagus selecting the region of interest to produce real-time 3D images can often demonstrate the key features during secundum ASD intervention. 3D full volume acquisition may be needed if the volume rate using focused live 3D acquisition is too low. The deep trans-gastric sagittal bicaval view best demonstrates the inferior rim and septal length and provides a good view from which to monitor device deployment. Precise measurement of the ASD is best performed using the MPR 4 panel format, but measurement of the rendered image is an alternative (Figure 10). Colour Doppler flow analysis of the size, position and mechanism of residual shunts is best performed with live 3D colour or biplane imaging. There are reports of using transthoracic 3DE to guide ASD closure from a subcostal view.[73,74]

VSD device closure

Transcatheter closure of VSDs has developed as an alternative treatment to surgical closure of muscular VSDs (mVSDs) and pmVSDs.[75–81] Specific advantages of 3DE over 2DE are improved visualisation of the VSD shape, size, and location as well as characterization of the tricuspid pouch and surrounding structures.[43,44,46,68–70] *En face* presentation of the ventricular septum from both RV and LV aspects can be accomplished most expeditiously from a four-chamber view using live 3D (Figure 12) or ECG-gated full-volume acquisition. Monitoring of interventional device hardware and device deployment is seen in a frontal four-chamber view (Figure 12). Following device deployment, live 3DE, cross plane or MPR imaging with colour flow Doppler is optimal for assessing the interventional result.

Additional applications of 3DE guidance: 3D TOE has been used during catheter-based closure of Fontan fenestrations,[82] ruptured sinus of Valsalva aneurysms,[83] coronary artery fistulas[84,85] prosthetic valve para-valvar leaks,[86–88] atrial switch baffle leaks or obstruction,[89,90] atrial septum trans–septal puncture,[91] and biventricular pacemaker synchrony assessment and lead placement.[92] Recently, intracardiac echocardiography transducers have been developed with 3D capability in a segment of ~60x15° using a 10-French probe. Early work has demonstrated visualisation of the atrial and ventricular septums, aortic valve, mitral valve and atrial appendages for guidance of intervention.[93–95]

Future Directions

Miniaturisation of 3D TOE probes for use in smaller patients and enhanced automation are likely future developments. The introduction of 3D intracardiac probes will provide an alternative to the TOE approach. The application of fusion imaging of 3D TEE with fluoroscopy, 3D rotational angiography, cardiac MRI, and CT angiography is also likely to expand as interventions become more complex.
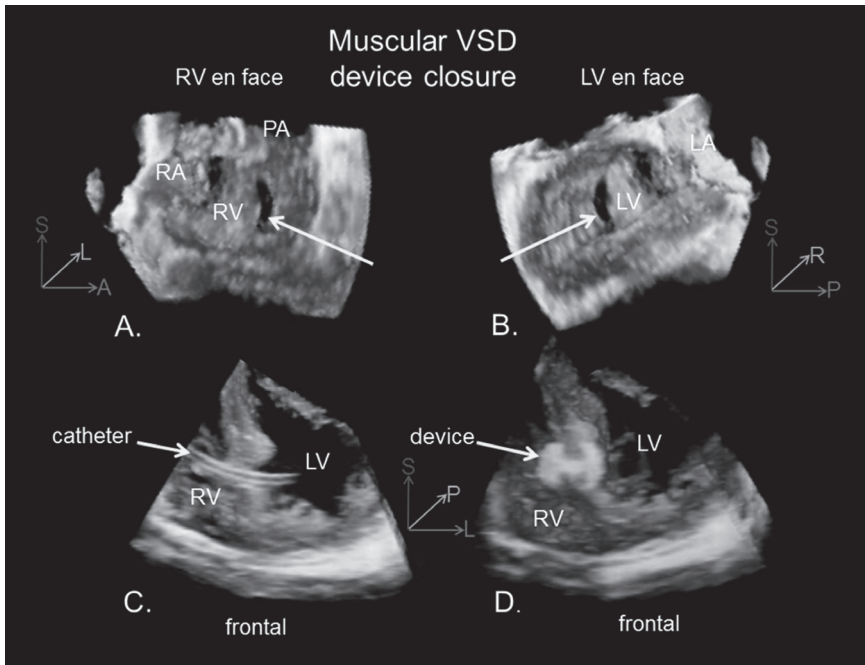
Figure 12 3DE permits en face visualisation of the ventricular septal defect to provide information on defect location, size and adjacent structures. In this example, 3D TOE was used. A muscular defect is seen from the right ventricular aspect (A) and LV aspect (B). During positioning of catheters (C) and device deployment (D) 3DE can assist. In each pane of this figure, the ventricular septal defect (VSD) is arrowed. RA, right atrium; LA, left atrium; RV, right ventricle; LV, left ventricle; PA, pulmonary artery; S, superior; L, left; R, right; P, posterior; A, anterior.

Recommendations

Use of 3DE to guide catheter based interventions

3DE is recommended to assist interventional closure of selected ASDs and VSDs, particularly multiple, irregularly shaped or residual defects.

Real-time 3D imaging is recommended for visualisation of catheters, delivery systems and devices during catheter intervention in CHD.

Use of 3DE to measure defects (either MPR or rendered 3D images) is recommended to assist interventional catheter procedures involving CHD.

THREE-DIMENSIONAL ECHOCARDIOGRAPHIC ASSESSMENT OF VENTRICULAR VOLUMES AND VENTRICULAR FUNCTION

There are many challenges with assessment of the RV and LV in patients with CHD, including abnormal cardiac position, abnormal connections, septal defects, non-contractile

patch material, and abnormal loading conditions. These difficulties are additive to generic considerations such as adequate temporal resolution to determine the chamber volume throughout the cardiac cycle with accuracy. Above all, however, in CHD ventricular geometry may be far removed from the normal geometry around which software packages have been designed, so that analysis algorithms may not be valid. Nonetheless, 3DE has been applied in CHD because assessment of cardiac volumes and function are being increasingly used to plan patient management,[54] and subjective assessment is unreliable.[96]

3DE assessment of the right ventricle

Assessment of RV size and function is important in clinical practice, particularly in patients with repaired tetralogy of Fallot (TOF) and other surgical repairs utilizing an RV to pulmonary artery conduit where RV measurements impact on the timing of pulmonary valve replacement. The position of the RV immediately behind the sternum complicates imaging windows, and sub-costal imaging may not be adequate beyond the early childhood years. Prominent trabeculations complicate endocardial border delineation, and normal RV geometry is complex with a triangular appearance in the sagittal plane and a crescent shape in the coronal plane. RV inflow and outflow tracts are also located in different imaging planes. All these hinder capturing the RV in its entirety by ultrasound and preclude the use of a simple geometrical formula to calculate volumes and ejection fraction (EF). 3DE has potential advantages for assessment of RV volume because it makes few assumptions about ventricular shape. Three 3DE techniques have been applied to measure RV volumes and EF, namely summation of discs, semi-automated border detection and knowledge-based reconstruction.

Summation of discs

The semi-automated method of disc summation is conceptually most comparable to MRI analysis and has been validated in children by water displacement[97] and MRI.[98] Feasibility of this method is good in healthy children (Table 4), although a recent study in older patients found feasibility in < 60%.[99] Although there is excellent correlation with MRI-derived RV volumes, the values from 3DE tend to be lower.[98]

   The disc summation method retains landmarks which may be abnormally positioned or absent in CHD.[18,113] Unfortunately, summation of disks methodology has been removed from some software packages, thereby removing the closest correlate with MRI.

Semi-automated border detection

This is the most common 3DE method to assess RV volumes and EF. A full-volume 3D data set is acquired and segmented into four-chamber, sagittal, and coronal views (Figure 13A). Key RV and LV anatomical landmarks are defined, and end-diastolic and end-systolic contours are manually drawn in each view to construct a dynamic polyhedron model of the RV (Figure 13A and B). In healthy adults, this methodology is feasible;[101,102.] volumes and EF correlate well with MRI, although 3DE underestimates volumes compared to MRI (Table 4). Acquisition time is significantly shorter for 3DE than for MRI (~5 vs.

Table 4 Published data on estimation of RV volumes by different echocardiographic techniques compared to values derived from magnetic resonance imaging.

Echo method and Reference	Population	N	Feasibility (%)	EDV Correlation/ agreement with MRI	ESV Correlation with MRI	EF Correlation with MRI	Mean difference EDV	Reproducibility (EDV) ICC (%) or limits of agreement (ml)	Test-retest
Method of discs									
Lu et al [98]	Healthy children	20	85%	r = 0.98	r = 0.96	r = 0.89	-3.2±7.0 ml	Intra: 2.1% ±5.3% Inter: 5.4%±9.2%	
Renella et al [99]	Varied, including normal and CHD	70	58%	-	-	-	-	Intra: -1.9 ml (-5.1 to 1.3) Inter: -2.0ml (-6.0 to 2.1)	-0.50 (-3.5 to 2.5)
Semi-automated border detection									
Maffessanti et al [100]	Healthy adults	540	94%	-	-	-	-	Intraobserver COV 2–8.6% Interobserver COV 7–15%	-
Tamborini et al [101]	Healthy adults	245	94%		-	-	-10 ml	Intra: 0.6±5.1 Inter: 0.9±20.3	0.2±6.9
Leibundgut et al [102]	Adults with cardiac dysfunction	100	92%	r = 0.84	r = 0.83	r = 0.72	-10 ml	Intra: ICC 0.93 Inter: ICC 0.95	
Jenkins et al [103]	Adults with cardiac dysfunction	54	93%	r = 0.6	r = 0.55	r = 0.78	-3±10 ml	Intra: r = 0.94, 1±3ml Inter: r = 0.76, 0±10	r = 0.91, 0±5
Dragulescu et al [104]	Children with CHD	70 (36 vs. MRI)	91%	r = 0.98	r = 0.98	r = 0.85	18.2±17.8	Intra: COV 5.4 Inter: 8	
Khoo et al [17]	Children with CHD	54	52%	r = 0.91	r = 0.9	r = 0.76	-19.3±6 14	Inter: ICC 0.97, 11.6±7.0	
Grewal et al [105]	Adults with CHD	25		r = 0.88	r = 0.89		-9%, max 34%	Inter: 10%	

Table 4 Published data on estimation of RV volumes by different echocardiographic techniques compared to values derived from magnetic resonance imaging. (continued)

Echo method and Reference	Population	N	Feasibility (%)	EDV Correlation/ agreement with MRI	ESV Correlation with MRI	EF Correlation with MRI	Mean difference EDV	Reproducibility (EDV) ICC (%) or limits of agreement (ml)	Test-retest
Van der Zwaan et al [106,107]	Adults with CHD	62	81%	r = 0.93	r = 0.91	r = 0.74	34 ml LOA -32 to 99	Intra: 1±12 Inter: ±	7%
Iriart et al [108]	Adults with repaired TOF	34	92%	r = 0.99 ICC = 0.99	r = 0.98 ICC = 0.98	r = 0.86 ICC = 0.85	18.7± 12.2	Inter: 0.4±0.3	
Grapsa et al [109]	Adults normal+PAH	80		r = 0.75 -3.7 ml LOA 52.6 ml	r = 0.74	-1.3% LOA 12.5		Inter: ICC 0.89	10.6%
Knowledge based reconstruction									
Dragulescu et al [110]	Children with TOF	30	100%	r = 0.99	r = 0.99	r = 0.87	-2.5±3.7ml	Intra: r = 0.997, Interr = 0.995	
Dragulescu et al [104]	Children with TOF (40 vs. MRI)	70	98%	r = 0.99	r = 0.99	r = 0.94	6.6±10.7	Intra: COV 3.4 Inter: COV 3.8	
Kutty et al [111]	Adolescents and adults with systemic RV	15	100%	r = 0.80	r = 0.82	r = 0.86	-4.3%	Intra: 3.2% Inter: 4.6%	
Single-beat full-volume capture									
Zhang et al [112]	adults normal and with cardiac dysfunction	61	96.7%	r = 0.97 Bias: 2.16 LOA: 15.1	r = 0.96 Bias: 2.6 LOA: 15.8	r = 0.71 Bias: 0.86 LOA: 16	2	Intra: ICC 0.97 Inter: ICC 0.97	EDV ICC 0.96, mean difference -1.7

EDV – end-diastolic volume, ESV – end-systolic volume, EF – ejection fraction, RV – right ventricle, MRI – magnetic resonance imaging, Intra - intraobserver, Inter - interobserver, Bias, LOA – bias and limits of agreement between two methods assessed by Bland Altman analysis, ICC – intra-class correlation coefficient.
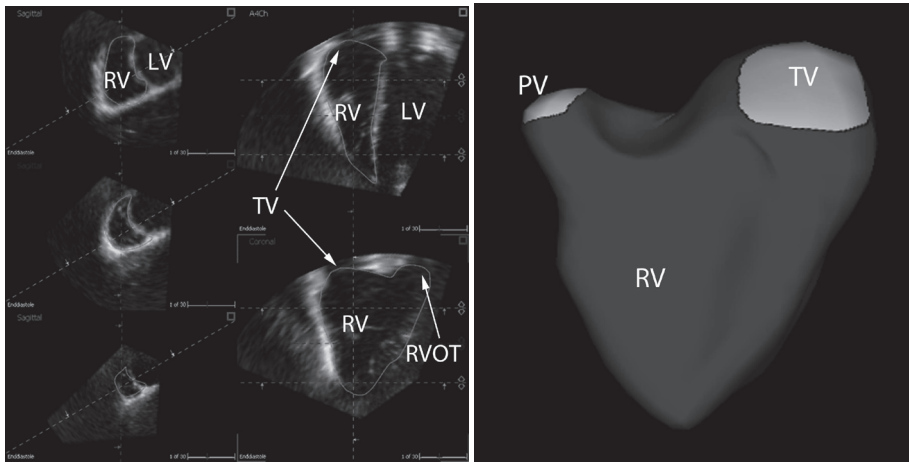
Figure 13 Measurement of right ventricular volume by transthoracic 3DE. (A) Analysis packages designed specifically for the right ventricle are based on user defined reference points and semi-automated tracking of the endocardial border. The green lines show the endocardial border in reference planes including sagittal (left panels), apical projection (upper right panel) and angled coronal planes (lower right panel). (B) Once the user defined planes have been set, a representative model of the right ventricle can be produced, the boundaries of which define EDV and ESV.

LV, left ventricle; RV, right ventricle; TV, tricuspid valve; RVOT, right ventricular outflow tract.

20 minutes).[17,106] In healthy adults and children, intra- and inter-observer reliability is good[98,101] (Table 4) but agreement with MRI worsens in adults with cardiac dysfunction (Table 4).[103,109]

In adults after TOF repair, correlation with MRI is good for end-systolic volume (ESV), end-diastolic volume (EDV)[104–106] and EF; however, 3DE produces lower volumes compared to MRI (Table 4).[105] Individual differences between the techniques can be substantial, and the limits of agreement are wide. The disparity between 3DE and MRI becomes larger in the severely dilated RV where there are particular difficulties in the incorporation of the whole RV, particularly the RV outflow tract in a single volume.[105,106,108,114] Intraobserver, interobserver and test-retest reliability varies among studies, but is generally acceptable (Table 4).[104,106,107] In children with hypoplastic left heart syndrome, 3DE has good reproducibility during serial follow up.[115] However, 3DE measurements are a mean 30% lower than MRI with larger differences in smaller patients, so the techniques cannot be used interchangeably.[116]

Most published RV data utilise full-volume 3DE datasets acquired over several cardiac cycles and normal adult ranges.[100] Recently, 3DE RV volumes and function has been studied using single-beat acquisition in adults.[112] Feasibility was very good (96.7%) as were correlation and agreement with MRI; however, the reduced temporal resolution remains a concern for application to younger patients with higher heart rates.

Knowledge-based 3D reconstruction

Knowledge-based 3D reconstruction evaluates 3D RV volumes from a series of 2DE images localized using a magnetic tracking system (Figure 14).[117] RV anatomic landmarks are identified on the images, which are processed over the Internet using a reference lesion-specific MRI database. This technique has been validated against MRI in children after TOF repair.[110,118] Bias, intra- and inter-observer reliability were good, and knowledge-based 3D reconstruction was slightly better than semi-automated border detection method in this regard. In adults with a systemic RV[111,119] and pulmonary arterial hypertension, values have shown good agreement with MRI.[120,121] Limitations of the knowledge-based technique include the necessity for a tracked ultrasound transducer and for the patient to remain still throughout the study.
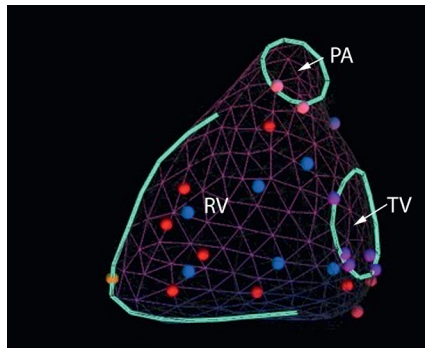
Figure 14 RV volume calculated using knowledge-based reconstruction. This technique is based on placing reference points on transthoracic 2DE images of different projections of the right ventricle, using a defined protocol and a tracked probe. Each of the points (red, blue, purple, pink, and orange) represents a specific reference point. The full volume is reconstructed by uploading the information to a server which is linked to a disease specific atlas to complete the contouring and volume generation.
TV, tricuspid valve; RV, right ventricle; PA, pulmonary artery.

3DE assessment of the LV

Reliable assessment of LV volume and function is important in patients with CHD. 2DE has important limitations in CHD because, in contrast to 3DE, it makes assumptions of LV shape, which are frequently invalid in this population. Thus, 3DE can contribute significantly to the assessment of LV volumes, function and mass.

Analysis methods

The 3DE dataset is obtained from an apical or modified transducer position to include the entire LV volume, which is usually feasible except when the LV is severely dilated. Current software tracks the endocardium of the LV throughout the cardiac cycle and therefore depends on adequate image quality and acoustic windows. Vendors typically display reference planes used to define the endocardial border (Figure 15) as well as the 'shell' of the LV itself (Figure 16). Current tracking algorithms involve user definition of key reference

points followed by semi-automated tracking of the endocardium, but the operator can manually override the initial automated selection of the endocardial border.[122]
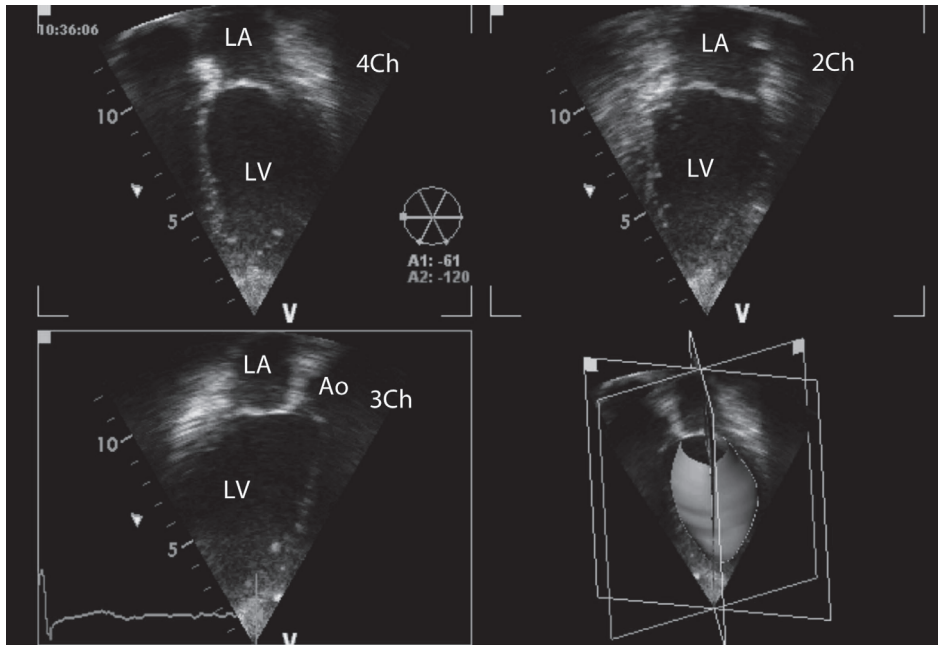
Figure 15 'Triplane' view of the left ventricle. This view permits visualisation of the apical four-chamber, two-chamber and three-chamber views as well as the volume defined by the endocardial border of the three reference planes.

LA, left atrium; LV, left ventricle; Ao, aorta.
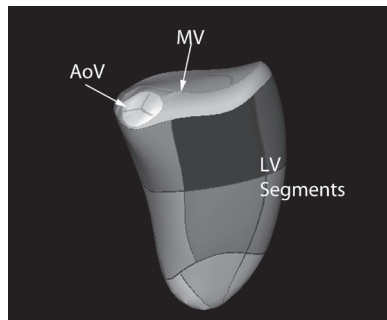
Figure 16 Segmental view of LV. 3DE can be used to assess LV volume, ejection fraction and synchrony based on tracking of the endocardial border of the ventricle. A standard segmentation of the ventricle is used to colour encode the basal, mid and apical segments. Most software algorithms assume a central axis from the mitral valve to the LV apex so that this type of analysis has not been validated for ventricles of more complex shape.

AoV, aortic valve; MV, mitral valve.

Table 5 Results of published data comparing 3DE and MRI in patients with CHD and children.

Echocardiographic method	Population	n	Feasibility (%)	EDV Correlation/ agreement with MRI	ESV Correlation with MRI	EF Correlation with MRI	LV mass	Mean difference EDV	Reproducibility (EDV)
Disk summation									
Altman et al [124]	Children and adults with functional single ventricle	12		r = 0.98	r = 0.98	Mean diff. 4.4 ± 10%	Mean diff. 5.8 ± 19gr	-2.9 ± 8.1 ml	
Soriano et al [18]	Children with functional single ventricle	29	93%	r = 0.96	r = 0.94	r = 0.64	r = 0.84	-3.8 ± 13 ml	Intra: ICC 0.99 Inter: ICC 0.97
Friedberg et al [113]	Children with CHD	35		r = 0.96	r = 0.90	r = 0.75	r = 0.93	-0.49 ± 2.6 ml	Intra: ICC 0.98 Inter: ICC 0.97
Semi-automated border detection									
Bu et [125]	Healthy children	19		r = 0.97	r = 0.97	r = 0.86	r = 0.97	-6.83 ±9.66ml	Intra: 2.9%±3.0% Inter: 7%±5%
Van den Bosch,	Adults with CHD	32 22	91%	r = 0.95	r = 0.97	r = 0.88	r = 0.94		Intra: ICC 0.96 Inter: ICC 0.92 Inter: ICC 0.99
Riehle, et al [126]	Children and young adults with CHD	12		r = 0.99	r = 0.93	r = 0.69		-4.11 ±5.16ml	Intra: 0.4%±5.3% Inter: 3.3%±4.3%
Lu et al [127]	Healthy children	19		r = 0.96	r = 0.93	r = 0.88	r = 0.98	-6.93 ±9.71ml	Intra: 1.0%±5.2% Inter: 3.2%±3.8%
Laser et al [128]	Healthy children and children with tetralogy of Fallot	49		r = 0.95	r = 0.91				Intra: ICC 0.99 Inter: ICC 0.98
Poutanen et al [129]	Healthy children	30		r = 0.80	r = 0.88	r = 0.20	r = 0.81	-4.0 ± 19.6ml	Intra:ICC 0.92 Bias -1.0±13.0 Inter:ICC 0.83 bias 4.7±17.6
Ylanen et al [130]	Children with normal cardiac anatomy	71		r = 0.88	r = 0.83	r = 0.12		-24 ± 32ml	Intra: ICC 0.98 Inter: ICC 0.88

EDV – end-diastolic volume, ESV – end-systolic volume, EF – ejection fraction, LV– left ventricle, MRI – magnetic resonance imaging, Intra - intraobserver, Inter - interobserver, Bias, LOA – bias and limits of agreement between two methods assessed by Bland Altman analysis, ICC – intra-class correlation coefficient.

Despite difficult endocardial delineation and heterogeneous LV shapes, accurate determination of LV volume and function by 3DE has been reported in adults and children with CHD using MRI as the gold standard. Potential errors can still occur in children who have higher heart rates and smaller LV volumes compared with adults, which is offset by superior image quality. 3DE compares favourably with MRI but has a bias to producing lower LV EDV and ESV compared with MRI in patients with CHD in a meta-analysis of 3055 subjects from 95 studies.[123]

The repeatability of 3DE for estimation of LV volume is good and supports its role for serial follow up, although the values are not interchangeable with those obtained by MRI in the CHD population. Validation studies in children and adults with CHD are listed in Table 5.[98,113,125,126,129,130] 3DE is more accurate and reproducible than either M-mode or 2D Simpson's biplane method and is as feasible as 2DE in children.[127,131] These findings have also been validated in neonates and infants where 3DE has compared favorably with MRI even when LV volumes are small and heart rates are high.[113]

LV mass

3DE has been used to assess LV mass in children and compared to both 2DE and M-mode.[132] In younger patients, M-mode has remained the most widespread technique because of the availability of normal paediatric ranges.[133,134] 3DE methods are based on calculating the endo- and epicardial volumes, which are subtracted to compute the mass. 3DE values correlate well with MRI, with low inter- and intra-observer variability[135] but the limits of agreement remain wide[98,113,125,129] Therefore, the clinical application of 3DE for LV mass calculation in patients with CHD remains to be established.

3DE assessment of LV intra-ventricular dyssynchrony

The capability of 3DE to capture the entire LV volume offers the opportunity to assess global and regional LV function (Figure 16). Ventricular dyssynchrony is expressed as the standard deviation of the time taken for segments to reach their minimum systolic volume, indexed to the cardiac cycle length (Systolic Dyssynchrony Index (SDI)).[136] Normal values of SDI in children and adolescents are lower than the adult population.[137,138] 3DE estimates of LV dyssynchrony appear to be most repeatable if a 16-segment model is used as opposed to 12 or 6 segment models.[139] 3DE has been used to demonstrate increased LV dyssynchrony in children with Kawasaki disease[140] as well as dilated cardiomyopathy where the 16-segment SDI correlated negatively with 3DE EF and 2DE fractional shortening.[141] 3DE has also demonstrated LV dyssynchrony in patients with tricuspid atresia after Fontan palliation[142] and a high incidence of LV regional wall motion abnormalities in CHD patients.[143] Current software packages define abnormal wall motion with respect to the central LV axis, which has limitations for some CHD patients with an LV of unusual shape. Further difficulties in measurement of dyssynchrony occur where LV function is poor due to difficulties in accurate determination of the point of minimum systolic volume in segments where such curves are of low amplitude.[144] Caution is required when using 3DE as a modality to quantify electro-mechanical dyssynchrony in CHD in the absence of a significant body of evidence.

3D wall tracking of the left ventricle

Recent advances in 3D wall tracking have allowed for assessment of myocardial deformation in three dimensions from a single volume of the LV (Figure 17). The 3D technique has a potential advantage over 2D strain in that loss of tracking due to through plane motion can be avoided.[145] This permits a semi-automated analysis of longitudinal, radial, circumferential and 3D strain from a single volume. In addition, LV volume, EF and LV twist and torsion can be computed from the same volume. The major limitations of this technique remain temporal resolution and feasibility of incorporating the entire LV. Recent publications have reported normal values in children and adolescents[146,147] but this currently remains a research tool, and the place of such analysis in the management of patients with CHD remains to be established.
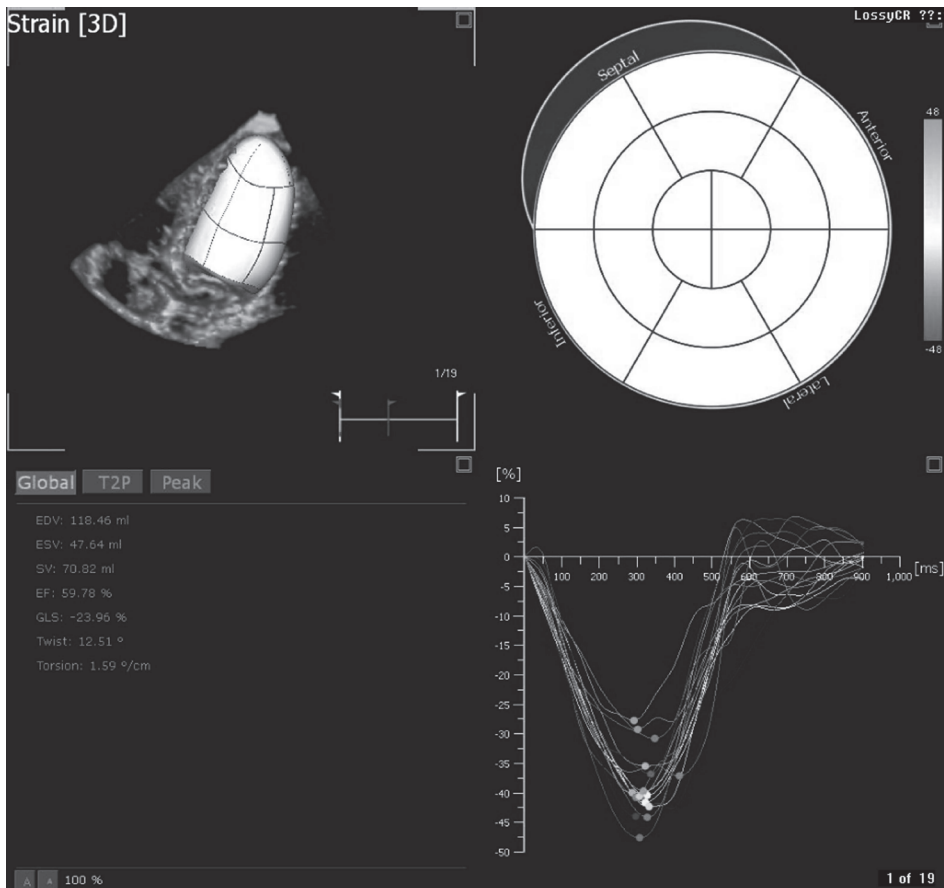
Figure 17 3D deformation analysis by wall tracking. Some software uses the 3D volume to track the myocardium of the left ventricle rather than simply the endocardial border. This permits analysis of deformation, twist and torsion of the whole of the left ventricle from a single volume. A limitation of the technique is that the temporal resolution is lower than 2DE.

Assessment of the functional single ventricle

Ventricular dysfunction is an important long-term complication in patients with functionally single ventricle circulation. 3DE based on disc summation appears feasible and compares favourably with MRI.[18,124] Semi-automated border detection has been applied to the serial assessment of RV volumes and EF in hypoplastic left heart syndrome[115] but with systematic underestimation of RV volume compared to MRI.[116] The differences may reflect the tendency for semiautomatic methods to skim the surface of trabeculations, geometric limitations and failure to include the entire ventricle by 3DE.

Future directions

Technical solutions such as the fusion of multiple 3DE volumes may assist in acquiring the entire ventricular cavity for the purposes of RV functional assessment.[148] The availability of the semi-automated method of disks algorithm for RV volumetry is desirable, as is the availability of analysis software that is purpose-designed, including the facility to landmark structures in normal and abnormal hearts. The availability of large studies to define normal RV and LV volumes and mass across a wide range of body size would enable these measurements to replace 2D measurements in clinical practice. The availability of automated, reproducible algorithms that provide for geometry-independent volumetric analysis of congenitally abnormal ventricles would enhance application in serial follow-up.

RECOMMENDATIONS

Assessment of ventricular volumes and function in CHD

Measurement of ventricular volumes and EF by 3DE is highly repeatable.

3DE has a systematic bias to produce lower values of volume than MRI so that measurements should not be used interchangeably.

Current implementation into clinical practice is hampered by a paucity of normal data from infancy through to adulthood.

Software developed for the normal LV or RV should not be applied to patients with congenitally abnormal ventricles without being validated.

The semi-automated summation of disc method is the least constrained by geometry and should be included with post-processing software particularly for ventricles of abnormal morphology.

3D ECHOCARDIOGRAPHIC ASSESSMENT OF ATRIOVENTRICULAR AND ARTERIAL VALVE FUNCTION IN CONGENITAL HEART DISEASE

3DE assessment of AV valves in CHD is one of the most frequently used applications of the technology in a clinical setting.[149,150] 3DE provides comprehensive information on AV

valve size, morphology and motion. The application of 3D colour flow Doppler can be used to visualise regions of AV valve regurgitation including the size, shape and number of regurgitant orifices.

The AV valves

Assessment of AV valve anatomy

3DE assessment of AV valves in CHD is driven by the need for better visualisation and understanding of the mechanism of the valve regurgitation during surgical planning. AV valve function is a complex interaction of atrial contraction[151] annular shape, contraction and motion;[152,153] leaflet size, shape[154,155] and the changes in its tensor strength,[156,157] chordal length and tension as well as papillary muscle contraction and position.[158,159] Ventricular coordination and contraction[160,161] also impact on AV valve function. 3DE assessment focuses on the valve annulus, leaflets, chords and papillary muscles, as these are the AV valve components that can be manipulated or repaired by current surgical techniques. Although quantitative 3DE assessment of the AV valve in CHD has been reported for AV septal defects[159,16] and tricuspid valves in hypoplastic left heart syndrome,[158,163] it is still not part of routine clinical practice. Commercially available quantitation software frequently assumes normal AV valve morphology and acquired disease, making it less valid for use in CHD. Currently, the assessment of AV valve regurgitation by 3DE remains largely qualitative[41] and is tailored to the individual valve anatomy. There are no data on the impact of 3DE on clinical outcomes in CHD but the technique may impact on the surgical approach.[164]

Quantitation of AV valve regurgitation

Assessment of AV valve regurgitation severity by 2DE has been demonstrated to guide management in the adult population[165] despite significant interobserver variation.[166] 2DE guidelines have been produced for quantitative assessment of valvular regurgitation in adults[167,168] but not children.[24] Poor reproducibility and accuracy result from morphologically abnormal valves, complex regurgitant jet morphology with an elliptical or linear regurgitant orifice and multiple jets, and effective regurgitant orifice area (EROA) calculation has not demonstrated major benefit compared to qualitative assessment.[169–171] EROA reference values relative to patient or valve size are not available, which is a significant limitation in the interpretation of results in growing patients with congenitally abnormal valves. 3DE methods analogous to MRI for estimation of valve regurgitation are encouraging[172–174] but are limited by the requirement of no significant interventricular shunts. 3DE quantification of AV valve regurgitation *vena contracta* area in CHD is a promising approach, is relatively simple to measure and is available on most 3DE navigation software. After acquiring a 3DE colour mapping dataset, the clinician can navigate within the MPR mode to directly measure the *vena contracta* area perpendicular to the regurgitant jet. Multiple validation studies in the adult population have shown strong correlation between 3DE *vena contracta* area of mitral regurgitation and MRI calculated EROA and

regurgitation fraction with high reproducibility.[175] Further validation in paediatric and CHD patients is still required.

Quantitation of aortic and pulmonary valve stenosis and regurgitation by 3DE

The aortic valve

The central role of echocardiography in the investigation of aortic valve disease is well established in both paediatric / congenital and adult practice.[24,176,177] As previously discussed, 3DE can define valve morphology and estimate LV volume and mass. Doppler derived pressure drop across valves is flow dependent, and accurate measurement of effective aortic valve orifice area is clinically important. This is particularly important in children where use of the continuity equation has not been recommended because of the potential for measurement error[24] MPR images can be adjusted to ensure an *en face* orientation to assist in direct measurement of the effective aortic valve area in children with aortic valve stenosis.[21,178] 'Cut off' values of area in children cannot be used because this is impacted by the size of the aortic valve, which is in turn related to the size of the child. Previous published work has addressed the normal aortic valve area across a wide age and size range,[179] but this normative data used a rotational probe rather than current real-time 3DE techniques. Thus, it is feasible to planimeter the effective aortic valve area in the paediatric population, but data on the impact of such measurements on timing of intervention or prognosis is lacking.

Echocardiographic quantification of aortic valve regurgitation has been addressed in several documents,[24,176,177] and standard indices include LV dimensions, regurgitant jet or *vena contracta* diameter, and diastolic reversal of flow in the aorta. Recent adult work has used 3DE colour estimation of the size of the 3DE derived *vena contracta* against 2DE and MRI with encouraging results.[180,181] This technique has not been validated in paediatric or congenital populations. Surgical planning for patients with aortic valve disease involves quantitation of aortic root size, with evidence of improved accuracy using 3DE in children[51] and validation of automated 3DE in adults.[182]

The pulmonary valve

Assessment of pulmonary valve stenosis in children and adults with CHD is normally based on Doppler-derived pressure drop across the valve.[24] Obtaining an *en face* image of the pulmonary valve by 2DE may be challenging, which hampers definitions of stenosis based on effective pulmonary valve orifice area. 3DE may assist in projecting the pulmonary valve *en face* either by real time 3DE, by cropping a multi-beat full volume, or by utilization of cross plane techniques. Pulmonary regurgitation is an important complication of many patients with CHD, particularly those with repaired TOF or with conduits from the RV to the pulmonary artery. Recent publications[54,114,183] emphasise the importance of quantifying the size and function of the RV by 3DE. The estimation of pulmonary regurgitation by 3DE remains semi quantitative; although there are published

data using 3DE to measure EROA,[184] it has not been adopted into CHD practice and has not been validated against cardiac MRI.

Recommendations

Atrioventricular valves

The use of 3DE to visualise AV valves, papillary muscles and chordal support is recommended to assist surgical planning.

3DE assessment of the location, size, shape and number of regurgitant jets and orifice area is recommended.

Measurement of EROA needs to be validated in children and adolescents and in a wide range of valve pathology before its measurement can be recommended to quantify AV valve regurgitation and impact timing of valve repair or replacement.

Post-processing software for AV anatomy and valve function needs to be used with caution as it may assume normal valve anatomy.

Arterial valves

3DE is recommended to assess the morphology of the aortic and pulmonary valves.

3DE is recommended for the measurement of annulus, root and effective orifice area measurement.

3DE colour flow Doppler measurements remain to be validated as a means of quantifying arterial valve regurgitation.

TRAINING IN THREE-DIMENSIONAL ECHOCARDIOGRAPHY

Requirements and recommendations for training have been an integral part of position statements and guidelines for echocardiography in CHD.[185–187] No such proposals have been produced for 3DE of CHD, and the European certification process for echocardiography of CHD does not currently include 3DE at all.[188] Training and education play a critical role in increasing the utility of 3DE, particularly in terms of its ability to improve outcomes.[189] There is no question that the adoption of 3DE into clinical routine has a learning curve and demands specific training.

Machines and transducers for 3DE are similar to those for 2DE. There are some fundamental differences in the approach to learning 2DE versus 3DE. In 2DE, the only image that can be interpreted is the acquired 2D image. A central component of training is the appropriate acquisition of images in planes that are largely predefined. In contrast, 3DE involves acquisition of a 3D dataset with extensive potential for post-processing. Training in 3DE must involve methods to develop and improve the ability to acquire optimal 3DE datasets and to post process the sonographic volumetric datasets to show cardiac morphology or quantify ventricular function. Recognition and evaluation of *en face* views of valves and septums must be learned as well as other details of complex intracardiac

anatomy uniquely available through 3DE. While these structures and views are familiar to surgeons, pathologists, and others who have an implicit understanding of cardiac anatomy, they pose a challenge to those who do not have such a frame of reference. One approach to helping bridge this gap has been the development of educational programmes and publications that include side-by-side depiction of pathology specimen photographs and 3DE images for a wide range of CHD.[60]

Training in acquisition has, of necessity, involved live scanning of subjects in a classroom or clinical setting. Although it provides an authentic learning experience, this mode of learning has practical limitations, including class size, availability of cooperative subjects with a wide spectrum of disease states, busy clinical settings, and issues related to privacy. Over the past few years, simulators to teach 2D TOE and TTE have become available but 3DE simulators are lacking.[190,191]

Training in post-processing has primarily occurred in the format of workshops involving manipulation of datasets from a wide range of pathologies.[192] This type of training requires high-quality 3DE datasets of a variety of CHD, a large number of portable computers and vendor-specific software. One of the challenges of 3DE training has been the high frequency of modifications of the user interface for both acquisition and post-processing.[189] While this is to be expected in the evolution of the modality, frequent changes of user interface may discourage adoption of 3DE. Stability of the user interface and consistency between manufacturers would help greatly in developing robust tools for training.

A further consideration is the wide variability in the use of 3DE between centres and adoption of 3DE within certification and training programmes. There are no specific guidelines for education related to 3DE in the published North American guidelines for core fellowship training in paediatric cardiology[185] and the revised guidelines include only vague references to 3DE experience for advanced fellowship training in non-invasive imaging[193] 3DE is not a current component of the European certification process in echocardiography of CHD. The absence of specific training standards for 3DE has resulted from the absence of guidelines and standards for the performance and interpretation of 3DE studies. This document should provide a framework for more structured 3DE training in the future.

With respect to what form such training should take, attendance at a formal training course in acquisition and post-processing of 3DE is essential to understand different 3D modalities and post-processing software. Sonographers and cardiologists in training should continue to establish their core skills in 2DE according to established training programmes. For trainees subspecialising in echocardiographic imaging, many should be able to gain the further experience in data acquisition and post-processing within their unit, provided 3DE is being widely used. Assessment should be competence based but acquisition of and post-processing of at least 50 volumes (mixed TTE / TOE) of different forms of CHD would seem reasonable. Competence should include assessment of cardiac morphology as well as quantitation of left ventricular volume and EF. If a centre does not offer exposure to a high volume of 3DE then a period of training of 3–6 months at a high volume centre would be appropriate. For the advanced practitioner, application of 3DE

in the catheterisation laboratory and during surgery requires advanced and rapid acquisition and post-processing skills and will generally require more experience and training than that outlined above. Application of 3DE to the RV or abnormally shaped ventricles will also require further experience and training. Trainers in 3D echocardiography will be drawn from cardiologists with many years of experience of acquisition and post-processing of structure and function using 3D echocardiography. It is hoped that the recommendations in this document, for examples those relating to image orientation, may assist in development of structured programs both for trainees and trainers.

Future Directions

Echocardiography simulators should be modified to include training in 3DE acquisition. The development of a comprehensive simulation-based educational resource would require a large library of 3DE datasets encompassing a wide range of pathologic states. Training in post-processing should involve web-based access to 3DE analytic software in conjunction with an online library of 3DE datasets of various CHD lesions. In order to develop such libraries, anonymisation tools for Digital Imaging and Communications in Medicine (DICOM) datasets including removal of both DICOM headers and patient data displayed in the image are essential.

Recommendations

Training in 3DE

Training in 3DE should be an integral part of the training of the congenital echocardiographer. This should include the indications for and added value of 3DE in surgical and interventional planning and guidance.

Training should include 3DE dataset acquisition and post processing to demonstrate competence in assessment of cardiac morphology and quantification of cardiac function.

Operators should learn to recognize and evaluate cardiac views which are uniquely feasible by 3DE including *en face* views of valves and septums.

A degree of consistency of the user interface and uniformity of terminology between manufacturers would help greatly in developing robust non-proprietary tools for training.

ADVANCES IN THREE-DIMENSIONAL ECHOCARDIOGRAPHY

While the past decade has brought exciting advances to the fore in 3DE, there are many aspects that would benefit from improvements in technology that are tailored to the patient with CHD. We look forward to advances in transducer design and computer post-processing as well as research into novel methodologies, such as frame reordering[194] and image compounding,[148,195,196] which can achieve benefits in terms of field of view, endocardial border definition, enhanced temporal resolution and intraventricular flow.

Advances in 3D printing[197,198] and in holographic displays promise the ability to view, understand and utilize 3DE data better in clinical practice.

Novel measurements of ventricular volumes, 3D deformation, valvar morphology, valvar function and flows should be validated, automated, and lead to publication of robust normal ranges across a wide range of ages and body size. These enhancements should not be limited to left heart structures but need to be comprehensive to include the right heart and congenitally abnormal ventricles and valves. All of these measures need to undergo robust assessment of their repeatability and accuracy versus other imaging techniques.

The assessment of the impact of 3DE techniques on patient outcome remains a challenge. Many current 3D techniques have been adopted in an *ad hoc* manner to address specific clinical challenges such as surgical repair of CHD or guidance of interventional procedures but without robust analysis of impact on outcome. Quantitation of ventricular volumes, myocardial deformation, and cardiac function by 3DE needs to stimulate research studies that demonstrate whether or not 3DE measures can be used as surrogates for outcome.

The technical advances and increased use of 3DE techniques in clinical practice will place greater emphasis on improved methods for training and education in 3DE. This needs to be matched at the research and development stage by improvements in the software interface for acquisition and analysis of 3DE including, where appropriate, increased automation to improve workflow and reduce observer error.

REFERENCES

1. Hung J, Lang R, Flachskampf F, Shernan SK, McCulloch ML, Adams DB, Thomas J, Vannan M, Ryan T, Ase. 3D echocardiography: a review of the current status and future directions. *J Am Soc Echocardiogr* 2007;20:213-233.

2. Lang RM, Badano LP, Tsang W, Adams DH, Agricola E, Buck T, Faletra FF, Franke A, Hung J, de Isla LP, Kamp O, Kasprzak JD, Lancellotti P, Marwick TH, McCulloch ML, Monaghan MJ, Nihoyannopoulos P, Pandian NG, Pellikka PA, Pepi M, Roberson DA, Shernan SK, Shirali GS, Sugeng L, Ten Cate FJ, Vannan MA, Zamorano JL, Zoghbi WA, American Society of E, European Association of E. EAE/ASE recommendations for image acquisition and display using three-dimensional echocardiography. *Eur Heart J Cardiovasc Imaging* 2012;13:1-46.

3. Dekker DL, Piziali RL, Dong E, Jr. A system for ultrasonically imaging the human heart in three dimensions. *Comput Biomed Res* 1974;7:544-553.

4. von Ramm OT, Smith SW. Real time volumetric ultrasound imaging system. *J Digit Imaging* 1990;3:261-266.

5. Sheikh K, Smith SW, von Ramm O, Kisslo J. Real-time, three-dimensional echocardiography: feasibility and initial use. *Echocardiography* 1991;8:119-125.

6. Simpson JM. Real-time three-dimensional echocardiography of congenital heart disease using a high frequency paediatric matrix transducer. *Eur J Echocardiogr* 2008;9:222-224.

7. Acar P, Abadir S, Paranon S, Latcu G, Grosjean J, Dulac Y. Live 3D echocardiography with the pediatric matrix probe. *Echocardiography* 2007;24:750-755.

8. Sugeng L, Shernan SK, Salgo IS, Weinert L, Shook D, Raman J, Jeevanandam V, Dupont F, Settlemier S, Savord B, Fox J, Mor-Avi V, Lang RM. Live 3-dimensional transesophageal echocardiography initial experience using the fully-sampled matrix array probe. *J Am Coll Cardiol* 2008;52:446-449.

9. Rawlins DB, Austin C, Simpson JM. Live three-dimensional paediatric intraoperative epicardial echocardiography as a guide to surgical repair of atrioventricular valves. *Cardiol Young* 2006;16:34-39.

10. McGhie JS, Vletter WB, de Groot-de Laat LE, Ren B, Frowijn R, van den Bosch AE, Soliman OI, Geleijnse ML. Contributions of simultaneous multiplane echocardiographic imaging in daily clinical practice. *Echocardiography* 2014;31:245-254.

11. McGhie JS, van den Bosch AE, Haarman MG, Ren B, Roos-Hesselink JW, Witsenburg M, Geleijnse ML. Characterization of atrial septal defect by simultaneous multiplane two-dimensional echocardiography. *Eur Heart J Cardiovasc Imaging* 2014;15:1145-1151.

12. Kutty S, Colen TM, Smallhorn JF. Three-dimensional echocardiography in the assessment of congenital mitral valve disease. *J Am Soc Echocardiogr* 2014;27:142-154.

13. Faletra FF, Ramamurthi A, Dequarti MC, Leo LA, Moccetti T, Pandian N. Artifacts in three-dimensional transesophageal echocardiography. *J Am Soc Echocardiogr* 2014;27:453-462.

14. Lang RM, Badano LP, Tsang W, Adams DH, Agricola E, Buck T, Faletra FF, Franke A, Hung J, de Isla LP, Kamp O, Kasprzak JD, Lancellotti P, Marwick TH, McCulloch ML, Monaghan MJ, Nihoyannopoulos P, Pandian NG, Pellikka PA, Pepi M, Roberson DA, Shernan SK, Shirali GS, Sugeng L, Ten Cate FJ, Vannan MA, Zamorano JL, Zoghbi WA, American Society of E, European Association of E. EAE/ASE recommendations for image acquisition and display using three-dimensional echocardiography. *J Am Soc Echocardiogr* 2012;25:3-46.

15. Fenster A, Parraga G, Bax J. Three-dimensional ultrasound scanning. *Interface Focus* 2011;1:503-519.

16. Pandian NG, Roelandt J, Nanda NC, Sugeng L, Cao QL, Azevedo J, Schwartz SL, Vannan MA, Ludomirski A, Marx G, et al. Dynamic three-dimensional echocardiography: methods and clinical potential. *Echocardiography* 1994;11:237-259.

17. Khoo NS, Young A, Occleshaw C, Cowan B, Zeng IS, Gentles TL. Assessments of right ventricular volume and function using three-dimensional echocardiography in older children and adults with congenital heart disease: comparison with cardiac magnetic resonance imaging. *J Am Soc Echocardiogr* 2009;22:1279-1288.

18. Soriano BD, Hoch M, Ithuralde A, Geva T, Powell AJ, Kussman BD, Graham DA, Tworetzky W, Marx GR. Matrix-array 3-dimensional echocardiographic assessment of volumes, mass, and ejection fraction in young pediatric patients with a functional single ventricle: a comparison study with cardiac magnetic resonance. *Circulation* 2008;117:1842-1848.

19. Bharucha T, Ho SY, Vettukattil JJ. Multiplanar review analysis of three-dimensional echocardiographic datasets gives new insights into the morphology of subaortic stenosis. *Eur J Echocardiogr* 2008;9:614-620.

20. Bharucha T, Sivaprakasam MC, Roman KS, Vettukattil JJ. A multiplanar three dimensional echocardiographic study of mitral valvar annular function in children with normal and regurgitant valves. *Cardiol Young* 2008;18:379-385.

21. Bharucha T, Fernandes F, Slorach C, Mertens L, Friedberg MK. Measurement of effective aortic valve area using three-dimensional echocardiography in children undergoing aortic balloon valvuloplasty for aortic stenosis. *Echocardiography* 2012;29:484-491.

22. Lai WW, Geva T, Shirali GS, Frommelt PC, Humes RA, Brook MM, Pignatelli RH, Rychik J, Task Force of the Pediatric Council of the American Society of E, Pediatric Council of the American Society of E. Guidelines and standards for performance of a pediatric echocardiogram: a report from the Task

Force of the Pediatric Council of the American Society of Echocardiography. *J Am Soc Echocardiogr* 2006;19:1413-1430.

23. Ayres NA, Miller-Hance W, Fyfe DA, Stevenson JG, Sahn DJ, Young LT, Minich LL, Kimball TR, Geva T, Smith FC, Rychik J, Pediatric Council of the American Society of the E. Indications and guidelines for performance of transesophageal echocardiography in the patient with pediatric acquired or congenital heart disease: report from the task force of the Pediatric Council of the American Society of Echocardiography. *J Am Soc Echocardiogr* 2005;18:91-98.

24. Lopez L, Colan SD, Frommelt PC, Ensing GJ, Kendall K, Younoszai AK, Lai WW, Geva T. Recommendations for quantification methods during the performance of a pediatric echocardiogram: a report from the Pediatric Measurements Writing Group of the American Society of Echocardiography Pediatric and Congenital Heart Disease Council. *J Am Soc Echocardiogr* 2010;23:465-495; quiz 576-467.

25. Nanda NC, Kisslo J, Lang R, Pandian N, Marwick T, Shirali G, Kelly G. Examination protocol for three-dimensional echocardiography. *Echocardiography* 2004;21:763-768.

26. Anderson RH, Razavi R, Taylor AM. Cardiac anatomy revisited. *J Anat* 2004;205:159-177.

27. Simpson J, Miller O, Bell A, Bellsham-Revell H, McGhie J, Meijboom F. Image orientation for three-dimensional echocardiography of congenital heart disease. *Int J Cardiovasc Imaging* 2012;28:743-753.

28. Pushparajah K, Miller OI, Simpson JM. 3D echocardiography of the atrial septum: anatomical features and landmarks for the echocardiographer. *JACC Cardiovasc Imaging* 2010;3:981-984.

29. Pushparajah K, Barlow A, Tran VH, Miller OI, Zidere V, Vaidyanathan B, Simpson JM. A systematic three-dimensional echocardiographic approach to assist surgical planning in double outlet right ventricle. *Echocardiography* 2013;30:234-238.

30. Roberson DA, Cui W, Patel D, Tsang W, Sugeng L, Weinert L, Bharati S, Lang RM. Three-dimensional transesophageal echocardiography of atrial septal defect: a qualitative and quantitative anatomic study. *J Am Soc Echocardiogr* 2011;24:600-610.

31. Ojala T, Rosenthal E, Nugent K, Qureshi S, Simpson J. Live 3D echocardiography to guide closure of residual ASD. *JACC Cardiovasc Imaging* 2013;6:523-525.

32. Roberson DA, Cui VW. Three-dimensional transesophageal echocardiography of atrial septal defect device closure. *Curr Cardiol Rep* 2014;16:453.

33. Saric M, Perk G, Purgess JR, Kronzon I. Imaging atrial septal defects by real-time three-dimensional transesophageal echocardiography: step-by-step approach. *J Am Soc Echocardiogr* 2010;23:1128-1135.

34. Acar P, Abadir S, Roux D, Taktak A, Dulac Y, Glock Y, Fournial G. Ebstein's anomaly assessed by real-time 3-D echocardiography. *Ann Thorac Surg* 2006;82:731-733.

35. Hadeed K, Hascoet S, Dulac Y, Peyre M, Acar P. Tethering of tricuspid valve resulting from aberrant tendinous cords mimic ebstein's anomaly, three-dimensional echocardiography approach. *Echocardiography* 2014;31:E136-137.

36. Booker OJ, Nanda NC. Echocardiographic assessment of Ebstein's anomaly. *Echocardiography* 2015;32 Suppl 2:S177-188.

37. Badano LP, Agricola E, Perez de Isla L, Gianfagna P, Zamorano JL. Evaluation of the tricuspid valve morphology and function by transthoracic real-time three-dimensional echocardiography. *Eur J Echocardiogr* 2009;10:477-484.

38. Kutty S, Colen T, Thompson RB, Tham E, Li L, Vijarnsorn C, Polak A, Truong DT, Danford DA, Smallhorn JF, Khoo NS. Tricuspid regurgitation in hypoplastic left heart syndrome: mechanistic insights from 3-dimensional echocardiography and relationship with outcomes. *Circ Cardiovasc Imaging* 2014;7:765-772.

39. van Noord PT, Scohy TV, McGhie J, Bogers AJ. Three-dimensional transesophageal echocardiography in Ebstein's anomaly. *Interact Cardiovasc Thorac Surg* 2010;10:836-837.

40. Kutty S, Smallhorn JF. Evaluation of atrioventricular septal defects by three-dimensional echocardiography: benefits of navigating the third dimension. *J Am Soc Echocardiogr* 2012;25:932-944.

41. Takahashi K, Mackie AS, Rebeyka IM, Ross DB, Robertson M, Dyck JD, Inage A, Smallhorn JF. Two-dimensional versus transthoracic real-time three-dimensional echocardiography in the evaluation of the mechanisms and sites of atrioventricular valve regurgitation in a congenital heart disease population. *J Am Soc Echocardiogr* 2010;23:726-734.

42. Bharucha T, Anderson RH, Lim ZS, Vettukattil JJ. Multiplanar review of three-dimensional echocardiography gives new insights into the morphology of Ebstein's malformation. *Cardiol Young* 2010;20:49-53.

43. Acar P, Abdel-Massih T, Douste-Blazy MY, Dulac Y, Bonhoeffer P, Sidi D. Assessment of muscular ventricular septal defect closure by transcatheter or surgical approach: a three-dimensional echocardiographic study. *Eur J Echocardiogr* 2002;3:185-191.

44. Charakida M, Qureshi S, Simpson JM. 3D echocardiography for planning and guidance of interventional closure of VSD. *JACC Cardiovasc Imaging* 2013;6:120-123.

45. Chen FL, Hsiung MC, Nanda N, Hsieh KS, Chou MC. Real time three-dimensional echocardiography in assessing ventricular septal defects: an echocardiographic-surgical correlative study. *Echocardiography* 2006;23:562-568.

46. Acar P, Abadir S, Aggoun Y. Transcatheter closure of perimembranous ventricular septal defects with Amplatzer occluder assessed by real-time three-dimensional echocardiography. *Eur J Echocardiogr* 2007;8:110-115.

47. Sivakumar K, Singhi A, Pavithran S. Enface reconstruction of VSD on RV septal surface using real-time 3D echocardiography. *JACC Cardiovasc Imaging* 2012;5:1176-1180.

48. Mercer-Rosa L, Seliem MA, Fedec A, Rome J, Rychik J, Gaynor JW. Illustration of the additional value of real-time 3-dimensional echocardiography to conventional transthoracic and transesophageal 2-dimensional echocardiography in imaging muscular ventricular septal defects: does this have any impact on individual patient treatment? *J Am Soc Echocardiogr* 2006;19:1511-1519.

49. Marechaux S, Juthier F, Banfi C, Vincentelli A, Prat A, Ennezat PV. Illustration of the echocardiographic diagnosis of subaortic membrane stenosis in adults: surgical and live three-dimensional transoesophageal findings. *Eur J Echocardiogr* 2011;12:E2.

50. Shirali GS. Three dimensional echocardiography in congenital heart defects. *Ann Pediatr Cardiol* 2008;1:8-17.

51. Noel CV, Choy RM, Lester JR, Soriano BD. Accuracy of matrix-array three-dimensional echocardiographic measurements of aortic root dilation and comparison with two-dimensional echocardiography in pediatric patients. *J Am Soc Echocardiogr* 2012;25:287-293.

52. Martin R, Hascoet S, Dulac Y, Peyre M, Mejean S, Hadeed K, Cazavet A, Leobon B, Acar P. Comparison of two- and three-dimensional transthoracic echocardiography for measurement of aortic annulus diameter in children. *Arch Cardiovasc Dis* 2013;106:492-500.

53. Hlavacek A, Lucas J, Baker H, Chessa K, Shirali G. Feasibility and utility of three-dimensional color flow echocardiography of the aortic arch: The "echocardiographic angiogram". *Echocardiography* 2006;23:860-864.

54. Valente AM, Cook S, Festa P, Ko HH, Krishnamurthy R, Taylor AM, Warnes CA, Kreutzer J, Geva T. Multimodality imaging guidelines for patients with repaired tetralogy of fallot: a report from the AmericanSsociety of Echocardiography: developed in collaboration with the Society for Cardiovascular Magnetic Resonance and the Society for Pediatric Radiology. *J Am Soc Echocardiogr* 2014;27:111-141.

55. Anwar AM, Soliman O, van den Bosch AE, McGhie JS, Geleijnse ML, ten Cate FJ, Meijboom FJ. Assessment of pulmonary valve and right ventricular outflow tract with real-time three-dimensional echocardiography. *Int J Cardiovasc Imaging* 2007;23:167-175.

56. Bharucha T, Sivaprakasam MC, Haw MP, Anderson RH, Vettukattil JJ. The angle of the components of the common atrioventricular valve predicts the outcome of surgical correction in patients with atrioventricular septal defect and common atrioventricular junction. *J Am Soc Echocardiogr* 2008;21:1099-1104.

57. Faletra FF, Nucifora G, Ho SY. Real-time 3-dimensional transesophageal echocardiography of the atrioventricular septal defect. *Circ Cardiovasc Imaging* 2011;4:e7-9.

58. van den Bosch AE, Ten Harkel DJ, McGhie JS, Roos-Hesselink JW, Simoons ML, Bogers AJ, Meijboom FJ. Surgical validation of real-time transthoracic 3D echocardiographic assessment of atrioventricular septal defects. *Int J Cardiol* 2006;112:213-218.

59. van den Bosch AE, van Dijk VF, McGhie JS, Bogers AJ, Roos-Hesselink JW, Simoons ML, Meijboom FJ. Real-time transthoracic three-dimensional echocardiography provides additional information of left-sided AV valve morphology after AVSD repair. *Int J Cardiol* 2006;106:360-364.

60. Shirali G SJ. Pediatric Aspects of Three-Dimensional Echocardiography Comprehensive Atlas of 3D Echocardiography. Philadelphia: Lippincott,Williams and Wilkins, 2012:311-310.

61. Abadir S, Leobon B, Acar P. Assessment of tricuspid regurgitation mechanism by three-dimensional echocardiography in an adult patient with congenitally corrected transposition of the great arteries. *Arch Cardiovasc Dis* 2009;102:459-460.

62. Kottayil BP, Sunil GS, Kappanayil M, Mohanty SH, Francis E, Vaidyanathan B, Balachandran R, Nair SG, Kumar RK. Two-ventricle repair for complex congenital heart defects palliated towards single-ventricle repair. *Interact Cardiovasc Thorac Surg* 2014;18:266-271.

63. Del Pasqua A, Sanders SP, de Zorzi A, Toscano A, Iacobelli R, Pierli C, Pasquini L, Di Donato R, Rinelli G. Impact of three-dimensional echocardiography in complex congenital heart defect cases: the surgical view. *Pediatr Cardiol* 2009;30:293-300.

64. Acar P, Saliba Z, Bonhoeffer P, Aggoun Y, Bonnet D, Sidi D, Kachaner J. Influence of atrial septal defect anatomy in patient selection and assessment of closure with the Cardioseal device; a three-dimensional transoesophageal echocardiographic reconstruction. *Eur Heart J* 2000;21:573-581.

65. Abdel-Massih T, Dulac Y, Taktak A, Aggoun Y, Massabuau P, Elbaz M, Carrie D, Acar P. Assessment of atrial septal defect size with 3D-transesophageal echocardiography: comparison with balloon method. *Echocardiography* 2005;22:121-127.

66. Taniguchi M, Akagi T, Kijima Y, Sano S. Clinical advantage of real-time three-dimensional transesophageal echocardiography for transcatheter closure of multiple atrial septal defects. *Int J Cardiovasc Imaging* 2013;29:1273-1280.

67. Bhaya M, Mutluer FO, Mahan E, Mahan L, Hsiung MC, Yin WH, Wei J, Tsai SK, Zhao GY, Yin WH, Pradhan M, Beniwal R, Joshi D, Nabavizadeh F, Singh A, Nanda NC. Live/Real time three-dimensional transesophageal echocardiography in percutaneous closure of atrial septal defects. *Echocardiography* 2013;30:345-353.

68. Cheng TO, Xie MX, Wang XF, Wang Y, Lu Q. Real-time 3-dimensional echocardiography in assessing atrial and ventricular septal defects: an echocardiographic-surgical correlative study. *Am Heart J* 2004;148:1091-1095.

69. van den Bosch AE, Ten Harkel DJ, McGhie JS, Roos-Hesselink JW, Simoons ML, Bogers AJ, Meijboom FJ. Feasibility and accuracy of real-time 3-dimensional echocardiographic assessment of ventricular septal defects. *J Am Soc Echocardiogr* 2006;19:7-13.

70. Hsu JH, Wu JR, Dai ZK, Lee MH. Real-time three-dimensional echocardiography provides novel and useful anatomic insights of perimembranous ventricular septal aneurysm. *Int J Cardiol* 2007;118:326-331.

71. Butera G, Biondi-Zoccai G, Sangiorgi G, Abella R, Giamberti A, Bussadori C, Sheiban I, Saliba Z, Santoro T, Pelissero G, Carminati M, Frigiola A. Percutaneous versus surgical closure of secundum atrial septal defects: a systematic review and meta-analysis of currently available clinical evidence. *EuroIntervention* 2011;7:377-385.

72. Du ZD, Hijazi ZM, Kleinman CS, Silverman NH, Larntz K, Amplatzer I. Comparison between transcatheter and surgical closure of secundum atrial septal defect in children and adults: results of a multicenter nonrandomized trial. *J Am Coll Cardiol* 2002;39:1836-1844.

73. Chen FL, Hsiung MC, Hsieh KS, Li YC, Chou MC. Real time three-dimensional transthoracic echocardiography for guiding Amplatzer septal occluder device deployment in patients with atrial septal defect. *Echocardiography* 2006;23:763-770.

74. Roman KS, Nii M, Golding F, Benson LN, Smallhorn JF. Images in cardiovascular medicine. Real-time subcostal 3-dimensional echocardiography for guided percutaneous atrial septal defect closure. *Circulation* 2004;109:e320-321.

75. Lock JE, Block PC, McKay RG, Baim DS, Keane JF. Transcatheter closure of ventricular septal defects. *Circulation* 1988;78:361-368.

76. Knauth AL, Lock JE, Perry SB, McElhinney DB, Gauvreau K, Landzberg MJ, Rome JJ, Hellenbrand WE, Ruiz CE, Jenkins KJ. Transcatheter device closure of congenital and postoperative residual ventricular septal defects. *Circulation* 2004;110:501-507.

77. Butera G, Carminati M, Chessa M, Piazza L, Micheletti A, Negura DG, Abella R, Giamberti A, Frigiola A. Transcatheter closure of perimembranous ventricular septal defects: early and long-term results. *J Am Coll Cardiol* 2007;50:1189-1195.

78. Carminati M, Butera G, Chessa M, De Giovanni J, Fisher G, Gewillig M, Peuster M, Piechaud JF, Santoro G, Sievert H, Spadoni I, Walsh K, Investigators of the European VSDR. Transcatheter closure of congenital ventricular septal defects: results of the European Registry. *Eur Heart J* 2007;28:2361-2368.

79. Butera G, Chessa M, Carminati M. Percutaneous closure of ventricular septal defects. State of the art. *J Cardiovasc Med (Hagerstown)* 2007;8:39-45.

80. El Said HG, Bratincsak A, Gordon BM, Moore JW. Closure of perimembranous ventricular septal defects with aneurysmal tissue using the Amplatzer Duct Occluder I: lessons learned and medium term follow up. *Catheter Cardiovasc Interv* 2012;80:895-903.

81. Lucas V. Closure of perimembranous ventricular septal defects with aneurysmal tissue using the Amplatzer Duct Occluder I. *Catheter Cardiovasc Interv* 2012;80:904.

82. Giannakoulas G, Thanopoulos V. Three-dimensional transesophageal echocardiography for guiding percutaneous fontan fenestration closure. *Echocardiography* 2014;31:E230-231.

83. Raslan S, Nanda NC, Lloyd L, Khairnar P, Reilly SD, Holman WL. Incremental value of live/real time three-dimensional transesophageal echocardiography over the two-dimensional technique in the assessment of sinus of valsalva aneurysm rupture. *Echocardiography* 2011;28:918-920.

84. Esper SA, Fink R, Rhodes JF, Jr., Harrison JK, Mackensen GB. A coronary artery fistula successfully closed with the precise guidance of three-dimensional echocardiography. *J Cardiothorac Vasc Anesth* 2014;28:194-195.

85. Mishra J, Puri HP, Hsiung MC, Misra S, Khairnar P, Laxmi Gollamudi B, Patel A, Nanda NC, Yin WH, Wei J, Tsai SK, Sudhakar S. Incremental value of live/real time three-dimensional over two-dimensional transesophageal echocardiography in the evaluation of right coronary artery fistula. *Echocardiography* 2011;28:805-808.

86.   Singh P, Manda J, Hsiung MC, Mehta A, Kesanolla SK, Nanda NC, Tsai SK, Wei J, Yin WH. Live/
real time three-dimensional transesophageal echocardiographic evaluation of mitral and aortic valve
prosthetic paravalvular regurgitation. *Echocardiography* 2009;26:980-987.

87.   Cavalcante JL, Rodriguez LL, Kapadia S, Tuzcu EM, Stewart WJ. Role of echocardiography in percuta-
neous mitral valve interventions. *JACC Cardiovasc Imaging* 2012;5:733-746.

88.   Alli OO, Hsiung MC, Guvenc T, Neill J, Elguindy M, Ahmed MI, Gaba S, Nanda NC. Incremental
value of three-dimensional transesophageal echocardiography over the two-dimensional technique in
percutaneous closure of aortic paraprosthetic regurgitation. *Echocardiography* 2014;31:1154-1158.

89.   Cua CL, Kollins K, Roble S, Holzer RJ. Three-dimensional image of a baffle leak in a patient with a
Mustard operation. *Echocardiography* 2014;31:E315-316.

90.   Soriano BD, Stout KK, Cailes CD, Jones TK. Transcatether closure of an atrial redirection baffle leak.
Ann Pediatr Cardiol 2009;2:85-86.

91.   Faletra FF, Nucifora G, Ho SY. Imaging the atrial septum using real-time three-dimensional trans-
esophageal echocardiography: technical tips, normal anatomy, and its role in transseptal puncture. *J Am
Soc Echocardiogr* 2011;24:593-599.

92.   Doring M, Braunschweig F, Eitel C, Gaspar T, Wetzel U, Nitsche B, Hindricks G, Piorkowski C.
Individually tailored left ventricular lead placement: lessons from multimodality integration between
three-dimensional echocardiography and coronary sinus angiogram. *Europace* 2013;15:718-727.

93.   Fontes-Carvalho R, Sampaio F, Ribeiro J, Gama Ribeiro V. Three-dimensional intracardiac echocardi-
ography: a new promising imaging modality to potentially guide cardiovascular interventions. *Eur Heart J
Cardiovasc Imaging* 2013;14:1028.

94.   Maini B. Real-time three-dimensional intracardiac echocardiography: an early single-center experience.
J Invasive Cardiol 2015;27:E5-E12.

95.   Silvestry FE, Kadakia MB, Willhide J, Herrmann HC. Initial experience with a novel real-time three-di-
mensional intracardiac ultrasound system to guide percutaneous cardiac structural interventions: a phase
1 feasibility study of volume intracardiac echocardiography in the assessment of patients with structural
heart disease undergoing percutaneous transcatheter therapy. *J Am Soc Echocardiogr* 2014;27:978-983.

96.   Bellsham-Revell HR, Simpson JM, Miller OI, Bell AJ. Subjective evaluation of right ventricular systolic
function in hypoplastic left heart syndrome: how accurate is it? *J Am Soc Echocardiogr* 2013;26:52-56.

97.   Hoch M, Vasilyev NV, Soriano B, Gauvreau K, Marx GR. Variables influencing the accuracy of right
ventricular volume assessment by real-time 3-dimensional echocardiography: an in vitro validation
study. *J Am Soc Echocardiogr* 2007;20:456-461.

98.   Lu X, Nadvoretskiy V, Bu L, Stolpen A, Ayres N, Pignatelli RH, Kovalchin JP, Grenier M, Klas B, Ge
S. Accuracy and reproducibility of real-time three-dimensional echocardiography for assessment of right
ventricular volumes and ejection fraction in children. *J Am Soc Echocardiogr* 2008;21:84-89.

99.   Renella P, Marx GR, Zhou J, Gauvreau K, Geva T. Feasibility and reproducibility of three-dimensional
echocardiographic assessment of right ventricular size and function in pediatric patients. *J Am Soc
Echocardiogr* 2014;27:903-910.

100.   Maffessanti F, Muraru D, Esposito R, Gripari P, Ermacora D, Santoro C, Tamborini G, Galderisi M,
Pepi M, Badano LP. Age-, body size-, and sex-specific reference values for right ventricular volumes and
ejection fraction by three-dimensional echocardiography: a multicenter echocardiographic study in 507
healthy volunteers. *Circ Cardiovasc Imaging* 2013;6:700-710.

101.   Tamborini G, Marsan NA, Gripari P, Maffessanti F, Brusoni D, Muratori M, Caiani EG, Fiorentini
C, Pepi M. Reference values for right ventricular volumes and ejection fraction with real-time three-
dimensional echocardiography: evaluation in a large series of normal subjects. *J Am Soc Echocardiogr*
2010;23:109-115.

102. Leibundgut G, Rohner A, Grize L, Bernheim A, Kessel-Schaefer A, Bremerich J, Zellweger M, Buser P, Handke M. Dynamic assessment of right ventricular volumes and function by real-time three-dimensional echocardiography: a comparison study with magnetic resonance imaging in 100 adult patients. *J Am Soc Echocardiogr* 2010;23:116-126.

103. Jenkins C, Chan J, Bricknell K, Strudwick M, Marwick TH. Reproducibility of right ventricular volumes and ejection fraction using real-time three-dimensional echocardiography: comparison with cardiac MRI. *Chest* 2007;131:1844-1851.

104. Dragulescu A, Grosse-Wortmann L, Fackoury C, Mertens L. Echocardiographic assessment of right ventricular volumes: a comparison of different techniques in children after surgical repair of tetralogy of Fallot. *Eur Heart J Cardiovasc Imaging* 2012;13:596-604.

105. Grewal J, Majdalany D, Syed I, Pellikka P, Warnes CA. Three-dimensional echocardiographic assessment of right ventricular volume and function in adult patients with congenital heart disease: comparison with magnetic resonance imaging. *J Am Soc Echocardiogr* 2010;23:127-133.

106. van der Zwaan HB, Helbing WA, McGhie JS, Geleijnse ML, Luijnenburg SE, Roos-Hesselink JW, Meijboom FJ. Clinical value of real-time three-dimensional echocardiography for right ventricular quantification in congenital heart disease: validation with cardiac magnetic resonance imaging. *J Am Soc Echocardiogr* 2010;23:134-140.

107. van der Zwaan HB, Geleijnse ML, Soliman OI, McGhie JS, Wiegers-Groeneweg EJ, Helbing WA, Roos-Hesselink JW, Meijboom FJ. Test-retest variability of volumetric right ventricular measurements using real-time three-dimensional echocardiography. *J Am Soc Echocardiogr* 2011;24:671-679.

108. Iriart X, Montaudon M, Lafitte S, Chabaneix J, Reant P, Balbach T, Houle H, Laurent F, Thambo JB. Right ventricle three-dimensional echography in corrected tetralogy of fallot: accuracy and variability. *Eur J Echocardiogr* 2009;10:784-792.

109. Grapsa J, O'Regan DP, Pavlopoulos H, Durighel G, Dawson D, Nihoyannopoulos P. Right ventricular remodelling in pulmonary arterial hypertension with three-dimensional echocardiography: comparison with cardiac magnetic resonance imaging. *Eur J Echocardiogr* 2010;11:64-73.

110. Dragulescu A, Grosse-Wortmann L, Fackoury C, Riffle S, Waiss M, Jaeggi E, Yoo SJ, Friedberg MK, Mertens L. Echocardiographic assessment of right ventricular volumes after surgical repair of tetralogy of Fallot: clinical validation of a new echocardiographic method. *J Am Soc Echocardiogr* 2011;24:1191-1198.

111. Kutty S, Li L, Polak A, Gribben P, Danford DA. Echocardiographic knowledge-based reconstruction for quantification of the systemic right ventricle in young adults with repaired D-transposition of great arteries. *Am J Cardiol* 2012;109:881-888.

112. Zhang QB, Sun JP, Gao RF, Lee AP, Feng YL, Liu XR, Sheng W, Liu F, Yang XS, Fang F, Yu CM. Feasibility of single-beat full-volume capture real-time three-dimensional echocardiography for quantification of right ventricular volume: validation by cardiac magnetic resonance imaging. *Int J Cardiol* 2013;168:3991-3995.

113. Friedberg MK, Su X, Tworetzky W, Soriano BD, Powell AJ, Marx GR. Validation of 3D echocardiographic assessment of left ventricular volumes, mass, and ejection fraction in neonates and infants with congenital heart disease: a comparison study with cardiac MRI. *Circ Cardiovasc Imaging* 2010;3:735-742.

114. Selly JB, Iriart X, Roubertie F, Mauriat P, Marek J, Guilhon E, Jamal-Bey K, Thambo JB. Multivariable assessment of the right ventricle by echocardiography in patients with repaired tetralogy of Fallot undergoing pulmonary valve replacement: a comparative study with magnetic resonance imaging. *Arch Cardiovasc Dis* 2015;108:5-15.

115. Kutty S, Graney BA, Khoo NS, Li L, Polak A, Gribben P, Hammel JM, Smallhorn JF, Danford DA. Serial assessment of right ventricular volume and function in surgically palliated hypoplastic left heart syndrome using real-time transthoracic three-dimensional echocardiography. *J Am Soc Echocardiogr* 2012;25:682-689.

116. Bell A, Rawlins D, Bellsham-Revell H, Miller O, Razavi R, Simpson J. Assessment of right ventricular volumes in hypoplastic left heart syndrome by real-time three-dimensional echocardiography: comparison with cardiac magnetic resonance imaging. *Eur Heart J Cardiovasc Imaging* 2014;15:257-266.

117. Hubka M, Bolson EL, McDonald JA, Martin RW, Munt B, Sheehan FH. Three-dimensional echocardiographic measurement of left and right ventricular mass and volume: in vitro validation. *Int J Cardiovasc Imaging* 2002;18:111-118.

118. Sheehan FH, Kilner PJ, Sahn DJ, Vick GW, 3rd, Stout KK, Ge S, Helbing WA, Lewin M, Shurman AJ, Buechel EV, Litt HI, Waiss MP. Accuracy of knowledge-based reconstruction for measurement of right ventricular volume and function in patients with tetralogy of Fallot. *Am J Cardiol* 2010;105:993-999.

119. Moroseos T, Mitsumori L, Kerwin WS, Sahn DJ, Helbing WA, Kilner PJ, Shurman A, Litt H, Sheehan FH. Comparison of Simpson's method and three-dimensional reconstruction for measurement of right ventricular volume in patients with complete or corrected transposition of the great arteries. *Am J Cardiol* 2010;105:1603-1609.

120. Bhave NM, Patel AR, Weinert L, Yamat M, Freed BH, Mor-Avi V, Gomberg-Maitland M, Lang RM. Three-dimensional modeling of the right ventricle from two-dimensional transthoracic echocardiographic images: utility of knowledge-based reconstruction in pulmonary arterial hypertension. *J Am Soc Echocardiogr* 2013;26:860-867.

121. Leary PJ, Kurtz CE, Hough CL, Waiss MP, Ralph DD, Sheehan FH. Three-dimensional analysis of right ventricular shape and function in pulmonary hypertension. *Pulm Circ* 2012;2:34-40.

122. van den Bosch AE, Robbers-Visser D, Krenning BJ, Voormolen MM, McGhie JS, Helbing WA, Roos-Hesselink JW, Simoons ML, Meijboom FJ. Real-time transthoracic three-dimensional echocardiographic assessment of left ventricular volume and ejection fraction in congenital heart disease. *J Am Soc Echocardiogr* 2006;19:1-6.

123. Shimada YJ, Shiota T. A meta-analysis and investigation for the source of bias of left ventricular volumes and function by three-dimensional echocardiography in comparison with magnetic resonance imaging. *Am J Cardiol* 2011;107:126-138.

124. Altmann K, Shen Z, Boxt LM, King DL, Gersony WM, Allan LD, Apfel HD. Comparison of three-dimensional echocardiographic assessment of volume, mass, and function in children with functionally single left ventricles with two-dimensional echocardiography and magnetic resonance imaging. *Am J Cardiol* 1997;80:1060-1065.

125. Bu L, Munns S, Zhang H, Disterhoft M, Dixon M, Stolpen A, Sonka M, Scholz TD, Mahoney LT, Ge S. Rapid full volume data acquisition by real-time 3-dimensional echocardiography for assessment of left ventricular indexes in children: a validation study compared with magnetic resonance imaging. *J Am Soc Echocardiogr* 2005;18:299-305.

126. Riehle TJ, Mahle WT, Parks WJ, Sallee D, 3rd, Fyfe DA. Real-time three-dimensional echocardiographic acquisition and quantification of left ventricular indices in children and young adults with congenital heart disease: comparison with magnetic resonance imaging. *J Am Soc Echocardiogr* 2008;21:78-83.

127. Lu X, Xie M, Tomberlin D, Klas B, Nadvoretskiy V, Ayres N, Towbin J, Ge S. How accurately, reproducibly, and efficiently can we measure left ventricular indices using M-mode, 2-dimensional, and 3-dimensional echocardiography in children? *Am Heart J* 2008;155:946-953.

128. Laser KT, Bunge M, Hauffe P, Argueta JR, Kelter-Klopping A, Barth P, Sarikouch S, Burchert W, Kececioglu D, Korperich H. Left ventricular volumetry in healthy children and adolescents: comparison

of two different real-time three-dimensional matrix transducers with cardiovascular magnetic resonance. *Eur J Echocardiogr* 2010;11:138-148.

129. Poutanen T, Ikonen A, Jokinen E, Vainio P, Tikanoja T. Transthoracic three-dimensional echocardiography is as good as magnetic resonance imaging in measuring dynamic changes in left ventricular volume during the heart cycle in children. *Eur J Echocardiogr* 2001;2:31-39.

130. Ylanen K, Eerola A, Vettenranta K, Poutanen T. Three-dimensional echocardiography and cardiac magnetic resonance imaging in the screening of long-term survivors of childhood cancer after cardiotoxic therapy. *Am J Cardiol* 2014;113:1886-1892.

131. Balluz R, Liu L, Zhou X, Ge S. Real time three-dimensional echocardiography for quantification of ventricular volumes, mass, and function in children with congenital and acquired heart diseases. *Echocardiography* 2013;30:472-482.

132. Poutanen T, Jokinen E. Left ventricular mass in 169 healthy children and young adults assessed by three-dimensional echocardiography. *Pediatr Cardiol* 2007;28:201-207.

133. Foster BJ, Mackie AS, Mitsnefes M, Ali H, Mamber S, Colan SD. A novel method of expressing left ventricular mass relative to body size in children. *Circulation* 2008;117:2769-2775.

134. Khoury PR, Mitsnefes M, Daniels SR, Kimball TR. Age-specific reference intervals for indexed left ventricular mass in children. *J Am Soc Echocardiogr* 2009;22:709-714.

135. van den Bosch AE, Robbers-Visser D, Krenning BJ, McGhie JS, Helbing WA, Meijboom FJ, Roos-Hesselink JW. Comparison of real-time three-dimensional echocardiography to magnetic resonance imaging for assessment of left ventricular mass. *Am J Cardiol* 2006;97:113-117.

136. Kapetanakis S, Kearney MT, Siva A, Gall N, Cooklin M, Monaghan MJ. Real-time three-dimensional echocardiography: a novel technique to quantify global left ventricular mechanical dyssynchrony. *Circulation* 2005;112:992-1000.

137. Cui W, Gambetta K, Zimmerman F, Freter A, Sugeng L, Lang R, Roberson DA. Real-time three-dimensional echocardiographic assessment of left ventricular systolic dyssynchrony in healthy children. *J Am Soc Echocardiogr* 2010;23:1153-1159.

138. Ten Harkel AD, Van Osch-Gevers M, Helbing WA. Real-time transthoracic three dimensional echocardiography: normal reference data for left ventricular dyssynchrony in adolescents. *J Am Soc Echocardiogr* 2009;22:933-938.

139. Ojala T, Mathur S, Vatanen A, Sinha MD, Jahnukainen K, Simpson J. Repeatability and agreement of real time three-dimensional echocardiography measurements of left ventricular mass and synchrony in young patients. *Echocardiography* 2015;32:522-527.

140. Yu Y, Sun K, Xue H, Chen S, Yang J. Usefulness of real-time 3-dimensional echocardiography to identify and quantify left ventricular dyssynchrony in patients with Kawasaki disease. *J Ultrasound Med* 2013;32:1013-1021.

141. Baker GH, Hlavacek AM, Chessa KS, Fleming DM, Shirali GS. Left ventricular dysfunction is associated with intraventricular dyssynchrony by 3-dimensional echocardiography in children. *J Am Soc Echocardiogr* 2008;21:230-233.

142. Ho PK, Lai CT, Wong SJ, Cheung YF. Three-dimensional mechanical dyssynchrony and myocardial deformation of the left ventricle in patients with tricuspid atresia after Fontan procedure. *J Am Soc Echocardiogr* 2012;25:393-400.

143. Raedle-Hurst TM, Mueller M, Rentzsch A, Schaefers HJ, Herrmann E, Abdul-Khaliq H. Assessment of left ventricular dyssynchrony and function using real-time 3-dimensional echocardiography in patients with congenital right heart disease. *Am Heart J* 2009;157:791-798.

144. Sonne C, Sugeng L, Takeuchi M, Weinert L, Childers R, Watanabe N, Yoshida K, Mor-Avi V, Lang RM. Real-time 3-dimensional echocardiographic assessment of left ventricular dyssynchrony: pitfalls in patients with dilated cardiomyopathy. *JACC Cardiovasc Imaging* 2009;2:802-812.

145. Wu VC, Takeuchi M, Otani K, Haruki N, Yoshitani H, Tamura M, Abe H, Lin FC, Otsuji Y. Effect of through-plane and twisting motion on left ventricular strain calculation: direct comparison between two-dimensional and three-dimensional speckle-tracking echocardiography. *J Am Soc Echocardiogr* 2013;26:1274-1281 e1274.

146. Kaku K, Takeuchi M, Tsang W, Takigiku K, Yasukochi S, Patel AR, Mor-Avi V, Lang RM, Otsuji Y. Age-related normal range of left ventricular strain and torsion using three-dimensional speckle-tracking echocardiography. *J Am Soc Echocardiogr* 2014;27:55-64.

147. Zhang L, Gao J, Xie M, Yin P, Liu W, Li Y, Klas B, Sun J, Balluz R, Ge S. Left ventricular three-dimensional global systolic strain by real-time three-dimensional speckle-tracking in children: feasibility, reproducibility, maturational changes, and normal ranges. *J Am Soc Echocardiogr* 2013;26:853-859.

148. Yao C, Simpson JM, Schaeffter T, Penney GP. Multi-view 3D echocardiography compounding based on feature consistency. *Phys Med Biol* 2011;56:6109-6128.

149. Said SM, Dearani JA, Burkhart HM, Connolly HM, Eidem B, Stensrud PE, Schaff HV. Management of tricuspid regurgitation in congenital heart disease: is survival better with valve repair? *J Thorac Cardiovasc Surg* 2014;147:412-417.

150. Yamagishi S, Masuoka A, Uno Y, Katogi T, Suzuki T. Influence of bidirectional cavopulmonary anastomosis and concomitant valve repair on atrioventricular valve annulus and function. *Ann Thorac Surg* 2014;98:641-647; discussion 647.

151. Swanson JC, Krishnamurthy G, Kvitting JP, Miller DC, Ingels NB, Jr. Electromechanical coupling between the atria and mitral valve. *Am J Physiol Heart Circ Physiol* 2011;300:H1267-1273.

152. Salgo IS, Gorman JH, 3rd, Gorman RC, Jackson BM, Bowen FW, Plappert T, St John Sutton MG, Edmunds LH, Jr. Effect of annular shape on leaflet curvature in reducing mitral leaflet stress. *Circulation* 2002;106:711-717.

153. Nii M, Roman KS, Macgowan CK, Smallhorn JF. Insight into normal mitral and tricuspid annular dynamics in pediatrics: a real-time three-dimensional echocardiographic study. *J Am Soc Echocardiogr* 2005;18:805-814.

154. Ando M, Takahashi Y. Variations of atrioventricular septal defects predisposing to regurgitation and stenosis. *Ann Thorac Surg* 2010;90:614-621.

155. Kanani M, Elliott M, Cook A, Juraszek A, Devine W, Anderson RH. Late incompetence of the left atrioventricular valve after repair of atrioventricular septal defects: the morphologic perspective. *J Thorac Cardiovasc Surg* 2006;132:640-646, 646 e641-643.

156. Krishnamurthy G, Itoh A, Swanson JC, Miller DC, Ingels NB, Jr. Transient stiffening of mitral valve leaflets in the beating heart. *Am J Physiol Heart Circ Physiol* 2010;298:H2221-2225.

157. Swanson JC, Krishnamurthy G, Itoh A, Kvitting JP, Bothe W, Craig Miller D, Ingels NB, Jr. Multiple mitral leaflet contractile systems in the beating heart. *J Biomech* 2011;44:1328-1333.

158. Takahashi K, Inage A, Rebeyka IM, Ross DB, Thompson RB, Mackie AS, Smallhorn JF. Real-time 3-dimensional echocardiography provides new insight into mechanisms of tricuspid valve regurgitation in patients with hypoplastic left heart syndrome. *Circulation* 2009;120:1091-1098.

159. Takahashi K, Mackie AS, Thompson R, Al-Naami G, Inage A, Rebeyka IM, Ross DB, Khoo NS, Colen T, Smallhorn JF. Quantitative real-time three-dimensional echocardiography provides new insight into the mechanisms of mitral valve regurgitation post-repair of atrioventricular septal defect. *J Am Soc Echocardiogr* 2012;25:1231-1244.

160. Ypenburg C, Lancellotti P, Tops LF, Bleeker GB, Holman ER, Pierard LA, Schalij MJ, Bax JJ. Acute effects of initiation and withdrawal of cardiac resynchronization therapy on papillary muscle dyssynchrony and mitral regurgitation. *J Am Coll Cardiol* 2007;50:2071-2077.

161. Bharucha T, Khan R, Mertens L, Friedberg MK. Right ventricular mechanical dyssynchrony and asymmetric contraction in hypoplastic heart syndrome are associated with tricuspid regurgitation. *J Am Soc Echocardiogr* 2013;26:1214-1220.

162. Takahashi K, Guerra V, Roman KS, Nii M, Redington A, Smallhorn JF. Three-dimensional echocardiography improves the understanding of the mechanisms and site of left atrioventricular valve regurgitation in atrioventricular septal defect. *J Am Soc Echocardiogr* 2006;19:1502-1510.

163. Nii M, Guerra V, Roman KS, Macgowan CK, Smallhorn JF. Three-dimensional tricuspid annular function provides insight into the mechanisms of tricuspid valve regurgitation in classic hypoplastic left heart syndrome. *J Am Soc Echocardiogr* 2006;19:391-402.

164. Colen TM, Khoo NS, Ross DB, Smallhorn JF. Partial zone of apposition closure in atrioventricular septal defect: are papillary muscles the clue. *Ann Thorac Surg* 2013;96:637-643.

165. Kusunose K, Cremer PC, Tsutsui RS, Grimm RA, Thomas JD, Griffin BP, Popovic ZB. Regurgitant volume informs rate of progressive cardiac dysfunction in asymptomatic patients with chronic aortic or mitral regurgitation. *JACC Cardiovasc Imaging* 2015;8:14-23.

166. Thomas N, Unsworth B, Ferenczi EA, Davies JE, Mayet J, Francis DP. Intraobserver variability in grading severity of repeated identical cases of mitral regurgitation. *Am Heart J* 2008;156:1089-1094.

167. Zoghbi WA, Enriquez-Sarano M, Foster E, Grayburn PA, Kraft CD, Levine RA, Nihoyannopoulos P, Otto CM, Quinones MA, Rakowski H, Stewart WJ, Waggoner A, Weissman NJ, American Society of E. Recommendations for evaluation of the severity of native valvular regurgitation with two-dimensional and Doppler echocardiography. *J Am Soc Echocardiogr* 2003;16:777-802.

168. Lancellotti P, Moura L, Pierard LA, Agricola E, Popescu BA, Tribouilloy C, Hagendorff A, Monin JL, Badano L, Zamorano JL, European Association of E. European Association of Echocardiography recommendations for the assessment of valvular regurgitation. Part 2: mitral and tricuspid regurgitation (native valve disease). *Eur J Echocardiogr* 2010;11:307-332.

169. Choi J, Heo R, Hong GR, Chang HJ, Sung JM, Shin SH, Cho IJ, Shim CY, Chung N. Differential effect of 3-dimensional color Doppler echocardiography for the quantification of mitral regurgitation according to the severity and characteristics. *Circ Cardiovasc Imaging* 2014;7:535-544.

170. Prakash A, Lacro RV, Sleeper LA, Minich LL, Colan SD, McCrindle B, Covitz W, Golding F, Hlavacek AM, Levine JC, Cohen MS. Challenges in echocardiographic assessment of mitral regurgitation in children after repair of atrioventricular septal defect. *Pediatr Cardiol* 2012;33:205-214.

171. Biner S, Rafique A, Rafii F, Tolstrup K, Noorani O, Shiota T, Gurudevan S, Siegel RJ. Reproducibility of proximal isovelocity surface area, vena contracta, and regurgitant jet area for assessment of mitral regurgitation severity. *JACC Cardiovasc Imaging* 2010;3:235-243.

172. Thavendiranathan P, Liu S, Datta S, Walls M, Nitinunu A, Van Houten T, Tomson NA, Vidmar L, Georgescu B, Wang Y, Srinivasan S, De Michelis N, Raman SV, Ryan T, Vannan MA. Automated quantification of mitral inflow and aortic outflow stroke volumes by three-dimensional real-time volume color-flow Doppler transthoracic echocardiography: comparison with pulsed-wave Doppler and cardiac magnetic resonance imaging. *J Am Soc Echocardiogr* 2012;25:56-65.

173. Ge S, Bu L, Zhang H, Schelbert E, Disterhoft M, Li X, Li X, Sahn D, Stolpen A, Sonka M. A real-time 3-dimensional digital Doppler method for measurement of flow rate and volume through mitral valve in children: a validation study compared with magnetic resonance imaging. *J Am Soc Echocardiogr* 2005;18:1-7.

174. Lu X, Nadvoretskiy V, Klas B, Bu L, Stolpen A, Ayres NA, Sahn DJ, Ge S. Measurement of volumetric flow by real-time 3-dimensional doppler echocardiography in children. *J Am Soc Echocardiogr* 2007;20:915-920.

175. Maragiannis D, Little SH. 3D vena contracta area to quantify severity of mitral regurgitation: a practical new tool? *Hellenic J Cardiol* 2013;54:448-454.

176. Lancellotti P, Tribouilloy C, Hagendorff A, Moura L, Popescu BA, Agricola E, Monin JL, Pierard LA, Badano L, Zamorano JL, European Association of E. European Association of Echocardiography recommendations for the assessment of valvular regurgitation. Part 1: aortic and pulmonary regurgitation (native valve disease). *Eur J Echocardiogr* 2010;11:223-244.

177. Joint Task Force on the Management of Valvular Heart Disease of the European Society of C, European Association for Cardio-Thoracic S, Vahanian A, Alfieri O, Andreotti F, Antunes MJ, Baron-Esquivias G, Baumgartner H, Borger MA, Carrel TP, De Bonis M, Evangelista A, Falk V, Iung B, Lancellotti P, Pierard L, Price S, Schafers HJ, Schuler G, Stepinska J, Swedberg K, Takkenberg J, Von Oppell UO, Windecker S, Zamorano JL, Zembala M. Guidelines on the management of valvular heart disease (version 2012). *Eur Heart J* 2012;33:2451-2496.

178. Cognet T, Seguela PE, Thomson E, Bouisset F, Lairez O, Hascoet S, Carrie D, Acar P. Assessment of valvular surfaces in children with a congenital bicuspid aortic valve: preliminary three-dimensional echocardiographic study. *Arch Cardiovasc Dis* 2013;106:295-302.

179. Poutanen T, Tikanoja T, Sairanen H, Jokinen E. Normal mitral and aortic valve areas assessed by three- and two-dimensional echocardiography in 168 children and young adults. *Pediatr Cardiol* 2006;27:217-225.

180. Perez de Isla L, Zamorano J, Fernandez-Golfin C, Ciocarelli S, Corros C, Sanchez T, Ferreiros J, Marcos-Alberca P, Almeria C, Rodrigo JL, Macaya C. 3D color-Doppler echocardiography and chronic aortic regurgitation: a novel approach for severity assessment. *Int J Cardiol* 2013;166:640-645.

181. Ewe SH, Delgado V, van der Geest R, Westenberg JJ, Haeck ML, Witkowski TG, Auger D, Marsan NA, Holman ER, de Roos A, Schalij MJ, Bax JJ, Sieders A, Siebelink HM. Accuracy of three-dimensional versus two-dimensional echocardiography for quantification of aortic regurgitation and validation by three-dimensional three-directional velocity-encoded magnetic resonance imaging. *Am J Cardiol* 2013;112:560-566.

182. Calleja A, Thavendiranathan P, Ionasec RI, Houle H, Liu S, Voigt I, Sai Sudhakar C, Crestanello J, Ryan T, Vannan MA. Automated quantitative 3-dimensional modeling of the aortic valve and root by 3-dimensional transesophageal echocardiography in normals, aortic regurgitation, and aortic stenosis: comparison to computed tomography in normals and clinical implications. *Circ Cardiovasc Imaging* 2013;6:99-108.

183. Festa P, Ait-Ali L, Minichilli F, Kristo I, Deiana M, Picano E. A new simple method to estimate pulmonary regurgitation by echocardiography in operated fallot: comparison with magnetic resonance imaging and performance test evaluation. *J Am Soc Echocardiogr* 2010;23:496-503.

184. Pothineni KR, Wells BJ, Hsiung MC, Nanda NC, Yelamanchili P, Suwanjutah T, Prasad AN, Hansalia S, Lin CC, Yin WH, Young MS. Live/real time three-dimensional transthoracic echocardiographic assessment of pulmonary regurgitation. *Echocardiography* 2008;25:911-917.

185. Sanders SP, Colan SD, Cordes TM, Donofrio MT, Ensing GJ, Geva T, Kimball TR, Sahn DJ, Silverman NH, Sklansky MS, Weinberg PM, American Society of E, Society of Pediatric E, American College of Cardiology F, American Heart A, American College of Physicians Task Force on Clinical C. ACCF/AHA/AAP recommendations for training in pediatric cardiology. Task force 2: pediatric training guidelines for noninvasive cardiac imaging endorsed by the American Society of Echocardiography and the Society of Pediatric Echocardiography. *J Am Coll Cardiol* 2005;46:1384-1388.

186. Mertens L, Seri I, Marek J, Arlettaz R, Barker P, McNamara P, Moon-Grady AJ, Coon PD, Noori S, Simpson J, Lai WW, Writing Group of the American Society of E, European Association of E, Association for European Pediatric C. Targeted neonatal echocardiography in the neonatal intensive care unit: practice guidelines and recommendations for training. *Eur J Echocardiogr* 2011;12:715-736.

187. Mertens L, Helbing W, Sieverding L, Daniels O, Working Group on Cardiac Imaging of the Association for European Paediatric C. Guidelines from the Association for European Paediatric Cardiology: standards for training in paediatric echocardiography. *Cardiol Young* 2005;15:441-442.

188. Mertens L, Miller O, Fox K, Simpson J. Certification in echocardiography of congenital heart disease: experience of the first 6 years of a European process. *Eur Heart J Cardiovasc Imaging* 2013;14:142-148.

189. Pellikka PA, Douglas PS, Miller JG, Abraham TP, Baumann R, Buxton DB, Byrd BF, 3rd, Chen P, Cook NL, Gardin JM, Hansen G, Houle HC, Husson S, Kaul S, Klein AL, Lang RM, Leong-Poi H, Lopez H, Mahmoud TM, Maslak S, McCulloch ML, Metz S, Nagueh SF, Pearlman AS, Pibarot P, Picard MH, Porter TR, Prater D, Rodriguez R, Sarano ME, Scherrer-Crosbie M, Shirali GS, Sinusas A, Slosky JJ, Sugeng L, Tatpati A, Villanueva FS, von Ramm OT, Weissman NJ, Zamani S. American Society of Echocardiography Cardiovascular Technology and Research Summit: a roadmap for 2020. *J Am Soc Echocardiogr* 2013;26:325-338.

190. Bose RR, Matyal R, Warraich HJ, Summers J, Subramaniam B, Mitchell J, Panzica PJ, Shahul S, Mahmood F. Utility of a transesophageal echocardiographic simulator as a teaching tool. *J Cardiothorac Vasc Anesth* 2011;25:212-215.

191. Jelacic S, Bowdle A, Togashi K, VonHomeyer P. The use of TEE simulation in teaching basic echocardiography skills to senior anesthesiology residents. *J Cardiothorac Vasc Anesth* 2013;27:670-675.

192. Jenkins C, Monaghan M, Shirali G, Guraraja R, Marwick TH. An intensive interactive course for 3D echocardiography: is 'crop till you drop' an effective learning strategy? *Eur J Echocardiogr* 2008;9:373-380.

193. Srivastava S, Printz BF, Geva T, Shirali GS, Weinberg PM, Wong PC, Lang P. Task Force 2: Pediatric Cardiology Fellowship Training in Noninvasive Cardiac Imaging. *J Am Coll Cardiol* 2015;66:687-698.

194. Perrin DP, Vasilyev NV, Marx GR, del Nido PJ. Temporal enhancement of 3D echocardiography by frame reordering. *JACC Cardiovasc Imaging* 2012;5:300-304.

195. de Vecchi A, Gomez A, Pushparajah K, Schaefter T, Nordsletten DA, Simpson JM, Penney GP, Smith NP. Towards a fast and efficient approach for modelling the patient-specific ventricular haemodynamics. *Prog Biophys Mol Biol* 2014;116:3-10.

196. Gomez A, de Vecchi A, Jantsch M, Shi W, Pushparajah K, Simpson JM, Smith NP, Rueckert D, Schaefter T, Penney GP. 4D Blood Flow Reconstruction Over the Entire Ventricle From Wall Motion and Blood Velocity Derived From Ultrasound Data. *IEEE Trans Med Imaging* 2015;34:2298-2308.

197. Olivieri LJ, Krieger A, Loke YH, Nath DS, Kim PC, Sable CA. Three-dimensional printing of intracardiac defects from three-dimensional echocardiographic images: feasibility and relative accuracy. *J Am Soc Echocardiogr* 2015;28:392-397.

198. Samuel BP, Pinto C, Pietila T, Vettukattil JJ. Ultrasound-Derived Three-Dimensional Printing in Congenital Heart Disease. *J Digit Imaging* 2015;28:459-461.

PART III

Simultaneous multiplane
2D-echocardiography and ventricular
function

CHAPTER 8

Normal myocardial strain values using 2D speckle tracking echocardiography in healthy adults aged 20 to 72 years

Myrthe E. Menting
Jackie S. McGhie
Laurens P. Koopman
Wim B. Vletter
Willem A. Helbing
Annemien E. van den Bosch
Jolien W. Roos-Hesselink

ABSTRACT

Aims

Evaluation of left ventricular (LV) myocardial deformation by speckle-tracking echocardiography (STE) is useful for clinical and research purposes. However, strain measurements depend on the used software. Normative data for QLAB 10 (Philips) are scarce. Additionally, little is known about the influence of anthropometric factors. We aimed to establish normal adult STE-derived strain and strain rate values, and to evaluate associations with anthropometrics.

Methods

One hundred fifty-five healthy subjects aged 20 to 72 years ($\geq$ 28 subjects per decile) were prospectively gathered and examined with electrocardiography and two-dimensional echocardiography. With STE, we assessed peak systolic LV global longitudinal strain (GLS), segmental longitudinal strain and strain rate from the three standard apical views.

Results

We included 147 healthy subjects (age 44.6±13.7 years, 50% female, LV GLS -20.8±2.0%). Men had significantly lower GLS than women (-20.1±1.8% vs. -21.5±2.0%, $P<$ .001). GLS was significantly lower in subjects with age above 55 years ($P =$ .029), higher blood pressure ($P<$ .001), higher body surface area (BSA, $P<$ .001), larger LV end-systolic and end-diastolic volumes (both $P<$ .001), lower LV ejection fraction ($P<$ .001) and some indices of diastolic function. After multivariable regression analysis, the correlation with systolic blood pressure, E-wave and LV end-systolic volume remained significant. The systolic strain rates of most segments correlated with BSA.

Conclusions

Our study resulted in normative LV GLS values assessed with QLAB 10. Male sex, higher BSA and higher blood pressure negatively influence GLS. Therefore, these factors should be taken into account for strain interpretation in clinical practice.

INTRODUCTION

The quantification of cardiac chamber dimensions and function is the cornerstone of cardiac imaging.[1] Conventional two-dimensional (2D) and Doppler echocardiography are the most commonly used noninvasive modalities and are valuable tools, especially for the assessment of global systolic and diastolic function. The most widely used measurement for left ventricular (LV) systolic function in a clinical setting is ejection fraction. However, this parameter is limited in abnormally shaped or dilated LVs due to the geometric assumptions used in the 2D-biplane method. In addition, regional systolic dysfunction could be missed with this method.[1]

During the last decade, 2D speckle-tracking echocardiography (STE) has become available that provides quantitative assessment of global and segmental ventricular function by measuring myocardial deformation, largely independent of angle and ventricular geometry.[2,3] Longitudinal strain (LS), one of the measures of deformation, is the most widely used type of strain and is a robust index for clinical studies.[4] With the use of myocardial deformation imaging, ventricular dysfunction may be detected in a pre-clinical phase.[5]

Although STE is widely used for the assessment of LV function, myocardial deformation parameters are dependent on the equipment that is used and therefore, results of machines and software packages from different vendors are not interchangeable.[4,6] However, there has been an improvement in between-vendor concordance in LV global longitudinal strain (GLS) as the work of the joint standardization task force.[7] Erasmus MC routinely uses the Philips iE33 and EPIQ7 ultrasound systems, and QLAB software for analyzing datasets (Philips Medical Systems, Best, The Netherlands). Normal reference values of STE-derived LS are scarce using QLAB software (Philips Medical Systems),[8] especially strain values established with the software versions after the standardization initiative.[7] Because of this lack of adequate normal data, the clinical value of STE data in patients is suboptimal. In addition, little is known about the influence of anthropometric factors on these strain values.

The aim of this prospective cohort study was to obtain normal LV LS and strain rate values in healthy volunteers aged from 20 to 72 years. Secondly, we wanted to identify the influence of age, sex, body mass index (BMI), body surface area (BSA), blood pressure, ECG findings and ventricular size and volumes on strain.

METHODS

Study population

This prospective cohort study was conducted in 2014–2015 in 155 healthy volunteers aged 20 to 72 years, who were stratified into five age groups: 20 to 29, 30 to 39, 40 to 49, 50 to 59, and 60 to 72 years (n≥ 28 in each group, equal distribution in sex). The subjects were recruited via an advertisement for healthy subjects. The inclusion criteria required that subjects had normal results on physical examination and electrocardiography (ECG). Subjects were excluded when they met any of the following criteria: (prior) cardiovascular

disease; cardiovascular risk factors consisting of hypertension, diabetes mellitus or hyper-cholesterolemia; systemic disease or medication known to influence cardiac function; or the finding of cardiac abnormalities during examination. Professional athletes, morbidly obese subjects (BMI > 40 kg/m^2), pregnant women and women with breast implants were also excluded.

All procedures were in accordance with the ethical standards of the institutional research committee and with the 1964 Helsinki declaration and its later amendments. Informed consent was obtained from all participants.

Clinical assessment

The subjects' visit consisted of physical examination, 12-lead ECG, venous blood sampling, and 2D-echocardiography. Physical examination included height, weight, blood pressure, saturation, and results of heart, lungs and abdominal findings. Blood samples were taken to determine serum creatinine as an indicator for renal function.

Echocardiographic image acquisition

All echocardiographic studies were performed by 2 experienced sonographers (JM, WV). Two-dimensional greyscale harmonic images were obtained in the left lateral decubitus position using an iE33 or EPIQ7 ultrasound system equipped with a transthoracic broad-band X5–1 matrix transducer (composed of 3040 elements with 1–5 MHz). Standard apical 4-chamber (A4C), 2-chamber (A2C) and 3-chamber (A3C) views were obtained for STE at frame rates of ≥ 50 frames/sec.[9]

Conventional echocardiographic measurements

For chamber measurements we used the current guidelines of the American Society of Echocardiography and the European Association of Cardiovascular Imaging.[1] From the 4C, pulsed-wave Doppler examination was performed to obtain peak mitral inflow velocities at early (E) and late (A) diastole and E deceleration time. Tissue Doppler imaging was performed to obtain myocardial tissue velocity at the septal mitral annulus at early diastole (E'). LV end-diastolic, LV end-systolic and LV ejection fraction were derived with the biplane method of disks based on one cardiac cycle using QLAB software.

Speckle-tracking analysis

The data sets were blinded regarding the subject's ID. Offline analyses were performed by 2 independent observers (MM, JM) using QLAB 10. Cardiac cycles were defined by the positioning of R-waves. Aortic valve closure time was used to define end-systole[3] by selecting the frame of closure on the 3C view.

To assess peak systolic LV LS and strain rate, the endocardial and epicardial borders were traced in the 4C, 3C and 2C on an end-diastolic frame. The program automatically divided the walls in several segments (LV algorithm based on 17-segment model) and tracked these points on a frame-by-frame basis. When tracking was suboptimal, we readjusted the borders. Segments with persistently inadequate tracking were excluded

from analysis. Peak systolic strain and strain rate values were defined as the peak values on the curves during the ejection phase of one cardiac cycle. Figure 1 shows examples of LS analyses (GLS, LS-4C, LS-3C and LS-2C). Data were exported to a spreadsheet program (Excel; Microsoft Corporation, Redmond, WA, USA). All references to strain changes consider the absolute value of the number, so that higher or increase in LS means a more negative number and lower or decrease means a less negative number.[10]
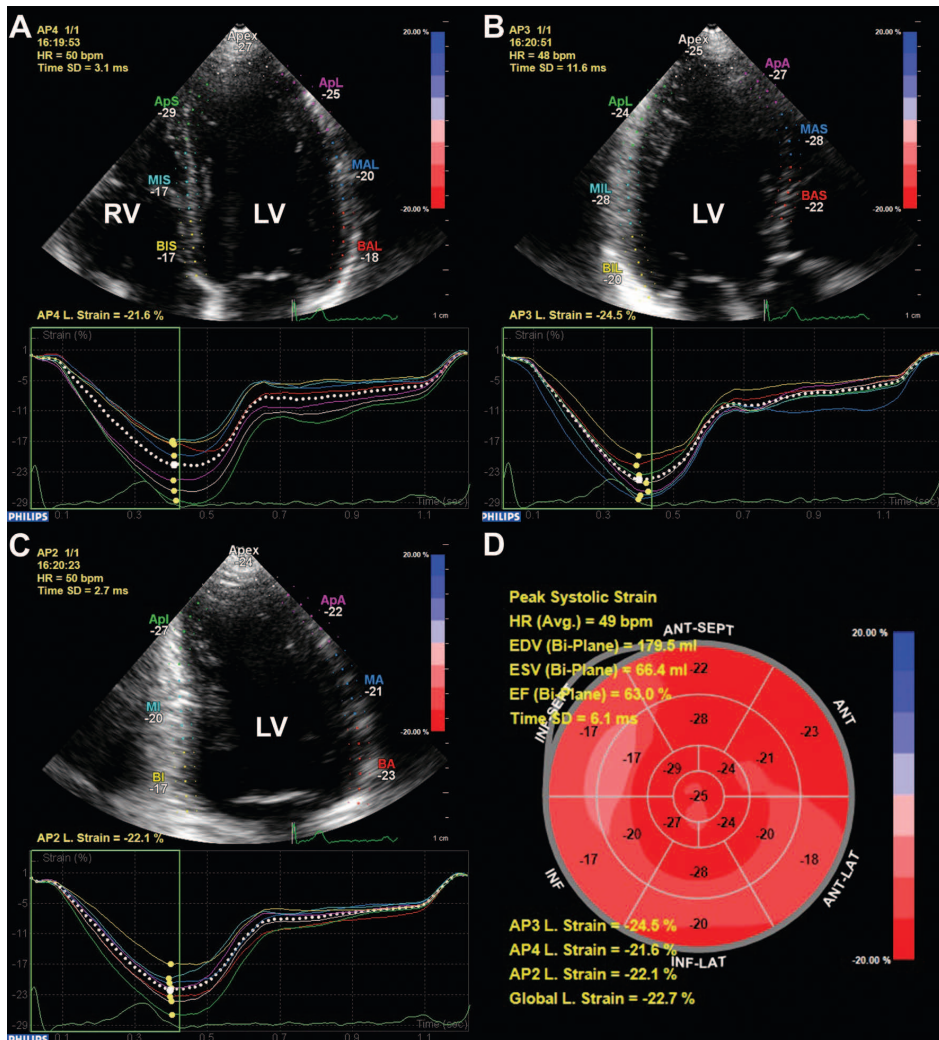
Figure 1 Example of left ventricular longitudinal strain measurements in a healthy individual
The left ventricle was traced in the apical four-, three-, and two-chamber views at end-diastole. The walls were automatically divided into seven segments at each view, and the global longitudinal strain at each view was calculated (**A-C**). The segmental strains were plotted in a bull's eye, and the left ventricular global longitudinal strain based on a 17-segment model was calculated (**D**).
AP2=apical two-chamber; AP3=apical three-chamber; AP4=apical four-chamber; GL=global longitudinal; LV=left ventricle; RV=right ventricle

Statistical analysis

The data distribution was checked using histograms and the Shapiro-Wilk test. Depending on the distribution, continuous data are presented as mean ± standard deviation (SD), or median with first and third quartile [Q1-Q3] or interquartile range [IQR]. Categorical data are presented as frequencies and percentages. For comparison of normally distributed continuous variables in one group, we used the paired t-test and between two groups the Student's t-test. In case of skewed distribution, the Mann-Whitney-U test was applied. For comparison of frequencies the chi-square test was used. Linear regression analysis was used to explore the relationship between strain and baseline characteristics. Variables that reached $P< .001$ and did not show collinearity with other variables were included in a multivariable model. In case of collinear variables, the variable with the highest correlation coefficient was included. All statistical analyses were performed using SPSS statistics version 21 (IBM Corp., Armonk, NY, USA). The statistical tests were two-sided and a $P< 0.05$ was considered statistically significant.

Intra-observer agreement (MM) was assessed by repeated analysis in a sample of 20 subjects (n = 4 per decile, randomly selected) > 1 month after the initial analysis, in randomly mixed order, and blinded to the initial results. Assessment of inter-observer agreement was performed by a second observer (JM) in the same sample. The agreement between 2 measurements was determined as the mean of the differences ±1.96SD.[11] Additionally, the coefficient of variation was provided (SD of the differences of 2 measurements divided by their mean).

RESULTS

Study population

Of the 155 subjects who came to our medical center, 147 were included (age 44.6±13.7 years, 50% female). Table 1 shows the characteristics of the study population per age group. Eight subjects were excluded for various reasons: breast implants (n = 2), valvular pathology (n = 2), surgically closed patent ductus arteriosus (n = 1), hypertension (n = 1), morbid obesity (n = 1), and right bundle branch block on ECG (n = 1). Due to technological reasons, the echocardiographic images of 2 subjects had not been exported to the QLAB working station.

Left ventricular longitudinal strain

Among the 145 remaining subjects, the feasibility of LV peak systolic LS-4C and LS-2C was 99%, LS-3C 97%, and GLS 97%. Figure 2 shows the feasibility per segment on each view. The mean GLS of the healthy subjects was -20.8±2.0%. The mean GLS, LS-4C, LS-3C, LS-2C and segmental strains per age group are summarized in Table 2. GLS did not decrease significantly with advancing age as continuous variable (Figure 3). However, comparing GLS of subjects > 55 years old (n = 35) versus ≤ 55 years (n = 106), resulted
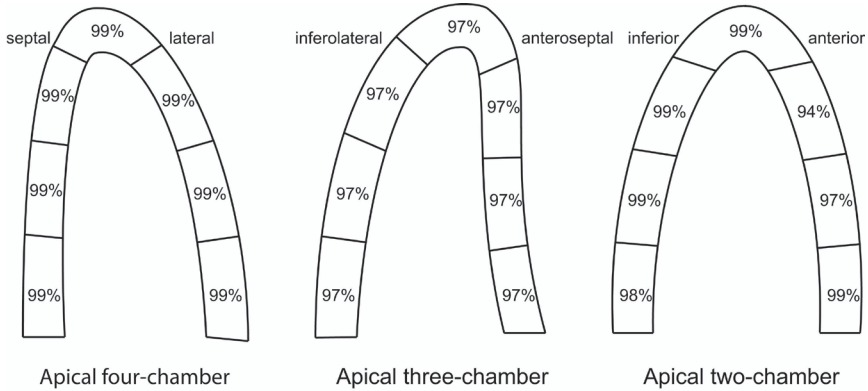
Figure 2 The feasibility of strain calculation per segment. Each number reflects the percentage of possible strain measurements of that segment in our cohort.
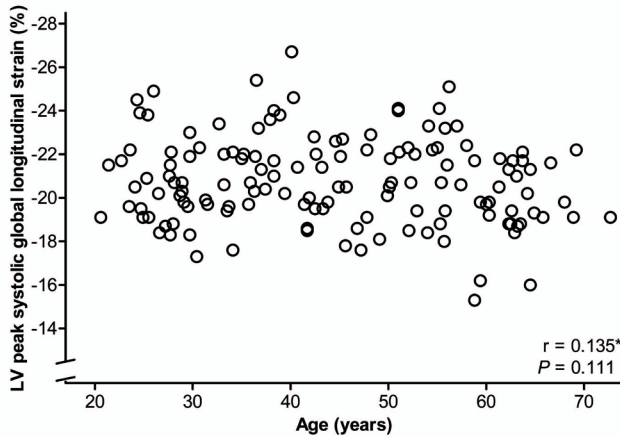
Figure 3 Correlation between left ventricular peak systolic global longitudinal strain and age. This scatter plot represents one person's left ventricular peak systolic global longitudinal strain value versus his/her age. No significant relationship could be observed between these two variables.
*To aid interpretation of the Pearson's correlation coefficient, global longitudinal strain has been analyzed as positive number. LV= left ventricular.

in a lower strain in the older subjects (-20.2±2.0% vs. -21.0±2.0%, P = 0.029). In all age groups, the apical segments showed higher peak systolic strain than the basal segments.

Relationships with left ventricular global longitudinal strain

Males had significantly lower GLS than females (-20.1±1.8% vs. -21.5±2.0%, P< 0.001). Figure 4 presents the median GLS for males and females stratified by age.

Table 3 shows the results of univariable and multivariable regression analyses with GLS as dependent variable. There was a linear decrease in GLS with increasing blood pressure and BSA, but no relationship was found with age as continuous variable. A higher GLS

Table 1 Characteristics of the study population

Characteristic		Age group (y)				
		20–29	**30–39**	**40–49**	**50–59**	**60–72**
		n = 32	**n = 28**	**n = 28**	**n = 31**	**n = 28**
Sex, female		16 (50%)	14 (50%)	14 (50%)	16 (52%)	14 (50%)
Age (y)		26±3	35±3	44±3	55±3	64±3
Current smoker		2 (6%)	1 (4%)	4 (14%)	5 (16%)	1 (4%)
Physical examination						
	Body mass index (kg/m²)	22.3±2.1	24.1±3.4	24.6±3.7	25.4±2.8	25.8±3.1
	Body surface area (m²)	1.84±0.17	1.89±0.18	1.92±0.22	1.92±0.18	1.90±0.19
	Systolic blood pressure (mmHg)	124±13	121±10	123±12	130±15	137±17
	Diastolic blood pressure (mmHg)	76±8	78±7	80±10	83±11	83±8
ECG						
	Sinus rhythm	32 (100%)	28 (100%)	28 (100%)	31 (100%)	28 (100%)
	Heart rate (bpm)	61±11	60±8	61±10	62±9	65±10
	PR interval (ms)	156±24	150±21	156±24	159±16	173±18
	QRS duration (ms)	96±8	97±9	97±9	95±10	97±10
Echocardiography, left ventricle						
	End-diastolic dimension (mm)	46.4±3.2	46.9±3.2	45.3±3.9	44.8±4.5	44.0±5.1
	End-systolic dimension (mm)	28.6±3.2	28.3±3.3	28.4±4.6	28.2±4.2	28.0±6.2
	E-wave (m/s)	0.80±0.16	0.75±0.16	0.66±0.15	0.65±0.11	0.59±0.13
	A-wave (m/s)	0.39±0.14	0.43±0.08	0.47±0.10	0.56±0.12	0.62±0.17
	Deceleration time (ms)	177±29	181±32	185±29	194±31	216±64

Table 1 Characteristics of the study population (continued)

Characteristic	Age group (y)				
	20–29	30–39	40–49	50–59	60–72
	n = 32	n = 28	n = 28	n = 31	n = 28
E' (cm/s)	12.5±1.8	10.4±1.6	9.2±1.6	8.2±1.8	6.8±1.7
E/A ratio	2.27±0.77	1.80±0.40	1.43±0.38	1.21±0.34	1.01±0.32
E/E' ratio	6.45±1.35	7.27±1.47	7.29±1.71	8.11±1.44	9.04±2.42
End-systolic volume (mL)	47±11	47±13	51±15	45±12	48±16
End-diastolic volume (mL)	117±23	120±23	125±31	116±21	116±31
End-systolic volume / BSA (mL/m^2)	25.4±5.1	24.7±6.2	26.2±5.5	23.2±5.1	25.0±6.9
End-diastolic volume / BSA (mL/m^2)	63.9±9.5	63.1±9.9	64.1±10.9	60.5±8.0	60.6±12.2
Ejection fraction, biplane (%)	60.4±3.6	61.4±5.0	59.2±4.5	61.9±5.3	59.2±4.5

Values are presented as n (%) or mean±SD.
E, peak mitral inflow velocity at early diastole; A, peak mitral inflow velocity at late diastole; E', early diastolic annular myocardial velocity.

Table 2 Left ventricular peak systolic global and segmental longitudinal strain

Age (y)		20–29	30–39	40–49	50–59	60–72	P-value*
		n = 31	n = 28	n = 27	n = 30	n = 27	
GLS (%)		-20.8±1.9	-21.3±1.9	-20.7±2.2	-21.1±2.4	-20.0±1.5	0.189
LS-4C		-21.1±2.0	-21.4±2.1	-20.9±2.5	-21.0±2.9	-19.9±1.7	0.068
	Basal septal	-16.4±2.3	-16.9±2.7	-16.5±3.2	-15.8±3.5	-14.1±2.7	0.001
	Mid septal	-18.6±3.1	-18.6±2.7	-16.8±3.7	-17.0±3.3	-16.0±2.8	0.001
	Apical septal	-27.0±3.4	-27.3±2.7	-27.4±3.9	-28.4±4.6	-27.1±3.6	0.377
	Apex	-25.2±2.5	-25.1±2.5	-24.5±3.2	-25.2±3.9	-23.9±2.6	0.349
	Apical lateral	-23.4±2.5	-23.1±3.1	-21.8±3.7	-22.0±3.8	-20.7±2.4	0.003
	Mid lateral	-18.9±3.4	-20.2±2.7	-20.5±3.0	-20.1±3.4	-18.5±2.8	0.883
	Basal lateral	-19.1±2.5	-19.3±3.0	-19.3±3.3	-19.3±3.6	-19.1±2.1	0.961
LS-3C		-20.2±2.5	-21.5±2.4	-21.4±2.5	-21.4±3.3	-20.8±2.7	0.264
	Basal inferolateral	-17.3±3.7	-18.5±3.1	-19.8±3.6	-18.9±3.5	-19.9±4.0	0.016
	Mid inferolateral	-21.2±3.6	-22.8±4.1	-22.3±3.2	-21.9±4.4	-21.2±4.2	0.748
	Apical lateral	-21.4±3.2	-22.2±3.2	-21.5±3.6	-22.3±4.5	-20.6±2.8	0.684
	Apex	-22.4±3.2	-23.4±3.0	-23.4±4.4	-23.4±4.7	-22.2±3.5	0.586
	Apical anterior	-23.3±4.1	-24.7±4.1	-25.3±5.7	-24.4±6.2	-24.3±4.4	0.273
	Mid anteroseptal	-19.7±3.1	-20.4±3.7	-20.0±4.3	-20.8±4.6	-19.8±2.9	0.449
	Basal anteroseptal	-17.4±3.2	-19.4±3.2	-18.2±2.8	-19.4±3.7	-18.4±3.8	0.131
LS-2C		-20.9±2.1	-21.0±2.1	-20.1±2.6	-20.8±2.5	-19.3±1.9	0.015
	Basal inferior	-16.8±2.9	-16.9±3.0	-17.1±3.5	-16.5±3.7	-15.2±3.2	0.087
	Mid inferior	-19.3±2.9	-18.7±3.0	-18.1±3.3	-18.3±3.2	-17.0±2.6	0.006
	Apical inferior	-25.5±3.0	-25.9±2.7	-24.5±3.4	-26.2±3.3	-24.4±2.8	0.258
	Apex	-23.4±2.7	-24.0±2.6	-22.3±3.0	-24.0±3.3	-21.9±2.3	0.155
	Apical anterior	-21.7±3.0	-22.0±3.2	-20.6±3.3	-22.5±3.9	-19.5±2.7	0.084
	Mid anterior	-21.1±3.2	-20.9±3.1	-19.2±3.3	-19.8±3.9	-19.4±3.4	0.006
	Basal anterior	-19.1±2.9	-19.4±4.3	-19.7±3.8	-19.3±3.1	-18.6±3.2	0.359

Values are presented as mean±SD. *Using linear regression analysis.
GLS, global longitudinal strain; LS, longitudinal strain; 4C, apical four-chamber; 3C, apical three-chamber; 2C, apical two-chamber.

Table 3 Univariable and multivariable regression analyses of left ventricular global longitudinal strain

| | LV GLS | | | | | LV GLS / BSA | | | | |
| | Univariable | | Multivariable | | | Univariable | | Multivariable | | |
	Pearson's r	P-value	Unstandard-ized β	Standard-ized β	P-value	Pearson's r	P-value	Unstandard-ized β	Standar-dized β	P-value
Age (y)	-0.14	0.111				-0.13	0.127			
Sex (female)	0.34	**< 0.001**				0.64	**< 0.001**	1.04	0.29	**< 0.001**
Physical examination										
Body surface area (m²)	-0.35	**< 0.001**	0.92	0.09	0.337					
Body mass index (kg/m²)	-0.26	**0.002**								
Systolic blood pressure (mmHg)	-0.40	**< 0.001**	-0.04	-0.26	**0.001**	-0.44	**< 0.001**	-0.03	-0.21	**< 0.001**
Diastolic blood pressure (mmHg)	-0.36	**< 0.001**				-0.44	**< 0.001**			
ECG										
Heart rate (bpm)	-0.21	**0.012**				-0.05	0.523			
QRS duration (ms)	-0.14	0.089				-0.38	**< 0.001**	-0.01	-0.04	0.512
Echocardiography, left ventricle										
End-diastolic dimension (mm)	0.08	0.324				-0.15	0.087			
End-systolic dimension (mm)	0.02	0.855				-0.15	0.072			
E-wave (m/s)	0.34	**< 0.001**	1.99	0.16	**0.031**	0.39	**< 0.001**	1.53	0.14	**0.014**
A-wave (m/s)	-0.01	0.870				0.03	0.771			
Deceleration time (ms)	-0.17	0.050				-0.22	**0.009**			
E' (cm/s)	0.26	**0.002**				0.30	**< 0.001**			
E/A-ratio	0.19	**0.021**				0.21	**0.011**			
E/E'-ratio	0.01	0.907				0.02	0.809			
End-diastolic volume (mL)	-0.32	**< 0.001**				-0.62	**< 0.001**			
End-systolic volume (mL)	-0.53	**< 0.001**	-0.07	-0.47	**< 0.001**	-0.70	**< 0.001**	-0.06	-0.43	**< 0.001**
Ejection fraction, biplane (%)	0.69	**< 0.001**				0.58	**< 0.001**			

Global longitudinal strain has been analyzed as positive number to aid interpretation of correlations. Bold font indicates statistically significant correlations. Variables that reached a *P*< 0.001 and did not show collinearity with other variables were included in the multivariable model. In case of collinear variables, the variable with the highest correlation coefficient was included in the multivariable model. IV, left ventricle; GLS, global longitudinal strain; BSA, body surface area; E, peak mitral inflow velocity at early diastole; A, peak mitral inflow velocity at late diastole; E', early diastolic annular myocardial velocity.
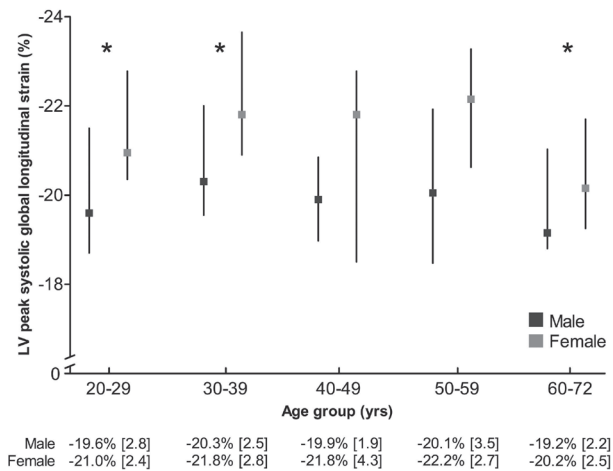
Figure 4 Median left ventricular global longitudinal strain stratified by sex and age. *P< 0.05. Strain values are presented as median [IQR] by sex and age group.
LV= left ventricular.

was associated with more favorable indices of diastolic function and with smaller LV end-diastolic and end-systolic volumes.

Because of the relationship between GLS and BSA, we additionally performed univariable regression analysis of GLS indexed for BSA. Indexing for BSA strengthened most of the significant correlations with the subjects' characteristics. In multivariable analysis, sex, systolic blood pressure, E wave and LV end-systolic volume remained significant predictors for GLS indexed for BSA (Table 3).

Left ventricular longitudinal strain rate

LV peak systolic strain rates per age group are given in Table 4. Linear regression analysis showed lower strain rates on the A4C and A2C with increasing age. Strain rates were comparable between men and women. Correlation analysis between strain rate and BSA showed that on the A4C 6 out of 7 segments correlated significantly, on the A3C 1 out of 7, and on the A2C 5 out of 7.

Intra-observer and inter-observer agreement

The intra-observer agreement for GLS was 0.01±0.57%, and the inter-observer agreement -0.67±0.91%. Figure 5 presents the linear correlation and Bland-Altman plots for the intra-observer and inter-observer measurements.

Table 4 Left ventricular peak systolic strain rates per age group

Age (y)	20–29	30–39	40–49	50–59	60–72	P-value*
	n = 31	n = 28	n = 27	n = 30	n = 27	
Apical four-chamber						
Basal septal (s^{-1})	-0.79±0.12	-0.84±0.11	-0.81±0.18	-0.77±0.14	-0.69±0.13	0.002
Mid septal	-0.92±0.15	-0.92±0.15	-0.85±0.18	-0.87±0.17	-0.78±0.13	0.002
Apical septal	-1.26±0.18	-1.26±0.16	-1.25±0.19	-1.25±0.16	-1.16±0.20	0.134
Apex	-1.22±0.17	-1.16±0.13	-1.12±0.18	-1.12±0.19	-1.02±0.14	< 0.001
Apical lateral	-1.22±0.22	-1.11±0.16	-1.01±0.23	-1.04±0.23	-0.90±0.13	< 0.001
Mid lateral	-1.00±0.13	-1.03±0.14	-0.98±0.17	-0.99±0.15	-0.91±0.13	0.026
Basal lateral	-1.00±0.16	-0.97±0.17	-0.99±0.16	-0.90±0.16	-0.91±0.12	0.008
Apical three-chamber						
Basal inferolateral	-0.93±0.15	-1.01±0.17	-0.98±0.18	-0.94±0.14	-0.93±0.23	0.733
Mid inferolateral	-1.03±0.18	-1.09±0.19	-1.06±0.17	-1.05±0.15	-1.02±0.20	0.547
Apical lateral	-1.00±0.17	-1.05±0.13	-1.00±0.14	-1.02±0.21	-0.93±0.15	0.097
Apex	-1.01±0.13	-1.06±0.11	-1.05±0.17	-1.04±0.21	-0.99±0.19	0.948
Apical anterior	-1.05±0.16	-1.11±0.15	-1.12±0.24	-1.09±0.26	-1.09±0.24	0.405
Mid anteroseptal	-0.97±0.13	-0.99±0.16	-0.99±0.20	-0.97±0.16	-0.94±0.20	0.873
Basal anteroseptal	-0.84±0.16	-0.95±0.16	-0.92±0.15	-0.92±0.18	-0.87±0.19	0.595
Apical two-chamber						
Basal inferior	-0.80±0.15	-0.79±0.09	-0.80±0.15	-0.77±0.13	-0.71±0.12	0.013
Mid inferior	-0.92±0.15	-0.87±0.11	-0.89±0.16	-0.89±0.13	-0.83±0.13	0.053
Apical inferior	-1.17±0.14	-1.17±0.12	-1.12±0.15	-1.13±0.11	-1.06±0.16	0.004
Apex	-1.08±0.14	-1.07±0.10	-1.01±0.15	-1.03±0.11	-0.96±0.13	0.001
Apical anterior	-1.01±0.17	-1.00±0.12	-0.95±0.16	-0.99±0.16	-0.91±0.15	0.028
Mid anterior	-0.98±0.17	-0.98±0.16	-0.92±0.14	-0.91±0.17	-0.91±0.16	0.005
Basal anterior	-0.89±0.17	-0.89±0.15	-0.90±0.17	-0.87±0.13	-0.84±0.14	0.088

Values are presented as mean±SD. *Using linear regression analysis.

DISCUSSION

To our best knowledge, this prospective cohort study, consisting of 147 healthy volunteers and who are stratified per age decade, is the first study reporting normal LV LS values after the strain standardization initiative of the task force.[10] Sex, BSA and blood pressure were the most important anthropometric factors that influence LV GLS assessed with QLAB, whereas age did not. Strain rates were lower with increasing age and did not differ between men and women.

Left ventricular longitudinal strain

LV GLS was feasible in 97% of the subjects, and LS-4C and LS-2C even in 99%, which is an important amenity for the wider use of LS on a daily basis in the clinical setting. The mean GLS of our study cohort was -20.8±2.0%, which is comparable with the
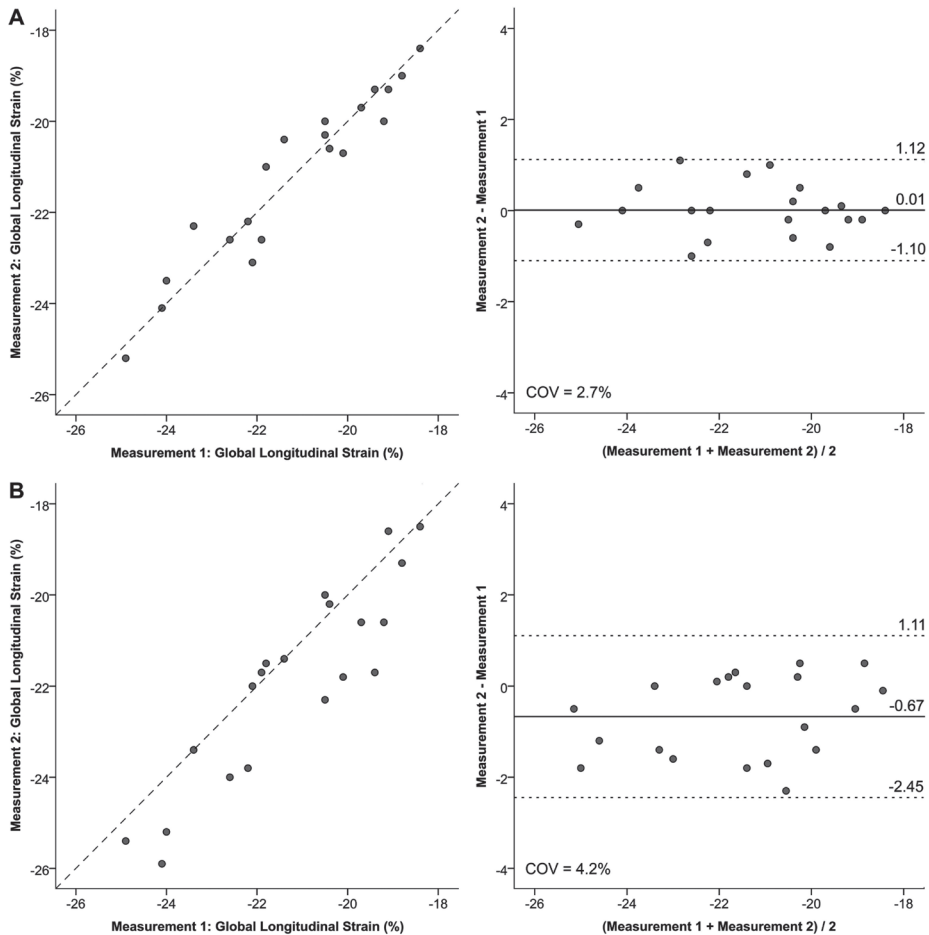
Figure 5 Linear correlation and Bland-Altman plots for intra-observer and interobserver measurements of left ventricular global longitudinal strain. First row (**A**) refers to intra-observer agreement with one observer analyzing the same dataset twice. Second row (**B**) refers to inter-observer agreement with two observers analyzing the same dataset. In the Bland-Altman plots on the right side, the striped lines depict the mean difference of two measurements, and the dashed lines depict the limits of agreement (1.96SD). COV=coefficient of variation.

reported -19.7% in a meta-analysis.[8] However, the majority of included studies in that meta-analysis used software of another vendor. Moreover, the included studies are dated and therefore newer versions of the software are already in use.

We observed LV segmental strain heterogeneity: LS gradually increased from the basal to apical segments in all age groups, which is in line with the results reported by Sun et al.[12] Nowadays, analyzing regional ventricular function becomes more and more important. An increasing number of studies state that it is especially the function of some of the regions that are impaired in different types of heart diseases, for example decreased basal strain in hypertrophic cardiomyopathy and aortic stenosis.[13,14] Even in patients with

primarily right-heart pathology, evaluating regional LV deformation could be of particular importance. Patients with repaired tetralogy of Fallot had a decreased LV septal strain indicating that right ventricular dysfunction negatively affects LV function, which is called ventricular-ventricular interaction.[15]

In our study, GLS correlated well with LV ejection fraction. Kalam et al.[16] performed a systematic review and meta-analysis which compared GLS against LV ejection fraction in predicting all-cause mortality and cardiac-related events. Both endpoints were stronger associated with GLS than with LV ejection fraction. Therefore, GLS appears to have superior prognostic value to ejection fraction for predicting major adverse events.

Relationships with sex, age and body surface area

The cutoff value for normal LV ejection fraction is higher in women than men.[1] The same should be applied for LS, because we found significant greater values in women, which corroborates with previous STE studies[12,17] and a recent study with feature-tracking cardiovascular magnetic resonance (CMR).[18] In a relatively large sample of the general population, where LS was measured with colour Doppler myocardial imaging,[19] no sex differences were found, neither in a meta-analysis by Yingchoncharoen et al.[8] The different vendors that have been included might have had an influence.

We did not observe a clear relationship between GLS and the age decades. This might be explained by our relatively low sample size. On the other hand, the absence of a relationship was also reported on GLS assessed with feature-tracking CMR.[18] However, we found a significant difference in strain between subjects ≤ 55 years old and subjects > 55. Dividing subjects in groups younger and older than 55 years has also been performed by Sun et al. resulting in a slightly lower strain in the older patients.[12] In a study including over 1200 healthy individuals with a maximum age of 89 years, systolic strain was also lower with increasing age.[20] Due to the fact that age often goes along with higher blood pressure and BSA, it seems plausible that at a certain age, decrease in strain could occur. However, we did not include subjects > 72 years. Those subjects may have a lower GLS than the subjects of our cohort, but this assumption has to be investigated. It is however not easy to include subjects above 72 years of age without history of or risk factors for cardiovascular disease.

We found a weak-to-moderate positive correlation between GLS and BSA. Such correlation had also been described with the use of feature-tracking CMR in healthy controls,[18] and, though weaker, with STE.[12] Because of this correlation and the possible interaction between BSA and other anthropometric and echocardiographic measurements, we decided to index GLS for BSA. This indexation resulted in stronger correlations regarding systolic and diastolic blood pressure, some diastolic function indices and LV end-diastolic and end-systolic volumes. Regarding our results, we advise to use sex and/or BSA specific values.

Relationship with blood pressure

Even though all our subjects were healthy and did not have hypertension, we still observed a moderate correlation between higher blood pressure and lower GLS. A similar correlation was also found in a meta-analysis with a larger sample of healthy subjects.[8] In patients with hypertension, decreased GLS was reported in the presence of a normal or even supranormal LV ejection fraction.[21] As a compensatory mechanism for preserving the ejection fraction, these patients had an increased twist compared to normal controls.[21] It is generally known that, besides aging[22], hypertension is associated with alterations in diastolic LV function.[23] In our healthy cohort, some of the diastolic function indices, such as E wave, deceleration time, E', and E/A ratio showed significant relationships with GLS. Even after implementation the "E wave" in a multivariable regression model, it remained a significant determinant for GLS. A recently published paper of the CARDIA study described that higher cumulative exposure to blood pressure over 25 years from young adulthood to middle age was associated with lower LV LS and diastolic dysfunction, but not with LV ejection fraction.[24] These findings reflect that LS is a load dependent parameter and that a relatively small increase in afterload will result in lower LS. The fact that GLS correlates with blood-pressure values at the time of echocardiography in our cohort, makes no distinction whether GLS is just a pure reflection of the current degree of afterload or a reasonable and sensitive marker for incipient LV dysfunction caused by chronic hypertension. The definition of hypertension is traditionally based on office blood-pressure measurements.[25] However, blood pressure could be elevated in the office and normal out of the office which is termed white-coat hypertension, whereas masked hypertension refers to a normal blood pressure in the office and abnormally high out of the medical environment.[23] Hence, out-of-office blood-pressure measurements play an important role in hypertension management,[23,25] but home and ambulatory blood-pressure monitoring both have their limitations. It would be helpful if STE-derived strain can serve, already in a preclinical state, as an objective diagnostic tool to determine the severity of hypertension without the interference of overestimation (white-coat hypertension) or underestimation (masked hypertension). Whether decreased strain really can serve as an early marker and reasonable predictor of hypertension and future heart failure in this patient population has to be investigated in a follow-up study.

Left ventricular longitudinal strain rate

In contrast to LS, strain rates of most of the segments did significantly decrease over the age decades, but regarding sex no clear differences were found. Studies evaluating the effects of age on strain rate are scarce, and studies reporting strain rates measured with the newer STE software versions even more. Although not measured with STE but with Doppler imaging, strain rate showed significant dependence on age in some studies.[19,20,26] It has been supposed that slower calcium cycling with age leads to longer systolic contraction periods. This physiological mechanism may be an explanation for the fact that decrease in tissue displacement is less age-related than decrease in velocity.[26,27] Therefore, peak systolic strain could be preserved despite lower peak strain rate.

Intra-observer and inter-observer agreement

The intra-observer and inter-observer agreement were excellent and evidently better than previously reported by others.[12,17] Recent publications showed that reproducibility of GLS measurements was superior to LV ejection fraction.[28,29] The improvement is probably a result of the more automated software that now have been used and is an important finding making GLS more sound for clinical use.

Study limitations

Between-vendor variability is often mentioned as a limitation to the clinical application of strain imaging. In this study, we only used Philips ultrasound equipment and QLAB software. However, after the implementation of the standardization process, the variability of GLS in the later-developed software versions between two leading ultrasound manufactures have been reduced[7] making the values reported by us more widely applicable nowadays.

Due to the relatively small sample size and the single-center study design, conclusions should be interpreted with caution. We did not obtain strain values of subjects from 73 years or older, which form a great part of the current patient population. We measured strain on 2D views which could lead to through-plane artifact. The ongoing developments of 3D strain are promising to overcome this limitation.

CONCLUSIONS

Our study resulted in normative LV LS values assessed with QLAB 10 in a healthy population aged 20 to 72 years. Sex, BSA, older age and blood pressure influence GLS. For interpretation of strain results in clinical practice, it is crucial to take these factors into account.

REFERENCES

1. Lang RM, Badano LP, Mor-Avi V, et al: Recommendations for cardiac chamber quantification by echocardiography in adults: an update from the american society of echocardiography and the European association of cardiovascular imaging. *Eur Heart J Cardiovasc Imaging* 2015;16:233-271.
2. Teske AJ, De Boeck BW, Melman PG, et al: Echocardiographic quantification of myocardial function using tissue deformation imaging, a guide to image acquisition and analysis using tissue Doppler and speckle tracking. *Cardiovasc Ultrasound* 2007;5:27.
3. Mor-Avi V, Lang RM, Badano LP, et al: Current and evolving echocardiographic techniques for the quantitative evaluation of cardiac mechanics: ASE/EAE consensus statement on methodology and indications endorsed by the Japanese Society of Echocardiography. *Eur J Echocardiogr* 2011;12:167-205.
4. Nagata Y, Takeuchi M, Mizukoshi K, et al: Intervendor variability of two-dimensional strain using vendor-specific and vendor-independent software. *J Am Soc Echocardiogr* 2015;28:630-641.
5. Mondillo S, Galderisi M, Mele D, et al: Speckle-tracking echocardiography: a new technique for assessing myocardial function. *J Ultrasound Med* 2011;30:71-83.

6. Koopman LP, Slorach C, Manlhiot C, et al: Assessment of myocardial deformation in children using Digital Imaging and Communications in Medicine (DICOM) data and vendor independent speckle tracking software. *J Am Soc Echocardiogr* 2011;24:37-44.

7. Yang H, Marwick TH, Fukuda N, et al: Improvement in Strain Concordance between Two Major Vendors after the Strain Standardization Initiative. *J Am Soc Echocardiogr* 2015;28:642-648 e647.

8. Yingchoncharoen T, Agarwal S, Popovic ZB, et al: Normal ranges of left ventricular strain: a meta-analysis. *J Am Soc Echocardiogr* 2013;26:185-191.

9. Rosner A, Barbosa D, Aarsaether E, et al: The influence of frame rate on two-dimensional speckle-tracking strain measurements: a study on silico-simulated models and images recorded in patients. *Eur Heart J Cardiovasc Imaging* 2015;16:1137-1147.

10. Voigt JU, Pedrizzetti G, Lysyansky P, et al: Definitions for a Common Standard for 2D Speckle Tracking Echocardiography: Consensus Document of the EACVI/ASE/Industry Task Force to Standardize Deformation Imaging. *J Am Soc Echocardiogr* 2015;28:183-193.

11. Bland JM, Altman DG: Statistical methods for assessing agreement between two methods of clinical measurement. *Lancet* 1986;1:307-310.

12. Sun JP, Lee AP, Wu C, et al: Quantification of left ventricular regional myocardial function using two-dimensional speckle tracking echocardiography in healthy volunteers--a multi-center study. *Int J Cardiol* 2013;167:495-501.

13. Serri K, Reant P, Lafitte M, et al: Global and regional myocardial function quantification by two-dimensional strain: application in hypertrophic cardiomyopathy. *J Am Coll Cardiol* 2006;47:1175-1181.

14. Carstensen HG, Larsen LH, Hassager C, et al: Tissue Velocities and Myocardial Deformation in Asymptomatic and Symptomatic Aortic Stenosis. *J Am Soc Echocardiogr* 2015.

15. Menting ME, van den Bosch AE, McGhie JS, et al: Assessment of ventricular function in adults with repaired tetralogy of Fallot using myocardial deformation imaging. *Eur Heart J Cardiovasc Imaging* 2015;16(12):1347-57..

16. Kalam K, Otahal P, Marwick TH: Prognostic implications of global LV dysfunction: a systematic review and meta-analysis of global longitudinal strain and ejection fraction. *Heart* 2014;100:1673-1680.

17. Takigiku K, Takeuchi M, Izumi C, et al: Normal range of left ventricular 2-dimensional strain: Japanese Ultrasound Speckle Tracking of the Left Ventricle (JUSTICE) study. *Circ J* 2012;76:2623-2632.

18. Taylor RJ, Moody WE, Umar F, et al: Myocardial strain measurement with feature-tracking cardiovascular magnetic resonance: normal values. *Eur Heart J Cardiovasc Imaging* 2015;16:871-881.

19. Kuznetsova T, Herbots L, Richart T, et al: Left ventricular strain and strain rate in a general population. *Eur Heart J* 2008;29:2014-2023.

20. Dalen H, Thorstensen A, Aase SA, et al: Segmental and global longitudinal strain and strain rate based on echocardiography of 1266 healthy individuals: the HUNT study in Norway. *Eur J Echocardiogr* 2010;11:176-183.

21. Ahmed MI, Desai RV, Gaddam KK, et al: Relation of torsion and myocardial strains to LV ejection fraction in hypertension. *JACC Cardiovasc Imaging* 2012;5:273-281.

22. Mantero A, Gentile F, Gualtierotti C, et al: Left ventricular diastolic parameters in 288 normal subjects from 20 to 80 years old. *Eur Heart J* 1995;16:94-105.

23. Mancia G, Fagard R, Narkiewicz K, et al: 2013 ESH/ESC guidelines for the management of arterial hypertension: the Task Force for the Management of Arterial Hypertension of the European Society of Hypertension (ESH) and of the European Society of Cardiology (ESC). *Eur Heart J* 2013;34:2159-2219.

24. Kishi S, Teixido-Tura G, Ning H, et al: Cumulative Blood Pressure in Early Adulthood and Cardiac Dysfunction in Middle Age: The CARDIA Study. *J Am Coll Cardiol* 2015;65:2679-2687.

25.   Fagard RH, Cornelissen VA: Incidence of cardiovascular events in white-coat, masked and sustained hypertension versus true normotension: a meta-analysis. *J Hypertens* 2007;25:2193-2198.

26.   Sun JP, Popovic ZB, Greenberg NL, et al: Noninvasive quantification of regional myocardial function using Doppler-derived velocity, displacement, strain rate, and strain in healthy volunteers: effects of aging. *J Am Soc Echocardiogr* 2004;17:132-138.

27.   Lakatta EG, Sollott SJ: Perspectives on mammalian cardiovascular aging: humans to molecules. *Comp Biochem Physiol A Mol Integr Physiol* 2002;132:699-721.

28.   Knackstedt C, Bekkers SC, Schummers G, et al: Fully automated versus standard tracking of left ventricular ejection fraction and longitudinal strain: the FAST-EFs Multicenter Study. *J Am Coll Cardiol*. 2015;29;66(13):1456-66.

29.   Farsalinos KE, Daraban AM, Ünlü S, et al: Head-to-head comparison of global longitudinal strain measurements among nine different vendors: the EACVI/ASE inter-vendor comparison study. *J Am Soc Echocardiogr* 2015:28(10):1171-1181, e2.

CHAPTER 9

A novel 13-segment standardized model for assessment of right ventricular function using two-dimensional iRotate echocardiography

Jackie S. McGhie
Myrthe E. Menting
Wim B. Vletter
René Frowijn
Jolien W. Roos-Hesselink
Osama I.I. Soliman
Heleen B. van der Zwaan
Marcel L. Geleijnse
Annemien E. van den Bosch

ABSTRACT

Aims

The aim of this study was to evaluate the feasibility of transthoracic two-dimensional (2D) iRotate, a new echo modality, to assess the whole right ventricle (RV) from a single transducer position based on anatomic landmarks.

Methods and results

The anatomic landmarks were first defined based on three-dimensional echocardiographic datasets using multiplane reconstruction analyses. Thereafter, we included 120 healthy subjects (51% male, age range 21–67 years). Using 2D iRotate, four views of the RV could be acquired based on these landmarks. The anterior, lateral, inferior wall (divided into three segments: basal-mid-apical), and RVOT anterior wall of the RV were determined. The feasibility of visualization of RV segments and tricuspid annular plane systolic excursion (TAPSE) and tissue Doppler imaging (TDI) measurements were assessed. To evaluate this model for diseased RVs, a small pilot study of 20 patients was performed. In 98% of healthy subjects and 100% of patients, iRotate mode was feasible to assess the RV from one single transducer position. In total, 86% and 95%, respectively, of the RV segments could be visualized. The visualization of the RVOT anterior wall was worse 23% and 75%, respectively. TAPSE and TDI measurements on all four views were feasible 93% and 92%, respectively, of the healthy subjects and in 100% of the patients.

Conclusion

With 2D iRotate, a comprehensive evaluation of the entire normal and diseased RV is feasible from a fixed transducer position based on anatomic landmarks. This is less time-consuming than the multi-view approach and enhances accuracy of RV evaluation. Imaging of the RVOT segment remains challenging.

INTRODUCTION

Assessment of right ventricular (RV) function is increasingly recognized as a prognostic factor in a variety of diseases such as left sided heart failure, pulmonary hypertension, and congenital heart disease in the acute phase and during follow up.[1] In everyday clinical practice, two-dimensional (2D) transthoracic echocardiography (TTE) remains the technique that is most often used for the assessment of ventricular function. Unlike the left ventricle (LV) that can be completely visualized from one apical window, for a comprehensive evaluation of RV size and function a multiview approach is necessary.[2–6] However, this multiview approach is impractical in a routine setting. It is time-consuming, operator dependent, and inaccurate due to the complex RV geometry. Current echocardiographic methodologies do not provide a robust assessment of RV function. Serial follow-up of RV measurements and function parameters result in significant inaccuracies from oblique plane acquisitions due to the lack of fixed landmarks.[2,4] A standardized echocardiographic approach taken from one acoustic window where an anatomic landmark in the image plane can be used to identify a specific RV wall could increase the accuracy of assessment of RV function in routine follow up. The aim of this study was: (1) to investigate if there are unique anatomic landmarks that could be used as a reference point to depict a specific RV wall from one standard acoustic window, the apical window, (2) to evaluate the feasibility of 2D transthoracic iRotate mode, a new echo modality, to comprehensively assess the RV based on these anatomic landmarks, and (3) to demonstrate in a small pilot group of patients with a diseased RV the feasibility of this technique for further investigation.

METHODS

Definition of Anatomic Landmarks Based on 3D Echo

In order to identify anatomic landmarks, seen in views that demonstrate specific RV walls, and to determine how to steer a 2D imaging plane (iRotate, Philips Medical systems, Best, The Netherlands) using a matrix-array transducer in order to acquire these views, we first examined several three-dimensional (3D) echocardiographic datasets. A total of 15, 3D datasets, acquired from the apical window, from normal subjects, and from patients with acquired and congenital (dilated RVs) heart disease, were examined with the TomTec 4D cardio-View 3.0 (TomTec-Arena version 1.2, TomTec, Munich, Germany) using the multiplane reconstruction analysis (MPR). The TomTec software features a quad screen display with three 2D cut planes (sagittal, transverse, coronal) and a 3D volume cube, created from a 3D volume dataset. With MPR three planes (sagittal, transverse, coronal) can be positioned through a region of interest and moved simultaneously. The four-chamber (4C) view displayed in the sagittal plane was adjusted to center the inter-ventricular septum (IVS)-RV apex along the midline and then transected at the base of the right and left ventricle (Figure 1A). The corresponding short-axis view, displayed in the transverse plane, shows: anterior, lateral and inferior wall of the RV (Figure 1B, C). With the MPR, it is
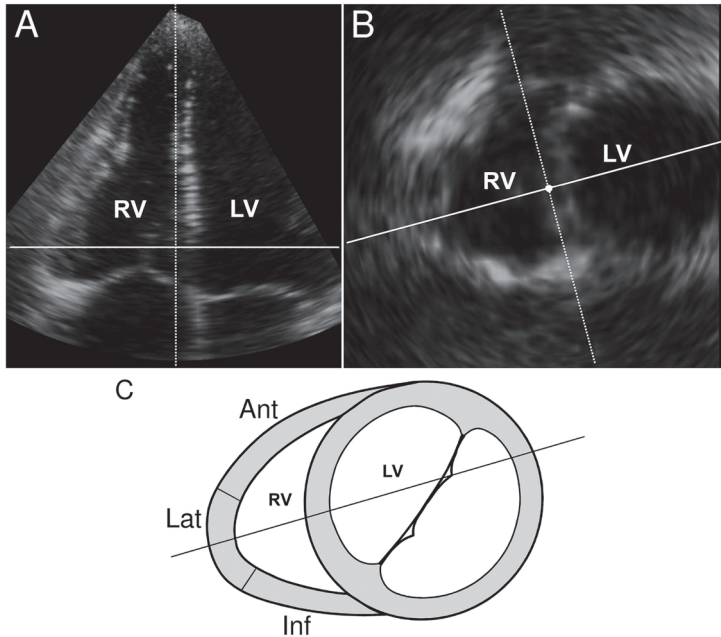
Figure 1 A. Display of the sagittal plane from the TomTec 4D Cardio-View multi-plane reconstruction analysis program showing the right side of the inter-ventricular septum (IVS) along the centerline. The white solid line depicts the position of the cut plane for the transverse image. **B.** Display of the transvers plane showing the basal short axis view of the right ventricle (RV). The cut plane (white solid line) transverses the lateral wall of the RV, IVS and left ventricle (LV). **C.** Schematic drawing of the transvers plane of the RV as seen in B. The RV walls displayed are as follows: Ant: anterior; Lat: lateral; Inf: inferior.

possible to rotate around the IVS in this transverse plane; thereby, anatomic landmarks could be defined in the corresponding sagittal plane.

Identified Anatomic Landmarks

In all examined 3D datasets, the four walls (anterior, lateral, inferior and RVOT anterior wall) of the RV could be identified according to a unique anatomic landmark. The anatomic landmarks that we identified were as follows:

– Mitral valve (standard 4C view): showing the lateral wall of the RV
– Coronary sinus: showing the anterior wall of the RV
– Aortic valve: showing the inferior wall of the RV
– RVOT: showing the RVOT anterior and inferior wall of the RV

The rotation around the IVS and the corresponding anatomic landmark identified in the sagittal plane are shown in Figure 2.
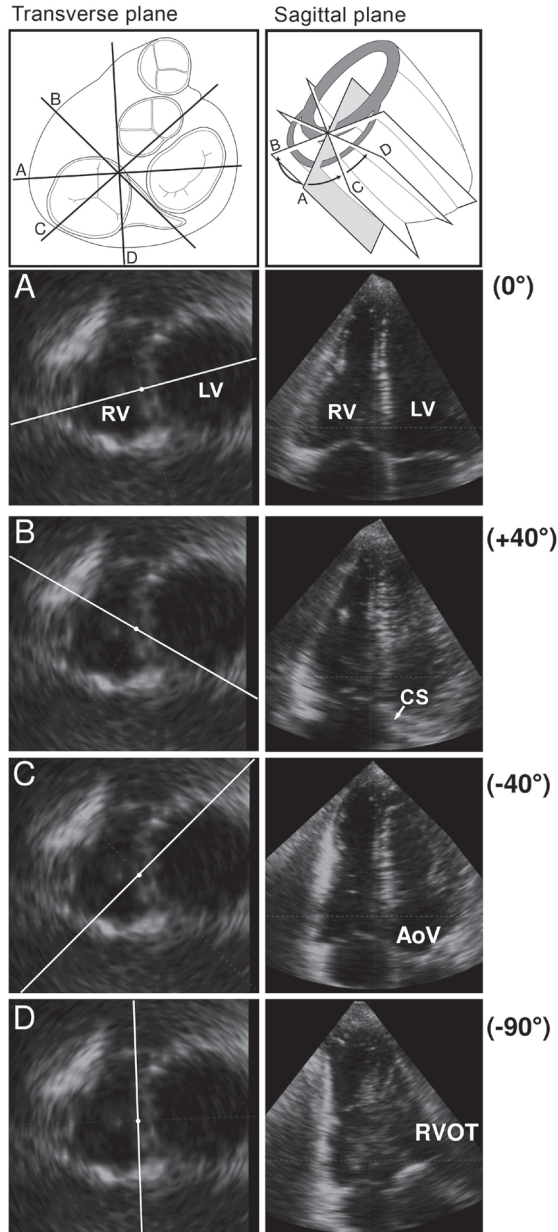
Figure 2 Schematic drawings and multiplane reconstruction of echocardiographic images displayed using the TomTec 4D Cardio-View analysis program. **Left**: schematic drawing and echocardiographic images of the cut planes A-D displaying the right ventricle (RV) in the transvers plane, viewed from the RV aspect. LV=left ventricle. **Right**: schematic drawing and echocardiographic images of the cut planes A-D from the RV and corresponding landmark in the sagittal plane. **A.** Four chamber view (0°). Landmark mitral valve giving rise to the lateral wall. **B.** Coronary sinus view (+40°). Landmark coronary sinus (CS) giving rise to the anterior wall. **C.** Aortic view (-40°). Landmark aortic valve (AoV) giving rise to the inferior wall. **D.** Coronal view (-90°). Landmark right ventricular outflow tract (RVOT) giving rise to the RVOT anterior wall.

Assessment of RV Function with iRotate Mode

The study was conducted in two phases: First, our proposed model was examined in healthy subjects, and then, a pilot study on patients with a diseased RV was performed.

Healthy Population

We prospectively recruited 120 healthy subjects (51% male, age range 21–67 years) with no medical history or current symptoms that suggested cardiovascular disease. All subjects underwent physical examination, a standard 12-lead electrocardiogram and a detailed echocardiogram with the addition of four apical views of the RV, according to the unique anatomic landmarks as described above. Exclusion criteria were any abnormal findings on the physical examination, electrocardiogram, or echocardiogram. The study was carried out according to the principles of the Declaration of Helsinki and approved by the local medical ethics committee. Written informed consent was obtained from all subjects.

Pilot Study Patients

An additional, pilot test population, which is comprised of 20 adult patients (55% male, age range 18–70) with RV pathology, consequent to congenital heart disease, was studied to observe if this 13-segment model was feasible in a diseased state. We did not perform this pilot test to evaluate RV function in a quantitative manner. The patients prospectively included were referred to the echocardiography department for routine measurements of their cardiac function and had a sufficient acoustic window. Ten patients had a volume overloaded RV due to atrial septal defect (n = 4), tetralogy of Fallot with severe residual pulmonary regurgitation (n = 6). Ten patients had a pressure overloaded RV (Doppler tricuspid regurgitation velocity > 3m/sec), pulmonary hypertension (n = 3), pulmonary homograft stenosis (n = 2), systemic RV consequent to an atrial switch operation in infancy for D-transposition of the great arteries (n = 5). All patients were in New York Heart Association (NYHA) class I or II. A complete 2D echocardiogram including four additional apical RV views was acquired as for the healthy subjects.

Transthoracic 2D iRotate Mode

Two experienced echocardiographers (JMcG, WV) performed the 2D echocardiograms including four additional apical views of the RV acquired with iRotate mode. In iRotate mode a full electronic rotation of 360° (adjustable by 5° steps) can be performed.[7] All studies were acquired in harmonic imaging using an iE33 or EPIQ7 ultrasound system (Philips Medical systems) equipped with a X5–1 matrix-array transthoracic probe. From the apical window, a standard apical 4C view was adjusted to acquire a focused non-foreshortened RV view with the (IVS)-RV apex centered along, or as near as possible, to the midline of the sector. With the iRotate mode an approximate 130° electronic rotation was performed. Using the anatomic landmarks, as defined above, four standard views of the RV were acquired during end-expiratory breath-hold (Figure 3).
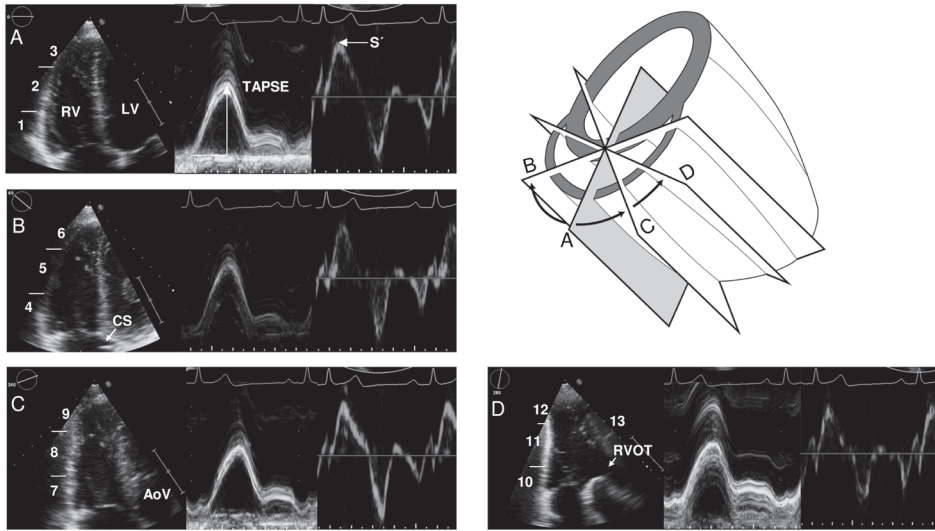
Figure 3 Schematic drawing of the cut planes (A-D) with their corresponding echocardiographic images: **Left:** 2D right ventricle (RV) image. **Center:** Tricuspid annular plane systolic excursion (TAPSE). **Right:** Tricuspid annular peak systolic velocity (S') for each cut plane in a healthy subject. Mean value of TAPSE and S' calculated from all views is 33mm and 13.9 cm/sec respectively.**A.** Four chamber view with segments 1–3; **B.** coronary sinus view with segments 4–6; **C.** aortic view with segments 7–9; **D.** coronal view with segments 10–13.

– Four chamber view, 0°
– Coronary sinus view at approximately +40° (slight posterior angulation of the transducer maybe necessary)
– Aortic view at approximately -40° (slight anterior angulation of the transducer maybe necessary)
– Coronal view (RVOT) at approximately -90°

Images of a pressure and volume overloaded RV acquired with 2D iRotate are shown in Figure 4.

Learning Curve

The impact of a learning curve on the feasibility of endocardial borders delineation of RV segments in our proposed model was sought by comparing data from the first consecutive 20 subjects with the following consecutive 20 subjects.

Right Ventricular Wall Segmentation according to the Echocardiographic Views

We analyzed the walls of the RV in the four views and divided each wall into three segments: basal, mid-, and apical segment (segments 1–12). In the coronal view, the RVOT anterior wall was defined as the 13th segment (Figure 3). The IVS was not included in this model, as it does not exclusively reflect RV function.[4,8] In total, the visualization of the RV
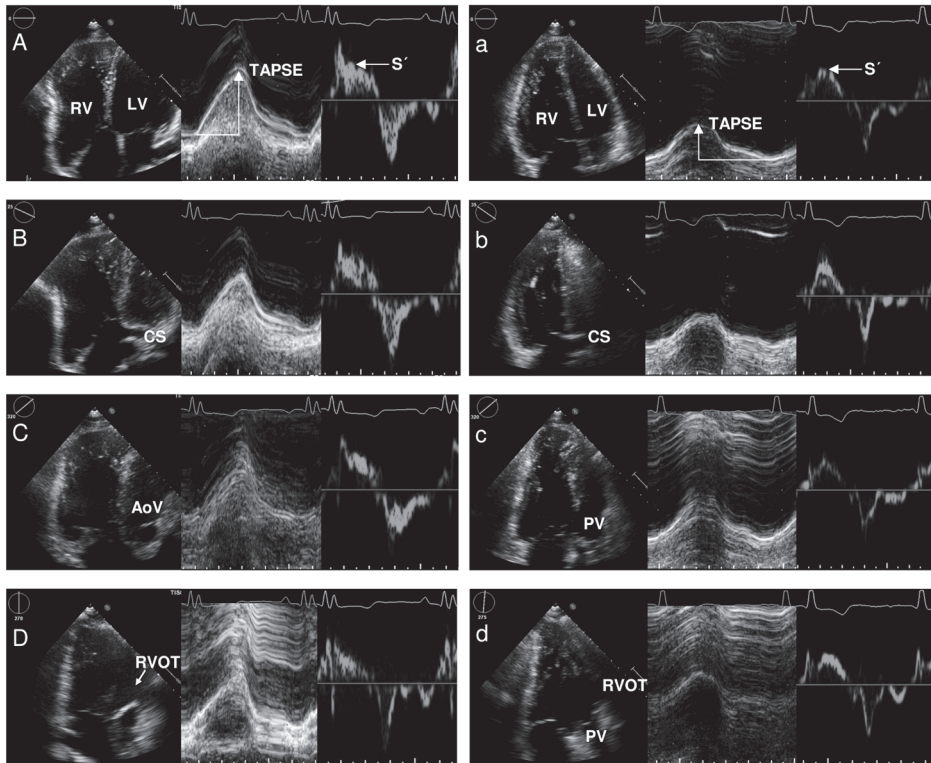
Figure 4 Left (A-D): 2D iRotate in a patient with severe residual pulmonary regurgitation and impaired RV systolic function. **Left:** 2D right ventricle (RV) image. **Center:** Tricuspid annular plane systolic excursion (TAPSE). **Right:** Tricuspid annular peak systolic velocity (S'). Mean value of TAPSE and S' calculated from all views is 17 mm and 6.1 cm/sec respectively.
Right (a-d): 2D iRotate in a patient with a systemic RV and impaired systolic function. **Left:** 2D right ventricle (RV) image. **Center:** Tricuspid annular plane systolic excursion (TAPSE). **Right:** Tricuspid annular peak systolic velocity (S'). Mean value of TAPSE and TDI S' calculated from all views is 17mm and 8.2 cm/sec respectively.
Note: both mean values of TAPSE and S' are lower than in the healthy subjects.
A(a)=four chamber view, B(b)= coronary sinus view, C(c)=Aortic view, D(d)= Coronal view.

wall was evaluated for 13 segments. An experience echocardiographer (JMcG) analyzed all the 13 segments in a dynamic format and graded each segment: 0 = not visible; 1 = partially visible (part of the segment or the whole segment is visible during only part of the cardiac cycle); 2 = visible (the whole segment is visible during the entire cardiac cycle), and 3 = optimal (excellent delineation of endocardium during the entire cardiac cycle).

TAPSE and TDI

Tricuspid annular plane systolic excursion (TAPSE) was measured with 2D echocardiography-guided M-mode, and tricuspid annular peak systolic velocity (S') was measured with the pulsed wave tissue Doppler imaging technique (TDI) in all four RV images

acquired with iRotate mode at the: (1) lateral tricuspid annulus in the four chamber view, (2) anterior tricuspid annulus in the coronary sinus view, (3) inferior annulus in the aortic view, and (4) inferior annulus in the coronal view. All measurements, as stated in the guidelines, were obtained with the ultrasound beam as parallel as possible to the direction of the tricuspid annular motion of that segment.[4] With sporadic use, when the ultrasound beam was not parallel to the tricuspid annular motion, a TAPSE measurement was taken directly on the 2D image at the end-diastolic position of the tricuspid annulus taken at the beginning of the QRS complex and its greatest apical long-axis displacement. All recordings were performed during end-expiratory breath-hold.

Statistical Analysis

Continuous variables are presented as mean ± standard deviation (SD), and categorical variables are presented as frequencies and percentages. Intra-observer agreement (JMcG) and inter-observer agreement (JMcG and MM) of the TAPSE and TDI peak systolic velocity (S') were assessed by repeated analysis in 30 data sets at least 2 months after the initial analysis. The agreement between two measurements was determined as the mean of the differences ± 1.96SD.[9] Additionally, the coefficient of variation (SD of the differences of two measurements divided by their mean) was provided. All statistical analyses were performed using SPSS statistics version 21.0 (IBM Corp., Armonk, NY, USA). A p-value of < 0.05 was considered significant.

RESULTS

Healthy Population

The normal population comprised of 120 subjects with normal cardiac anatomy and function. Baseline characteristics of the normal population are listed in Table 1.

The additional acquisition time for our proposed model of 4 additional RV views is approximately 1–2 minutes. The iRotate mode, to assess the RV from the standard apical window, was feasible in 118 of the 120 (98%) healthy subjects. Two subjects were excluded from the study due to absence of an apical window. One or more of the RV views could not be acquired with iRotate mode in an additional 6 subjects.

Visualization of 13 Segments of the Right Ventricle

The feasibility of the RV segments is shown in Figure 5. In the first 20 subjects, 83% (215/260 segments) of the segments could be visualized; when excluding the RVOT segment, this was 88% (212/240 segments). In the following 20 subjects, 86% (224/260 segments) of the segments could be visualized; when excluding the RVOT segment, this was 91% (218/240 segments).

Table 1 Baseline characteristics of Healthy Subjects

Characteristic	n = 120
Age, yrs	43 ± 13
Men, n (%)	61 (51%)
Height, cm	174 ± 9
Weight, kg	74 ± 12
BMI, kg/m²	24 ± 3
Systolic blood pressure, mmHg	125 ± 14
Diastolic blood pressure, mmHg	79 ± 9
QRS duration, ms	96 ± 9

Baseline characteristics are expressed as mean ± SD or n
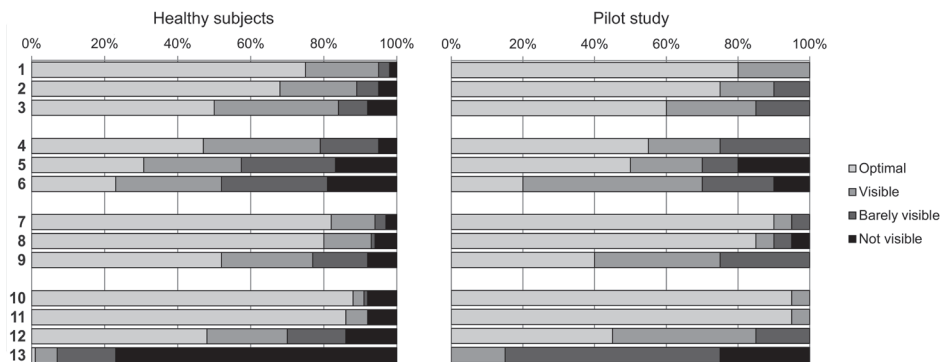
Figure 5 Feasibility of the RV segments for each view. **Left:** Healthy subjects (n = 120). 1344 (86%) of the total 1560 RV right ventricular segments were visualized. Note: this low percentage is mainly due to the poor visibility of the 13th segment. **Right:** Pilot study (n = 20). 248 (95%) of the total 260 RV right ventricular segments were visualized. Basal-mid-apical segment: 1–3 (four chamber view), 4–6 (coronary sinus view), 7–9 (aortic view), 10–12 (coronal view), 13 (right ventricular outflow tract anterior wall).

In total, 1344 (86%) of 1560 RV segments could be visualized. The RVOT segment was only visualized in 27 (23%) subjects. After exclusion of this segment, 1317 (91%) of the total 1440 RV segments were visualized.

TAPSE and TDI Measurements

The feasibility per view and measurement of the TAPSE and the TDI velocity S' are shown in Table 2. The TAPSE and TDI velocity S' were lower in the coronal view than the mitral, aortic and coronary sinus views.

Intra- and Inter-Observer Variability

The mean differences and coefficients of variation for the intra- and inter-observer agreement of the TASPE and TDI velocity S' are displayed in Table 3.

Table 2 Mean values of TAPSE and TDI (S') for each RV view (n = 120)

View	TAPSE mm			TDI (S') cm/sec		
	N (%)	Mean ± SD	Range	N (%)	Mean ± SD	Range
Four chamber	117 (98%)	26 ± 4	17–37	116 (97%)	12.0 ± 2.0	7.9–16.9
Coronary sinus	113 (94%)	27 ± 4	17–36	111 (93%)	12.0 ± 2.0	6.7–18.1
Aortic view	116 (97%)	25 ± 4	17–33	113 (94%)	11.1 ± 2.1	6.3–15.6
Coronal view	111 (93%)	23 ± 3	14–33	110 (92%)	9.9 ± 1.9	6.1–14.0

Table 3 Intra- and Inter-Observer Variability Measurements for TAPSE and TDI (S') (n = 30)

		Intra-Observer		Inter-Observer	
		Mean Difference	Coefficient of Variation (%)	Mean difference	Coefficient of variation (%)
TAPSE	Four chamber	0.0 ± 1.7	7	-0.4 ± 1.5	6
	Coronary sinus	-0.4 ± 2.5	10	0.0 ± 2.1	9
	Aortic view	-0.2 ± 2.5	10	0.0 ± 1.7	7
	Coronal view	-0.5 ± 1.8	8	0.3 ± 1.9	9
TDI(S')	Four chamber	0.3 ± 1.3	12	0.2 ± 0.6	8
	Coronary sinus	0.0 ± 1.4	13	0.3 ± 0.9	5
	Aortic view	0.3 ± 1.2	13	0.1 ± 0.7	7
	Coronal view	0.1 ± 0.8	9	0.0 ± 0.5	5

Pilot Study Patients

All patients in the pilot group had at least moderate RV dilatation. The RV systolic function varied between the diseased states. The iRotate mode was feasible in all study patients; the feasibility of the RV segments is shown in Figure 5. In total, 248 (95%) of 260 RV segments could be visualized. The RVOT segment was classed partially visible in 12 and visible in three patients. TAPSE and TDI velocity S' were feasible in all views in all patients.

DISCUSSION

The current study shows that among unselected healthy subjects, a 13 segment standardized model for RV assessment is feasible using 2D iRotate mode, based on unique anatomic landmarks and achieved from a single acoustic window. The visibility of the RVOT anterior wall remains challenging; however, the visibility was higher in the diseased RV.

It is recommended to record multiple 2D images for assessment of RV function.[4,6,10] This multi-view approach, based on several acoustic windows, is susceptible to error (oblique views, operator dependency) and is a major limitation of RV assessment due to the lack of reproducibility on serial follow-up. Moreover, as this approach is not always feasible in the routine setting, often only the apical 4C view is acquired and an RV analyses consists

of dimension, right ventricular fractional area change (RVFAC), TAPSE and TDI (S') measurements. RV linear dimensions and regional function assessment are dependent on probe rotation and different views, and it is therefore recommended to state the window from which the measurement was performed in order to permit inter-study comparison.[4,6] Our study provides a robust and standardized RV segmentation.

With the introduction of transthoracic 3D echocardiography, the assessment of RV size and function in adults and children was thought to improve and solve some of the problems of 2D echocardiography.[11] Theoretically, 3D echocardiography could provide all information that could be added using our proposed model. Several studies have extensively investigated RV function and found that 3D echocardiography improved the accuracy and reproducibility of RV assessment and identified RV dysfunction quite accurately.[12] However, most published data compose of small and rather selective patient populations based on moderate to good image quality.[13] In a real-world setting Renella, et al.[13] evaluated 3DE of the RV in pediatric and congenital heart disease patients (age 1–20yrs), and they found that RV volumes were measurable in only 58% of the patients. Moreover, current ASE/EACVI recommendations acknowledge the limitations of performing 3D RV assessment in every patient.[6]

In this study, a comprehensive evaluation of the RV can be achieved, from one acoustic window, with 2D iRotate mode based on anatomic landmarks. Compared to the standard multiview approach, 2D iRotate evaluation of the RV takes only a few minutes making it very attractive and robust for routine use in the echo laboratory and at bedside. There is a short learning curve for data acquisition based on the fact that there was minimal increase in the feasibility score (83–86%) after the first 20 subjects. However, with less experienced echocardiographers, the learning curve could possibly be slightly longer. Of note, the 2D iRotate mode is limited to the matrix-array transducer. Furthermore, a true non-foreshortened right-ventricular view with the IVS-RV apex centered along, or as near as possible, to the midline of the sector is mandatory.

The feasibility of the RV segments, excluding the RVOT anterior wall is good, with 81% of the segments adequately visible. The feasibility of the apical segments is less when compared to the mid and basal segments, probably due to the sharp curvature of the RV apex and also, the known difficulty in obtaining high quality 2D images in the near field, which could contribute to this finding.[14]

The feasibility of RVOT anterior wall is poor, visible in only 23% of the subjects of which 16% were scored partially visible. Reduced feasibility was also observed in the anterior wall in the coronary sinus view when compared to the feasibility of the lateral wall (mitral view), inferior wall (aortic view), and inferior wall (coronal view). This suboptimal visualization of the most anterior segments of the RV could be explained by the retrosternal position of the heart in the thorax. Also the long axis of the normal sized heart is superior-inferior (vertical), which again would contribute to the difficulty in visualizing the most anterior segments, with echocardiography.[15]

RV wall deformation consists of three components: radial, longitudinal, and circumferential. Despite their limitations, TAPSE and TDI (S') are simple and reproducible

measurements used to assess RV longitudinal systolic function.[4,16,17] As far as we know our current study is the first study to assess multiple TAPSE and TDI (S¢) measurements from the tricuspid annulus. TAPSE was feasible in one view or more in 93% or more and TDI (S¢) 92% or more healthy subjects. Both measurements fell into consistent ranges for normal subjects as stated in the guidelines for the apical 4C view (reference values: TAPSE 16–30mm, TDI 10–19 cm/s).[4] Inter- and intra-observer variability were acceptable as coefficients of variation were < 10% and < 14% respectively. Recently, Forsha et al investigated RV strain in an 18-segment model of the RV in 40 healthy subjects.[14] The RV strain analysis was feasible and the global peak strain and peak dyssynchrony measures fell into consistent range for normal subjects. The authors acknowledged that the lack of universal standardized RV views is an obvious limitation of the study. In our study we provide standardized RV views and segmentation as the basis for future RV analysis.

The Pilot Study

These patients were included simply to demonstrate whether this model is feasible in the diseased RV. The results are encouraging; the feasibility of the segments is similar to the normal RV. The feasibility of the apical segment, as in the healthy subjects, remains less when compared to the mid- and basal segment. However, feasibility of the segments in the coronal and RVOT view appears to be slightly better than in the healthy subjects. This could be explained by the fact that in the diseased RV (dilated or hypertrophic), the long axis of the heart is often more horizontal and therefore the sternum will compromise the image quality to a lesser degree.[15] Also in the dilated RV, the apex is moved automatically more to the center of the 2D sector and the rotation around the RV with iRotate mode be noted to be easier than in the normal RV.

Clinical Implementations

One of the critical limitations of 2D echo recordings is the potential for variability in the 2D planes during follow-up. Well-defined anatomic landmarks result in robust image orientation, precise echocardiographic follow-up, and less oblique plane acquisition, implying that this simple approach could minimize or avoid such variability. With this method of scanning, the RV walls are visualized in their long axis. This could allow strain and strain rate imaging to be performed on more segments of the RV and its complex contraction pattern to be evaluated in more detail. Further studies are warranted to investigate these issues.

Limitations

This study provides a novel model of RV assessment of a potential value. There are some study limitations. First, we did not perform test-retest repeatability in this study. Our study comprised of a relatively small sample of RV pathology. Our model might not be feasible in patients with extremely dilated LVs because we will be unable to align the (IVS)-RV apex in the center of the imaging sector. Therefore, the clinical utility and the incremental value of our proposed model need to be confirmed in a larger population.

Moreover, a direct comparative study between our 2D iRotate model and 3DE in a large consecutive series is warranted.

CONCLUSION

2D transthoracic iRotate mode enables a comprehensive evaluation of the normal and diseased RV. Our proposed approach provides a standardized protocol for RV acquisition and assessment from a single acoustic window with a fixed transducer position, using simple anatomic landmarks. The anterior, lateral, inferior, and outflow tract anterior wall of the RV could be assessed, reducing acquisition time compared to the multiview approach and enhances the accuracy of RV evaluation. Further studies are warranted to discover the full potential of this new technique for evaluation of the RV in various diseased states.

ACKNOWLEDGEMENTS

REFERENCES

1. Haddad F, Doyle R, Murphy DJ, Hunt SA. Right ventricular function in cardiovascular disease, part II: pathophysiology, clinical importance, and management of right ventricular failure. *Circulation* 2008;117:1717-1731.

2. Horton KD, Meece RW, Hill JC. Assessment of the right ventricle by echocardiography: a primer for cardiac sonographers. *J Am Soc Echocardiogr* 2009;22:776-792; quiz 861-772.

3. Mertens LL, Friedberg MK. Imaging the right ventricle--current state of the art. *Nat Rev Cardiol* 2010;7:551-563.

4. Rudski LG, Lai WW, Afilalo J, Hua L, Handschumacher MD, Chandrasekaran K, Solomon SD, Louie EK, Schiller NB. Guidelines for the echocardiographic assessment of the right heart in adults: a report from the American Society of Echocardiography endorsed by the European Association of Echocardiography, a registered branch of the European Society of Cardiology, and the Canadian Society of Echocardiography. *J Am Soc Echocardiogr* 2010;23:685-713; quiz 786-688.

5. Valsangiacomo Buechel ER, Mertens LL. Imaging the right heart: the use of integrated multimodality imaging. *Eur Heart J* 2012;33:949-960.

6. Lang RM, Badano LP, Mor-Avi V, Afilalo J, Armstrong A, Ernande L, Flachskampf FA, Foster E, Goldstein SA, Kuznetsova T, Lancellotti P, Muraru D, Picard MH, Rietzschel ER, Rudski L, Spencer KT, Tsang W, Voigt JU. Recommendations for cardiac chamber quantification by echocardiography in adults: an update from the American Society of Echocardiography and the European Association of Cardiovascular Imaging. *Eur Heart J Cardiovasc Imaging* 2015;16:233-270.

7.   McGhie JS, Vletter WB, de Groot-de Laat LE, Ren B, Frowijn R, van den Bosch AE, Soliman OI, Geleijnse ML. Contributions of simultaneous multiplane echocardiographic imaging in daily clinical practice. *Echocardiography* 2014;31:245-254.

8.   Schwarz K, Singh S, Dawson D, Frenneaux MP. Right ventricular function in left ventricular disease: pathophysiology and implications. *Heart Lung Circ* 2013;22:507-511.

9.   Bland JM, Altman DG. Statistical methods for assessing agreement between two methods of clinical measurement. *Lancet* 1986;1:307-310.

10. Jurcut R, Giusca S, La Gerche A, Vasile S, Ginghina C, Voigt JU. The echocardiographic assessment of the right ventricle: what to do in 2010? *Eur J Echocardiogr* 2010;11:81-96.

11. van der Zwaan HB, Helbing WA, McGhie JS, Geleijnse ML, Luijnenburg SE, Roos-Hesselink JW, Meijboom FJ. Clinical value of real-time three-dimensional echocardiography for right ventricular quantification in congenital heart disease: validation with cardiac magnetic resonance imaging. *J Am Soc Echocardiogr* 2010;23:134-140.

12. van der Zwaan HB, Geleijnse ML, McGhie JS, Boersma E, Helbing WA, Meijboom FJ, Roos-Hesselink JW. Right ventricular quantification in clinical practice: two-dimensional vs. three-dimensional echocardiography compared with cardiac magnetic resonance imaging. *Eur J Echocardiogr* 2011;12:656-664.

13. Renella P, Marx GR, Zhou J, Gauvreau K, Geva T. Feasibility and reproducibility of three-dimensional echocardiographic assessment of right ventricular size and function in pediatric patients. *J Am Soc Echocardiogr* 2014;27:903-910.

14. Forsha D, Risum N, Kropf PA, Rajagopal S, Smith PB, Kanter RJ, Samad Z, Sogaard P, Barker P, Kisslo J. Right ventricular mechanics using a novel comprehensive three-view echocardiographic strain analysis in a normal population. *J Am Soc Echocardiogr* 2014;27:413-422.

15. Buck T FA, Monaghan M,ed. Three-dimensional Echocardiography 2nd Edition. Berlin: Springer-Verlag Berlin and Heidelberg 2015:31.

16. Koestenberger M, Ravekes W, Everett AD, Stueger HP, Heinzl B, Gamillscheg A, Cvirn G, Boysen A, Fandl A, Nagel B. Right ventricular function in infants, children and adolescents: reference values of the tricuspid annular plane systolic excursion (TAPSE) in 640 healthy patients and calculation of z score values. *J Am Soc Echocardiogr* 2009;22:715-719.

17. Meluzin J, Spinarova L, Bakala J, Toman J, Krejci J, Hude P, Kara T, Soucek M. Pulsed Doppler tissue imaging of the velocity of tricuspid annular systolic motion; a new, rapid, and non-invasive method of evaluating right ventricular systolic function. *Eur Heart J* 2001;22:340-348.

CHAPTER 10

Quantitative assessment of the entire right ventricle from one acoustic window:
an attractive approach

Jackie S. McGhie
Myrthe E. Menting
Wim. B. Vletter
René Frowijn
Jolien W. Roos-Hesselink
Heleen B. van der Zwaan
Osama I.I. Soliman
Marcel L. Geleijnse
Annemien E. van den Bosch

ABSTRACT

Aims

The aim of this prospective study was to evaluate the feasibility and establish normal values of functional right ventricle (RV) parameters as assessed in our four, long-axis view RV model using iRotate echocardiography. Furthermore, we evaluated the potential use of this model in patients with abnormally loaded RVs.

Method and results

One hundred and fifty-five healthy subjects aged 20–72 years (≥ 28 subjects per decile) were prospectively recruited. We used non-dedicated RV speckle-tracking software to test the feasibility and to establish normal range values of peak systolic global longitudinal RV strain (RV-GLS) from the RV free-walls (septum was excluded). Also normal range values for: dimensions, tricuspid annular plane systolic excursion (TAPSE) and tricuspid annular peak systolic velocity (TDI-S′) were established. The feasibility of RV-GLS was 88, 84, and 62%, respectively, in the lateral, inferior, and anterior free wall. Mean RV-GLS normal value was -24.5 ± 4.9% for lateral wall and -25.4 ± 5.0% for anterior wall. Mean RV-GLS for the inferior wall was -23.2 ± 4.4% in the aortic (Ao) view and -20.7 ± 5.0% in the coronal (CV) view. The feasibility of mean RV-GLS was 100% in the anterior, lateral and inferior walls in abnormally dilated RVs.

Conclusion

The feasibility of all RV parameters assessed in the four-view iRotate model is good to excellent. Normal values for RV dimension and function of the anterior, inferior and lateral RV walls have been established. Further studies and dedicated RV speckle-tracking software are warranted to discover the full potential of this new technique.

INTRODUCTION

Right ventricular function (RVF) has been increasingly recognized as a prognostic factor in a variety of disease states such as left sided heart failure, pulmonary hypertension and congenital heart lesions.[1] Therefore, accurate and reproducible quantification of RV function is a cornerstone in cardiac imaging.[2] Ideally, RV assessment should be simple, accurate and inexpensive. In current routine clinical practice systolic RVF is commonly assessed by measuring tricuspid annular plane systolic excursion (TAPSE), right ventricular fractional area change (RVFAC), and tricuspid annular peak systolic velocity (S′) using tissue Doppler imaging (TDI). More recently, peak global RV longitudinal strain from the apical four-chamber (A4C) view using two-dimensional (2D) speckle-tracking echocardiography (STE) has demonstrated an incremental value to conventional echo parameters.[3] However, the accuracy of these parameters for assessing the RV is inherently limited because the parameter reflects only a limited region of the RV.

Structured multiple-view strain analyses assessment of the RV could be of incremental value in patients with RV dysfunction. We previously introduced a 13-segment standardized model, based on anatomic landmarks for assessing the RV from one apical view using 2D-transthoracic echocardiography (TTE) iRotate mode.[4] This novel four-view approach with the RV walls visualized in their long-axis may have the potential to allow analyses of all of the above mentioned function parameters resulting in an extensive and concise evaluation of the RV.

The aim of this prospective study was to evaluate the feasibility and establish normal values of different RV parameters as assessed in this multi-view iRotate RV model. In addition, the influence of age, sex and body surface area (BSA) will be studied and finally the potential use of this method in patients with abnormally loaded RVs investigated.

METHODS

Study population

From 2014 to 2015, 155 healthy subjects aged 20–72 years were prospectively recruited and were stratified into 5 age groups: 20–29, 30–39, 40–49, 50–59 and 60–72 years (n≥ 28 in each group, equal distribution in sex). The inclusion criteria required that all subjects had normal results on physical examination and electrocardiography (ECG). Subjects were excluded when they met any of the following criteria: professional athletes, morbidly obese subjects (BMI > 40 kg/m^2); (prior) cardiovascular disease; present cardiovascular risk factors; systemic disease or the finding of cardiac abnormalities during examination at our outpatient clinic.

The study was carried out according to the principles of the Declaration of Helsinki and approved by the local medical ethics committee. Written informed consent was obtained from all subjects.

Pilot Study Patients

Twenty adult patients (55% male, age range 18–70) with RV pathology, consequent to congenital heart disease, were prospectively studied to evaluate RV function using this novel four-view approach.[4] All patients were referred for routine echocardiographic assessment of cardiac function and had a sufficient acoustic window. Ten patients had a volume overloaded RV due to an atrial septal defect (n = 4) and tetralogy of Fallot with severe pulmonary regurgitation (n = 6). Ten patients had a pressure overloaded RV (Doppler tricuspid regurgitation velocity > 3m/sec), due to pulmonary hypertension (n = 3), pulmonary homograft stenosis (n = 2) and a systemic RV consequent to an atrial switch operation (n = 5). All patients were in New York Heart Association (NYHA) class I or II.

Echocardiographic acquisition

Two experienced sonographers (J.S.M., W.B.V.) performed a standard 2D-TTE. All studies were acquired, in the left lateral decubitus position, in harmonic imaging using an iE33 or EPIQ7 ultrasound system (Philips Medical Systems, Best, the Netherlands) equipped with an X5–1 matrix-array transducer (composed of 3040 elements with 1–5 MHz). Four additional RV views, based on anatomical landmarks, were acquired with iRotate mode which allows an electronic rotation of 360º (adjustable in 5º steps). The views acquired were: a focused non-foreshortened RV view with the interventricular septum (IVS)-RV centred along or as near to the midline of the sector (4C, 0º) showing the lateral RV wall, coronary sinus view (CS ± +40º) showing the anterior RV wall, aortic view (Ao ± -40º) showing the RV inferior wall and coronal view (CV ± -90º) showing the RV outflow tract (RVOT) anterior wall and inferior wall of the RV as seen in Figure 1.[4] All images were acquired at frame rates of ≥ 50 frames/sec.[5] Real-time 3D-TTE was performed immediately after the 2D-TTE with the same ultrasound unit and transducer. A four-or six-beat full volume data set (27 ± 8 vol/s, range 13–51) of the RVwas acquired from the apical window during a single breath hold.

Conventional echocardiographic measurements

2D-TTE and Tissue Doppler

RV linear dimensions were measured in the four focused RV views as stated in guidelines.[2] RVFAC, (calculated as end-diastolic area - end-systolic area / end-diastolic area x 100%), was only measured in the focused 4C view. TAPSE was measured with 2D echocardiography-guided M-mode and TDI-S' in all four RV views. With sporadic use, when the ultrasound beam was not parallel to the tricuspid annular motion, a TAPSE was measured directly on the 2D image at the end-diastolic position of the tricuspid annulus taken at the beginning of the QRS complex and its greatest apical long-axis displacement. Intra- and inter-observer variability test was not performed for TAPSE and TDI-S′ as this has been presented in our previous article.[4]
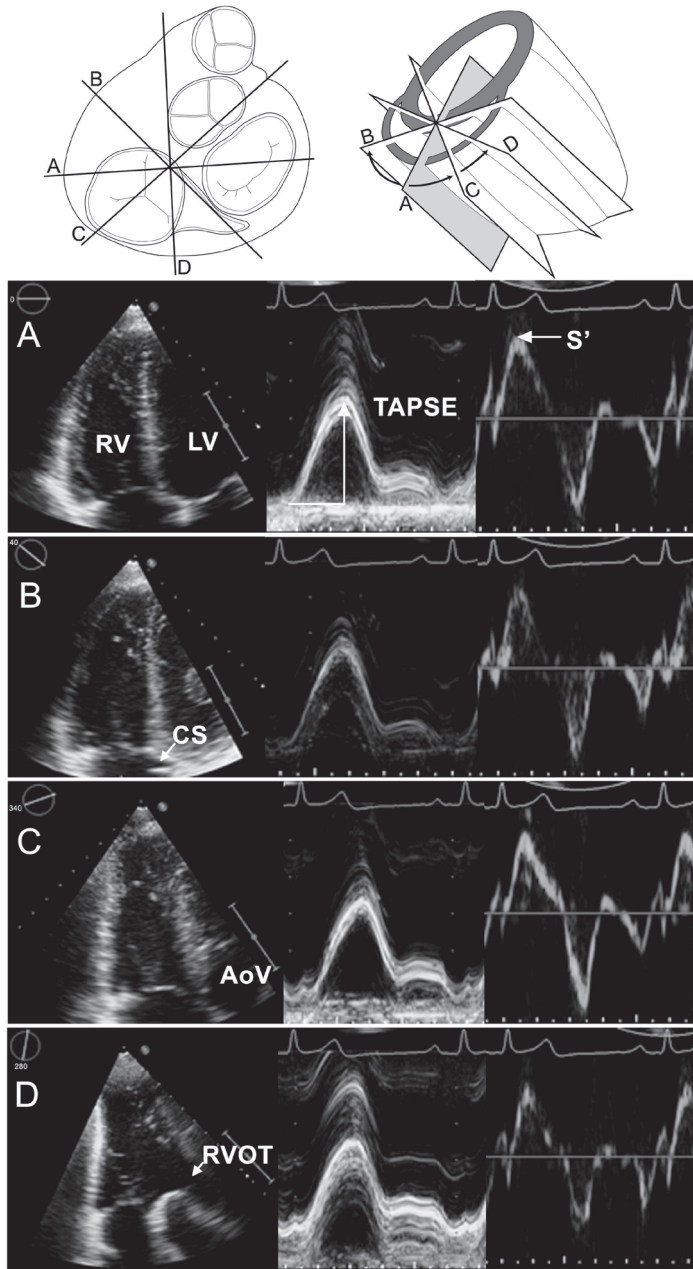
Figure 1 Schematic drawings of the cut planes (**A-D**) with corresponding echocardiographic images.
Top left: displaying the right ventricle (RV) in the transvers plane viewed from the RV aspect.Top right: displaying the RV in the sagittal plane.(**A**) focused four-chamber view (0°), lateral wall; (**B**) coronary sinus view (+40°) anterior wall; (**C**) aortic view (-40°), inferior wall; (**D**) coronal view (-90°), inferior wall and RVOT anterior wall.Left: 2D RV image. Centre: Tricuspid annular plane systolic excursion (TAPSE). Right: Tricuspid annular peak systolic velocity (TDI-S'').LV, left ventricle; CS, coronary sinus; AoV, aortic valve; RVOT, right ventricle outflow tract.

RV 2D Speckle-Tracking

The four RV datasets were digitally exported to a TomTec server (TomTec Imaging Systems, Munich, Germany). Data analysis was performed offline by two independent observers (J.S.M., M.E.M.), using DICOM grayscale images. To assess peak systolic global longitudinal RV strain (RV-GLS) the endocardial boarder was traced in the RV; focused 4C, CS, Ao and CV-view using an LV algorithm based 16-segment model wall motion tracking software (2D CPA 1.2.3.6; TomTec Imaging Systems, Munich, Germany).

Two cardiac cycles were analysed; all views were flipped displaying the RV on the right of the screen. The endocardium was manually traced in the chosen end-diastolic frame. If the tracking results were inadequate, an end-systolic frame was traced; if this persisted the data set was excluded. The RVOT anterior wall in the CV-view was excluded in this study due to poor visibility and persistent inadequate tracking.

Peak systolic RV-GLS was obtained from each segment from software generated curves. Free wall three-segment peak systolic RV-GLS (analysed in this manuscript) was calculated from the arithmetic mean of the strain values in 3 segments of the RV free-wall obtained from the six-segment model. In all four views, the IVS strain values were excluded (Figure 2).
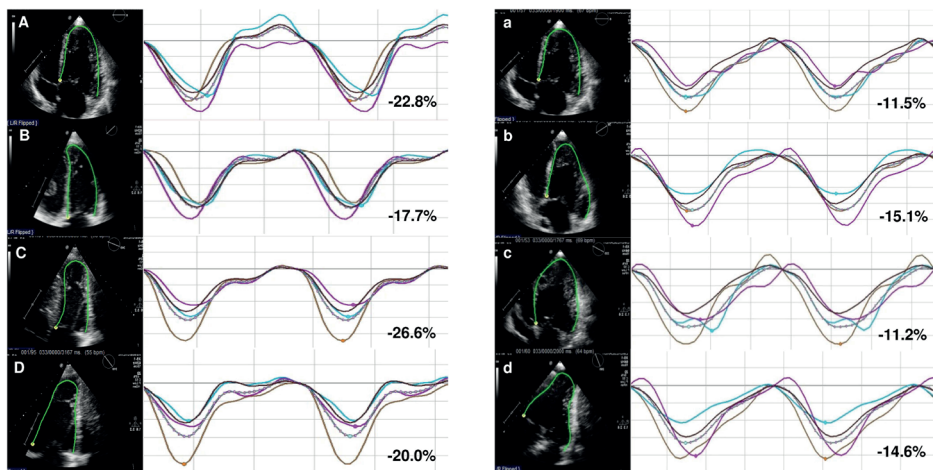
Figure 2 Peak systolic (three-segment) global right ventricular longitudinal strain measurement (dotted line). Left; 2D iRotate RV-GLS in a healthy subject. Right; 2D iRotate RV-GLS in a patient with a systemic RV. (Note: All images are flipped displaying the right ventricle on the right of the screen). (**A, a**) Focused four-chamber view, lateral wall; (**B, b**) coronary sinus view, anterior wall; (**C, c**) aortic view, inferior wall; (**D, d**) coronal view, inferior wall.

Real-time 3D echocardiography

The 3DE datasets were digitally exported to a TomTec server (TomTec Imaging Systems) and analyzed offline using TomTec 4D- RV function 2.0 software. After placing set landmarks RV volume and ejection fraction (EF) were automatically calculated over the entire

cardiac cycle. If inadequate tracking occurred the endocardial contours were manually adjusted.

Statistical analysis

The distribution of data was checked using histograms and the Shapiro-Wilk test. Depending on the data distribution, continuous data are presented as mean ± standard deviation (SD). Categorical data are presented as frequencies and percentages. For comparison of normally distributed continuous variables in one group we used the paired *t*-test, between two groups the Student's *t*-test. In case of skewed distribution, the Mann-Whitney *U*-test was applied. For comparison of frequencies the χ^2-test or Fisher's exact test was used. Linear regression analysis was used to explore the relationship between echocardiographic measurements and baseline characteristics. All statistical analyses were performed using the Statistical Package for Social Sciences version 21 (SPSS Inc., Armonk, NY, USA). The statistical tests were two-sided and a *P*< 0.05 was considered statistically significant.

Intra-observer agreement was assessed by repeated analysis in a representative sample of subjects at least one month after the initial analysis and blinded to the initial results. Assessment of inter-observer agreement was performed by a second observer (M.E.M.) in the same sample. The agreement between two measurements was determined as the mean of the differences ±1.96SD.[6] Additionally, the coefficient of variation was provided (SD of the differences of two measurements divided by their mean).

Venn diagrams illustrate the sensitivity of TAPSE, TDI-S' and RV-GLS in the diseased RV for this four view RV model. Cut-off values were determined as the normal range mean ± 1.96SD. Comparisons of proportions were done with a two-sided *Z*-test.

RESULTS

Study Population

Of the 155 subjects who participated in this study, we included 147 (mean age 44.6±13.7 years, 50% female). Eight subjects were excluded for one of the following reasons: breast implants (n = 2), valvular pathology (n = 2), surgically closed patent ductus arteriosus (n = 1), hypertension (n = 1), morbid obesity (n = 1), and right bundle branch block on ECG (n = 1). Table 1 shows the characteristics of the study population per age group. From 147 participants the focused 4C view was feasible in 145 (95%) subjects, CS view in 142 (97%), the Ao view in 142 (97%) and CV view in 139 (95%).

Conventional echocardiographic measurements

RV chamber parameters

The standard parameters from the focused 4C view are displayed in Table 2 together with the basal and longitudinal diameter of the three additional views. The focused 4C view RV diameters were: basal 28–49mm, longitudinal 67–97mm. The basal diameter in the

Table 1 Characteristics of the study population

	Age group (years)				
	20–29	**30–39**	**40–49**	**50–59**	**60–72**
Characteristic	**n = 32**	**n = 28**	**n = 28**	**n = 31**	**n = 28**
Sex, female	16 (50%)	14 (50%)	14 (50%)	16 (52%)	14 (50%)
Age (years)	26±3	35±3	44±3	55±3	64±3
Current smokers	2 (6%)	1 (4%)	4 (14%)	5 (16%)	1 (4%)
Physical examination					
Height (m)	1.75±0.08	1.75±0.09	1.76±0.12	1.74±0.08	1.73±0.09
Weight (kg)	68.8±10.0	74.0±12.2	76.6±15.0	77.2±12.2	77.1±12.9
Body mass index (kg/m^2)	22.3±2.1	24.1±3.4	24.6±3.7	25.4±2.8	25.8±3.1
Body surface area (m^2)	1.84±0.17	1.89±0.18	1.92±0.22	1.92±0.18	1.90±0.19
Systolic blood pressure (mmHg)	124±13	121±10	123±12	130±15	137±17
Diastolic blood pressure (mmHg)	76±8	78±7	80±10	83±11	83±8
ECG					
Sinus rhythm	32 (100%)	28 (100%)	28 (100%)	31 (100%)	28 (100%)
Heart rate	61±11	60±8	61±10	62±9	65±10
PR interval	156±24	150±21	156±24	159±16	173±18
QRS duration (ms)	96±8	97±9	97±9	95±10	97±10

focused 4C and CS view and longitudinal diameter in all four views were larger in men than women. RV end-diastolic and end-systolic areas were larger in men than women.

RV function parameters

TAPSE and TDI-S' measurements were analysable in, respectively, 99 and 98% of the RV walls. The standard functional parameters measured from all RV views are displayed in Table 2 and 3. TAPSE showed no statistically significant correlation with the sex and with the age only in the inferior wall in the Ao and CV view. TDI-S' correlated significantly with age in all four views (all $P < 0.01$).

Right ventricular longitudinal strain

Adequate tracking for strain analyses was obtained in 448 of the 588 RV walls (76%). The feasibility of STE was lowest in the anterior RV wall (CS view) 62% compared to the lateral RV wall (4C view), 88%, and inferior RV wall (in Ao and in CV view), 84%. Mean RV-GLS normal values measured were; lateral wall (4C view): -25.4 ± 5.0%, anterior wall (CS view): -24.5 ± 4.9%, inferior wall (Ao view): -23.2 ± 4.4% and inferior wall (CV view): -20.7 ± 5.0%. The RV-GLS of the inferior wall (CV view) was decreased compared to the anterior and lateral wall. Mean strain values were comparable between

Table 2 Right ventricular chamber echocardiographic parameters stratified by sex

Parameter	Total Mean ± SD	Range*	Male Mean ± SD	Female Mean ± SD	P-value
RV basal-diameter (mm)					
Four-chamber view (*n* = 142)	38.8 ± 5.2	28.4–49.2	40.8 ± 5.3	36.7 ± 4.4	**< 0.001**
Coronary sinus view (*n* = 131)	40.7 ± 6.2	28.3–53.1	42.4 ± 6.1	38.9 ± 5.8	**0.001**
Aortic view (*n* = 135)	35.0 ± 6.9	21.2–48.8	35.1 ± 7.8	35.0 ± 5.8	0.901
Coronal view (*n* = 128)	37.8 ± 5.7	26.4–49.2	38.3 ± 5.9	37.3 ± 5.5	0.341
RV longitudinal diameter (mm)					
Four-chamber view (*n* = 141)	82.1 ± 7.6	66.9–97.3	84.7 ± 7.3	79.5 ± 7.0	**< 0.001**
Coronary sinus view (*n* = 127)	80.8 ± 7.6	65.6–96.0	83.5 ± 7.4	78.1 ± 6.8	**< 0.001**
Aortic view (*n* = 131)	81.4 ± 7.2	67.0–95.8	84.4 ± 6.9	78.4 ± 6.4	**< 0.001**
Coronal view (*n* = 123)	87.2 ± 8.4	70.4–104.0	91.3 ± 7.9	83.3 ± 7.0	**< 0.001**
Four-chamber view					
RV end-diastolic area (cm²) (*n* = 125)	24.9 ± 5.1	14.7–35.1	28.0 ± 4.2	21.9 ± 4.0	**< 0.001**
RV end-systolic area (cm²)	14.5 ± 3.7	7.1–24.0	16.6 ± 3.4	12.5 ± 2.9	**< 0.001**
Normalized to BSA					
RV end-diastolic area	13.2 ± 2.3	8.6–17.8	13.9 ± 2.2	12.5 ± 2.2	**< 0.001**
RV end-systolic area	7.7 ± 1.7	4.3–11.1	8.2 ± 1.7	7.1 ± 1.6	**< 0.001**
TAPSE (mm)					
Four-chamber view (*n* = 144)	26.0 ± 3.8	18.4–33.6	26.0 ± 4.0	26.3 ± 3.5	0.334
Coronary sinus view (*n* = 140)	26.4 ± 3.5	19.4–33.4	26.6 ± 3.6	26.2 ± 3.4	0.481
Aortic view (*n* = 143)	24.5 ± 3.6	17.3–31.7	24.0 ± 3.7	25.0 ± 3.5	0.111
Coronal view (*n* = 136)	22.9 ± 3.3	16.3–29.5	22.4 ± 3.4	23.0 ± 3.1	0.064
TDI-S' (cm/s)					
Four-chamber view (*n* = 143)	12.0 ± 2.1	7.8–16.2	11.9 ± 2.0	12.1 ± 2.1	0.564
Coronary sinus view (*n* = 138)	12.0 ± 2.0	8.0–16.0	11.8 ± 2.0	11.2 ± 2.0	0.386
Aortic view (*n* = 140)	11.0 ± 2.0	7.0–15.0	10.8 ± 2.0	11.8 ± 2.0	0.245
Coronal view (*n* = 135)	9.8 ± 1.8	6.2–13.4	9.7 ± 1.7	9.8 ± 2.0	0.946
RV-GLS (%)					
Four-chamber view (*n* = 128)	-25.4 ± 5.0	15.4–35.4	-25.0 ± 5.0	-25.8 ± 5.0	0.368
Coronary sinus view (*n* = 88)	-24.5 ± 4.9	14.7–34.3	-24.6 ± 5.2	-24.5 ± 4.5	0.920
Aortic view (*n* = 119)	-23.2 ± 4.4	14.4–32.0	-22.4 ± 4.2	-23.8 ± 4.5	0.079
Coronal view (*n* = 113)	-20.7 ± 5.0	10.7–30.7	-19.2 ± 4.1	-22.1 ± 5.4	**0.002**

* Range = mean ± 2SD

Table 3 RV function parameters (TAPSE, TDI, RV FAC, 3DE) per age group

Mean ± SD	Age group (years)					P-value*
	20–29	30–39	40–49	50–59	60–72	
TAPSE (mm)						
Four-chamber view (*n* = 144)	26.4 ± 3.9	27.2 ± 3.3	24.7 ± 3.9	25.6 ± 3.2	25.9 ±4.3	0.264
Coronary sinus view (*n* = 140)	26.5 ± 3.6	26.8 ± 2.9	25.8 ± 3.6	26.4 ± 3.3	26.2 ± 4.3	0.661
Aortic view (*n* = 143)	26.1 ± 3.4	25.3 ± 3.0	23.7 ± 3.8	23.6 ± 4.0	23.5 ± 3.3	**0.001**
Coronal view (*n* = 136)	24.4 ± 3.1	24.0 ± 2.4	22.4 ± 2.7	21.9 ± 3.9	21.6 ± 3.3	**< 0.001**
TDI-S' (cm/s)						
Four-chamber view (*n* = 143)	12.7 ± 1.8	12.8 ± 1.7	11.7 ± 2.4	11.6 ± 1.8	11.3 ± 2.2	**< 0.001**
Coronary sinus view (*n* = 138)	12.5 ± 2.4	12.6 ± 1.5	11.7 ± 2.2	11.8± 1.6	11.2 ± 1.9	**0.005**
Aortic view (*n* = 140)	11.9 ± 1.9	11.5 ± 1.8	10.9 ± 2.2	10.6 ± 1.9	10.1 ± 1.9	**< 0.001**
Coronal view (*n* = 135)	10.5 ± 1.6	10.7 ± 1.5	9.7 ± 1.8	9.3 ± 1.9	8.6 ± 1.7	**< 0.001**
RV-GLS (%)						
Four-chamber view (*n* = 128)	-24.8 ± 4.5	-26.2 ± 4.6	-26.8 ± 6.4	-25.6 ± 4.7	-23.8 ± 4.8	0.459
Coronary sinus view (*n* = 88)	-24.8 ± 4.4	-24.3 ± 5.0	-25.8 ± 6.0	-23.3 ± 4.0	-24.4 ± 5.4	0.646
Aortic view (*n* = 119)	-24.0 ± 5.2	-23.6 ± 3.5	-22.0 ± 4.0	-22.7 ± 4.8	-23.2 ± 4.2	0.410
Coronal view (*n* = 113)	-21.0 ± 5.6	-21.2 ± 4.5	-20.2 ± 4.8	-20.6 ± 5.8	-20.7 ± 4.8	0.851
RVFAC (%) (*n* = 125)	41.2 ± 6.6	43.6 ± 6.2	42.6 ± 8.5	42.6 ± 8.7	44.5 ± 7.2	0.196
3DE						
End-diastolic volume (mL)	108.7 ± 33.2	102.6 ± 17.1	110.1 ± 30.9	111.4 ± 22.3	117.3 ± 31.5	0.386
End-systolic volume (mL)	44.4 ± 15.7	42.4 ± 8.6	47.3 ± 15.0	46.4 ± 10.3	52.4 ± 13,4	0.077
Stroke volume (mL)	63.2 ± 16.7	60.5 ± 10.5	62.7 ± 17.3	65.2 ± 13.9	64.8 ± 19.2	0.804
EF (%) (*n* = 97)	59.1 ± 3.7	59.0 ± 3.7	57.3 ± 4.7	58.7 ± 4.1	54.9 ± 3.1	**0.003**

RV, right ventricle; TAPSE, tricuspid annular plane systolic excursion; TDI-S', tissue Doppler imaging; RVFAC, right ventricular fractional area change; 3DE, three dimensional echocardiography
*Using linear regression analysis

men and women except in the inferior wall in the coronal view (male, -19.2 ± 4.4% versus female, -22.1 ± 5.4%, *p* = 0.002; Table 2). No statistically significant correlation was found between RV-GLS and age (Figure 3), blood pressure (systolic and diastolic) or QRS duration in all 4 views.

Intra and Inter-observer variability

Intra-and interobserver variability for RV strain was evaluated in a random subset of 20 subjects for all four views Intra-observer variability was: 4C, 0.2 ± 2.6%; CS, 0.7 ± 3.2%; Ao, 0.2 ± 2.4% and CV, 0.5 ± 2.5%. Inter-observer variability was: 4C, 0.2 ± 2.9%; CS, 0.1 ± 3.0%; Ao, -1.1 ± 3.9% and CV, -0.1 ± 3.1%.
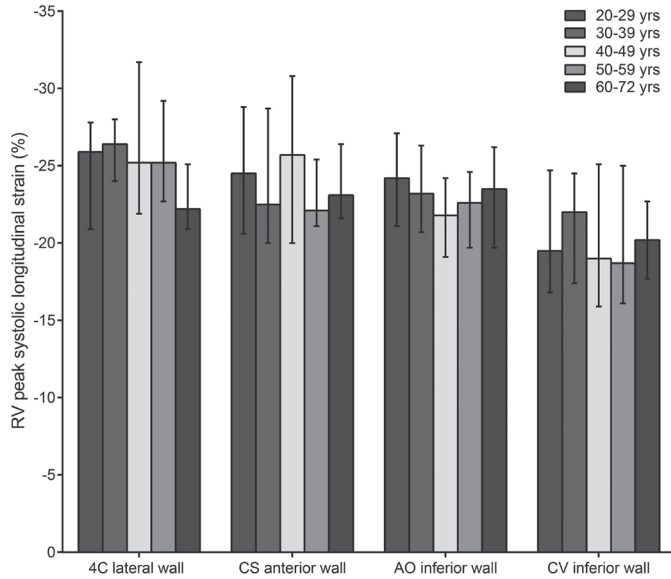
Figure 3 Peak systolic (three-segment) global right ventricular longitudinal strain per age group. RV, right ventricle; 4C, four-chamber; CS, coronary sinus; Ao, aortic; CV, coronal view

Pilot Study

In the pilot group, the basal and longitudinal dimensions of the RV were in all four views increased compared to the normal values. TAPSE, TDI-S′ and strain measurements were feasible in all views in all patients. Figure 4 shows a Venn diagram of the three RVF

Figure 4 Venn diagram of the standard apical four-chamber view (n = 20).Patients in the pilot group with RV dysfunction. Cut-off values are shown in the figure. Pink c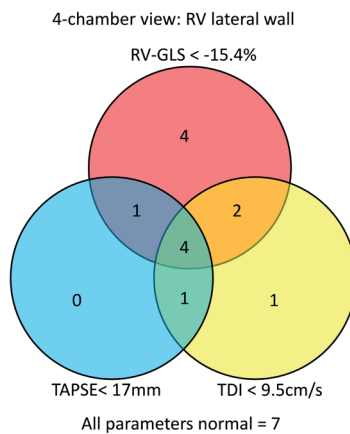ircle, peak systolic (three-segment) global right ventricular longitudinal strain RV-GLS; blue circle, tricuspid annular plane systolic excursion (TAPSE); yellow circle, tricuspid annular peak systolic velocity TDI-S'

parameters as evaluated in the 4C-view using the cut off value for TAPSE and TDI-S′ as stated in the 2015 guidelines and the RV-GLS lower level of normal as determined in this study (calculated as mean ± 1.96SD). Figure 5 shows a Venn diagram of the 4 RV views, only using lower level of normal values as determined in this study (calculated as mean ± 1.96SD). Abnormal values were seen in 45% for TAPSE, 39% for RV-GLS and 20% for TDI-S′ (TAPSE vs RV-GLS P < 0.001 and TAPSE vs TDI-S′ P < 0.001). The inferior wall from the coronal view seems relative insensitive for detection of abnormalities: abnormalities were seen in 30 vs. 61% an average in the other three walls (P< 0.001)
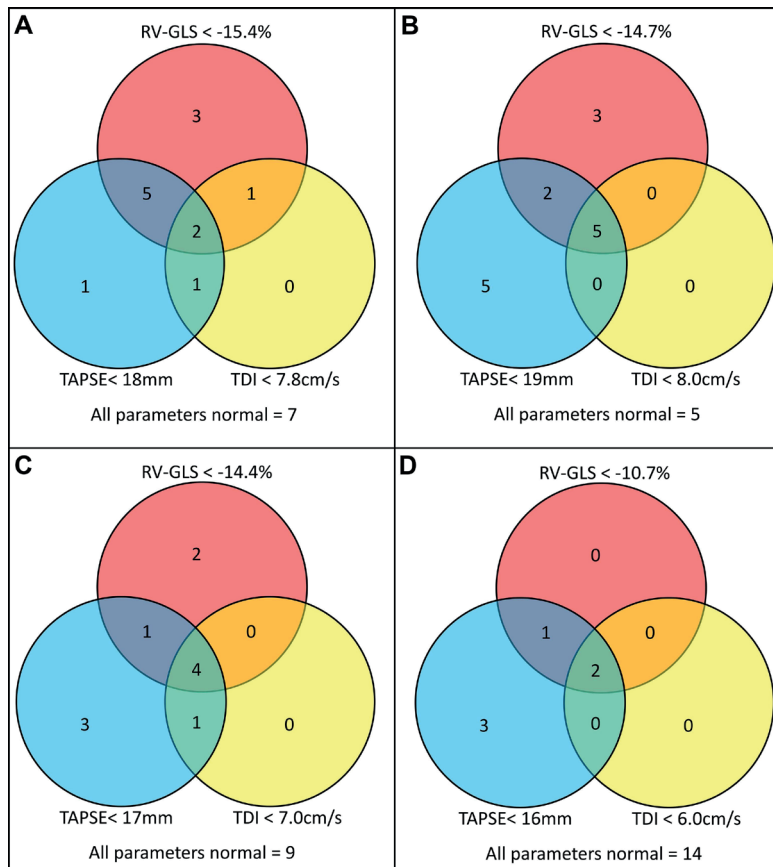
Figure 5 Venn diagram of the four right ventricular views (*n* = 20). Patients in the pilot group with RV dysfunction. Cut-off values are shown in the figure. (**A**) Four-chamber view (lateral wall), (**B**) Coronary sinus view (anterior wall), (**C**) aortic view (inferior wall), (**D**) coronal view (inferior wall). Pink circle, peak systolic (three-segment) global right ventricular longitudinal strain RV-GLS; blue circle, tricuspid annular plane systolic excursion (TAPSE); yellow circle, tricuspid annular peak systolic velocity TDI-S'.

DISCUSSION

This is a new step in the assessment of RVF providing a reproducible and fast assessment of regional and global function of the RV that is easily applicable in daily clinical practice. Multi-view imaging of the RV using iRotate mode has a short- learning curve and additional acquisition time.[4]

Conventional echocardiographic RV dimensions and areas

Interpretation of data depends upon the availability of robust reference limits that define 'normalcy'.[7] The two most recent large studies for reference ranges for the RV stress the importance of incorporating sex, age and biometric data.[7,8] This prospective study consisting of 147 healthy volunteers who are stratified per age decade is the first study publishing normal recommendations for RV dimensions and function for this novel four-view iRotate approach.

The unindexed focused 4C-view RV diameters in our study were found to be larger than the normal range values as stated in the EACVI/ASE 2015 guidelines; basal 28–49 versus 25–41mm and longitudinal 67–97 versus 59–83mm. RV areas indexed for BSA (as recommended in the 2015 guidelines) were also increased. In concordance with the literature dimensions and indexed areas were significantly larger in men than women.[7,8]

The larger RV size could be explained by the non-foreshortened RV view which is acquired with the (IVS)-RV apex centred along the midline of the 2D sector.[4] Thereby, the heart is sectioned in a slightly different way than the standard 4C-view and the focused 4C-view stated in 2005 and 2015 guidelines respectively.[2,9] In addition, for the non-indexed parameters it is important to note that the average height in our cohort of Dutch healthy subjects was 175 ± 9 cm compared with 170 ± 10 cm in the NORRE study and 171 ± 10 cm in the study from D'Oronzio et a l.[7,8]

RV function parameters (TAPSE and TDI-S′)

Despite their limitations TAPSE and TDI-S′ are simple and reproducible measurements used to assess RV longitudinal systolic function in daily practice. In our study, the feasibility of these parameters were > 90% for all four views compared to 85% for RVFAC and 66% for real-time 3DE. This study presents normal values for TAPSE and TDI-S′ taken at four points around the tricuspid annulus giving additional information and a more complete assessment of this complex RV. Both measurements from all four views fell within the normal range for the 4C-view as stated in the 2015 guidelines.[2] The lowest TAPSE and TDI-S′ value measured was from the inferior wall in the CV-view. A significant difference between TAPSE and age groups could only be found in the inferior wall and for TDI-S′ measurements in all four views.

Right ventricular longitudinal strain

Adequate tracking for RV strain analyses was obtained in 76% of the RV walls and the feasibility of STE was lowest in the anterior (CS-view) RV wall. These suboptimal findings

most probably result from the retrosternal position of the RV in the thorax and its thin walls.

Prognostic value of peak systolic global longitudinal (excluding the IVS) STE derived strain from the apical 4c view has been shown in diseased states.[2,10]

This multi-view study, differs in two-fold from the recent multi-view studies from Forsha and Rajagopal; (1) standardized RV views were assessed, Forsha et al acknowledge that the lack of universal standardized views is a limitation in their study, (2) focuses on tracking of the RV free walls, excluding the septum which reflects not just RV but also LV contractile function.[2,11–13]

Normal values for RV-GLS are scarce; the 2015 recommendations state -29% ± 4.5% but add that the data is limited and may vary depending on vendor and software version. The RV-GLS values from all four RV views fell within the normal range of the RV lateral free wall strain as stated in the 2015 guidelines.[2] It is interesting to note that the lowest strain values were seen in the inferior wall (CV-view) along with the lowest TAPSE and TDI-S' value. Compared with several published studies we did not find a significant correlation with strain and age and it was only in the inferior wall (CV-view) that we found a statistically significant difference in the strain values between men and women.[11,14,15]

The Pilot Study

These patients were included to examine whether RV-GLS was feasible in the diseased RV. It is encouraging to see that feasibility is 100% in the varying diseased states. No definite conclusions can be taken from the Venn diagrams as the group is too small. However, it's interesting to note that functional parameters from the inferior wall were found to be normal in more of the patients from this pilot group when compared to the anterior and lateral wall and that TDI-S' seems the least discriminative. Further larger studies are needed to evaluate the full potential of this model with normal range values as mentioned by us.

Limitations

This is a single centre study on a cohort of Dutch healthy subjects with the use of single vendor specific software so our reference values may not apply to other populations and equipment.

Secondly, STE is dependent on good image quality. The visualization of the anterior wall of the RVOT was only possible in a small group in the normal and pilot study population and was thus omitted from this study. Third, the software used is designed for the LV, which we adapted for the RV.

CONCLUSION

Two-dimensional transthoracic iRotate mode is a very attractive way to assess the RVF of anterior, lateral, inferior and sporadically the RVOT anterior wall in a standardised way.

The feasibility is good for all RV parameters, especially in the dilated RV. Normal values of RV dimension and function have been established. Further studies and a dedicated RV speckle tracking software are warranted to discover the full potential of this new technique for evaluation of the RV in various diseased states.

FUNDING

REFERENCES

1. Haddad F, Doyle R, Murphy DJ, Hunt SA. Right ventricular function in cardiovascular disease, part II: pathophysiology, clinical importance, and management of right ventricular failure. *Circulation* 2008;117:1717-1731.

2. Lang RM, Badano LP, Mor-Avi V, Afilalo J, Armstrong A, Ernande L, Flachskampf FA, Foster E, Goldstein SA, Kuznetsova T, Lancellotti P, Muraru D, Picard MH, Rietzschel ER, Rudski L, Spencer KT, Tsang W, Voigt JU. Recommendations for cardiac chamber quantification by echocardiography in adults: an update from the American Society of Echocardiography and the European Association of Cardiovascular Imaging. *Eur Heart J Cardiovasc Imaging* 2015;16:233-270.

3. Sachdev A, Villarraga HR, Frantz RP, McGoon MD, Hsiao JF, Maalouf JF, Ammash NM, McCully RB, Miller FA, Pellikka PA, Oh JK, Kane GC. Right ventricular strain for prediction of survival in patients with pulmonary arterial hypertension. *Chest* 2011;139:1299-1309.

4. McGhie JS, Menting ME, Vletter WB, Frowijn R, Roos-Hesselink JW, Soliman OI, van der Zwaan HB, Geleijnse ML, van den Bosch AE. A Novel 13-Segment Standardized Model for Assessment of Right Ventricular Function Using Two-Dimensional iRotate Echocardiography. *Echocardiography* 2016;33:353-361.

5. Rosner A, Barbosa D, Aarsaether E, Kjonas D, Schirmer H, D'Hooge J. The influence of frame rate on two-dimensional speckle-tracking strain measurements: a study on silico-simulated models and images recorded in patients. *Eur Heart J Cardiovasc Imaging* 2015;16:1137-1147.

6. Bland JM, Altman DG. Statistical methods for assessing agreement between two methods of clinical measurement. *Lancet* 1986;1:307-310.

7. Kou S, Caballero L, Dulgheru R, Voilliot D, De Sousa C, Kacharava G, Athanassopoulos GD, Barone D, Baroni M, Cardim N, Gomez De Diego JJ, Hagendorff A, Henri C, Hristova K, Lopez T, Magne J, De La Morena G, Popescu BA, Penicka M, Ozyigit T, Rodrigo Carbonero JD, Salustri A, Van De Veire N, Von Bardeleben RS, Vinereanu D, Voigt JU, Zamorano JL, Donal E, Lang RM, Badano LP, Lancellotti P. Echocardiographic reference ranges for normal cardiac chamber size: results from the NORRE study. *Eur Heart J Cardiovasc Imaging* 2014;15:680-690.

8. D'Oronzio U, Senn O, Biaggi P, Gruner C, Jenni R, Tanner FC, Greutmann M. Right heart assessment by echocardiography: gender and body size matters. *J Am Soc Echocardiogr* 2012;25:1251-1258.

9. Lang RM, Bierig M, Devereux RB, Flachskampf FA, Foster E, Pellikka PA, Picard MH, Roman MJ, Seward J, Shanewise JS, Solomon SD, Spencer KT, Sutton MS, Stewart WJ, Chamber Quantification Writing G, American Society of Echocardiography's G, Standards C, European Association of E. Rec-

ommendations for chamber quantification: a report from the American Society of Echocardiography's Guidelines and Standards Committee and the Chamber Quantification Writing Group, developed in conjunction with the European Association of Echocardiography, a branch of the European Society of Cardiology. *J Am Soc Echocardiogr* 2005;18:1440-1463.

10. Haeck ML, Scherptong RW, Marsan NA, Holman ER, Schalij MJ, Bax JJ, Vliegen HW, Delgado V. Prognostic value of right ventricular longitudinal peak systolic strain in patients with pulmonary hypertension. *Circ Cardiovasc Imaging* 2012;5:628-636.

11. Fine NM, Chen L, Bastiansen PM, Frantz RP, Pellikka PA, Oh JK, Kane GC. Reference Values for Right Ventricular Strain in Patients without Cardiopulmonary Disease: A Prospective Evaluation and Meta-Analysis. *Echocardiography* 2015;32:787-796.

12. Forsha D, Risum N, Kropf PA, Rajagopal S, Smith PB, Kanter RJ, Samad Z, Sogaard P, Barker P, Kisslo J. Right ventricular mechanics using a novel comprehensive three-view echocardiographic strain analysis in a normal population. *J Am Soc Echocardiogr* 2014;27:413-422.

13. Rajagopal S, Forsha DE, Risum N, Hornik CP, Poms AD, Fortin TA, Tapson VF, Velazquez EJ, Kisslo J, Samad Z. Comprehensive assessment of right ventricular function in patients with pulmonary hypertension with global longitudinal peak systolic strain derived from multiple right ventricular views. *J Am Soc Echocardiogr* 2014;27:657-665 e653.

14. Chia EM, Hsieh CH, Boyd A, Pham P, Vidaic J, Leung D, Thomas L. Effects of age and gender on right ventricular systolic and diastolic function using two-dimensional speckle-tracking strain. *J Am Soc Echocardiogr* 2014;27:1079-1086 e1071.

15. Muraru D, Onciul S, Peluso D, Soriani N, Cucchini U, Aruta P, Romeo G, Cavalli G, Iliceto S, Badano LP. Sex- and Method-Specific Reference Values for Right Ventricular Strain by 2-Dimensional Speckle-Tracking Echocardiography. *Circ Cardiovasc Imaging* 2016;9:e003866.

CHAPTER 11

Summary and general discussion

SUMMARY AND GENERAL DISCUSSION

In this summary and general discussion I will address the research questions, discuss my findings and deliberate on clinical implications and future directions of Simultaneous Multiplane Imaging (SMPI).

The general introduction (**Chapter 1**) of this thesis gives a short summery of the evolution of echocardiography and provides the reasoning why I found it necessary to investigate the potential contributions of this new imaging modality to cardiovascular imaging. A new generation transthoracic two-dimensional and three-dimensional (2D/3D) echocardiographic matrix transducers have opened up a new way of echocardiographic imaging. One of the new features of this transducer is (SMPI) which permits the use of a full electronic rotation of 360° (iRotate) and a simultaneous adjustable biplane (xPlane) of the 2D image. Because of the shortcomings of 3D echocardiography (3DE) as it stands today this thesis would probably not have been written. Unlike 2D images, which are instantly available, 3D datasets in most applications only reveal their true information after they have been analysed. This requires special knowledge of the 3D analysis software, skills on 3D dataset cropping and 3D orientation. This is time consuming and has a longer learning curve than 2D image analysis, and therefore physicians and sonographers in many hospitals are dissatisfied with 3D echocardiography.[1]

From our earlier experience of SMPI with transesophageal echocardiography (TEE) and applying SMPI in transthoracic echocardiography (TTE) in daily clinical practice we found a dedicated article on this technique warranted. In **Chapter 2** we present several ways in which we think SMPI can be of benefit on a daily bases in a routine echocardiography-laboratory. Transthoracic biplane and triplane echocardiographic imaging has been available since 2003, the scarcity of literature and data suggest that the potential of this technique was not fully appreciated and/or the technology was not sufficient.[2] With SMPI modes, a goal-orientated or limited echocardiogram will only require two acoustic windows without manual rotation of the transducer. This would cut down scanning time and produce accurate cross-sectional images of the heart for 2D quantitative analyses. The sonographer and/or young doctor in training is expected to benefit greatly from this approach. Sengupta et al in 2004 already concluded that biplane imaging effectively reduces sonographer time in a high-volume echocardiography laboratory but also recognized that improvements in technology and transducer size were still necessary.[3] We agree with Sengupta's statement from 2004. The benefit of simultaneously displayed images from the apical window not only reveals that you are scanning from the true apical long axis but also gives the ability to perform measurements on two orthogonal planes in the same heartbeat. This will increase the accuracy of 2D-TTE-volume calculations. In other echocardiographic calculations i.e. stroke volume and regurgitant volume; both calculated with geometric assumptions, xPlane imaging may also improve the accuracy of the calculation. Both the mitral annulus (MA) and the LV outflow tract (LVOT) are often assumed to be circular in shape, whereas they have been confirmed, in multiple studies with different imaging modalities, to be saddle-like or oval.[4–6] In this thesis we

demonstrated that xPlane imaging enables us to measure the major and minor axis and/or the true cross sectional area of the MA and LVOT. Obviously dedicated studies should be performed to confirm these advantages.

SIMULTANEOUS MULTIPLANE 2D-ECHOCARDIOGRAPHY IN CONGENITAL AND VALVULAR HEART DISEASE

The atrial septal secundum defect (ASD) is one of the most common lesions in adult congenital heart disease. In the past decade, transcatheter closure of an ASD has gradually become the treatment of choice, rather than surgery.[7,8] The choice between surgical or percutaneous closure of the ASD relies on four essential criteria; location, diameter, tissue rim length and morphology. In this study (**Chapter 3**) we sought to assess the value of SMPI in measurements of the ASD and rim length. SMPI (iRotate and xPlane) could reliably assess the dimensions and rim length of an ASD when compared with 2D TEE.

SMPI allows the sonographer, once the largest diameter of the ASD has been visualized in the subcostal four-chamber view, to make a 90° rotation with iRotate or apply xPlane mode, by placing the cursor in the center of the defect giving the corresponding orthogonal plane. Both diameters and rim length of the ASD can be measured, in xPlane mode also from the same heartbeat. If the defect can be centered in the middle of the sector, a full 360° of the defect can be performed and all rims including the aortic rim visualized. In xPlane mode, as the frame rate drops by half and imaging is performed from the subcostal window with the region of interest in the far field, the true edges of a thin floppy inter-atrial septum maybe difficult to interpret. The ASD diameter can be overestimated and the rim length underestimated. Therefore, it is suggested that only in patients with a poor acoustic window a TEE is still required for pre-intervention evaluation.

In non-dedicated congenital heart disease centers, it is often assumed that an ASD is always in the center of the inter-atrial septum and circular in shape. However, this is often not the case.[7] In general cardiology, echocardiographic textbooks, the subcostal four-chamber view is advised for scanning of the inter-atrial septum.[9] As an ASD maybe oval or slit like in shape it is important that both the major and minor axis of the defect is visualized. A thorough multi-view examination of the inter-atrial septum from the subcostal window applying sweeps is mandatory, the defect may lie outside the region of the fossa ovalis or there maybe multiple defects present. For a less experienced sonographer this is a virtually impossible task, and often results in the patient being referred for a diagnostic TEE. The xPlane mode allows a controlled sweep across the inter-atrial septum from the standard subcostal four-chamber view, defects outside the oval fossa will now be easier to be detected by a non-congenital sonographer. The diagnoses of an ASD will become less operator- dependent but most importantly a diagnostic TEE will not always be necessary. A study should be initiated involving several peripheral hospitals to investigate, if there is a reduction in diagnostic TEEs performed by non-congenital cardiologist when SMPI is applied.

Mitral valve (MV) prolapse (**Chapter 4**) is one of the most common valvular abnormalities in industrialized countries.[10] The definition of the site and extent of MV prolapse plays a crucial role not only in the surgical referral but also for the operative plan. Different pathology requires different levels of surgical expertise based on the complexity of lesions seen with echocardiography.[11,12] Our study sought to assess the value of transthoracic 2D, 2D xPlane and 3D echocardiography for the definition of the site and extent of MV prolapse in patients who underwent MV surgery. We found that 2D xPlane imaging can assess the MV in a systematic manner and correctly diagnose the site and extent of the prolapse. Most patients may thus be operated on without the need for an outpatient pre-operative TEE. If necessary, a pre-operative TEE in the operating room may further refine the diagnosis and guide the surgical approach.

Unfortunately, many physicians are of the opinion that 2D TTE is not reliable enough to provide the surgeon or interventionist with the essential pre-intervention information and consider TEE obligatory. However, it should be recognised that the newer technology has improved TTE quality and we stress that TEE is a semi- invasive procedure that is not without procedural risk.[13–15] More recently, with 3D TTE, we have been introduced to the unique "enface" view and the spatial relationship of structures can be seen more clearly. We found that 2D xPlane imaging may be superior to enface 3D imaging as this requires more expertise, is more critically dependent on image quality and suffers from limited temporal and spatial resolution. Thin and curving structures like the fossa-ovalis and non-thickened valves often appear with large holes within them, the size of which can be easily influenced by the 3D gain setting.[16] In 3DE, the angle of insonation must be tailored to the region of interest and ideally should be orthogonal to the relevant structure. The ease of SMPI (xPlane and iRotate mode) to explore the heart for eccentric regurgitation jets, visualized with colour Doppler, makes it an attractive technique to explore cardiac morphology.

Paravalvular leakage (PVL) is an important issue in transcatheter aortic valve implantation (TAVI) because of its probable impact on mortality (**Chapter 5**).[17,18] Ideally, the circumferential extent of PVL serves as measure of severity. Unfortunately, the colour Doppler analysis of the short-axis TAVI view suffers from important limitations that may result in PVL severity underestimation because of impaired echocardiographic window quality and interaction of calcium, crushed native material or the stent prosthesis with the echo beam.[19,20] Colour Doppler imaging from an apical window does not suffer from this limiting interaction but the routinely used 3-chamber and 5-chamber apical views reflect only a very small proportion of the TAVI prosthesis circumference. iRotate echocardiography may be able to study the whole circumference of the TAVI prosthesis from an apical view.

In a study in 41 consecutive patients the value of iRotate echocardiography was investigated. It was shown that the whole TAVI prosthesis circumference could be reconstructed in all patients without a loss in spatial and temporal resolution compared to normal 2D scanning and with good inter-observer variability and test test-retest reproducibility. Overall, iRotate PVL circumferential extent was highly correlated with short-axis (SAX) circumferential extent (r = 0.84, $p < 0.001$). A bias of 6.0% (limits of agreement: ± 19.7%)

with a significant larger circumferential extent with iRotate (13.7% ± 17.0% vs. 7.7% ± 10.1%, *p* < 0.001) was observed. The main issue not answered by this study is obviously whether iRotate overestimates or SAX analysis underestimates circumferential extent of PVL. One potential factor that could have led to overestimation by iRotate may be the non-central position of the echo beam in the TAVI stent, in particular in patients with abnormally shaped stent frames. This issue may be explored in future studies in which the circumferential extent of PVL should be correlated with regurgitant volumes assessed by magnetic resonance imaging.

A transcatheter tricuspid valve intervention (TTVI), via repair or replacement of the tricuspid valve, is much less common compared to transcatheter pulmonary or aortic valve replacement.[21,22] However, in patients with residual TR, often found after complex initial surgical repair and with numerous comorbidities there is a high risk of a poor outcome after TV reoperation.[23] Therefore, TTVI could be an attractive alternative and a comprehensive pre-intervention evaluation of the TV apparatus mandatory. Detailed literature on scanning of the TV using echocardiography but more importantly the pros and cons of these individual echocardiographic modalities is scarce. In **Chapter 6,** a book section to be published in the "Practical manual of tricuspid valve disease", we describe in detail the transthoracic imaging modalities and scanning procedure alongside the incremental advantages of 3D-TTE over 2D-TTE. There is accumulating evidence that 3D-TTE has incremental values in the assessment of TV disease, in particular for the annulus, compared with 2D-TTE. However, assessment of right-sided structures with echocardiography is more difficult due to the anterior location of the right heart and since 3DE is dependent on 2DE quality, this will be very challenging. The SMPI modalities we speculate could have incremental value when 3D-TTE image quality is not optimal. The xPlane imaging mode allows the measurements of the two axes diameters of the TV annulus in the same heartbeat. Also we have demonstrated in earlier studies that the 2D-TTE iRotate mode provides a standard methodology for serial assessment of right ventricular function.[24] The feasibility of segmental RV wall analysis approached 95% in subjects with normal- and patients with dilated-RVs. Likewise, assessment of right ventricular strain in subjects with normal and dilated RV has been shown feasible and reproducible using the 2D-TTE iRotate mode.[25] Translating our initial feasibility studies of the 2D-TTE iRotate mode into direct TV assessment could be speculated in several aspects. It could be used for more robust serial follow up of disease progression before- and reverse remodelling after percutaneous interventions or surgery involving the TV. Likewise, recovery of RV function after TV repair or replacement could be more accurately quantified. The 2D-TTE iRotate mode could be used as well for comprehensive and robust serial assessment of TV annulus size and function

For paediatric cardiology, SMPI is available on their 2DE/3DE matrix transducer; the operating frequency range is 2–7MHz. These frequencies are lower than the dedicated 2D paediatric transducer entailing that it remains superior to that of their matrix transducer for this patient group. Even with this known drawback, 3DE has become important in the management of these patients, particularly with pre-surgical planning, guidance of

catheter interventions and functional assessment of the heart. The acoustic window of the paediatric patient is clearly superior to that of the adult patient making 3D imaging more attractive, and the role of SMPI maybe of less importance. In this consensus paper (**Chapter 7**), providing a review of the optimal applications of 3D echocardiography in congenital heart disease (CHD), we also address the technical limitations of the technique in this patient population. The acoustic window of the older and /or operated child can sometimes be disappointing and it is this group that could benefit from SMPI. The full use of SMPI in CHD still has to be explored.

SIMULTANEOUS MULTIPLANE 2D-ECHOCARDIOGRAPHY AND VENTRICULAR FUNCTION

Quantification of cardiac chambers and function is the cornerstone of cardiac imaging.[26] During the last decade, 2D speckle tracking echocardiography (STE) has become available and offers objective measurements to quantify regional and global ventricular function, independent of angle and ventricular geometry.[26] With the use of STE, ventricular dysfunction can be detected in a pre-clinical phase.[27,28] However, information on normal ranges of STE-derived measures and the prognostic value of is limited.[27–29] We initiated an echocardiographic study with 155 healthy individuals, the Navigator study, to obtain normal values of all echocardiographic parameters. These subjects were recruited in a stratified fashion to provide at least fourteen participants of each sex, representing each age decade from 20 to 72 years. In **Chapter 8** we established normal values for LV global longitudinal strain (GLS). Sex, body surface area and blood pressure were found to influence LV GLS whereas age did not. The apical 4-chamber (A4C), 2-chamber (A2C) and 3-chamber (A3C) images for strain analyses were acquired randomly by two highly experienced sonographers, using the standard manual rotation technique or with iRotate mode. Two interesting points were observed during the acquisitions acquired with iRotate mode. First; the known anatomic landmarks better depicted the view than the degree of rotation, the correct orientation for the A2C and A3C were often not seen at the suggested 60° and 120° orientation as stated in the text books.[30] Second, when the transducer was not correctly placed on the true LV apex, rotating to the A2C view would immediately show an incorrect image, indicating that the LV has not been cut in its true long axis. Correct alignment of the A4C and A2C cannot be guaranteed with manual rotation. During manual rotation, you tend to lift; tilt and turn the transducer whilst optimizing the image quality, correct alignment to your original A4C view however, is not guaranteed. As all trained sonographers appreciate, in the normal heart, if the transducer position is incorrect the LV will be foreshortened and appear more spherical with minimal tapering of the apex.[30] In a dilated LV this difference in shape is less distinct and an incorrect transducer position could go unnoticed. Incorrect alignment will lead to incorrect volume calculations with the modified bi-plane -Simpson's method of disk summation.[31]

The ease and use of iRotate mode from a fixed transducer position to assess the LV using anatomic landmarks triggered us into thinking about the possibility of applying this technique to assess the right ventricle (RV). Assessment of RV function is increasingly recognized as a prognostic factor in a variety of diseases such as left sided heart failure, pulmonary hypertension and congenital heart disease in the acute phase and during follow up.[32] Repeated assessment of RV size and function represents a crucial step in initiation and guiding of therapy, follow-up and prediction of out-come in patients with acquired and congenital heart disease.[33–35] The RV has a complex geometric shape which requires a 2D multi-view scanning protocol to fully assess it. Current echocardiographic methodologies do not provide a robust assessment of RV function. Since the introduction of 3DE a lot of data has been collected and studies performed. The feasibility varies between 52% and 94%.[36,37] In a real world setting Renella et al, evaluated 3DE of the RV in paediatric and congenital heart disease patients (age 1–20 years), and found that RV volumes were measurable in only 58% of the patients.[38] This patient group, expectably, has a better image quality compared to the adult patient population. Feasibility of 3DE of the RV in the adult patient population group in a real world setting is expected to be lower and stresses the need for a robust non-3D echo technique to assess the RV.

A standardized echocardiographic approach taken from one acoustic window, where an anatomic landmark in the image plane is used to identify a specific RV wall, increase the accuracy of assessment of RV function in routine follow up. We found (**Chapter 9**) that the anterior, lateral, inferior and right ventricular outflow tract (RVOT) anterior wall could be identified according to a unique anatomic landmark among normal subjects and patients with dilated RVs. Our proposed 13 segment standardized model for RV assessment using iRotate mode, from a single acoustic window, was highly feasible. However, the visibility of the RVOT anterior wall remains challenging. This suboptimal visualization of the most anterior segments of the RV could be explained by the retrosternal position of the heart in the thorax. Also the long axis of the normal sized heart is superior-inferior (vertical), which again would contribute to the difficulty in visualizing the most anterior segments of the RV.[39] Luckily, the visibility was higher in the diseased RV, probably due to the fact that the long axis of the diseased RV (dilated or hypertrophic) is more horizontal and will be less compromised by the sternum. Additional RV function information was also accessible through the multiple; tricuspid annular plane systolic excursion (TAPSE) and peak systolic velocity tissue (S¢) using tissue Doppler imaging (TDI) measurement around the tricuspid annulus.

Our new approach will reduce acquisition time and should enhance the accuracy for evaluating the RV. Well defined anatomic landmarks result in robust image orientation, precise echocardiographic follow up and less oblique plane acquisition compared to the standard manual multiview approach entailing several acoustic windows.

Interpretation of data depends upon the availability of robust reference limits that define 'normalcy'.[40] In **Chapter 10** we publish normal recommendations for RV dimensions and function based on our novel four-view iRotate approach from the 155 healthy individuals included in the Navigator study. The RV diameters in our study were found to be larger

than the normal range values as stated in the EACVI/ASE 2015 guidelines; basal 28–49 versus 25–41mm and longitudinal 67–97 versus 59–83mm. RV areas indexed for BSA (as recommended in the 2015 guidelines) were also increased. The larger RV size could be explained by the non-foreshortened RV view that is acquired with the (IVS)-RV apex centred along the midline of the 2D sector.[24] Thereby, the heart is sectioned in a slightly different way than the standard four chamber (4C) view and the focused 4C-view stated in 2005 and 2015 guidelines respectively.[26,31] In addition, for the non-indexed parameters it is important to note that the average height in our cohort of Dutch healthy subjects, known for their tallness,[41] was 175 ± 9cm compared to 170 ± 10cm in the NORRE study and 171 ± 10cm in the study from D'Oronzio et al.[40,42] In accordance with the literature dimensions and the indexed areas were significantly larger in men than in women.[40,42] TAPSE and TDI-S′ taken at four points around the tricuspid annulus gave additional information and a more complete assessment of the RV. A significant difference between TAPSE and age groups could only be found in the inferior wall and for TDI-S′ measurements in all four views.

In the last decade, 2D STE has become available which offers objective measurements to quantify regional and global ventricular function independent of angle and ventricular geometry.[43] However, the accuracy of these parameters for assessing the RV is inherently limited because the parameter reflects only a limited region of the RV; the lateral wall from the A4C view. Our model allows RV global longitudinal strain (GLS) values to be acquired from all four RV views. RV-GLS values for all four RV views fell within the normal range of the RV lateral free wall strain as stated in the 2015 guidelines.[26] Compared with several published studies we did not find a significant correlation with strain and age and it was only in the inferior wall (CV-view) that we found a statistically significant difference in the strain values between men and women.[44–46]

Pilot study patients were included in this thesis to examine first whether this novel four-view approach was feasible (**Chapter 9**) and second whether RV-GLS could be measured in all four views (**Chapter 10**) in pressure and volume overloaded RVs. It is encouraging to see that the feasibility for the RV walls, TAPSE, TDI-S′ and RV-GLS is good. It is now important that large studies are carried out to evaluate the full potential of this technique.

CONCLUSIONS AND FUTURE PERSPECTIVES

This thesis introduces a new echocardiographic imaging modality: Simultaneous Multiplane Imaging (SMPI), and provides practically based studies demonstrating the added value of SMPI in daily clinical practice. SMPI allows you to record multiple 2D images from one transducer position. With the primary image being based on anatomic landmarks and the secondary image depicted by the number of degrees the reproducibility of follow up echocardiograms should increase. Also, the accuracy of cross-sectional imaging is more robust, for example showing the LV in its true long axis is more reliable. This is extremely important when LV volume and function are quantified. SMPI gives more insight

into structural and congenital heart disease compared to standard 2D-echocardiography. With percutaneous procedures becoming more routine, detailed pre-and-post procedural information on morphology is essential. Further studies exploring the full ability of SMPI in this field are warranted. Analyses of the RV has reached a new dimension, similar to the LV we now have a 13-segment model, recordable from one transducer position. Since it is known that peak global RV longitudinal strain has incremental value over conventional echo parameters our novel four-view approach may play an important role in the assessment of RV function. However, the analyses software as written in Chapter 9 makes use of an algorithm developed for the LV whose geometric form is totally different to that of the RV. Accuracy and reproducibility in quantification analyses is of utmost importance, therefore new analyses software with a dedicated RV algorithm and fully automatic border detection, with minimal manual correction, is essential. This would allow along with segmental RV-GLS more accurate time-to-peak analyses. Subsequently studies with our 13-segment model will obviously be required to critically evaluate this new software in various diseased states.

Prior to two-dimensional SMPI, a similar modality was already available in 3D-echocardiography analyses software, known under various names including multiplane reconstruction (MPR) mode. Using this MPR mode, a 3D image can be interpreted and calculations performed for area and volume measurements. With our SMPI experience further development should be made in the 3D analyses software to allow an increased number of standard 2D cross-sections to be displayed simultaneously on one screen. You would immediately have a direct overview of all images and reporting will become more accurate and less time consuming. If needed extra cross-sections can always be created.

Whether SMPI is here to stay will depend upon future developments, I think for the next ten years 3D will still be an "add on" imaging technique with SMPI playing a very important role in daily routine echocardiographic examinations. In the real-world setting of tomorrow further development in hard and software is essential for optimal image quality along with a higher frame rate. With the increased number of obese patients penetration and resolution in the far field needs to improve. The same applies for the near field resolution for optimal visualization of the RVOT anterior wall. Secondly, the possibility to steer the ultrasound beam electronically in the elevation plane would be advantageous; overcoming the loss of transducer contact due to the acute angle needed to visualize this wall from the apical window. To achieve these goals, a good working relationship between clinicians and engineers is essential.

New technology of today and in the future in all aspects of echocardiography places great pressure on the day-to-day running of a department. For example, a major issue faced in many institutions is the integration of 3D echocardiography onto the work floor. SMPI is a quick, simple to use, and easy to understand echo modality which could bridge the gap between 2D and 3D thinking. At the moment, in many departments, top of the range echo-machines are functioning as elaborate ECG machines, the workload is so high that all the extra-modalities are left dormant. Time has to be created to ensure that these new echo modalities including analyses software can be learnt and applied. A tailored

request for an echocardiogram for example would ensure scanning time is used more efficiently and the sonographer would have time to invest in gaining knowledge of present and future echocardiographic technology. The cost-effectiveness would be seen in the long term as expensive imaging techniques are replaced by a cheaper dedicated echocardiogram to answer the same clinical question.

REFERENCES

1. Buck T FA, Monaghan M,ed. Three-dimensional Echocardiography 2nd Edition. Berlin: Springer-Verlag Berlin and Heidelberg 2015:31.
2. Sugeng L, Kirkpatrick J, Lang RM, Bednarz JE, Decara JM, Lammertin G, Spencer KT. Biplane stress echocardiography using a prototype matrix-array transducer. *J Am Soc Echocardiogr* 2003;16:937-941.
3. Sengupta PP, Chandrasekaran K, Prince DJ, Dyke RA, Khandheria BK. Role of biplane echocardiography in a large-volume clinical practice: revamping strategies for echocardiography in a limited time. *J Am Soc Echocardiogr* 2005;18:757-760.
4. Anwar AM, Soliman OI, ten Cate FJ, Nemes A, McGhie JS, Krenning BJ, van Geuns RJ, Galema TW, Geleijnse ML. True mitral annulus diameter is underestimated by two-dimensional echocardiography as evidenced by real-time three-dimensional echocardiography and magnetic resonance imaging. *Int J Cardiovasc Imaging* 2007;23:541-547.
5. Gordic S, Nguyen-Kim TD, Manka R, Sundermann S, Frauenfelder T, Maisano F, Falk V, Alkadhi H. Sizing the mitral annulus in healthy subjects and patients with mitral regurgitation: 2D versus 3D measurements from cardiac CT. *Int J Cardiovasc Imaging* 2014;30:389-398.
6. Otani K, Takeuchi M, Kaku K, Sugeng L, Yoshitani H, Haruki N, Ota T, Mor-Avi V, Lang RM, Otsuji Y. Assessment of the aortic root using real-time 3D transesophageal echocardiography. *Circ J* 2010;74:2649-2657.
7. Podnar T, Martanovic P, Gavora P, Masura J. Morphological variations of secundum-type atrial septal defects: feasibility for percutaneous closure using Amplatzer septal occluders. *Catheter Cardiovasc Interv* 2001;53:386-391.
8. Roberson DA, Cui W, Patel D, Tsang W, Sugeng L, Weinert L, Bharati S, Lang RM. Three-dimensional transesophageal echocardiography of atrial septal defect: a qualitative and quantitative anatomic study. *J Am Soc Echocardiogr* 2011;24:600-610.
9. Otto CM. Clinical Echocardiography. Philadelphia: Saunders Elsevier, 2009:430
10. Iung B, Baron G, Butchart EG, Delahaye F, Gohlke-Barwolf C, Levang OW, Tornos P, Vanoverschelde JL, Vermeer F, Boersma E, Ravaud P, Vahanian A. A prospective survey of patients with valvular heart disease in Europe: The Euro Heart Survey on Valvular Heart Disease. *Eur Heart J* 2003;24:1231-1243.
11. Adams DH, Anyanwu AC. Seeking a higher standard for degenerative mitral valve repair: begin with etiology. *J Thorac Cardiovasc Surg* 2008;136:551-556.
12. Adams DH, Anyanwu AC. The cardiologist's role in increasing the rate of mitral valve repair in degenerative disease. *Curr Opin Cardiol* 2008;23:105-110.
13. Daniel WG, Erbel R, Kasper W, Visser CA, Engberding R, Sutherland GR, Grube E, Hanrath P, Maisch B, Dennig K, et al. Safety of transesophageal echocardiography. A multicenter survey of 10,419 examinations. *Circulation* 1991;83:817-821.

14. Minardi G, Pino PG, Manzara CC, Pulignano G, Stefanini GG, Viceconte GN, Leonetti S, Madeo A, Gaudio C, Musumeci F. Preoperative scallop-by-scallop assessment of mitral prolapse using 2D-transthoracic echocardiography. *Cardiovasc Ultrasound* 2010;8:1.

15. Monin JL, Dehant P, Roiron C, Monchi M, Tabet JY, Clerc P, Fernandez G, Houel R, Garot J, Chauvel C, Gueret P. Functional assessment of mitral regurgitation by transthoracic echocardiography using standardized imaging planes diagnostic accuracy and outcome implications. *J Am Coll Cardiol* 2005;46:302-309.

16. Faletra FF, Ramamurthi A, Dequarti MC, Leo LA, Moccetti T, Pandian N. Artifacts in three-dimensional transesophageal echocardiography. *J Am Soc Echocardiogr* 2014;27:453-462.

17. Kodali SK, Williams MR, Smith CR, Svensson LG, Webb JG, Makkar RR, Fontana GP, Dewey TM, Thourani VH, Pichard AD, Fischbein M, Szeto WY, Lim S, Greason KL, Teirstein PS, Malaisrie SC, Douglas PS, Hahn RT, Whisenant B, Zajarias A, Wang D, Akin JJ, Anderson WN, Leon MB, Investigators PT. Two-year outcomes after transcatheter or surgical aortic-valve replacement. *N Engl J Med* 2012;366:1686-1695.

18. Lefevre T, Kappetein AP, Wolner E, Nataf P, Thomas M, Schachinger V, De Bruyne B, Eltchaninoff H, Thielmann M, Himbert D, Romano M, Serruys P, Wimmer-Greinecker G, Group PEI. One year follow-up of the multi-centre European PARTNER transcatheter heart valve study. *Eur Heart J* 2011;32:148-157.

19. Geleijnse ML, Di Martino LF, Vletter WB, Ren B, Galema TW, Van Mieghem NM, de Jaegere PP, Soliman OI. Limitations and difficulties of echocardiographic short-axis assessment of paravalvular leakage after corevalve transcatheter aortic valve implantation. *Cardiovasc Ultrasound* 2016;14:37.

20. Pibarot P, Hahn RT, Weissman NJ, Monaghan MJ. Assessment of paravalvular regurgitation following TAVR: a proposal of unifying grading scheme. *JACC Cardiovasc Imaging* 2015;8:340-360.

21. Aboulhosn J, Cabalka AK, Levi DS, Himbert D, Testa L, Latib A, Makkar RR, Boudjemline Y, Kim DW, Kefer J, Bleiziffer S, Kerst G, Dvir D, McElhinney DB. Transcatheter Valve-in-Ring Implantation for the Treatment of Residual or Recurrent Tricuspid Valve Dysfunction After Prior Surgical Repair. *JACC Cardiovasc Interv* 2017;10:53-63.

22. El-Eshmawi A, Tang GH, Verma S, Yanagawa B, Ruel M, Adams DH. Innovations in tricuspid valve intervention. *Curr Opin Cardiol* 2017.

23. Nath J, Foster E, Heidenreich PA. Impact of tricuspid regurgitation on long-term survival. *J Am Coll Cardiol* 2004;43:405-409.

24. McGhie JS, Menting ME, Vletter WB, Frowijn R, Roos-Hesselink JW, Soliman OI, van der Zwaan HB, Geleijnse ML, van den Bosch AE. A Novel 13-Segment Standardized Model for Assessment of Right Ventricular Function Using Two-Dimensional iRotate Echocardiography. *Echocardiography* 2016;33:353-361.

25. McGhie JS, Menting ME, Vletter WB, Frowijn R, Roos-Hesselink JW, van der Zwaan HB, Soliman OI, Geleijnse ML, van den Bosch AE. Quantitative assessment of the entire right ventricle from one acoustic window: an attractive approach. *Eur Heart J Cardiovasc Imaging* 2016.

26. Lang RM, Badano LP, Mor-Avi V, Afilalo J, Armstrong A, Ernande L, Flachskampf FA, Foster E, Goldstein SA, Kuznetsova T, Lancellotti P, Muraru D, Picard MH, Rietzschel ER, Rudski L, Spencer KT, Tsang W, Voigt JU. Recommendations for cardiac chamber quantification by echocardiography in adults: an update from the American Society of Echocardiography and the European Association of Cardiovascular Imaging. *Eur Heart J Cardiovasc Imaging* 2015;16:233-270.

27. Forsey J, Friedberg MK, Mertens L. Speckle tracking echocardiography in pediatric and congenital heart disease. *Echocardiography* 2013;30:447-459.

28. Mondillo S, Galderisi M, Mele D, Cameli M, Lomoriello VS, Zaca V, Ballo P, D'Andrea A, Muraru D, Losi M, Agricola E, D'Errico A, Buralli S, Sciomer S, Nistri S, Badano L, Echocardiography Study Group Of The Italian Society Of C. Speckle-tracking echocardiography: a new technique for assessing myocardial function. *J Ultrasound Med* 2011;30:71-83.

29. Geyer H, Caracciolo G, Abe H, Wilansky S, Carerj S, Gentile F, Nesser HJ, Khandheria B, Narula J, Sengupta PP. Assessment of myocardial mechanics using speckle tracking echocardiography: fundamentals and clinical applications. *J Am Soc Echocardiogr* 2010;23:351-369; quiz 453-355.

30. Otto CM. Clinical Echocardiography. Philadelphia: Saunders Elsevier, 2009:43-45.

31. Lang RM, Bierig M, Devereux RB, Flachskampf FA, Foster E, Pellikka PA, Picard MH, Roman MJ, Seward J, Shanewise JS, Solomon SD, Spencer KT, Sutton MS, Stewart WJ, Chamber Quantification Writing G, American Society of Echocardiography's G, Standards C, European Association of E. Recommendations for chamber quantification: a report from the American Society of Echocardiography's Guidelines and Standards Committee and the Chamber Quantification Writing Group, developed in conjunction with the European Association of Echocardiography, a branch of the European Society of Cardiology. *J Am Soc Echocardiogr* 2005;18:1440-1463.

32. Haddad F, Doyle R, Murphy DJ, Hunt SA. Right ventricular function in cardiovascular disease, part II: pathophysiology, clinical importance, and management of right ventricular failure. *Circulation* 2008;117:1717-1731.

33. Davlouros PA, Niwa K, Webb G, Gatzoulis MA. The right ventricle in congenital heart disease. *Heart* 2006;92 Suppl 1:i27-38.

34. Piran S, Veldtman G, Siu S, Webb GD, Liu PP. Heart failure and ventricular dysfunction in patients with single or systemic right ventricles. *Circulation* 2002;105:1189-1194.

35. Voelkel NF, Quaife RA, Leinwand LA, Barst RJ, McGoon MD, Meldrum DR, Dupuis J, Long CS, Rubin LJ, Smart FW, Suzuki YJ, Gladwin M, Denholm EM, Gail DB, National Heart L, Blood Institute Working Group on C, Molecular Mechanisms of Right Heart F. Right ventricular function and failure: report of a National Heart, Lung, and Blood Institute working group on cellular and molecular mechanisms of right heart failure. *Circulation* 2006;114:1883-1891.

36. Khoo NS, Young A, Occleshaw C, Cowan B, Zeng IS, Gentles TL. Assessments of right ventricular volume and function using three-dimensional echocardiography in older children and adults with congenital heart disease: comparison with cardiac magnetic resonance imaging. *J Am Soc Echocardiogr* 2009;22:1279-1288.

37. Tamborini G, Marsan NA, Gripari P, Maffessanti F, Brusoni D, Muratori M, Caiani EG, Fiorentini C, Pepi M. Reference values for right ventricular volumes and ejection fraction with real-time three-dimensional echocardiography: evaluation in a large series of normal subjects. *J Am Soc Echocardiogr* 2010;23:109-115.

38. Renella P, Marx GR, Zhou J, Gauvreau K, Geva T. Feasibility and reproducibility of three-dimensional echocardiographic assessment of right ventricular size and function in pediatric patients. *J Am Soc Echocardiogr* 2014;27:903-910.

39. Buck T FA, Monaghan M,ed. Three-dimensional Echocardiography 2nd Edition 2015:216.

40. Kou S, Caballero L, Dulgheru R, Voilliot D, De Sousa C, Kacharava G, Athanassopoulos GD, Barone D, Baroni M, Cardim N, Gomez De Diego JJ, Hagendorff A, Henri C, Hristova K, Lopez T, Magne J, De La Morena G, Popescu BA, Penicka M, Ozyigit T, Rodrigo Carbonero JD, Salustri A, Van De Veire N, Von Bardeleben RS, Vinereanu D, Voigt JU, Zamorano JL, Donal E, Lang RM, Badano LP, Lancellotti P. Echocardiographic reference ranges for normal cardiac chamber size: results from the NORRE study. *Eur Heart J Cardiovasc Imaging* 2014;15:680-690.

41. Collaboration NCDRF. A century of trends in adult human height. *Elife* 2016;5.

42. D'Oronzio U, Senn O, Biaggi P, Gruner C, Jenni R, Tanner FC, Greutmann M. Right heart assessment by echocardiography: gender and body size matters. *J Am Soc Echocardiogr* 2012;25:1251-1258.

43. Sachdev A, Villarraga HR, Frantz RP, McGoon MD, Hsiao JF, Maalouf JF, Ammash NM, McCully RB, Miller FA, Pellikka PA, Oh JK, Kane GC. Right ventricular strain for prediction of survival in patients with pulmonary arterial hypertension. *Chest* 2011;139:1299-1309.

44. Chia EM, Hsieh CH, Boyd A, Pham P, Vidaic J, Leung D, Thomas L. Effects of age and gender on right ventricular systolic and diastolic function using two-dimensional speckle-tracking strain. *J Am Soc Echocardiogr* 2014;27:1079-1086 e1071.

45. Fine NM, Chen L, Bastiansen PM, Frantz RP, Pellikka PA, Oh JK, Kane GC. Reference Values for Right Ventricular Strain in Patients without Cardiopulmonary Disease: A Prospective Evaluation and Meta-Analysis. *Echocardiography* 2015;32:787-796.

46. Muraru D, Onciul S, Peluso D, Soriani N, Cucchini U, Aruta P, Romeo G, Cavalli G, Iliceto S, Badano LP. Sex- and Method-Specific Reference Values for Right Ventricular Strain by 2-Dimensional Speckle-Tracking Echocardiography. *Circ Cardiovasc Imaging* 2016;9:e003866.

APPENDIX

Nederlandse Samenvatting

In 2011 kreeg het Erasmus MC, Thoraxcentrum, de beschikking over een nieuwe generatie transthoracale tweedimensionale en driedimensionale (2D/3D) echocardiografische matrixtransducer, met aanzienlijk hogere 2D-echocardiografische beeldkwaliteit. Door deze aanzienlijk hogere beeldkwaliteit ontstond een nieuwe beeldvormingsmodaliteit: *simultaneous multiplane* 2D-*echocardiografie imaging* (SMPI). Bij deze nieuwe modaliteit kan er gebruik worden gemaakt van een volledige (360°) elektronische rotatie van een 2D-opname (iRotate) en een gelijktijdig instelbare biplane 2D-opname gedurende dezelfde hartslag (xPlane).

Dit proefschrift is gericht op de potentiële voordelen van deze nieuwe beeldvormings-modaliteit voor cardiovasculaire beeldvorming en patiëntenzorg. Het proefschrift bestaat uit drie delen, namelijk een algemene inleiding over de techniek van SMPI, de waarde ervan bij aangeboren hartafwijkingen en klepafwijkingen, en de waarde bij de beoordeling van ventrikelfunctie.

DEEL I: SIMULTANEOUS MULTIPLANE 2D-ECHOCARDIOGRAFIE

Hoofdstuk 1 bevat zowel een algemene inleiding, waarin een korte samenvatting van de ontwikkeling van de echocardiografie wordt gegeven, als een onderbouwing voor het onderzoeken van de potentiële voordelen van deze nieuwe beeldvormingsmodaliteit voor cardiovasculaire beeldvorming. Deze nieuwe 2D-echocardiografische modaliteit, *simultaneous multiplane imaging* (SMPI), wordt uitgebreid besproken in **Hoofdstuk 2**. Dit hoofdstuk bevat tevens praktijkvoorbeelden van dagelijkse toepassingen van SMPI in het echolaboratorium en het voordeel van deze beeldvormingsmodaliteit ten opzichte van de huidige gangbare 2D-echocardiografische beeldvorming.

DEEL II: SIMULTANEOUS MULTIPLANE 2D-ECHOCARDIOGRAFIE BIJ AANGEBOREN HARTAFWIJKINGEN EN KLEPAFWIJKINGEN

In **Hoofdstuk 3** beoordeelden we de waarde van *simultaneous multiplane imaging* (SMPI) voor het bepalen van de grootte van een atriumseptum secundum defect (ASD) en de afmeting van de weefselrand. ASD is een van de meest voorkomende aangeboren hartaf-wijkingen bij volwassenen. In de loop der tijd is percutane sluiting de meest voorkomende behandeling van een ASD geworden. De grootte van het defect en de afmeting van de weefselrand zijn echter van belang bij de keuze van de behandeling, waarbij transoe-sofageale echocardiografie (TEE) wordt gezien als de meest geschikte pre-interventie beeldvormingsmethode bij de volwassen patiënt. Volgens onze bevindingen kunnen de afmetingen van een ASD en de weefselrand betrouwbaar worden ingeschat met behulp van SMPI (iRotate en xPlane) in vergelijking met 2D TEE. Aangezien een ASD ovaal- of spleetvormig kan zijn, is het belangrijk dat zowel de lange als de korte as van het defect in beeld wordt gebracht. Voor een grondig multi-view onderzoek van het interatriale septum

van het subcostale venster moeten sweeps worden toegepast, aangezien het defect zich ook buiten de regio van de fossa ovalis kan bevinden of er meerdere defecten zouden kunnen zijn. Dit is een vrijwel onmogelijke opgave voor de minder ervaren echocardiografist. De xPlane-modaliteit maakt een gecontroleerde sweep over het interatriale septum vanuit een gangbare subcostale vierkameropname mogelijk, waardoor defecten buiten de fossa ovalis makkelijker te detecteren zijn voor een niet-congenitale echocardiografist. Hierdoor zal de diagnose van ASD minder operatorafhankelijk worden, maar het belangrijkst is dat een diagnostische TEE niet altijd zal hoeven te worden verricht.

Het doel van **Hoofdstuk 4** was om de waarde te beoordelen van 2D-, 2D-xPlane beeldvorming en 3D-echocardiografie voor de vaststelling en uitgebreidheid van de mitralisklepprolaps (MKP) bij patiënten die een mitralisklepoperatie hebben ondergaan. De locatie en uitgebreidheid van de MKP zijn essentieel voor het beoordelen van de toepasbaarheid van mitralisklepreparatie. Volgens onze bevindingen kan de mitralisklep systematisch worden beoordeeld en de locatie en uitgebreidheid van de MKP juist worden vastgesteld met behulp van 2D-xPlane beeldvorming. De meeste patiënten zouden dus wellicht kunnen worden geopereerd zonder dat poliklinische preoperatieve transoesofageale echocardiografie (TEE) noodzakelijk is. Indien nodig zou een preoperatieve TEE in de operatiekamer de diagnose kunnen verfijnen en een leidraad voor de chirurgische benadering kunnen vormen. Bovendien suggereren onze bevindingen dat 2D-xPlane beeldvorming superieur zou kunnen zijn ten opzichte van en-face 3D-beeldvorming, aangezien laatstgenoemde modaliteit meer expertise vereist, sterker afhankelijk is van beeldkwaliteit en een beperkte spatiale en temporale resolutie heeft.

In **Hoofdstuk 5** beoordeelden we de waarde van iRotate echocardiografie voor het inschatten van de omvang van paravalvulaire lekkage van een transkatheter aortaklep implantatie (TAVI) bij een gestandaardiseerde apicale opname. Paravalvulaire aortaregurgitatie na TAVI wordt regelmatig waargenomen, met name bij oudere versies van de protheses. Korte as-doorsneden hebben last van schaduweffecten veroorzaakt door kunstkleppen en verkalkingen, waardoor paravalvulaire lekkage moeilijk waarneembaar is. Met iRotate echocardiografie, bij een gestandaardiseerde apicale opname zonder last van schaduweffecten, kan de gehele omtrek van de TAVI protheses in alle patiënten gevisualiseerd en de uitgebreidheid van de paravalvulaire lekkage vastgelegd worden. Met de opgedane ervaring van transkatheter pulmonaal- en aortaklepvervanging is er een behoefte ontstaan deze katheterinterventies uit te breiden naar de tricuspidalisklep. Hoewel deze zogenoemde 'vergeten klep' opnieuw in de belangstelling is gekomen, bevat de huidige literatuur weinig relevante informatie. **Hoofdstuk 6**, een boekdeel, bevat een gedetailleerde beschrijving van het belang van de verschillende transthoracale echocardiografische modaliteiten voor een uitgebreide beoordeling van de tricuspidalisklep. Ook wordt er gespeculeerd op de toegevoegde waarde van SMPI voor beeldvorming van de tricuspidalisklep. **Hoofdstuk 7**, een consensus paper, bevat een expert-evaluatie van de optimale toepassingen van 3D-echocardiografie op aangeboren hartafwijkingen (AHA). Ook de technische beperkingen van de techniek in deze patiëntenpopulatie worden besproken. Het akoestische venster van het oudere en/of geopereerde kind kan soms tegenvallen, en deze groep zou baat

kunnen hebben bij SMPI. De volledige toepassing van SMPI op AHA moet nog worden onderzocht.

DEEL III: SIMULTANEOUS MULTIPLANE 2D-ECHOCARDIOGRAFIE EN VENTRICULAIRE FUNCTIE

Kwantificering van hartkamers en functie vormt de hoeksteen van cardiale beeldvorming. Steeds meer gepubliceerde informatie suggereert dat ventriculaire dysfunctie in een preklinische fase kan worden gedetecteerd met behulp van *speckle tracking echocardiografie* (STE). Wij hebben een echocardiografisch onderzoek opgezet met 155 gezonde proefpersonen, de Navigator-studie, om de normaalwaarden van echocardiografische parameters in de Nederlandse populatie te bepalen. Bij de werving van de proefpersonen is gebruikgemaakt van een gestratificeerde steekproef, zodat er van elk geslacht en van elk leeftijdsdecennium van 20 tot 72 jaar minimaal veertien deelnemers waren. In **Hoofdstuk 8** richten we ons op de linkerventrikel (LV). Beelden van de LV werden opgenomen vanuit het apicale venster met de gebruikelijke of iRotate 2D-echocardiografie. Met behulp van STE werden longitudinale strainwaarden bepaald en antropometrische associaties vastgesteld. Volgens onze bevindingen werden de longitudinale strainwaarden van de LV wel beïnvloed door geslacht, lichaamsoppervlak en bloeddruk, maar niet door leeftijd. In tegenstelling tot patiënten met verworven hartafwijkingen, waarbij de LV een belangrijke rol speelt, hebben patiënten met aangeboren hartafwijkingen vaker problemen met de rechterventrikel (RV). Voor aanvang van de Navigator-studie hebben we een concept ontwikkeld om met de iRotate-modaliteit de hele RV te beoordelen vanuit een vaste transducerpositie op basis van anatomische oriëntatiepunten, zoals reeds gedaan voor de LV.

In **Hoofdstuk 9** beschrijven we hoe we (zoals voor de LV) unieke anatomische oriëntatiepunten hebben bepaald die zouden kunnen worden gebruikt als referentiepunten voor een nauwkeurige opname van de hele RV, waardoor een gestandaardiseerd 13-segmentenmodel voor de beoordeling van de RV kon worden voorgesteld. Vervolgens hebben we de toepasbaarheid van deze *four-view iRotate approach* en dit voorgestelde 13-segmentenmodel geëvalueerd in een populatie van normale gezonde volwassen proefpersonen, de Navigator-studie, en in een kleine cohort van patiënten met abnormaal belaste RVs. Volgens onze bevindingen is het door ons voorgestelde gestandaardiseerde 13-segmentenmodel zeer toepasbaar bij het beoordelen van de RV met de iRotate-modaliteit vanuit één akoestisch venster. De anterieure wand van de RV-uitstroombaan is echter nog altijd moeilijk waarneembaar. Aanvullende informatie over de RV-functie was ook toegankelijk via het meerdere; *tricuspid annular plane systolic excursion* (TAPSE) en *peak systolic velocity tissue* (S¢) met behulp van een *tissue Doppler imaging* (TDI), meting rond de tricuspidalisannulus. Onze nieuwe benadering zal opnametijd verminderen en zou nauwkeurigere beoordeling van de RV mogelijk moeten maken.

De toepasbaarheid van de techniek die is beschreven in **Hoofdstuk 9** was veelbelovend. **Hoofdstuk 10** bevat standaard-aanbevelingen voor RV-dimensies en RV-functie,

gebaseerd op onze *four-view iRotate approach* van de 155 gezonde proefpersonen in de Navigator-studie. De RV-diameters in onze studie bleken groter te zijn dan de normale bereikwaarden in de *European Association of Cardiovascular imaging and the American Society of Echocardiografie 2015 guidelines*. Dit verschil zou kunnen worden verklaard door de niet-verkorte RV-opname die wordt verkregen wanneer de (IVS)-RV-apex is gecentreerd op de middellijn van de 2D-sector. Zodoende wordt het hart op een iets andere manier verdeeld dan bij de gangbare 4-kameropname en de gerichte 4-kameropname die in respectievelijk de 2005 en 2015 guidelines worden vermeld. Bovendien is het voor de niet-geïndexeerde parameters belangrijk om te vermelden dat de gemiddelde lengte in onze cohort van gezonde Nederlandse proefpersonen 175 ± 9 cm was, ten opzichte van 170 ± 10 cm in de NORRE-studie en 171 ± 10 cm in de studie van D'Oronzio *et al.* TAPSE en TDI-S′, gemeten op vier punten rond de tricuspidalisannulus, verschaften aanvullende informatie en maakten een vollediger beoordeling van de RV mogelijk. Evenals bij de LV werden met STE longitudinale strainwaarden voor de RV bepaald en antropometrische associaties vastgesteld. In vergelijking met een aantal gepubliceerde studies hebben wij geen significante correlatie tussen longitudinale strain en leeftijd gevonden. Alleen in de inferieure wand (coronale opname) hebben we een statistisch significant verschil in deze strainwaarden tussen mannen en vrouwen gevonden.

Een pilotstudie van patiënten met volume en/of door druk overbelaste RVs werden geïncludeerd in dit proefschrift om ten eerste te onderzoeken of deze nieuwe *four-view iRotate approach* toepasbaar was (**Hoofdstuk 9**) en ten tweede te onderzoeken of longitudinale strainwaarden van de RV konden worden gemeten in alle vier de opnamen (**Hoofdstuk 10**). De goede toepasbaarheid op de RV-wanden, TAPSE, TDI-S′ en longitudinale strain is bemoedigend. Uitgebreide studies moeten nu worden opgezet om het volledige potentieel van deze techniek te evalueren.

Tot slot bespreken we in **Hoofdstuk 11** onze bevindingen en de positie van *simultaneous multiplane* 2D-*echocardiografie* in de dagelijkse cardiale beeldvorming. Gezien de voortdurende innovaties op het gebied van ultrageluidtechnologie reflecteren we op de druk die er rust op de dagelijkse bedrijfsvoering van de echocardiografie-afdeling en het belang van een goede werkrelatie tussen clinici en technici voor het bereiken van deze doelen.

List of Publications

1. Simpson J, Lopez L, Acar P, Friedberg MK, Khoo NS, Ko HH, Marek J, Marx G, **McGhie JS**, Meijboom F, Roberson D, Van den Bosch A, Miller O, Shirali G. Three-dimensional Echocardiography in Congenital Heart Disease: An Expert Consensus Document from the European Association of Cardiovascular Imaging and the American Society of Echocardiography. *J Am Soc Echocardiogr* 2017;30:1-27.

2. Menting ME, van Grootel RW, van den Bosch AE, Eindhoven JA, **McGhie JS**, Cuypers JA, Witsenburg M, Helbing WA, Roos-Hesselink JW. Quantitative assessment of systolic left ventricular function with speckle-tracking echocardiography in adult patients with repaired aortic coarctation. *Int J Cardiovasc Imaging* 2016;32:777-787.

3. Menting ME, **McGhie JS**, Koopman LP, Vletter WB, Helbing WA, van den Bosch AE, Roos-Hesselink JW. Normal myocardial strain values using 2D speckle tracking echocardiography in healthy adults aged 20 to 72 years. *Echocardiography* 2016;33:1665-1675.

4. **McGhie JS**, Menting ME, Vletter WB, Frowijn R, Roos-Hesselink JW, van der Zwaan HB, Soliman OI, Geleijnse ML, van den Bosch AE. Quantitative assessment of the entire right ventricle from one acoustic window: an attractive approach. *Eur Heart J Cardiovasc Imaging* 2016.

5. **McGhie JS**, Menting ME, Vletter WB, Frowijn R, Roos-Hesselink JW, Soliman OI, van der Zwaan HB, Geleijnse ML, van den Bosch AE. A Novel 13-Segment Standardized Model for Assessment of Right Ventricular Function Using Two-Dimensional iRotate Echocardiography. *Echocardiography* 2016;33:353-361.

6. de Groot-de Laat LE, Ren B, **McGhie J**, Oei FB, Strachinaru M, Kirschbaum SW, Akin S, Kievit CM, Bogers AJ, Geleijnse ML. The role of experience in echocardiographic identification of location and extent of mitral valve prolapse with 2D and 3D echocardiography. *Int J Cardiovasc Imaging* 2016.

7. Menting ME, van den Bosch AE, **McGhie JS**, Eindhoven JA, Cuypers JA, Witsenburg M, Geleijnse ML, Helbing WA, Roos-Hesselink JW. Assessment of ventricular function in adults with repaired Tetralogy of Fallot using myocardial deformation imaging. *Eur Heart J Cardiovasc Imaging* 2015;16:1347-1357.

8. Menting ME, van den Bosch AE, **McGhie JS**, Cuypers JA, Witsenburg M, Geleijnse ML, Helbing WA, Roos-Hesselink JW. Ventricular myocardial deformation in adults after early surgical repair of atrial septal defect. *Eur Heart J Cardiovasc Imaging* 2015;16:549-557.

9. **McGhie JS**, de Groot-de Laat L, Ren B, Vletter W, Frowijn R, Oei F, Geleijnse ML. Transthoracic two-dimensional xPlane and three-dimensional echocardiographic analysis of the site of mitral valve prolapse. *Int J Cardiovasc Imaging* 2015;31:1553-1560.

10. Eindhoven JA, Menting ME, van den Bosch AE, **McGhie JS**, Witsenburg M, Cuypers JA, Boersma E, Roos-Hesselink JW. Quantitative assessment of systolic right ventricular function using myocardial deformation in patients with a systemic right ventricle. *Eur Heart J Cardiovasc Imaging* 2015;16:380-388.

11. Ren B, Vletter WB, **McGhie J**, Soliman OI, Geleijnse ML. Single-beat real-time three-dimensional echocardiographic automated contour detection for quantification of left ventricular volumes and systolic function. *Int J Cardiovasc Imaging* 2014;30:287-294.

12. Menting ME, Eindhoven JA, van den Bosch AE, Cuypers JA, Ruys TP, van Dalen BM, **McGhie JS**, Witsenburg M, Helbing WA, Geleijnse ML, Roos-Hesselink JW. Abnormal left ventricular rotation and twist in adult patients with corrected tetralogy of Fallot. *Eur Heart J Cardiovasc Imaging* 2014;15:566-574.

13. **McGhie JS**, Vletter WB, de Groot-de Laat LE, Ren B, Frowijn R, van den Bosch AE, Soliman OI, Geleijnse ML. Contributions of simultaneous multiplane echocardiographic imaging in daily clinical practice. *Echocardiography* 2014;31:245-254.

14. **McGhie JS**, van den Bosch AE, Haarman MG, Ren B, Roos-Hesselink JW, Witsenburg M, Geleijnse ML. Characterization of atrial septal defect by simultaneous multiplane two-dimensional echocardiography. *Eur Heart J Cardiovasc Imaging* 2014;15:1145-1151.

15. Eindhoven JA, Menting ME, van den Bosch AE, Cuypers JA, Ruys TP, Witsenburg M, **McGhie JS**, Boersma E, Roos-Hesselink JW. Associations between N-terminal pro-B-type natriuretic peptide and cardiac function in adults with corrected tetralogy of Fallot. *Int J Cardiol* 2014;174:550-556.

16. de Vette LC, Brugts JJ, **McGhie JS**, Roos-Hesselink JW. Long-lasting symptoms and diagnostics in a patient with unrecognized right sided heart failure: Why listening to the heart is so important. *World J Cardiol* 2014;6:345-348.

17. De Groot-de Laat LE, Ren B, **McGhie J**, Oei FB, Raap GB, Bogers JJ, Geleijnse ML. Real-world echocardiography in patients referred for mitral valve surgery: the gap between guidelines and clinical practice. *J Heart Valve Dis* 2014;23:721-726.

18. van der Linde D, Rossi A, Yap SC, **McGhie JS**, van den Bosch AE, Kirschbaum SW, Russo B, van Dijk AP, Moelker A, Krestin GP, van Geuns RJ, Roos-Hesselink JW. Ascending aortic diameters in congenital aortic stenosis: cardiac magnetic resonance versus transthoracic echocardiography. *Echocardiography* 2013;30:497-504.

19. Ruys TP, van der Bosch AE, Cuypers JA, Witsenburg M, Helbing WA, Bogers AJ, van Domburg R, **McGhie JS**, Geleijnse ML, Henrichs J, Utens E, Van der Zwaan HB, Takkenberg JJ, Roos-Hesselink JW. Long-term outcome and quality of life after arterial switch operation: a prospective study with a historical comparison. *Congenit Heart Dis* 2013;8:203-210.

20. Ren B, de Groot-de Laat LE, **McGhie J**, Vletter WB, Ten Cate FJ, Geleijnse ML. Geometric errors of the pulsed-wave Doppler flow method in quantifying degenerative mitral valve regurgitation: a three-dimensional echocardiography study. *J Am Soc Echocardiogr* 2013;26:261-269.

21. Eindhoven JA, van den Bosch AE, Ruys TP, Opic P, Cuypers JA, **McGhie JS**, Witsenburg M, Boersma E, Roos-Hesselink JW. N-terminal pro-B-type natriuretic peptide and its relationship with cardiac function in adults with congenital heart disease. *J Am Coll Cardiol* 2013;62:1203-1212.

22. Simpson J, Miller O, Bell A, Bellsham-Revell H, **McGhie J**, Meijboom F. Image orientation for three-dimensional echocardiography of congenital heart disease. *Int J Cardiovasc Imaging* 2012;28:743-753.

23. van der Zwaan HB, Geleijnse ML, Soliman OI, **McGhie JS**, Wiegers-Groeneweg EJ, Helbing WA, Roos-Hesselink JW, Meijboom FJ. Test-retest variability of volumetric right ventricular measurements using real-time three-dimensional echocardiography. *J Am Soc Echocardiogr* 2011;24:671-679.

24. van der Zwaan HB, Geleijnse ML, **McGhie JS**, Boersma E, Helbing WA, Meijboom FJ, Roos-Hesselink JW. Right ventricular quantification in clinical practice: two-dimensional vs. three-dimensional echocardiography compared with cardiac magnetic resonance imaging. *Eur J Echocardiogr* 2011;12:656-664.

25. Soliman OI, Anwar AM, Metawei AK, **McGhie JS**, Geleijnse ML, Ten Cate FJ. New Scores for the Assessment of Mitral Stenosis Using Real-Time Three-Dimensional Echocardiography. *Curr Cardiovasc Imaging Rep* 2011;4:370-377.

26. Scohy TV, Luthen C, **McGhie J**, Oei F. Three-dimensional transesophageal echocardiography: diagnosing intraoperative pulmonary artery thrombus. *Interact Cardiovasc Thorac Surg* 2011;12:840-841.

27. van Noord PT, Scohy TV, **McGhie J**, Bogers AJ. Three-dimensional transesophageal echocardiography in Ebstein's anomaly. *Interact Cardiovasc Thorac Surg* 2010;10:836-837.

28. Van Mieghem NM, Piazza N, Anderson RH, Tzikas A, Nieman K, De Laat LE, **McGhie JS**, Geleijnse ML, Feldman T, Serruys PW, de Jaegere PP. Anatomy of the mitral valvular complex and its implications for transcatheter interventions for mitral regurgitation. *J Am Coll Cardiol* 2010;56:617-626.

29. van der Zwaan HB, Helbing WA, **McGhie JS**, Geleijnse ML, Luijnenburg SE, Roos-Hesselink JW, Meijboom FJ. Clinical value of real-time three-dimensional echocardiography for right ventricular quantification in congenital heart disease: validation with cardiac magnetic resonance imaging. *J Am Soc Echocardiogr* 2010;23:134-140.

30. van der Zwaan HB, Helbing WA, Boersma E, Geleijnse ML, **McGhie JS**, Soliman OI, Roos-Hesselink JW, Meijboom FJ. Usefulness of real-time three-dimensional echocardiography to identify right ventricular dysfunction in patients with congenital heart disease. *Am J Cardiol* 2010;106:843-850.

31. Scohy TV, Geniets B, **McGhie J**, Bogers AJ. Feasibility of real-time three-dimensional transesophageal echocardiography in type A aortic dissection. *Interact Cardiovasc Thorac Surg* 2010;11:112-113.

32. Nemes A, Geleijnse ML, Soliman OI, Vletter WB, **McGhie JS**, Forster T, Ten Cate FJ. [Evaluation of the mitral valve by transthoracic real-time three-dimensional echocardiography]A mitralis billentyu vizsgalata transthoracalis real-time haromdimenzios echokardiografiaval. *Orv Hetil* 2010;151:854-863.

33. Scohy TV, Soliman OI, Lecomte PV, **McGhie J**, Kappetein AP, Hofland J, Ten Cate FJ. Intraoperative real time three-dimensional transesophageal echocardiographic

measurement of hemodynamic, anatomic and functional changes after aortic valve replacement. *Echocardiography* 2009;26:96-99.

34. Scohy TV, Matte G, van Neer PL, van der Steen AF, **McGhie J**, Bogers A, de Jong N. A new transesophageal probe for newborns. *Ultrasound Med Biol* 2009;35:1686-1689.

35. Scohy TV, Maat AP, **McGhie J**, ten Cate FJ, Bogers AJ. Three-dimensional transesophageal echocardiography: diagnosing the extent of pericarditis constrictiva and intraoperative surgical support. *J Card Surg* 2009;24:305-308.

36. Scohy TV, Gommers D, Schepp MN, **McGhie J**, de Jong N, Bogers AJ. Image quality using a micromultiplane transesophageal echocardiographic probe in older children during cardiac surgery. *Eur J Anaesthesiol* 2009;26:445-447.

37. Scohy TV, du Plessis F, **McGhie J**, de Jong PL, Bogers AJ. Rapid method for intraoperative assessment of aortic coarctation using three-dimensional echocardiography. *Eur J Echocardiogr* 2009;10:922-925.

38. Nemes A, Geleijnse ML, Soliman OI, Anwar AM, Vletter WB, **McGhie JS**, Csanady M, Forster T, Ten Cate FJ. [The role of real-time three-dimensional echocardiography in the evaluation of hypertrophic cardiomyopathy]A real-time haromdimenzios echokardiografia szerepe a hypertrophias cardiomyopathia vizsgalataban. *Orv Hetil* 2009;150:1925-1931.

39. Nemes A, Caliskan K, Soliman OI, **McGhie JS**, Geleijnse ML, ten Cate FJ. Diagnosis of biventricular non-compaction cardiomyopathy by real-time three-dimensional echocardiography. *Eur J Echocardiogr* 2009;10:356-357.

40. Yap SC, van Geuns RJ, Nemes A, Meijboom FJ, **McGhie JS**, Geleijnse ML, Simoons ML, Roos-Hesselink JW. Rapid and accurate measurement of LV mass by biplane real-time 3D echocardiography in patients with concentric LV hypertrophy: comparison to CMR. *Eur J Echocardiogr* 2008;9:255-260.

41. Scohy TV, Ten Cate FJ, Lecomte PV, **McGhie J**, de Jong PL, Hofland J, Bogers AJ. Usefulness of intraoperative real-time 3D transesophageal echocardiography in cardiac surgery. *J Card Surg* 2008;23:784-786.

42. Scohy TV, Lecomte PV, **McGhie J**, Meijer R, Gommers D, Hofland J, Ten Cate FJ. Intraoperative real time three-dimensional transesophageal echocardiographic evaluation of right atrial tumor. *Echocardiography* 2008;25:646-649.

43. Meijboom FJ, Roos-Hesselink JW, **McGhie JS**, Spitaels SE, van Domburg RT, Utens LM, Simoons ML, Bogers AJ. Consequences of a selective approach toward pulmonary valve replacement in adult patients with tetralogy of Fallot and pulmonary regurgitation. *J Thorac Cardiovasc Surg* 2008;135:50-55.

44. Anwar AM, **McGhie JS**, Meijboom FJ, Ten Cate FJ. Double orifice mitral valve by real-time three-dimensional echocardiography. *Eur J Echocardiogr* 2008;9:731-732.

45. Yap SC, van Geuns RJ, Meijboom FJ, Kirschbaum SW, **McGhie JS**, Simoons ML, Kilner PJ, Roos-Hesselink JW. A simplified continuity equation approach to the quantification of stenotic bicuspid aortic valves using velocity-encoded cardiovascular magnetic resonance. *J Cardiovasc Magn Reson* 2007;9:899-906.

46. Scohy TV, Gommers D, Jan ten Harkel AD, Deryck Y, **McGhie J**, Bogers AJ. Intra-operative evaluation of micromultiplane transesophageal echocardiographic probe in surgery for congenital heart disease. *Eur J Echocardiogr* 2007;8:241-246.

47. Nemes A, Geleijnse ML, Soliman OI, Anwar AM, Bosch JG, Krenning BJ, Yap SC, Vletter WB, **McGhie JS**, Forster T, Csanady M, Ten Cate FJ. [Real-time 3-dimensional echocardiography: can there be one more dimension?]Real-time 3-dimenzios echokardiografia--lehet egy dimenzioval tobb? *Orv Hetil* 2007;148:2451-2460.

48. Anwar AM, Soliman O, van den Bosch AE, **McGhie JS**, Geleijnse ML, ten Cate FJ, Meijboom FJ. Assessment of pulmonary valve and right ventricular outflow tract with real-time three-dimensional echocardiography. *Int J Cardiovasc Imaging* 2007;23:167-175.

49. Anwar AM, Geleijnse ML, Soliman OI, **McGhie JS**, Nemes A, ten Cate FJ. Evaluation of rheumatic tricuspid valve stenosis by real-time three-dimensional echocardiography. *Heart* 2007;93:363-364.

50. Anwar AM, Geleijnse ML, Soliman OI, **McGhie JS**, Frowijn R, Nemes A, van den Bosch AE, Galema TW, Ten Cate FJ. Assessment of normal tricuspid valve anatomy in adults by real-time three-dimensional echocardiography. *Int J Cardiovasc Imaging* 2007;23:717-724.

51. van den Bosch AE, van Dijk VF, **McGhie JS**, Bogers AJ, Roos-Hesselink JW, Simoons ML, Meijboom FJ. Real-time transthoracic three-dimensional echocardiography provides additional information of left-sided AV valve morphology after AVSD repair. *Int J Cardiol* 2006;106:360-364.

52. van den Bosch AE, Ten Harkel DJ, **McGhie JS**, Roos-Hesselink JW, Simoons ML, Bogers AJ, Meijboom FJ. Surgical validation of real-time transthoracic 3D echocardiographic assessment of atrioventricular septal defects. *Int J Cardiol* 2006;112:213-218.

53. van den Bosch AE, Ten Harkel DJ, **McGhie JS**, Roos-Hesselink JW, Simoons ML, Bogers AJ, Meijboom FJ. Feasibility and accuracy of real-time 3-dimensional echocardiographic assessment of ventricular septal defects. *J Am Soc Echocardiogr* 2006;19:7-13.

54. van den Bosch AE, Ten Harkel DJ, **McGhie JS**, Roos-Hesselink JW, Simoons ML, Bogers AJ, Meijboom FJ. Characterization of atrial septal defect assessed by real-time 3-dimensional echocardiography. *J Am Soc Echocardiogr* 2006;19:815-821.

55. van den Bosch AE, Robbers-Visser D, Krenning BJ, Voormolen MM, **McGhie JS**, Helbing WA, Roos-Hesselink JW, Simoons ML, Meijboom FJ. Real-time transthoracic three-dimensional echocardiographic assessment of left ventricular volume and ejection fraction in congenital heart disease. *J Am Soc Echocardiogr* 2006;19:1-6.

56. van den Bosch AE, Robbers-Visser D, Krenning BJ, **McGhie JS**, Helbing WA, Meijboom FJ, Roos-Hesselink JW. Comparison of real-time three-dimensional echocardiography to magnetic resonance imaging for assessment of left ventricular mass. *Am J Cardiol* 2006;97:113-117.

57. Nemes A, **McGhie JS**, ten Cate FJ. Real-time 3-dimensional echocardiographic evaluation of aortic dissection. *J Am Soc Echocardiogr* 2006;19:108 e101-108 e103.

58. Nemes A, Lagrand WK, **McGhie JS**, ten Cate FJ. Three-dimensional transesophageal echocardiography in the evaluation of aortic valve destruction by endocarditis. *J Am Soc Echocardiogr* 2006;19:355 e313-355 e314.

59. Nemes A, Geleijnse ML, van Geuns RJ, Caliskan K, Michels M, Soliman OI, **McGhie JS**, ten Cate FJ. Evaluation of pericardial hydatid cysts by different echocardiographic imaging modalities. *Int J Cardiovasc Imaging* 2006;22:647-651.

60. van den Bosch AE, Koning AH, Meijboom FJ, **McGhie JS**, Simoons ML, van der Spek PJ, Bogers AJ. Dynamic 3D echocardiography in virtual reality. *Cardiovasc Ultrasound* 2005;3:37.

61. van den Bosch AE, Meijboom FJ, **McGhie JS**, Roos-Hesselink JW, Ten Cate FJ, Roelandt JR. Enhanced visualisation of the right ventricle by contrast echocardiography in congenital heart disease. *Eur J Echocardiogr* 2004;5:104-110.

62. Roos-Hesselink JW, Meijboom FJ, Spitaels SE, van Domburg R, van Rijen EH, Utens EM, **McGhie J**, Bos E, Bogers AJ, Simoons ML. Decline in ventricular function and clinical condition after Mustard repair for transposition of the great arteries (a prospective study of 22-29 years). *Eur Heart J* 2004;25:1264-1270.

63. Al Hashimi H, Al Windy N, **McGhie JC**, Galema TW, Ten Cate FJ, Simoons ML. Role of echocardiography in the diagnosis and management of infective endocarditis. *Neth Heart J* 2004;12:64-68.

64. Al Hashimi H, Scholten MF, **McGhie J**. A usual presentation of an unusual diagnosis. *Neth Heart J* 2002;10:326-328.

65. Al Hashimi H, Scholten MF, **McGhie JS**. Left to right shunt as a result of acute infective endocarditis. *Neth Heart J* 2001;9:87.

66. Dall'Agata A, **McGhie J**, Taams MA, Cromme-Dijkhuis AH, Spitaels SE, Breburda CS, Roelandt JR, Bogers AJ. Secundum atrial septal defect is a dynamic three-dimensional entity. *Am Heart J* 1999;137:1075-1081.

67. Dall'Agata A, Cromme-Dijkhuis AH, Meijboom FJ, Spitaels SE, **McGhie JS**, Roelandt JR, Bogers AJ. Use of three-dimensional echocardiography for analysis of outflow obstruction in congenital heart disease. *Am J Cardiol* 1999;83:921-925.

68. Dall'Agata A, Cromme-Dijkhuis AH, Meijboom FJ, **McGhie JS**, Bol-Raap G, Nosir YF, Roelandt JR, Bogers AJ. Three-dimensional echocardiography enhances the assessment of ventricular septal defect. *Am J Cardiol* 1999;83:1576-1579, A1578.

69. Elhendy A, Zoet Nugteren S, Cornel JH, Fioretti PM, Bogers AJ, Roelandt JR, Krenning E, Postma-Tjoa J, **McGhie J**, Spitaels SE. Functional assessment of ALCAPA syndrome by dobutamine stress thallium-201 SPECT and echocardiography. *J Nucl Med* 1996;37:748-751.

70. Salustri A, Spitaels S, **McGhie J**, Vletter W, Roelandt JR. Transthoracic three-dimensional echocardiography in adult patients with congenital heart disease. *J Am Coll Cardiol* 1995;26:759-767.

71. Roos-Hesselink J, Perlroth MG, **McGhie J**, Spitaels S. Atrial arrhythmias in adults after repair of tetralogy of Fallot. Correlations with clinical, exercise, and echocardiographic findings. *Circulation* 1995;91:2214-2219.

72. Meijboom F, Hess J, Szatmari A, Utens EM, **McGhie J**, Deckers JW, Roelandt JR, Bos E. Long-term follow-up (9 to 20 years) after surgical closure of atrial septal defect at a young age. *Am J Cardiol* 1993;72:1431-1434.

73. Forster T, **McGhie J**, Rijsterborgh H, Meeter K, Balk A, Essed C, Roelandt J. Does the measurement of left ventricular isovolumic relaxation time allow early prediction of cardiac allograft rejection? *Acta Cardiol* 1992;47:459-471.

74. Sreeram N, Sutherland GR, **McGhie J**. Pseudoaneurysm of the right ventricular outflow tract: diagnosis by colour flow mapping. *Br Heart J* 1990;63:129-131.

75. Forster T, **McGhie J**, Rijsterborgh H, van de Borden S, Laird-Meeter K, Balk A, Essed C, Roelandt J. Can we assess the changes of ventricular filling resulting from acute allograft rejection with Doppler echocardiography? *J Heart Transplant* 1988;7:430-434.

76. Gussenhoven EJ, Taams MA, Roelandt JR, Ligtvoet KM, **McGhie J**, van Herwerden LA, Cahalan MK. Transesophageal two-dimensional echocardiography: its role in solving clinical problems. *J Am Coll Cardiol* 1986;8:975-979.

77. Pijpers L, Wladimiroff JW, **McGhie JS**, Bom N. Acute effect of maternal smoking on the maternal and fetal cardiovascular system. *Early Hum Dev* 1984;10:95-105.

78. Pijpers L, Wladimiroff JW, **McGhie J**. Effect of short-term maternal exercise on maternal and fetal cardiovascular dynamics. *Br J Obstet Gynaecol* 1984;91:1081-1086.

79. Wladimiroff JW, Vosters R, **McGhie JS**. Normal cardiac ventricular geometry and function during the last trimester of pregnancy and early neonatal period. *Br J Obstet Gynaecol* 1982;89:839-844.

80. Serruys PW, Meltzer RS, **McGhie J**, Roelandt J. [Transpulmonary contrast echocardiography. Initial experience]Echocardiographie de contraste transpulmonaire. Experience initiale. *Arch Mal Coeur Vaiss* 1982;75:249-260.

81. Meltzer RS, **McGhie J**, Roelandt J. Inferior vena cava echocardiography. *J Clin Ultrasound* 1982;10:47-51.

82. Wladimiroff JW, **McGhie JS**, Hovestreydt-Snijder RP, Tasseron EW. M-mode and pulsed Doppler ultrasound assessment of severe fetal bradycardia. A case report. *Br J Obstet Gynaecol* 1981;88:1246-1248.

83. Wladimiroff JW, **McGhie JS**. M-mode ultrasonic assessment of fetal cardiovascular dynamics. *Br J Obstet Gynaecol* 1981;88:1241-1245.

84. Wladimiroff JW, **McGhie J**. Ultrasonic assessment of cardiovascular geometry and function in the human fetus. *Br J Obstet Gynaecol* 1981;88:870-875.

85. Meltzer RS, Serruys PW, **McGhie J**, Hugenholtz PG, Roelandt J. Cardiac catheterization under echocardiographic control in a pregnant woman. *Am J Med* 1981;71:481-484.

86. Meltzer RS, Serruys PW, **McGhie J**, Verbaan N, Roelandt J. Pulmonary wedge injections yielding left-sided echocardiographic contrast. *Br Heart J* 1980;44:390-394.

PhD Portfolio

SUMMARY OF PHD TRAINING AND TEACHING ACTIVITIES

Name PhD student: J.S. McGhie
Erasmus MC Department: Cardiology
Research School: COEUR

PhD period: 2011–2016
Promotor(s): J.W. Roos-Hesselink
Supervisor: M.L. Geleijnse, A.E. van den Bosch

	Year	Workload (ECTS)
1. PhD training		
General academic and research skills		
- Workshop Systematic Literature Retrieval in PubMed, Erasmus medical library, Rotterdam, the Netherlands	2012	0.3
In-depth courses (e.g. Research school, Medical Training)		
- COEUR – Congenital Heart Disease	2013	1.5
National and International oral presentations		
- European Echocardiography Course on Congenital Heart Disease (x6)	2011–2016	12
- Clinical practice and technology in paediatric cardiology, Madrid, Spain	2011	1.0
- British Society of Echocardiography (AGM), Edinburgh, UK		1.0
- The Role of Cardiac Imaging: 3D Echocardiography, Venice, Italy		1.0
- Philips 3D Echocardiography training course, Hilvarenbeek, the Netherlands	2012	1.0
- Nederlandse Vereniging voor Cardiologie najaarscongres, Noordwijk, the Netherlands		1.5
- Congenital Heart Disease, "Focus echo", Erasmus MC, Rotterdam, the Netherlands		1.0
- Philips 3D Echocardiography training course, Amsterdam, the Netherlands		1.0
- Echography Symposium NVMBR, Ede, the Netherlands		1.0
- EuroEcho-Imaging Congress, Athens, Greece		1.5
- CVOI; Echocardiografische richtlijnen in de praktijk, meet de experts. Breda, the Netherlands	2013	1.0
- Regional Echo meeting; Tilburg, the Netherlands		2.0
- The Role of Cardiac Imaging: 3D Echocardiography, Venice, Italy		1.0
- Philips May 3D Echocardiography training course, Hilvarenbeek, the Netherlands	2014	1.0
- Philips 3D Echocardiography, October training course, Hilvarenbeek, the Netherlands		0.5
- EuroEcho-Imaging Congress, Vienna, Austria (Poster presentation)		1.0
- Philips March Basic echo-course, Eindhoven, the Netherlands	2015	1.0
- Philips November Basic echo-course, Eindhoven, the Netherlands		1.0
- EuroEcho-Imaging Congress, Seville, Spain		1.0
- EuroEcho-Imaging Congress, Leipzig, Germany	2016	1.0

International conferences

	Year	Workload (ECTS)
- European Society of Cardiology (ESC) congress, Paris, France	2011	1.0
- British Society of Echocardiography (AGM), Edinburgh, UK		1.0
- EuroEcho-Imaging Congress, Athens, Greece	2012	1.0
- EuroEcho-Imaging Congress, Vienna, Austria	2014	1.0
- EuroEcho-Imaging Congress, Seville, Spain	2015	2.0
- EuroEcho-Imaging Congress, Leipzig, Germany	2016	2.0
TOTAL (ECTS)		**42.3**

	Year	Workload (ECTS)
Seminars and workshops given		
- Siemens 3D RV workshops (x2). British Society of echocardiography (AGM), Edinburgh, UK	2011	3.0
- Siemens 3D RV workshops (x2). European Society of Cardiology (ESC) congress, Paris, France		3.0
- "Juniorkamerdag" Den Haag, the Netherlands	2015	2.0
- "Juniorkamerdag" Soestduinen, the Netherlands	2016	2.0
Other		
- Chairman: Congenital Session, EuroEcho-Imaging Congress, Athens, Greece	2012	
- Chairman: European Echocardiography Course on Congenital Heart Disease	2013–2016	
- Chairman: Congenital Session, EuroEcho-Imaging Congress, Seville, Spain	2015	
- European Congenital echocardiography exam committee meeting and workshop	2016	
- Chairman: Congenital Session, EuroEcho-Imaging Congress, Leipzig, Germany		
2. Teaching activities		
Lecturing		
- Advanced Congenital Echo course, Erasmus MC, Rotterdam, the Netherlands	2011	4.0
- Dordrecht Echo training, (ASZ) Dordrecht, the Netherlands		2.0
- Pulmonary Hypertension (Actelion), Rotterdam, the Netherlands		2.0
- 3D Echocardiography Course, Erasmus MC, Rotterdam, the Netherlands	2012	10.0
- Basic Congenital Echo course, Erasmus MC, Rotterdam, the Netherlands		4.0
- 3D Training Course, Erasmus MC, Rotterdam, the Netherlands		18.0
- Advanced Congenital Echo course, Erasmus MC, Rotterdam, the Netherlands	2013	4.0
- Pulmonary Hypertension (Actelion), Vlaardingen, the Netherlands		2.0
- COEUR – Congenital Heart Disease, Erasmus MC, Rotterdam, the Netherlands		1.0
- 3D Training Course Erasmus MC, Rotterdam, the Netherlands (Philips)		18.0
- 3D Training Course Erasmus MC, Rotterdam, the Netherlands (Siemens x2)		18.0
- Pulmonary Hypertension (Actelion), Middelburg, the Netherlands	2014	2.0
- Basic Congenital Echo course, Erasmus MC, Rotterdam, the Netherlands		4.0
- "Refereeravond, Rijmound Cardiologen", Rotterdam, the Netherlands		1.0
- 3D Training Course, Erasmus MC, Rotterdam, the Netherlands		18.0

- Image optimization and 3D echocardiography training, Regional hospitals, Rotterdam South, the Netherlands		4.0
- Advanced Congenital Echo course, Erasmus MC, Rotterdam, the Netherlands	2015	4.0
- Pulmonary Hypertension (Actelion), Dirksland, the Netherlands		2.0
- Nursing symposium "Inovations" Rotterdam, the Netherlands		2.0
- 3D Training Course, June, Erasmus MC, Rotterdam, the Netherlands		18.0
- "Juniorkamerdag" Den Haag, the Netherlands		1.0
- 3D Training Course, November, Erasmus MC, Rotterdam, the Netherlands		18.0
- Basic Congenital Echo course, Erasmus MC, Rotterdam, the Netherlands	2016	4.0
- Pulmonary Hypertension (Actelion), Bergen op Zoom, the Netherlands		2.0
- Advanced Congenital Echo course, Erasmus MC, Rotterdam, the Netherlands	2017	4.0

Supervising practicals and excursions

- EACVI CHD certification grader	2012–2016	8.0

Other

- Echo working group (NVVC) (4 x per jaar)	2011–2016	
- Hogeschool Inholland: Werkveldadviescommissie echocardiografie (1 x jaar)	2013–2016	
- EACVI CHD certification committee member	2014–2016	
Received honoree membership from the American Society of Echocardiography	2014–2015	
TOTAL (181 hrs = 6.5 ECTS)		**6.9**
TOTAL		**49 (ECTS)**

Curriculum Vitae

Jacqueline (Jackie) Susan McGhie was born on 6 February 1956 in Edinburgh, Scotland, United Kingdom. On completing secondary school in 1973, she started work at Newcastle General Hospital, as a student Physiological Measurement Technician (PMT). After achieving, an ONC, followed by an HNC in Medical Physic and Physiological Measurement, she was promoted to the position of Senior Technician. In 1977, several hospitals across the city of Newcastle were co-located into one centre, Freeman Hospital, where she operated as a Senior PMT before relocating, in March 1979, to the Thoraxcenter, Rotterdam, The Netherlands (now known as the Erasmus University Hospital). This move allowed her to increase her knowledge on echocardiography, especially the new two-dimensional technique that had recently been developed. From March 1979 up until today, she has held various positions in the department of echocardiography. Additionally, she has gained expertise in clinical and research echocardiography, in general cardiology, foetal cardiology, and has a special interest in adult congenital heart disease. In 2005, she acquired Dutch accreditation in echocardiography, and in 2007, European accreditation in congenital heart disease echocardiography. She is well known for her teaching qualities at national and international echo meetings. Furthermore, she is an active European exam committee member who aims to maintain a high standard of echocardiography in congenital heart disease throughout Europe. She is married to Wim Vletter and they have two sons: Guido and Alex.

Acknowledgements

The challenge I set myself was to have one article published on echocardiography as first author before retiring. Never did I expect to achieve the compilation of this book before you. Having worked with numerous doctoral students throughout my career, I have appreciated more than most, that this end result could only be accomplished with the support and help of a large number of people both in and out of hospital life. I would like to take the opportunity to express my appreciation to them personally in this book.

Firstly, for inspiring my career, Dr. S Hunter, the late Prof.dr. J.R.T.C. Roelandt and Dr. S. Spitaels. All three of you, with your brilliant minds and enthusiasm for echocardiography and congenital heart disease, I thank you deeply. You introduced me to and stimulated me in what has turned out to be a fascinating career for me.

My co-promoters (co-supervisors) Dr. M.L. Geleijnse and Dr. A.E. van den Bosch, dear Marcel and Annemien we have worked together for many years in different roles in the department of echocardiography. You Marcel, for the left side of the heart and you Annemien, first bi-ventricular, but sensibly choosing the right side of the heart. Your valuable scientific interrogation and stimulation encouraged me to take on this challenge. I am grateful for all your unwavering support throughout.

My promotor (supervisor), Prof.dr. J.W. Roos-Hesselink, dear Jolien, I am probably the oldest and possibly the most reluctant doctoral student you have had. Thank you for your confidence and belief in me; it has been an extremely challenging project made easier knowing I have your support.

To the members of the reading committee; Prof.dr. A.A.J. Bogers, Dr. F.J. ten Cate and Dr. F.J. Meijboom, I would like to thank you for finding time in your packed agendas not only for reading and critically reviewing my thesis, and being present today, but also for enabling me to have such an dynamic national and international career here at the Thoraxcentrum (Erasmus Medical Center, Rotterdam).

Dear Ad, we have worked together for a long time, intensely in the beginning, setting up echocardiography in the operating theatre. From there we established its potential use in structural and congenital heart disease. You and your team have, and still do, make me feel very welcome in your department. I would like to acknowledge them all. One memory that will stay with me always was the interpretation of our first 3D echo images of the heart. To me, they represented more of a lunar landscape, but to you, it was definitely the heart, the beginning of 3D, and a new era in echocardiography.

Dear, Folkert C and Folkert M, along with the scientific and dynamic work related discussions we shared, there was always time for relaxation and fun. You have both organized many courses and congresses always ensuring that our input was recognized and valued. You always made us feel we were all part of the same team.

Folkert C, I have known you ever since I first set foot in the Netherlands. I even think one of my first social experiences in Dutch life was at your party celebrating your own doctorate degree. Gosh how time flies. You have contributed so much to echocardiography worldwide and I am so pleased to have been a very small part of it. Even though you are retired, it's great to see you still remain so actively interested, resulting in regular participa-

tion in international teaching sessions, reviewing and writing medical articles. Thank you for joining me today.

Dear Folkert M, together we had a strong working relationship and helped to build a very successful department of echocardiography for adult congenital heart disease. We were pioneers in the field of congenital 3D echocardiography and initiated the annual echocardiography course in congenital heart disease, in the Netherlands, that still continues today. You kindly introduced me to the other two M's and since then I have become a faculty member of the annual European teaching course on echocardiography in congenital heart disease. I am pleased that the world of congenital echocardiography benefits from your knowledge and expertise to this day. Thank you Folkert, for joining me today.

To the remaining members of the defense committee; Prof.dr. J. Marek, Prof.dr. P.P.T. de Jaegere and Prof.dr.ir. N. de Jong.

Prof.dr. J. Marek, dear Jan, thank you for finding the time and making such an effort to be present today for my defense. It is so appreciated. We met for the first time many years ago at the European teaching course on echocardiography and annually thereafter. Your enthusiasm, and enormous talent for teaching inspired me. Being introduced to Prague by a true 'Pražan' was a wonderful experience and not one that I would have liked to miss.

Prof.dr. P.P.T. de Jaegere, dear Peter, thank you for finding the time to join me today, albeit on the other side of the table! You will understand that I am delighted to see that echocardiography now exists as a consideration by various cath-lab procedures. It is my hope that with the ongoing development in percutaneous valve implantation, it will not be long before it has become a permanent feature. Over the years, you have asked for my echo guidance in several of your cath-lab procedures and for that I would like to thank you, the technicians and nursing staff for making me feel so much a part of your team.

Prof.dr.ir. N. de Jong, dear Nico, the defense committee is complete now with an engineer onboard and I have a challenging task ahead. Thank you for giving up valuable time to join me today. We have attended many international congresses and shared many interesting discussions on echocardiography, both at conference and in your department. You have convinced me that progress in echocardiography is still on going and a fascinating journey lies ahead. I would like to take this opportunity to thank you and all your colleagues in the engineering department on the 23rd floor for the warm welcome I always receive.

Dr. O.I.I. Soliman, dear Osama, thank you for inviting me to join, the team of the "forgotten valve". As team we have managed to produce a very illustrative and practical chapter which I am proud to be allowed to print in this book. Also I would like to take this opportunity to thank you for reading my draft articles, you were always so enthusiastic and your comments were always constructive. The right ventricle has sparked your enthusiasm and hopefully together we can give this some more focus. I feel honored that you have been my co-author for many of my articles but above all I value your friendship.

Prof.dr. J. Simpson, dear John, thank you for inviting me to join your group of experts in writing a much needed 3D echocardiography in congenital heart disease consensus

paper and also for giving permission to include it in this book. The paper gives a clear and concise overview of this imaging modality and will be of help to many involved in this field of congenital heart disease. We met for the first time many years ago at the European teaching course on echocardiography and annually thereafter. Your enthusiasm, dynamic personality and enormous talent for teaching inspired me. To hear my hometown dialect, share a dram with you and enjoy that oh so wonderful sarcastic humor of the British always brings a smile to my face.

René Frowijn. Dear René, words are not enough to thank you for your tremendous support to my articles, numerous presentations and this book. From an IT perspective I must have been your world's worst nightmare, but I hope deep down you have enjoyed the ride.

Dr. Witsenburg, dear Maarten, I have benefitted more times than you can ever imagine from your immense knowledge of congenital heart disease. Your critical revision of the ASD article and your enthusiasm on hearing that I had accepted this PhD challenge has kept me going. I have very much appreciated working with you and continue to look forward to interesting times ahead.

Dr. van der Zwaan, dear Heleen, your help, constructive comments and scientific input for many of the articles in this book I have appreciated very much. The next episode of the famous 'forgotten chamber' (right ventricle) is now published. However, it still remains a continuing story. I would also like to take this opportunity to wish you every success in your career as a Cardiologist in whatever direction you choose. But most importantly, I would like to thank you and the three most important men in your life for the lovely times we have shared together.

Dr. Oei, dear Frans, I would like to thank you for reviewing and adding the final touch to the mitral valve article. I appreciate you finding the time to do this for me.

Myrthe and Marlies, my statisticians. Marlies, in your last year as a medical student you spent some time on a research project in our department. You introduced me gently to the world of statistics and our first scientific article was published with supporting statistical evidence. Good luck in your future career as a doctor, hopefully your dream to become a paediatric cardiologist will come true.

Myrthe, the meticulous, what a privilege it was for me to work with you. When you are on mission there is no stopping you. We made a good team, your statistical knowledge and my echo expertise has resulted in some solid based articles being published. SPSS or the "goochel doos" as I called it, was like putty in your hands. Thank you for presenting the information in a way that made sense. I would also like to acknowledge the initiation and completion of the Navigator study which you undertook. This data is, and continues to be, used in many studies, the echo department will be forever grateful to you. I wish you every success in your training and career as radiologist. It was a pleasurable experience to have worked with such a young academic.

Mihai and Ernst, I thank you for your constructive comments and scientific wisdom.

Mihai, I hope you have, like I have had, a dynamic career in echocardiography and your family settles well into Dutch life.

Ernest, without all your extra hard work, the deadline for the TAVI article would not have been reached, thank you. Good luck with all your research and have a good time in Holland.

Dr. Cuypers, dear Judith "als ik het kan, kun jij het ook" is what you wrote in your thesis for me. The end result is presented in this book and I only have the defense committee to face. If I am to believe you yet again, it will not be as bad as I fear. Thank you for your support.

To a great group, the backbone of the echo department, dear Debbie, Marianne, Lourus, Ellen, Linda, Anja, Beata and Kwaku. Our paths have crossed daily for many years, less intense since I moved over to the research lab, but it is always a pleasure to join you for lunch and catch up. Thank you for still considering me a team member.

My room mates in Ba302. It sounds like a book title and I could easily write a book on the comings and goings of room Ba302 over the years but I will only concentrate on the period concerning this thesis. Lotte, your hard work in persuading patients to participate in the mitral valve study resulted in our mitral valve xPlane article. I have thoroughly enjoyed working with you and wish you all the best with your own thesis. Claire, Stijn and Peter, conscientious hard workers and a doctorate as reward. Claire a long way from home, not only working on a doctorate but also trying to find your way in a completely new culture and working environment. You survived and have found your place in the echo-lab and Cardialysis. Thank you for accepting to be a co-author, your constructive comments and help throughout this period I have appreciated a great deal. Stijn you have had frustrating times getting your articles published but succeeded in the end. And Peter, you must be the best travelled "promivendi" I have ever known. Your encouragement, comments and IT wisdom was always welcome. Lenard and Hanna, the most recent roommates. Your open minds, enthusiasm, willingness to learn and to help me with IT and Pubmed problems and of course share in the disappointments when articles required reworking. It's a pleasure to have you onboard.

The inhabitants of room Ba308; Jannet, John, Iris, Vivan, Allard. Lidia and Roderik and all the other medical students working for a short period on various projects concerning congenital heart disease. Your eagerness to learn and to assist me in the complex world of submitting an article, the ins and outs of Pubmed and all other IT problems I am forever grateful. I wish all of you every success in your career as doctors.

The congenital team and my most direct colleges, Jolien, Maarten, Annemien, Judith, Dolf, Martijn, Tineke and Celeste, it continues to be a pleasure to work with you all. Your daily enthusiasm, encouragement and offers to help throughout have brought this project to a successful conclusion and I couldn't have done it without you.

Maud Bovelander, dear Maud, thank you for accepting the job of translating the summary of my thesis. You faced not just the challenge of translating the summary into Dutch but also understanding the language of cardiology! I hope my thesis is the first of a steady flow of requests for scientific translations. As a young, independent, self-employed Dutch-English-Dutch translator and editor, I wish you every success with your company 'em/dash'.

Dear Fiona and Jim, when I first mentioned my thoughts on the challenge of writing a scientific article, you did not hesitate to guarantee support and help with proof reading. That support has help tremendously and resulted in going from one scientific article to a whole thesis! Thank you both so much, not only for now, but for all times.

Dear Guido and Alex when I asked you both if you would be prepared to act, as para-nimfen for today you did not hesitate in your answer. You arrived as two wonderful gifts in my life, the only gift I know without a "gebruiksaanwijzing". It has been a wonderful and fascinating journey for me and I am so thrilled to have you standing at my side today. I hope I will make you proud.

Lastly, but most importantly, is to thank my dear Wim. This PhD was not a path we had anticipated, but you having supported me through the publication of many articles, the challenge to bring it to a good end became tempting. You voiced your concerns but guaranteed your total support. I could not have achieved it without your very constructive reviewing, scientific knowledge and household multitasking. Thank you for standing by my side throughout.